

# **The Role of Tissue Cell Polarity in Monocot Development**

**Annis Richardson**

Thesis submitted for the Degree of Doctor of Philosophy

University of East Anglia

John Innes Centre

September 2015

© This copy of the thesis has been supplied on condition that anyone who consults it is understood to recognise that its copyright rests with the author and that use of any information derived there from must be in accordance with current UK Copyright Law. In addition, any quotation or extract must include full attribution.

## Abstract

Nature exhibits huge diversity in organ shape, and yet all organs start as small bud-like peripheral outgrowths. Combinations of different spatial and temporal developmental switches in shape determine final organ shape. In plants shape arises through growth, which is defined by axiality and growth rates. Here I tested three hypotheses for how developmental switches in shape could arise: (1) growth rates alone are altered, (2) axiality alone is altered (3) both growth rates and axiality are altered. Using a multidisciplinary approach I explored which of the hypotheses was true for developmental switches in shape during organ development in two monocot models: early grass leaf development and the *Hooded* barley mutant. Developmental switches in shape were first volumetrically described using 3D imaging. Using this framework, computational models were generated to formulate hypotheses which could account for the switches in shape. Model predictions were then tested using whole-mount immunolocalisation of *SISTER OF PINFORMED 1* (*SoPIN1*), gene expression, and cell division and shape analyses. Synthetic biology was also used to generate a set of transgenic tools for future testing of the models. I found that a developmental switch in shape during early grass leaf development may arise through alterations in growth rates alone (hypothesis 1). In contrast, ectopic flower and wing formation in *Hooded* may arise through modulation of growth rates and axiality combined (hypothesis 2). In this case a single gene, *BKn3*, triggers the growth change, possibly through directly influencing tissue cell polarity (if axiality is defined by a polarity based axiality system), with differential effects on shape depending on where it is expressed. This suggests that novel developmental switches in shape could evolve due to single gene mutations, and that during evolution, modulation of growth may have been redeployed in different spatial and temporal patterns to trigger novel changes in shape, ultimately changing final form.

# Contents

Abstract .....	2
Contents .....	3
List of Tables .....	8
List of Figures .....	9
Acknowledgements.....	13
Introduction.....	15
1.1    Developmental switches .....	15
1.2    Growth in plant tissues .....	16
1.3    Growth and developmental switches in shape .....	18
1.4    Axiality systems .....	19
1.4.1    Polarity based axiality system.....	19
1.4.2    Stress based axiality system.....	23
1.4.3    Markers of axiality: PINs and hairs .....	24
1.5    The contribution of different tissues within the organ.....	25
1.6    Computational models at different scales .....	26
1.7    Exploring dicot and monocot development.....	27
1.8    This work .....	31
2    Grass Leaf Development.....	32
2.1    Leaf development in the grasses.....	32
2.2    Aim of this project.....	37
2.3    Describing a developmental switch in shape during primordial grass leaf development .....	37
2.4    The formation of the hood from a ring primordium could be accounted for by enhanced anisotropic growth towards the midvein .....	50
2.5    Axial information in the early grass leaf primordium .....	55
2.6    A change in axial information and/ or growth rate pattern may be required for the next shape transition from a hood to a cone.....	60
2.7    Axial information is oriented towards the midvein tip after the hood stage consistent with both model predictions .....	66
2.8    Exploring growth rate patterns across the grass leaf primordium .....	69
2.9    Discussion.....	77
2.9.1    Characterising developmental switches in shape during primordial stages of grass leaf development .....	77
2.9.2    Modelling the primordial stages of grass leaf development .....	77

2.9.3	<i>Predicted changes in growth during grass leaf development</i> .....	78
2.9.4	<i>The role of growth rate patterns in grass leaf development</i> .....	79
2.9.5	<i>The role of axial information in grass leaf development</i> .....	80
2.9.6	<i>Insights into the evolution of the grass leaf</i> .....	81
2.9.7	<i>Future work and concluding remarks</i> .....	82
<b>3</b>	<b>How Can a Single Gene Induce a Developmental Switch in Shape? The <i>Hooded</i> Barley Mutant</b> .....	<b>85</b>
<b>3.1</b>	<b>Barley floral development and the <i>Hooded</i> mutant</b> .....	<b>85</b>
3.1.1	<i>Morphology of wild-type barley</i> .....	85
3.1.2	<i>Morphology of the Hooded barley mutant</i> .....	87
3.1.3	<i>Previous studies in the Hooded mutant</i> . .....	90
<b>3.2</b>	<b>Aim of this project</b> .....	<b>92</b>
<b>3.3</b>	<b>Characterising a developmental switch in shape in the barley flower: Staging ectopic flower development</b> .....	<b>92</b>
<b>3.4</b>	<b>Ectopic expression of <i>BKn3</i> in the <i>Hooded</i> lemma precedes the formation of the ectopic meristem</b> .....	<b>104</b>
<b>3.5</b>	<b>The ectopic expression of <i>BKn3</i> in the <i>Hooded</i> lemma induces a reorientation in axial information at the cellular level</b> .....	<b>110</b>
<b>3.6</b>	<b>The ectopic expression of <i>BKn3</i> in the <i>Hooded</i> lemma induces changes in the expression pattern of candidate polarity organisers</b> .....	<b>123</b>
<b>3.7</b>	<b>Specific changes in growth in the lemma margin trigger the developmental switch in shape responsible for wing formation</b> .....	<b>136</b>
3.7.1	<i>Characterising a possible second developmental switch in shape in the Hooded mutant</i> .....	137
3.7.2	<i>Modelling Hooded lemma wing development as a consequence of changes in growth</i> .....	140
3.7.3	<i>Axial information may specifically reorient at the margin of the Hooded lemma</i> .....	144
3.7.4	<i><i>BKn3</i> may act cell autonomously in the margins to form the wings in the Hooded mutant</i> .....	148
<b>3.8</b>	<b>Discussion</b> .....	<b>151</b>
3.8.1	<i>Characterising the morphology of the wild-type and Hooded spike during development</i> .....	151
3.8.2	<i>There may be two independent developmental switches in shape in the Hooded mutant</i> .....	152
3.8.3	<i>Single genes are able to trigger developmental switches in shape through modulating growth rates and axiality</i> .....	153

	3.8.4	<i>BKn3 may influence axial information through modulating the expression of organiser components .....</i>	154
	3.8.5	<i>Future work and concluding remarks.....</i>	156
<b>4</b>		<b>Developing a Transgenic Toolkit in Barley .....</b>	<b>159</b>
	4.1	<b>Tools available in other species .....</b>	<b>159</b>
	4.2	<b>Aim of this work.....</b>	<b>162</b>
	4.3	<b>Spectral scan of barley flowers .....</b>	<b>163</b>
	4.4	<b>Design of the transformation constructs .....</b>	<b>164</b>
	4.4.1	<i>Selecting sequences.....</i>	165
	4.5	<b>Goldengate cloning of constructs.....</b>	<b>171</b>
	4.6	<b>Screening of plants.....</b>	<b>173</b>
	4.7	<b>Testing the heat shock inducible lines.....</b>	<b>179</b>
	4.8	<b>Discussion.....</b>	<b>182</b>
	4.8.1	<i>Development of a barley transgenic toolkit.....</i>	182
	4.8.2	<i>Future work .....</i>	182
<b>5</b>		<b>Discussion.....</b>	<b>185</b>
	5.1	<b>Summary of this work .....</b>	<b>185</b>
	5.2	<b>Developmental switches in shape arise from changes to growth rates alone and from changes in growth rates and axiality combined.....</b>	<b>186</b>
	5.3	<b>Single genes can trigger developmental switches in shape through modulating growth rates and axial information .....</b>	<b>187</b>
	5.4	<b>Modulating axial information with organiser regions .....</b>	<b>189</b>
	5.5	<b>The contribution of different tissues.....</b>	<b>190</b>
	5.6	<b>Monocots as developmental models .....</b>	<b>191</b>
	5.7	<b>Developmental switches in shape are involved in the evolution of new organ morphologies .....</b>	<b>193</b>
	5.8	<b>Computational modelling allows exploration of shape development at different scales .....</b>	<b>194</b>
	5.9	<b>Future directions.....</b>	<b>195</b>
	5.10	<b>Concluding remarks.....</b>	<b>199</b>
<b>6</b>		<b>Materials and methods .....</b>	<b>200</b>
	6.1	<b>General Methods .....</b>	<b>200</b>
	6.1.1	<i>DNA extraction.....</i>	200
	6.1.2	<i>RNA extraction .....</i>	200
	6.1.3	<i>cDNA synthesis.....</i>	200

6.1.4	PCR and colony PCR.....	201
6.1.5	Sequencing reactions .....	201
6.1.6	Heat shock transformation of <i>E.coli</i> .....	201
6.1.7	Heat shock of inducible transgenic lines .....	202
6.1.8	Electroporation transformation of <i>Agrobacterium tumefaciens</i> ..	202
6.1.9	Plasmid extraction from bacterial cultures .....	202
6.1.10	PCR purification.....	202
6.1.11	Restriction digest.....	203
6.1.12	Propidium iodide staining .....	203
6.1.13	Maize seed sterilisation.....	203
6.1.14	Optical projection tomography.....	204
<b>6.2</b>	<b>Plant Growth Conditions .....</b>	<b>205</b>
6.2.1	Timecourse samples .....	205
6.2.2	<i>In situ</i> hybridisation and immunolocalisation samples.....	206
6.2.3	Transgenic barley.....	206
<b>6.3</b>	<b>Generating transgenic barley lines:.....</b>	<b>206</b>
6.3.1	Goldengate cloning .....	206
6.3.2	Barley transformation, crossing and screening .....	208
<b>6.4</b>	<b>Tissue fixation and preparation for <i>in situ</i> hybridisation and immunolocalisations on sliced tissue .....</b>	<b>209</b>
<b>6.5</b>	<b><i>In situ</i> hybridisation .....</b>	<b>210</b>
6.5.1	Probe design.....	210
6.5.2	Probe preparation .....	211
6.5.3	<i>In situ</i> hybridisation protocol .....	211
6.5.4	Imaging .....	212
<b>6.6</b>	<b>Immunolocalisation .....</b>	<b>212</b>
6.6.1	Antibody information .....	212
6.6.2	Immunolocalisation protocol for sliced tissue.....	213
6.6.3	Whole-mount immunolocalisation of barley .....	213
<b>6.7</b>	<b>EdU/ PI staining of maize vegetative meristems.....</b>	<b>215</b>
6.7.1	Plant growth conditions .....	215
6.7.2	Protocol .....	215
6.7.3	Imaging .....	215
<b>6.8</b>	<b>Computational modelling.....</b>	<b>215</b>

	6.8.1	<i>The canvas</i> .....	216
	6.8.2	<i>The factors</i> .....	216
	6.8.3	<i>Networks</i> .....	217
	6.8.4	<i>Simulation details</i> .....	217
	6.8.5	<i>Polarity parameters</i> .....	218
	6.8.6	<i>Growth parameters</i> .....	219
	6.9	<b>List of plasmids generated</b> .....	<b>224</b>
	6.10	<b>List of primers used</b> .....	<b>225</b>
<b>7</b>		<b>Appendices</b> .....	<b>226</b>
	7.1	<b>Appendix A: Developing a whole-mount immunolocalisation protocol in barley</b> .....	<b>226</b>
	7.2	<b>Appendix B: Characterising barley morphology</b> .....	<b>229</b>
	7.3	<b>Appendix C: RNA <i>in situ</i> hybridisation probes</b> .....	<b>238</b>
	7.4	<b>Appendix D: Transgenic barley constructs</b> .....	<b>240</b>
<b>8</b>		<b>Abbreviations</b> .....	<b>251</b>
<b>9</b>		<b>References</b> .....	<b>252</b>

## List of Tables

<b>Table 2.1</b> Measurements describing a standard maize B73 juvenile leaf 6 .....	41
<b>Table 2.2</b> Dimensions of different stages of maize leaf development and the comparable model stages .....	66
<b>Table 3.1</b> Dimensions of the calculated T0 barley floret 5 morphology. ....	94
<b>Table 4.1</b> The different components for golden gate cloning with their related overhangs and endonuclease enzyme recognition sites as described by Weber et al 2011 [175].....	165
<b>Table 4.2</b> The L2 constructs transformed into barley and their component parts. ....	169
<b>Table 4.3</b> L1 components made for L2 construction .....	170
<b>Table 6.1</b> VIP machine program for paraffin embedded samples.....	210
<b>Table 6.2</b> VIP program for non-wax embedded samples .....	214
<b>Table 6.3</b> Factors used in the maize leaf models.....	221
<b>Table 6.4</b> Parameters for the diffusible factors in the maize leaf models .....	222
<b>Table 6.5</b> Factors used in the wing models .....	223
<b>Table 6.6</b> Parameters for diffusible factors in the wing models.....	223
<b>Table 6.7</b> Plasmids made during the project .....	224
<b>Table 6.8</b> List of primers used during the project.....	225

## List of Figures

<b>Figure 1.1</b> Diagram of a typical grass leaf after the initiation of flowering.....	28
<b>Figure 2.1</b> An example of a grass: maize seedling morphology.....	33
<b>Figure 2.2</b> Approximate fate map of the hood stage of maize leaf primordium development. .....	36
<b>Figure 2.3</b> 3D OPT imaging of the early stages of leaf development in B73 maize juvenile leaf 6.....	39
<b>Figure 2.4</b> Dimensions of B73 maize juvenile leaf 6 at P1, P2, P3 and P4... ..	42
<b>Figure 2.5</b> The <i>Poaceae</i> family tree .....	44
<b>Figure 2.6</b> OPT images of <i>Brachypodium distachyon</i> and <i>Fargesia rufa</i> . .....	45
<b>Figure 2.7</b> Monocot phylogeny.....	47
<b>Figure 2.8</b> OPT imaging of leaf primordium in the monocot species <i>Alium ameloprasum</i> (leek) and <i>Acorus calamus</i> . .....	49
<b>Figure 2.9</b> Modelling the transition from a ring to a hood shaped primordium. ....	52
<b>Figure 2.10</b> SoPIN1 localisation in early grass leaf primordia.....	57
<b>Figure 2.11</b> Whole-mount immunolocalisation of SoPIN1 in early barley leaf primordia ....	59
<b>Figure 2.12</b> Modelling the transition from a hood to cone shape with the distal tip model ... .....	61
<b>Figure 2.13</b> A switch in polarity allows the transition from a hood to a more cone-like shape in the proximo-marginal model .....	63
<b>Figure 2.14</b> Refining the proximo-marginal model for the transition from a hood shape to a cone like shape using a switch in growth rate pattern .....	65
<b>Figure 2.15</b> SoPIN1-YFP in transgenic <i>Brachypodium</i> at P3 stage of leaf development .....	67
<b>Figure 2.16</b> Whole-mount immunolocalisation of SoPIN1 in P2 stage barley primordia.....	68
<b>Figure 2.17</b> Schiff PI and EdU staining in maize primordia .....	72
<b>Figure 2.18</b> Cell area in a P1 and P3 primordium .....	73
<b>Figure 2.19</b> Cell files in calcofluor stained barley primordium .....	76
<b>Figure 3.1</b> The morphology of a wild-type barley flower .....	87
<b>Figure 3.2</b> The morphology of the <i>Hooded</i> mutant flower .....	89
<b>Figure 3.3</b> Whole spike morphology of wild-type and <i>Hooded</i> 2-row Bowman barley over 340 hours of inflorescence development. ....	97
<b>Figure 3.4</b> The morphology of the floret 5 during different times in development.....	99

<b>Figure 3.5</b> Graphs illustrating natural logarithm (ln) of the dimensions of developing barley inflorescence spikes and floret 5 in wild-type and <i>Hooded</i> samples.....	101
<b>Figure 3.6</b> Confocal images of the adaxial surface of calcofluor stained <i>Hooded</i> lemmas at different stages in development. ....	103
<b>Figure 3.7</b> Phylogenetic analysis of KNOTTED1 like proteins. ....	105
<b>Figure 3.8</b> Localisation of <i>BKn3</i> mRNA in central longitudinal sections through developing wild-type and <i>Hooded</i> barley flowers .....	109
<b>Figure 3.9</b> Guide phylogeny tree of the <i>PIN1</i> family .....	111
<b>Figure 3.10</b> RNA <i>in situ</i> hybridisation showing the localisation of <i>BKn3</i> , and barley <i>PIN1</i> homologues in developing barley florets. ....	113
<b>Figure 3.11</b> Immunolocalisation of PIN1a and SoPIN1 in developing barley flowers. ....	115
<b>Figure 3.12</b> Immunolocalisation of SoPIN1 in middle longitudinal sections of developing barley flowers. ....	117
<b>Figure 3.13</b> Whole-mount immunolocalisation of SoPIN1 on the adaxial side of wild-type lemmas.....	119
<b>Figure 3.14</b> Whole-mount immunolocalisation of SoPIN1 on the adaxial surface of developing <i>Hooded</i> lemmas. ....	121
<b>Figure 3.15</b> A summary diagram illustrating the relationship between <i>BKn3</i> expression, SoPIN1 localisation and morphology. ....	123
<b>Figure 3.16</b> Guide phylogenetic tree for NAM protein sequences and the map of the barley <i>NAM</i> mRNA sequence showing the region covered by the probe .....	125
<b>Figure 3.17</b> RNA <i>in situ</i> hybridisation of <i>NAM</i> mRNA in longitudinal sections through wild-type and <i>Hooded</i> barley flowers. ....	127
<b>Figure 3.18</b> Guide phylogenetic tree for YUCCA protein sequences and the map of barley <i>YUCCA</i> cDNA showing the region covered by the probe. ....	129
<b>Figure 3.19</b> RNA <i>in situ</i> hybridisation of <i>YUCCA</i> mRNA in longitudinal sections through wild-type and <i>Hooded</i> barley flowers. ....	130
<b>Figure 3.20</b> Guide phylogenetic tree for LAX protein sequences and the map of barley <i>LAX1</i> cDNA showing the region covered by the probe.....	131
<b>Figure 3.21</b> RNA <i>in situ</i> hybridisation of <i>LAX1</i> mRNA in longitudinal sections through wild-type and <i>Hooded</i> barley flowers. ....	133
<b>Figure 3.22</b> Summary cartoon of the localisation of <i>BKn3</i> , <i>LAX1</i> , <i>NAM</i> and <i>YUCCA</i> mRNA and the pattern of SoPIN1 localisation in longitudinal midsections through <i>Hooded</i> lemmas at different stages in development.....	135

<b>Figure 3.23</b> OPT images of <i>Hooded</i> lemmas showing the wing outgrowths at different stages of development.....	137
<b>Figure 3.24</b> The development of lemma shape in floret 5 of wild-type and <i>Hooded</i> inflorescence spikes over time.....	139
<b>Figure 3.25</b> GPT framework modelling of outgrowths. ....	143
<b>Figure 3.26</b> SEM images of the adaxial wing region in a mature <i>Hooded</i> lemma .....	145
<b>Figure 3.27</b> Cell file patterns in the adaxial surface of <i>Hooded</i> lemmas. ....	147
<b>Figure 3.28</b> RNA <i>in situ</i> hybridisation patterns of <i>BKn3</i> , <i>NAM</i> , <i>YUCCA</i> and <i>LAX1</i> in longitudinal sections through <i>Hooded</i> flowers at late stages in development .....	149
<b>Figure 3.29</b> Whole-mount immunolocalisation of <i>BKn3</i> in a developing lemma at approximately 260 hours.....	150
<b>Figure 4.1</b> Diagram illustrating the <i>CRE lox</i> clonal sector technique.....	161
<b>Figure 4.2</b> Screening of wild-type barley tissue for endogenous fluorescence.....	164
<b>Figure 4.3</b> <i>eGFP</i> expression in <i>pZmUbi::eGFP-T</i> barley lemmas. ....	166
<b>Figure 4.4</b> Phylogenetic tree showing the relationship between the PIP aquaporin proteins. ....	167
<b>Figure 4.5</b> The modification of the goldengate method to make clonal sector lines.....	172
<b>Figure 4.6</b> Expression of <i>HvPIP2.5-eGFP-T</i> in T1 barley plants. ....	174
<b>Figure 4.7</b> Expression and localisation of the <i>pZmUbi::loxmCHERRY-HDEL-Tlox/eGFP-HDEL-T</i> construct in T1 barley plants.....	175
<b>Figure 4.8</b> Expression and localisation of the <i>pHvHSP17::Cre/pZmUbi::loxmCHERRY-HDEL-Tlox/eGFP-HDEL-T</i> construct in T1 barley plants. ....	176
<b>Figure 4.9</b> Expression and localisation of the <i>pHvHSP17::Cre/pZmUbi::loxCyPET-HDEL-Tlox/Bkn3-mCHERRY-T/ pHvPIN1a::HvPIN1a-eGFP-T</i> construct in T1 barley plants.....	178
<b>Figure 4.10</b> Expression and localisation of the <i>pHvPIN1a::HvPIN1a-eGFP-T/DR5:mp35S::mCHERRY-T</i> construct.....	179
<b>Figure 4.11</b> Heat shock test on the expression and localisation of <i>mCHERRY</i> and <i>eGFP</i> in <i>pHvHSP17::Cre/pZmUbi::loxmCHERRY-HDEL-Tlox/eGFP-HDEL-T</i> T1 barley plants. ....	181
<b>Figure A1</b> Matrix of whole-mount immunolocalisation trial conditions .....	227
<b>Figure B1</b> The morphology of the wild-type barley spike over 380 hours of development. ....	230
<b>Figure B2</b> The morphology of the <i>Hooded</i> barley spike over 380 hours of development...232	

**Figure B3** The morphology of the wild-type and *Hooded* floret 5 over 380 hours.....234

**Figure B4** Confocal images of the adaxial surface of developing *Hooded* lemmas.....236

**Figure B5** SEM images of a mature wild-type lemma ..... 237

## Acknowledgements

**This thesis is dedicated to the memory of Professor Andrew Bangham (1947-2014), who was an indispensable source of wisdom and enthusiasm during my PhD.**

First and foremost, I would like to thank Enrico Coen for his supervision and for letting me travel both in body and mind, and for his patience during our thesis meetings. I would also like to thank my supervisory committee members; Cristobal Uauy, for his unending enthusiasm, and Xana Rebocho, my lab guardian angel. Thank you also to my collaborators, Sarah Hake and Devin O'Connor, without their enthusiasm (and antibodies) the leaf project would never have occurred.

Thank you to all of the members of the Coen lab, present and past, who have ridden the PhD wave with me and made me feel welcome from the moment I started in the lab. Particular thanks to Karen Lee, for teaching me OPT, Sam Fox for teaching me Goldengate cloning, Lucy Copsey for looking after my plants, Paul Southam and Richard Kennaway for helping me with the modelling, Jordi Chan for help with microscopy (and telling me that he was sure whole-mount immunos were easy) and to Des Bradley for being a fountain of knowledge. Also thanks to Claire Bushell, my immuno partner in crime, Cathy Mansfield, Mabon Ellis, Chris Whitewoods, Katie Abley and Tilly Eldridge for all of their laughing support.

Thanks also to Nick Brewin and Mike Merrick who made my rotation year run smoothly and helped me decide between projects. Thank you to my rotation supervisors and all of their lab members; Sophien Kamoun and Robert Sablowski.

Thank you to my friends both in Norwich and elsewhere who have kept me grounded and laughing throughout, particularly Claire Drurey (an incredible housemate), Richard Payne, Mike Rugen, Artemis Giannakopoulou, Matt Smith, Jo Harrison, Rachel Goddard, Lucy Gannon, Chris Judge, Hadrien Peyret, Philippa Borrill, Elyse Rigby, Ali Tamkin, Sophie Walker, Alex Lee, Harry Jubb, Imy Ogilvie, Oli Caspari, Jojo Shavisi, Gersh Rai and Hannah Morris.

I would also like to acknowledge some of the people who have inspired me and helped me to reach this point; Mrs Shields (my primary school teacher who inspired me to always ask why and how), Professor Melvin Askew (who has always been enthusiastic about my studies and work), Dr Stephen Tomkins (for taking a chance on me), Professor Marc Knight (for being an amazing summer project supervisor) and Professor Beverley Glover (for telling me to go to JIC for my PhD). Thank you also to Pap for his unending support and pride in his

granddaughter who chose to study biology, his thirst for life and learning is a continuous inspiration to me. Thank you to my brother, Lt Adam Richardson, who may not know it, but has inspired me to follow my instincts and work hard to achieve my goals, and has always challenged and questioned me.

Thank you to John Steele, without whom I would have fallen far harder at each hurdle life has thrown at me over the last 4 years.

Finally, to my parents who never told a little girl that she was dreaming when she said that she was going to go to Cambridge University and become a scientist, thank you.

## Introduction

Nature exhibits extraordinary diversity in organ shape and size. Shape can have a huge impact on an individual's fitness, for example, in plants the shape of petals can specify pollination syndromes [1] and the shape of leaves can influence photosynthetic capacity [2]. Despite the diversity in mature shape, all organs start as small peripheral outgrowths which have little to no resemblance to the mature form, these are termed buds in animal development and primordia in plants. Morphogenesis, how organ shape develops from these small peripheral outgrowths, is a central research area in developmental biology. An important question is how morphogenesis has been modified during evolution to generate new shapes.

During development organisms go through a series of distinct changes which can be temporally and environmentally regulated. These changes are often described as developmental switches. It may be that during evolution, developmental switches are adapted to generate new morphologies (or shapes).

### 1.1 Developmental switches

Developmental switches are usually associated with a change in identity or activity of a region which diverts from the one originally specified. For example, a well characterised, genetically controlled, developmental switch in identity is the transition from a vegetative meristem, which produces leaves, to an inflorescence meristem, which produces floral meristems. An interesting feature of the developmental switch from vegetative to inflorescence identity is that the expression of a single gene, such as the transcription factor *LEAFY*, is able to induce the switch [3]. These developmental switches in identity occur before organ initiation.

Developmental switches can also occur in relation to shape during organ development resulting in significant changes in morphology (or switches in shape). As an organ develops from a peripheral outgrowth, it will often progress through a series of precise shape transitions, which combine to generate the final mature shape. For example, during *Arabidopsis* leaf development the dome shaped primordium first develops into a simple rounded leaf, and the leaf margin is later elaborated through the initiation of serration outgrowths, which involves genetic and hormonal control [4, 5]. In the unusual leaves of the

*Monstera* plant family (also called swiss-cheese plants), in which perforations form an integral part of their shape, a normal continuous leaf is formed first and then later in development cell death is initiated in loci across the leaf to form the holes [6]. Developmental switches in shape are not unique to leaves, root structures in plants are also elaborated by the development of lateral roots from the main root axis, generating a branched structure, controlled by hormonal, genetic and environmental signals [7]. This phenomenon is also common across kingdoms. For example, in animals digit formation occurs late in development after limb formation has initiated, modifying the final shape of the limb. The final limb shape depends upon the level of genetically controlled signalling, or the size of gene expression domains. This is shown when comparing digits in pigs and bats which are reduced and extended respectively, depending on the size of the expression domain of transcription factors [8, 9]. Many of these developmental switches in shape during morphogenesis are under genetic control. How adjustments in gene behaviour result in developmental switches in shape is a key unanswered question in developmental biology.

In plants shape (morphogenesis) predominantly arises through a combination of growth and tissue deformation, due to the fact that cells are held in place relative to their neighbours by the rigid cell wall matrix. This makes investigating developmental switches in shape in plants simpler than animals, in which growth, tissue deformation, cell death and cell migration all have prominent roles. As tissue deformation is a resultant feature, it is likely that developmental switches in shape arise from changes in growth. The effects of growth during plant development can be very large, as illustrated by the development of the maize leaf; the maize leaf originates as a small primordium of around 100µm wide and 30µm high, with approximately 200 cells [10], whereas the mature maize leaf can be 10cm wide and over a meter long, composed of thousands of cells and many different tissue types. Manipulation of growth during organ formation could trigger new developmental switches in shape, resulting in novel mature organ morphologies. It may be that this link between growth and developmental switches in shape was exploited during evolution, generating the huge diversity of organ form now seen.

## **1.2 Growth in plant tissues**

Growth is defined as the increase in size over time and is driven by cell expansion. (Cell division compartmentalises the space within the tissue.) The growth of plant cells arises from the interaction between internal turgor pressure and the mechanical properties of the cell

wall [11], for example, when the walls are weakened the internal turgor pressure causes the cell to expand.

Plant cell walls are a network of polysaccharides and proteins. The properties of the cell wall can be altered through the activity of cell wall modulating enzymes like expansins, which loosen the cell wall [12, 13], and pectin methylesterases (PMEs), which can cause the cell wall to become more or less rigid depending on the environment within the wall [14]. One of the components of the cell wall is cellulose which is laid down in microfibril layers. Addition of cellulose to the cell wall stiffens it, and enables the cell to resist the stress placed upon it. Cellulose microfibrils are laid down in the cell wall by cellulose synthase enzymes, which are associated with the internal scaffold provided by microtubule arrays [15, 16]. Anisotropy in cell wall properties determines the orientation of cell growth, for example, cells have been observed to grow perpendicular to the walls with most cellulose reinforcement [17]. The interaction between cell wall stiffness and turgor pressure determines the amount that a cell grows. (Some recent work has also suggested that 3D geometry of the cell also adds to the mechanical constraints on growth [18].) This means that cell growth in plants is a mechanical process which is modulated by genes.

The cells in a plant tissue are connected via the cell wall matrix. Due to the connected nature of the tissue differential regions of growth throughout the tissue causes conflict between neighbouring regions of high and low growth rate. This conflict generates stresses in the cell wall matrix which result in tissue buckling and ultimately shape deformation [19]. Differential growth combined with tissue buckling forms the basis of plant tissue shape development, and has been explored using computational modelling [19-23].

Growth rates can be described as specified, the rate at which a region of tissue or a cell would grow in isolation, and resultant, the rate at which the tissue or cell actually grows due to the mechanical connectivity with other regions or cells. Through measuring resultant growth rate (we cannot measure specified growth rate due to the connected nature of the tissue which means that no region can achieve its full specified growth rate) using clonal sector analysis [10, 24], point tracking (e.g. using labelled particles on the organ surface or hairs) [25] and live imaging of cell outlines [21], it has become clear that growth within tissues can be isotropic, equal in all directions, or anisotropic, directional. Anisotropic growth can arise directly from specified anisotropy and indirectly (resultant anisotropy) due to conflict within the tissue. Clonal analysis in plants [10, 22, 24, 26-28], indicates that growth is often anisotropic, suggesting that anisotropic growth has a significant role in shape development.

Anisotropic growth has two components; axial information (from which the growth orientations are defined) and growth rates (separated into perpendicular and parallel growth rates relative to a given axiality).

Growth rates in a plant tissue are defined by the balance between turgor pressure and the resistance of the cell wall. This balance is influenced by genetically defined growth regulators which may be involved in transcriptional control of genes, biochemical modification of the cell wall or hormone regulation. Varying the expression of these genetic components across the tissue then leads to differential regions of specified growth rate. Different genetic factors can also influence the preferential orientation of growth of cells within different regions of the tissue to change shape.

The orientation of growth is specified with respect to an axiality system. Anisotropy in cell wall properties is guided with respect to this axis, resulting in oriented growth. Each cell has axial information and these cellular axes can be coordinated across a tissue, to generate a tissue level axis. The mechanism which coordinates cellular axes is called an axiality system. The axiality system can be influenced by altering the expression pattern of regulatory genes, sometimes establishing new axes of growth within a developing tissue.

### **1.3 Growth and developmental switches in shape**

It is likely that developmental switches in shape arise through changes in growth in plant tissues. But how is growth altered to generate new developmental switches in shape? As growth is composed of axiality and growth rates, there are three different ways that growth could be influenced:

1. Axiality alone is altered
2. Growth rates alone are altered
3. Both axiality and growth rates are altered

Both axiality and growth rates are under genetic control. Therefore, single gene mutations could lead to new developmental switches in shape if they were able to influence growth in any of these three ways.

## 1.4 Axiality systems

A coordinated axiality system within a tissue enables the orientation of growth of each cell to be specified with respect to their position within the tissue. Without coordination of the axiality system, tissues may grow more isotropically overall as each cell would grow with respect to its own axis. How an axiality system is defined is an active area of research in developmental biology, and there are currently two hypotheses. The first is the polarity based axiality system, the second is the stress based axiality system.

### 1.4.1 Polarity based axiality system

The polarity based axiality system hypothesises that axiality within the tissues is defined chemically. Self-organising chemical signals locally specify cellular polarities which can then be coordinated across the tissue to generate a tissue cell polarity field (coordinated cell polarities across a tissue). Axial information, from which growth is oriented, is locally provided by the cellular polarities. The cellular polarities influence the anisotropy of cell wall properties defining growth orientation (this could be through modulating microtubule alignment or altering the cell wall stiffness directly). Using this polarity based axiality system, axial information could be specified independently of growth.

The chemical signal (or morphogen) central to the polarity based model could be any diffusible factor (or group of components). The phytohormone auxin is a strong candidate of the polarity system, as it has been shown to be polarly transported through tissues by PIN (PIN-FORMED) auxin transporters [29] and it is linked with diverse changes in plant morphology [30-32]. Auxin has also been shown to be central to embryogenesis [33] and in shoot architecture (the *Arabidopsis pin1* mutant fails to form organ primordia, as do apices cultured in the auxin transport inhibitor NPA (1-N-Naphthylphthalamic acid) [30, 34]). How auxin acts to coordinate cellular polarities across a tissue is not known, although several hypotheses have been put forward based upon models of PIN protein localisation (PINs are used as markers of tissue cell polarity). Any model that underlies the polarity axiality system needs to explain both the cellular localisation of PINs and the coordination of PIN localisation across the tissue.

The up-the-gradient model, suggests that PIN proteins localise to the face of the cell which has the neighbour with the highest concentration of auxin [35], and that gradients of auxin across the tissue can generate tissue cell polarity. (The differences in concentration which trigger a change in PIN localisation can originate as small fluctuations, as the subsequent

transport of auxin is towards the cell with higher auxin concentration, reinforcing the initial concentration difference.) Using this model, simulations have shown that phylotactic patterns of PIN1 convergence points in the SAM can be accurately recreated [36]. There are two subfamilies of this category. One proposes that the concentration of auxin is directly sensed using a chemical based mechanism [35]. The other subfamily is mechanical based polarity which proposes that stress patterns in the cell walls bias the cellular localisation of PINs (possibly using microtubules) [37, 38], and that global coordination of cellular polarities arises through changes in the stress patterns generated by auxin in the tissue. These models result in the PIN proteins localising to the wall closest to regions of high auxin.

The with-the-flux model proposes that PIN proteins localise to the face of the cell which has the highest flux of auxin out of the cell [39, 40], and that gradients of auxin flux across the tissue generate the coordination of cellular polarities. Simulations using the with-the-flux model are able to accurately recreate vein patterning and development [36, 41].

A third model, intracellular partitioning [42], proposes that PINs become localised to the face of the cell with the lowest extracellular concentration of auxin due to a feedback loop of inhibitory factors in the cell's membrane. Through cell-cell coupling these polarities can then become locally coordinated across the tissue, generating tissue cell polarity patterns. This coordination occurs without the need for long range gradients of auxin concentration or flux. Intracellular partitioning combined with cell-cell coupling is able to recreate PIN1 patterns in the SAM and in veins (Katie Abley, JIC, unpublished).

Most of these models are able to account for PIN1 patterns seen in developing tissues to some extent, however not all of the biological components for the proposed polarising mechanisms have been identified. The up-the-gradient models rely upon a cell being able to sense the concentration of auxin in its neighbours or in the extracellular space using either a chemical or a more mechanical based mechanism. It was proposed that the possible extracellular auxin receptor ABP1 (AUXIN BINDING PROTEIN 1) [43] may be part of the chemical concentration sensing mechanism, however the functionality of ABP1 as an auxin receptor has recently been questioned [44]. The components of a mechanical polarity model have not been identified, although some suggest a direct link between microtubules and PIN localisation. Work in protoplasts could suggest that PINs require an intact cytoskeleton for polarisation [45], however this is not conclusively in support of mechanics as protoplast treatment could also inhibit any of the other mechanisms. Treatment with the microtubule depolymerising drug, oryzalin, only results in a broadening of the domain in which PIN1 is

localised [37, 45-47]. Similarly changing the mechanical properties of a tissue does not seem to affect PIN orientation (except in ablation experiments [37] but this could influence other orienting factors). Without direct links with microtubules, how mechanical stress is able to form discrete PIN convergence points across the meristem is not easily explained.

The with-the-flux model requires cells to be able to measure flux of auxin across a membrane. However, no flux-measuring protein has been identified and as auxin is able to diffuse into cells (i.e. it does not always require active transport) it may not be possible to measure accurately. Although recent work indicates that perhaps only a small percentage of the total auxin flux would need to be measured to initiate polarisation in the with-the-flux model (Przemysław Prusinkiewicz, University of Calgary, seminar talk, unpublished).

Intracellular partitioning does not need the cell to measure flux or concentration to become polarised, instead it requires several membrane bound proteins which mutually inhibit each other, but promote their own activation. It has been suggested that ROPs (RHO GTPASES OF PLANTS) could act as some of the components in this feedback loop [42], although this is yet to be tested thoroughly.

Irrespective of the method used to specify cell polarity, it could be that genetically defined 'organiser' regions are used to anchor cellular polarity coordination across the tissue, acting as plus (cellular polarity shifts to orient away from these regions) and minus (cellular polarity shifts to orient towards these regions) organisers [42]. Organiser regions could influence the polarity specifying factors directly (i.e. the components that respond to auxin to define the polarity within the cell) or they could influence auxin, either through modulating transport (using auxin import and export) or metabolism (auxin biosynthesis, conjugation, and degradation). This modulation could influence auxin gradients, either intracellularly or extracellularly, or auxin flux to bias the region of tissue immediately next to the organiser, resulting in the coordination of cell polarities across the tissue due to the feedback nature of the polarisation mechanisms proposed. Through modulating the distribution of organiser regions with a generic diffusible 'Polariser' component and differential growth rates, computational models have shown that diverse biological shapes can be formed [20-22, 24].

The first indication of a developing organ primordium is the formation of a PIN1 convergence point [48]. In the developing organ primordium the PIN1 polarity pattern could illustrate the new polarity field formed in response to the distribution of auxin across the meristem. The PIN1 convergence point may act as a new minus organiser, drawing auxin towards it,

coordinating the nearby cellular polarities. The localisation of epidermal PIN1 in a young developing leaf coordinates towards the tip of the midvein [49] (which forms in the site specified by the PIN1 convergence point), this is consistent with the role of a minus organiser. The developing midvein itself may act as a minus organiser by reducing epidermal auxin concentration through transporting auxin away from the epidermis into the developing vascular system. As the leaf develops the coordinated polarity field of PIN1 orients away from the boundary region, between the primordium and meristem, towards the leaf tip [49] this predicts that the boundary region may act as a new plus organiser. Boundary regions are defined by expression patterns of genes such as the NAC domain transcription factor *NAM* [50] (*NO APICAL MERISTEM* in *Petunia hybrida*, *CUP-SHAPED COTELYEDON* (*CUC*) genes in *Arabidopsis thaliana* [51]) and *LOB* (*LATERAL ORGAN BOUDARIES*) domain transcription factors [52]. Work in *Arabidopsis* shows that *NAM* and *LOB* domain transcription factors are found in the boundary between the primordium and the meristem, in the basal position predicted to be a plus organiser. Plus organisers are also proposed to increase auxin in the region, therefore they may have high expression of auxin biosynthesis genes like the *YUCCAs* [53]. Some work has been carried out on the expression patterns of *YUCCA* genes in rice [54] which indicate differential expression patterns, although no expression patterns in the primordial stage of leaf development have been recorded. Work on *SPI1* (*SPARSE INFLORESCENCE 1*, a *YUCCA*) in *Zea mays* (maize) suggests that *SPI1* is transiently expressed in the two outer cell layers of the meristem proximal to developing outgrowth [55], which could support the prediction of a basal plus organiser region. *YUCCA1* is also expressed at the base of developing leaf primordia in *Arabidopsis* [56], supporting the prediction made by the polarity based axiality model.

A key prediction made by the polarity based axiality model is that growth rate and growth orientation could be specified independently, and this is something that has not yet been shown. However, if auxin is able to modulate cell wall properties, through inducing cell wall modulating enzymes like the expansins [57], it may be that both axial information and growth rate are linked through the activity of auxin to some extent. This would mean that although it would be possible to separate changes in growth rate from axial information, changes in axial information (if it is determined by auxin) may not be separable from growth rate modulation.

Computational models that use a polarity based axiality system to set the axial information [20-22, 24] have found that the tissue can continually respond to the polarity field, or

respond to a polarity field which was locked at an earlier time step, without any significant change in resultant shape. This suggests that a locking mechanism may not always be essential during organ development.

If axiality is defined by a polarity based system, developmental switches in shape could be triggered by altering the spatial and temporal arrangement of axiality organiser regions. If a locking mechanism is used to fix the axiality, a developmental switch in shape could arise through the modulation of responsiveness windows during organ development.

#### **1.4.2 Stress based axiality system**

The stress based axiality system proposes that the axiality of a tissue is determined by the orientation of maximal stress patterns within the cell walls. Stress patterns are generated by differential growth within the connected tissue, and the tissue geometry. The mechanical stress (force per unit area) can be visualised by making small cuts in the tissue. Stress can act as compression (edges of the cut close) or tension (edges of the cut pull apart) [58]. As not all of the stress caused can be dissipated through tissue buckling and cell wall reinforcement during development, it is proposed that differential patterns of stress across a tissue could provide the orienting axis for anisotropic growth. This stress based axiality system proposes that maximal stress patterns are directly read by cells within the tissue and used to coordinate the cellular axes across the tissue.

How cells measure mechanical forces directly is not known. It has been shown that cells can respond to mechanical forces, for example, the expression of the *TOUCH3* transcription factor is activated in *Arabidopsis* in response to the application of touch [59]. However, although mechanosensitive ion channels have been identified [60, 61], how they function to measure stress is not understood. A major component of the cell which responds dramatically to mechanical forces is the microtubule network [62]. Microtubules have been observed to align along regions of maximal stress within the SAM (shoot apical meristem) and in developing primordia [63, 64]. It is proposed that mechanical stress could provide axial information through its influence on the alignment of microtubules which then feeds into the deposition of cellulose. This reinforces specific cell walls, biasing the orientation of cell growth. This is proposed to be the mechanism by which mechanical stress is able to directly define the axial information. (Although deposition of cellulose into the cell wall reinforces the cell wall from the stress imposed upon it, dissipating the stress.)

Computational models based upon mechanical axially have only so far considered the case of the meristem and primordia initiation [37]. During primordium outgrowth from the meristem, microtubules become aligned along the boundary region between the SAM and the primordium, whereas in the apex of the primordia they are more irregularly arranged [63]. This may induce a new axis of growth in the primordium as growth in the boundary region and adjacent to it will be perpendicular to the microtubules. However for outgrowth to occur, disassembly of highly aligned microtubules is required, possibly contradicting the proposed requirement of stress patterns for anisotropic growth (as the patterns of microtubules required to orient growth are disassembled, and therefore not present at the start of growth).

Recent preliminary work on the use of residual strain patterns (the strain remaining after dissipation of stress from cell wall reinforcement and tissue buckling) to define the axis from which growth is determined, suggest strain can define axially. However, if the tissue continually resets its axis in relation to the ever changing major stress patterns in the tissue, the axis will eventually be dissipated (Richard Kennaway, University of East Anglia, JIC, unpublished). This is consistent with the observation that cellulose deposition strengthens walls against stress imposed upon them, dissipating stress. These results suggest that a locking mechanism, like a window of developmental responsiveness, would be required to maintain a stress based axially system. In this case, changes in growth orientation would arise from specific reactivation of tissue responsiveness. However, the biological components of this stress based axially system are currently unknown.

### **1.4.3 Markers of axially: PINs and hairs**

To explore axially during development we need markers of cellular polarities. Through looking at the coordinated pattern of cellular polarities within a developing tissue we can assess the possible orientation of axially information. Several markers have been reported in the literature. One of the most commonly used markers is hair orientation in both animal and plant systems [65]. For example, through studying hair orientations in *Drosophila*, much has been discovered about planar polarity and many of the genes involved in defining tissue cell polarity (also called planar cell polarity) have been identified, including the receptor FRIZZLED [66]. In *Arabidopsis* the polarisation of hairs along the root towards the peak of auxin at the root tip have aided the discovery of genes involved in the polarising mechanism. For example, the *Arabidopsis aux1;ein2;gnom<sup>eb</sup>* mutant has hairs oriented towards the shoot and miss-localises RhoGTPases [67]. Other studies using the *Arabidopsis* root have identified

auxin as a key regulatory element for this polarisation of hair orientation [68]. However, as hairs form late in development they are poor markers of ontogeny and they may not be useful markers of axiality in younger stages of development.

The polar localisation of PIN proteins has been used extensively as a marker of tissue axiality in plants [65]. If axiality is determined by a polarity based system dependent on auxin, the polar cellular localisation of PINs within the tissue could provide a direct readout of axiality or even be a contributor of axiality. The use of PIN patterns to explore axiality is particularly useful in very young tissues where epidermal *PIN* expression is high. AtPIN1 has been used as a marker for axial information in published studies which modelled the development of the *Arabidopsis* leaf and petal [21, 22]. It may be that the polar localisation of PINs in internal tissues can also provide a readout of axial information within the organ. However, most studies so far have focussed on epidermal PIN1 patterns as a marker of axiality.

## **1.5 The contribution of different tissues within the organ**

The markers used to explore axiality within developing tissues focus on the axial information within the epidermal layer. There is much debate about whether the axial information in underlying tissues is the same and whether the epidermis is able to drive the development of the lower tissues [69, 70]. PIN1 localisation in developing veins is often oriented in the opposite direction to that in the epidermis. For example, in the developing *Arabidopsis* leaf epidermal PIN1 localises to the distal end of each cell towards the tip of the leaf [49], whereas in the developing midvein the PIN1 localises on the proximal face of the cell towards the base of the leaf [49].

Some research has suggested that the epidermis is able to guide the development of the leaf and whole plant [71]. For example, studies in which brassinosteroid signalling components were specifically expressed only in the epidermis were able to rescue the dwarf phenotype of the *bri1* mutant [71]. Other studies using chimera in *Nicotiana* have indicated that the development of the epidermis is also able to influence the mesophyll below [72]. Similarly altering cell division patterns in the epidermis of transgenic *Arabidopsis* can influence the final shape of the entire organ [73]. It is also suggested that the epidermis mechanically constrains the internal tissues, determining shape and size [74].

The opposite relationship has also been proposed. For example, veins could be the only tissues within a developing organ which respond to axiality cues. The veins could then ‘pull’

the rest of the tissue (including the epidermis) along due to the mechanical connectivity of the cells within the organ tissue. Models using this vein guided development are able to accurately recreate the mature shape of many broad leaves (Przemysław Prusinkiewicz, University of Calgary, seminar talk, unpublished). The underlying axiality theory used in these models is a polarity based axiality system, as veins form in response to auxin.

Other models treat the developing organ as a continuum, with no differentiation between specific tissues in the organ. These models, again using a polarity based axiality system, have been able to recreate the development of a range of organs, such as the *Arabidopsis* leaf 1 [21], the *Arabidopsis* fruit, the fruit of *Capsella rubella* (Tilly Eldridge, JIC, unpublished) and the *Antirrhinum* flower [24].

## 1.6 Computational models at different scales

The development of shape in plant organs is a complex process involving genes, growth rate patterns, axial information and tissue mechanics and can be explored at multiple scales; cellular, tissue and whole organ. The complexity of shape development means that it is not necessarily intuitive, therefore computational modelling provides a useful tool to explore how shape may develop.

There are many computational modelling tools available to explore shape development at different scales. Some focus on cellular dynamics [75], others focus on modulating a starting shape to a series of similar final shapes [23] (organ level) rather than the entire process of morphogenesis, others model morphogenesis from a start shape similar to early primordia, focussing on tissue level dynamics [20].

The Growing Polarised Tissue framework (GPT framework) [20] uses the polarity based axiality hypothesis to orient growth, and dispenses with the need to define cellular parameters (thus reducing the computational power required) by approximating the biological tissue as a continuous connected canvas. Despite its simplifications the GPT-framework has been used successfully as a tool to explore the development of shape in a diverse range of plant organs, from the simple *Arabidopsis thaliana* leaf [21], to the heart shaped *Capsella rubella* fruit (Tilly Eldridge, JIC, unpublished), to the complex *Antirrhinum* flower [24]. These models have provided extensive predictions about shape development at both the tissue and cellular level. These predictions are testable through clonal sector analysis, live cell tracking and PIN1 localisation patterns. GPT framework models can also be

used to predict the organ shape of different mutants, i.e. make organ level predictions. For example, the removal of the palate zone in the *Antirrhinum* flower model predicts the effect on the overall morphology in the mature flower, this prediction matches the phenotype of the *cupuliformis* mutant ([76], Alexandra Rebocho, JIC, unpublished). The ability of GPT framework models, which are built focussing on the tissue level dynamics, to make predictions at multiple scales of development makes them a powerful tool to explore shape development. This modelling method is yet to be used to model the development of a monocot tissue.

## 1.7 Exploring dicot and monocot development

Within the angiosperms (flowering plants) there are two broad classifications based upon fundamental morphological differences; dicots and monocots. The dicots produce two cotyledons (embryonic leaves) and leaves generally have reticulate venation and a distinct petiole and lamina. The monocots are a monophyletic group and are characterised by a single cotyledon with leaves that are typically ensheathing at the base with linear venation.

Much of the work exploring the mechanism of morphogenesis has so far focussed on dicot model species, such as *Arabidopsis thaliana* [21, 22] and *Antirrhinum majus* [24]. In particular, work in the last five years has focussed on how dicot leaves with reticulate venation, and broad laminae develop. This research has included work on *Arabidopsis thaliana* which has a simple round leaf shape in leaf 1 [21], with later leaves going on to develop margin serrations, and close relatives such as *Arabidopsis lyrata* which has lobed leaves and *Cardamine hirsuta* which has compound leaves [77]. This work has highlighted the role of differential growth rates across the developing leaf and anisotropic growth in generating the final leaf shape. Work on serration and lobe development has also indicated that cis-regulatory changes in single genes can generate new shapes during evolution [77, 78]. For example, research has indicated that the regulation of the gene *RCO* (*REDUCED COMPLEXITY*), could generate the difference between simple and lobed leaves in the *Arabidopsis* and *Cardamine* lineages [77]. This morphology change is possibly through modulating growth rates locally in the developing leaf margins and taking advantage of the prepattern of axial information (as marked by AtPIN1) present for serration development. This work has intimated the role of axially and growth rate patterns in defining shape and the possible role of single genes in modulating this. Of interest is whether these common factors are also involved in the development of the distinct monocot leaf.

Monocot development has been proposed to be somewhat simpler than that of dicots in some respects, as it is thought to be linear (for example the leaves often have long thin files of cells). However, final leaf shape can be complex and many plants undergo a necessary series of shape transitions during early development, proposing that perhaps changes in growth (either axiality or growth rates or both) could be central to the development and evolution of monocot organ shapes. For example, the grasses (the Poaceae family) have a distinctive leaf structure.

The grass leaf has a complex modular structure (Figure 1.1). It has a basal region (the sheath) which encircles the meristem and all younger leaves in such a way that every leaf has to form within a 'chimney' of older leaves. The middle region is composed of two tissues; the ligule, which is an epidermal outgrowth proposed to have a role in preventing water entering the sheath region, and the auricles, which are two wedges of stiffened tissue with a role in controlling the angle at which the upper, flattened region (the blade) bends away from the main axis of the plant. This specialised structure using both 3D and 2D elements enables the plant to keep the meristem close to the ground, surrounded by protective layers of leaves during vegetative growth, whilst still growing in height to compete with neighbours for light. This specialised growth habit and leaf shape is common to the grasses and may be one of the key traits (an evolutionary innovation) that has led to the huge success of the grass family.

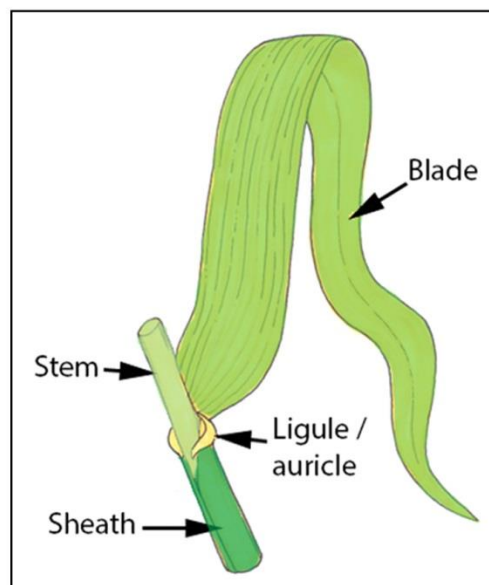


**Figure 1.1 Diagram of a typical grass leaf after the initiation of flowering.**

The leaf has a lower sheath, a middle ligule and auricle, and an upper blade region. Before flowering the stem remains very short, keeping the meristem at the base of the plant, the sheath wraps around the meristem (and any younger leaves) and extends vertically. After

the switch to flowering the stem begins to elongate, extending through the 'chimney' formed by the wrapped sheaths, eventually exposing the mature flower.

Extensive research has highlighted the role of different genes in defining specific regions within the grass leaf and of hormonal signalling in defining leaf shape, many of these pathways act very early in development. For example, like in dicots the first indication of an incipient primordia is the downregulation of class 1 *KNOX* genes [79] and the formation of the primordia and development of the organ is dependent upon auxin and auxin transport [80-82]. These genetic studies have also highlighted differences to dicot leaf developmental programs. For example, studies in rice on the role of *OsWOX3* (WUSCHEL-LIKE-HOMEODOMAIN) and *OsYAB3* (YABBY) in leaf development, found that in contrast to their homologues' polarised expression patterns and roles in defining the abaxial- adaxial axis in *Arabidopsis* [83, 84], they are expressed more uniformly in the developing leaf and do not function to define the abaxial/adaxial axis. Instead *OsWOX3* and *OsYAB3* act to regulate the level of differentiation within the developing leaf [85]. Similarly the mutant phenotypes of maize *roughsheath2* and *Antirrhinum phantastica* differ, despite the genes sharing similar roles, in that they both repress class 1 *KNOX* expression in the developing primordia [86]. This suggests that despite common elements there are differing developmental programs in monocots and dicots, highlighting the importance of studying development in monocots as well as dicots.

Extensive clonal sector analysis in mature maize leaves has explored the role of oriented growth in the development of the leaf, which suggests that growth is strongly anisotropic during grass leaf development [10, 26]. Experiments in the maize mutant *tangled*, have also shown that strict control over the cell division plane is not essential for the formation of the leaf shape [87], despite the linear nature of grass leaf development, suggesting that cell elongation can compensate for disorganised cell division patterns. This indicates the grass leaf shape is predominantly formed through the control of anisotropic growth. However, studies have not explored the relative roles of growth rates and axial information in the development of the mature shape in detail.

Grass leaf development undergoes a series of shape changes (developmental switches in shape) not seen in dicot leaf development. One of the clearest is the formation of the ligule as this involves the definition of a new axis of growth. However, although loss of the ligule does alter leaf shape, in that the angle at which the blade bends from the main axis of the plant is reduced, the overall shape of the leaf, with a cylindrical base and an oval blade, is not altered. There are mutants in grasses which have significantly altered final shapes, for

example the *hoja loca* maize mutant can form tube leaves (Sarah Hake and Aaron Sluis, UC Berkeley, unpublished). Interestingly early stages of maize leaf development undergo a series of distinct shape transitions which are not seen in the *hoja loca* mutant (Sarah Hake and Aaron Sluis, UC Berkeley, unpublished). These developmental switches in shape may arise through modulation of all or select components of growth. Whether these early leaf primordium shape transitions are conserved in all grasses is not known, if they are, perhaps the growth changes which cause the characteristic developmental switches in shape underlie the formation of the grass leaf.

Another mutant in which leaf shape is altered is the *Knotted1 (Kn1)* mutant in maize. In *Kn1* the leaf develops marginal outgrowths (flaps) and swellings in the blade (knots) due to the ectopic expression of the *KN1* transcription factor [88]. The homologous mutant in barley (*Hooded, Hd*) has a dramatic phenotype with the development of an inverted ectopic flower on one of the external floral organs [89, 90]. The significant shape transition in *Hd* suggests that the *KN1* gene family may be able to induce developmental switches in morphology possibly through modulating axial information. Despite the clear prediction of an inversion of the axial information, (possibly through the inversion of polarity system) no study has yet looked at tissue cell polarity in the *Hd* mutant and the consequent morphology changes.

Both of these cases, the precise shape transitions during maize leaf development and the inversion in the *Hd* mutant, provide useful tools to explore how manipulation of growth can induce developmental switches in shape.

The observation that the grasses undergo a series of key shape transitions during early development, vital for the formation of the correct mature leaf shape, and the existence of mutants which predict changes in axial information during the formation of leaves and floral organs, makes them different to existing dicot models. These essential shape changes during early development, particularly make monocots an excellent model system to test how developmental switches in shape arise from the modulation of the different components of growth, and how single genes are able to trigger developmental switches. Through assessing this in monocot models, this will allow future comparisons between dicot and monocot developmental programs and how they were modified to generate such distinct morphologies during evolution.

## 1.8 This work

This work aimed to explore how developmental switches in shape arise from changes to growth and how single genes can modulate growth. The project particularly focused on the modulation of the different components of anisotropic growth; axiality and growth rates. Overall I tested three hypothetical scenarios for how growth could be manipulated to generate developmental switches in shape:

1. Axiality alone is altered
4. Growth rates alone are altered
5. Both axiality and growth rates are altered

Employing a multidisciplinary approach, these hypotheses were tested using a wild-type (grass leaf development) and a mutant (the *Hooded* mutant in barley) developmental switch in shape. The *Hooded* barley mutant was also used to test how a single gene (*BKn3*) was able to induce a developmental switch in shape. To do this I made several assumptions, firstly that axiality is provided by a polarity based axiality system, second that PINs are markers of the orientation of the axis, and third that the tissue can be treated as a continuum. It was hoped that using this approach, how growth could be modulated to generate developmental switches in shape could be identified and therefore, mechanisms behind evolutionary innovative morphologies could be inferred.

Through this project I also aimed to develop a set of tools for the study of grass development. These tools were generated through 3D imaging timecourses in maize and barley, as well as development of protocols for RNA *in situ* hybridisation and protein immunolocalisation in barley tissues. In addition to this a set of transgenic barley plants for the study of grass development were generated.

## 2 Grass Leaf Development

Developmental switches in shape, which occur during organ development, influence the final shape of the organ and may underlie key evolutionary changes in leaf morphology. These developmental switches in shape are triggered by changes in growth. Growth can be modulated through altering growth rates or axiality alone or a combination of both. How growth has been modulated to generate key leaf morphologies during evolution is a key question in plant developmental biology.

### 2.1 Leaf development in the grasses

Members of the Poaceae (the grasses) uniquely combine both 3D and 2D shape in their leaves. The Grasses are the 5<sup>th</sup> largest plant family and account for more than 20% of the earth's vegetation cover [91, 92], occupying nearly every biome on the planet. This success is in part due to their specialised leaf structure. (A typical grass plant structure is shown in Figure 2.1.A, which illustrates the long thin grass leaves which are initiated at 180° to each other.) The grass leaf is modular in structure (shown in the colour coded image of maize leaf 2 in Figure 2.1.B), with a lower wrapped region which forms a 3D tube (the sheath, Figure 2.1.B, pink), a middle hinge region (the ligule and auricle, Figure 2.1.B, blue) which controls the angle at which the upper flat (2D) region (the blade, Figure 2.1.B, purple) bends away from the main axis of the plant. The base of the leaf is separated from the next leaf by the internode, below the meristem.

The modular shape of the grass leaf enables the plant to grow in height to compete with neighbours for light, whilst not extending the stem and exposing the SAM which is responsible for regrowth. This growth habit is possible because the 3D sheath of the leaf acts as a pseudostem vertically supporting the upper blade allowing it to grow in height. During vegetative growth the true stem does not elongate significantly and the SAM remains close to the ground surrounded by layers of wrapped leaves (the approximate position of the vegetative SAM is indicated by the white arrow in Figure 2.1.A). This is particularly evident when dissecting a vegetative grass plant as successive layers of leaves need to be removed to access the meristem. A dissection of the maize seedling in Figure 2.1.A is shown in Figure 2.1.C, illustrating the successive layers of leaves. Optical projection tomography (OPT) imaging of the base of a young maize seedling (like the one in Figure 2.1.A in the position indicated by the yellow box) shows the tight wrapping of the successive leaf layers, each

coloured differently in Figure 2.1.D. The wrapping of older leaves around younger leaves and the SAM protects them to an extent from herbivore grazing and from sudden temperature changes like frosts, enabling the plant to rapidly regrow after damage. This growth habit, made possible by the specialised leaf structure, is one of the innovative features which has contributed to the evolutionary success of the grasses.



**Figure 2.1 An example of a grass: maize seedling morphology**

*A:* B73 maize seedling, the white arrow indicates the position of the SAM during vegetative growth. *B:* Leaf 2 colour-coded to show the modular nature of the maize leaf with the sheath

(pink), ligule and auricle (blue) and the blade (purple). C: the outer leaves dissected from the maize seedling in A, *i*: leaf 1, *ii*: leaf 2, *iii*: leaf 3, *iv*: leaf 4, *v*: leaf 5 still wrapped around younger leaves and the meristem. D: Optical Projection Tomography (OPT) image of a longitudinal slice through the base of a maize seedling, roughly in the position indicated by the yellow box in A (some outer leaves have been removed). Showing the tight wrapping of the older leaves, protecting the meristem. Successive leaf layers surrounding the meristem (pink) are coloured from light green to dark green. Scale bars in A-C are 1cm, the scale bar in D is 100 $\mu$ m.

The grass *Zea mays* (maize) has been used extensively as a grass model system and much of the understanding of grass leaf development so far has come from analyses of clonal sector patterns, histology sections, genetics, SEM imaging and more recently CT imaging [93].

Developmental stages have been characterised using the plastochron which is the period of time it takes for the next leaf to initiate. Broadly the P number corresponds to the number of younger leaves between the leaf and the apical meristem, i.e. P0 is the youngest, P1 has one leaf between it and the meristem, P2 has two leaves between it and the apical meristem, etc. These stages have then been used to define broad phases of leaf development during which different events occur: founder recruitment, primordial growth and post-primordial growth [94]. Each of these different phases of development exhibit key developmental switches in shape which combine to influence the final form of the grass leaf.

During founder recruitment [94] the leaf primordium initiates as the midvein region, in the periphery of the meristem, 180° from the last initiated midvein, and spreads around the meristem to recruit a ring of founder cells from the two outer cell layers of the meristem [95]. This is the P0 primordium, before outgrowth has occurred.

During primordial growth (P1 to P4), the founder cells grow out to form a ring (P1) that is approximately 42 cells in circumference and three cells high [96], totalling around 200 cells [10]. The cells in the base of the ring primordium are called the disc of insertion. The midvein region then grows out and the primordium folds over the meristem forming a hood (P2). The margins then grow as the axis widens and the lamina edges eventually overlap at around P4. This wrapping of the margins can be up to 1.5 times around the main axis [95]. At this stage the primordium predominantly consists of blade tissue, with the as yet mostly unelaborated sheath initials below [93].

During post-primordial development (P4, onwards) cells start to differentiate. For example at the end of P3 and early P4 the sheath margins grow out of the disc of insertion as two overlapping leaf margins [93]. The ligule is also defined at the end of primordial growth in P3 (preligule band) [97] and begins to develop at P4-P5 stage with periclinal divisions in the epidermal cell layer at the boundary between the sheath and blade regions [95, 97]. Before ligule initiation, cells are undifferentiated and divide to form files along the length of the primordium. After ligule initiation, more transverse divisions in the blade and cell differentiation occur, and the sheath elongates rapidly [95, 97]. Cell divisions cease basipetally (from the tip to the base of the leaf) [95, 96]. The internodes (stem) do not elongate significantly until the sheath has completed most of its growth and the transition to flowering has been initiated.

These studies allow a rough fate map of a maize primordium to be built as shown in Figure 2.2. The initial disc of insertion gives rise to all of the modules of the maize leaf: the internode (yellow), the sheath (pink), the ligule/auricle (which will form in the boundary between the sheath and blade, blue) and the blade (purple). The first region to grow during the primordial stages of leaf development is the blade; the ligule, sheath, and internode develop later. The blade is formed by the major part of the primordium [10]. The blade margin originates as the distal rim of the ring primordium. I will refer to the region opposite the midvein as the 'keyhole' region from now on (marked with a blue arrowhead, the position of the midvein is marked with a pink arrowhead, in Figure 2.2). The sheath originates from an overlapping ring of founder cells below the blade region (pink region in Figure 2.2) [93, 95].

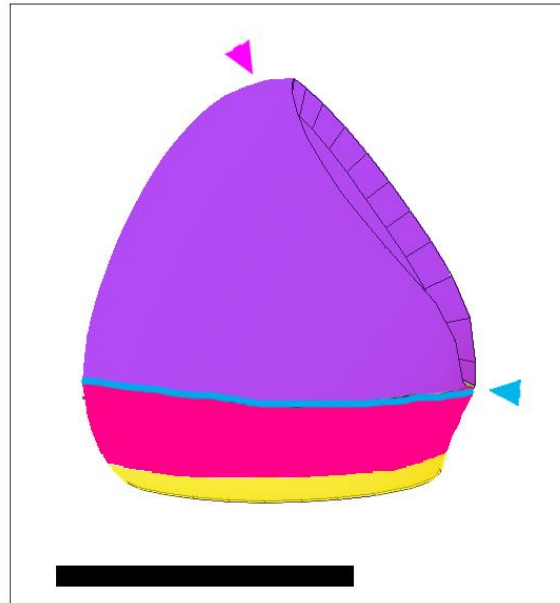


**Figure 2.2 Approximate fate map of the hood stage of maize leaf primordium development.** Approximately based on Scanlon et al 1997 [10]. The diagram indicates the location of tissue which will become the blade (purple), the ligule/auricle (blue), the sheath (pink) and the internode (yellow) but is still undifferentiated in the hood stage (P2) primordium. The position of the midvein (pink) and keyhole (blue) regions are indicated by the arrowheads. Scale bar is 100 $\mu$ m.

Generally grass leaf development is described as linear with long files of cells forming the leaf tissue and anisotropic clonal sectors extending along the leaf proximodistally [10, 96, 98]. This suggests that grass leaf development involves strong anisotropic growth.

Extensive genetic work in both maize and rice has also identified many genes involved in leaf development, and in specifying specific regions of the leaf. For example, many genes involved in abaxial/adaxial patterning like maize *MILKWEEDPOD* (a *KANADI* related gene) [99], maize *ROLLED LEAF 1* (a HDZIP III specific to adaxial patterning, [100]) and rice *SHALLOT LIKE 1* (involved in abaxial patterning,[101]) have been identified. As well as genes needed to specify different leaf domains, like maize *NARROWSHEATH 1 AND 2* (*WOX* transcription factors involved in lateral cell recruitment [102]), maize *LEAFBLADELESS1* [103] (involved in adaxial identity) and the *LIGULELESS* genes in rice and maize [104-107] (required for the correct formation of the ligule and auricle). Some of the genes identified have similar roles to their homologues in *Arabidopsis*, allowing their roles to be inferred, however many act differently, and some are not found in *Arabidopsis*. Auxin, which is involved in *Arabidopsis* leaf development, has also been shown to have a role in grass leaf development. Treatment

of maize primordia with auxin inhibitors such as NPA, which also inhibit leaf initiation [10, 108], disrupts leaf development, causing the loss of the sheath margin. So far not all of the genetic components involved in grass leaf development have been found, and it is not fully understood how all of the genetic and hormonal elements interlink to generate the final grass leaf.

Although some common elements are shared with leaf development in the dicot model system *Arabidopsis*, such as auxin, the mechanism responsible for the grass leaf shape cannot be fully inferred from comparative studies as the grass leaf structure is very distinct. The characteristic grass leaf shape is probably due to a series of key developmental switches in shape, particularly during the primordial stages of development. These developmental switches in shape may be crucial to establishing the overall shape of the grass leaf and are likely to be triggered by changes in growth. Changes in growth could be achieved through modulating axiality or growth rates alone or both combined. Which of these mechanisms of growth changes are central to the development of the evolutionarily important grass leaf has not been explored.

## **2.2 Aim of this project**

The aim of this project was to use a multidisciplinary approach to explore how changes in growth act during primordial stages of grass leaf development to trigger key developmental switches in shape. By doing this I aimed to gain insight into how the grass leaf may have evolved through modulation of growth to generate new organ shapes.

This work was done in collaboration with Dr Devin O'Connor (The Sainsbury Laboratory, The University of Cambridge), Professor Sarah Hake (UC Berkeley, California) and Dr Alexandra Rebocho (John Innes Centre, Norwich). For clarity, the work I did will be referred to in the first person.

## **2.3 Describing a developmental switch in shape during primordial grass leaf development**

To begin to explore how developmental switches in shape are achieved through modulation of growth in grass leaf development, I first needed to define a developmental switch in shape

which was involved in the formation of the grass leaf. As the broad shape of an organ is often determined early in development I used 3D imaging techniques to map the earliest (primordial) stages of development, during which the literature had described a series of shape transitions from a ring to a hood to a cone. I used Optical Projection Tomography (OPT) [109, 110] to image early stages of maize B73 juvenile leaf 6 development, enabling me to calculate approximate dimension changes between different morphological transitions. 3D imaging showed a clear progression of shape transitions in early maize leaf development from a ring, to a hood, to a cone shape (Figure 2.3) which had previously been seen in published SEM images.

The progression in developmental shape changes is illustrated in Figure 2.3. The ring (P1) primordium (Figure 2.3.A) is several cells high (Figure 2.3.A.i) and is thinner in leaf thickness (Figure 2.3.A.ii). The ring primordium forms a complete collar around the meristem which is visible in transverse views above the sample and in cross-sections through the primordium and meristem (Figure 2.3.A.iii and iv respectively). The ring primordium then transitions to form a hood shaped primordium (Figure 2.3.B).

The hood (P2) primordium arches over the meristem at the midvein (Figure 2.3.B.i, pink arrowhead indicates the midvein position) and has very restricted growth in the keyhole region opposite, both in height and in width (blue arrowhead, Figure 2.3.B.i side view and ii cross-section). During this shape transition from a ring to a hood, the primordium maintains the collar around the meristem (Figure 2.3.B.iii view from above and iv transverse cross-section).

The P3 primordium then transitions from the hood shape to a more cone-like shape (Figure 2.3.C.i side view and ii cross-section) which still maintains the ring around the meristem at the base (Figure 2.3.C.iii view from above and iv transverse cross-section through the base). Eventually the lateral margins of the leaf wrap around the meristem and younger leaves (Figure 2.3.D.i side view, ii cross-section, and iv transverse cross-section through the base showing the wrapping leaf margins) as the leaf continues to elongate (Figure 2.3.D.i and ii), forming a tightly wrapped cone (Figure 2.3.D, P4 stage).

Without this characteristic series of developmental switches in shape, from a ring to a hood to a cone, during primordial development the shape of the mature maize leaf is abnormal. For example the maize *hoja loca* mutant can form ring like primordia which fail to progress through these shape transitions and develop into tube leaves (Aaron Sluis and Sarah Hake,

UC Berkeley, unpublished). This suggests that the developmental switches in shape during primordial stages of development may be crucial for correct grass leaf development.

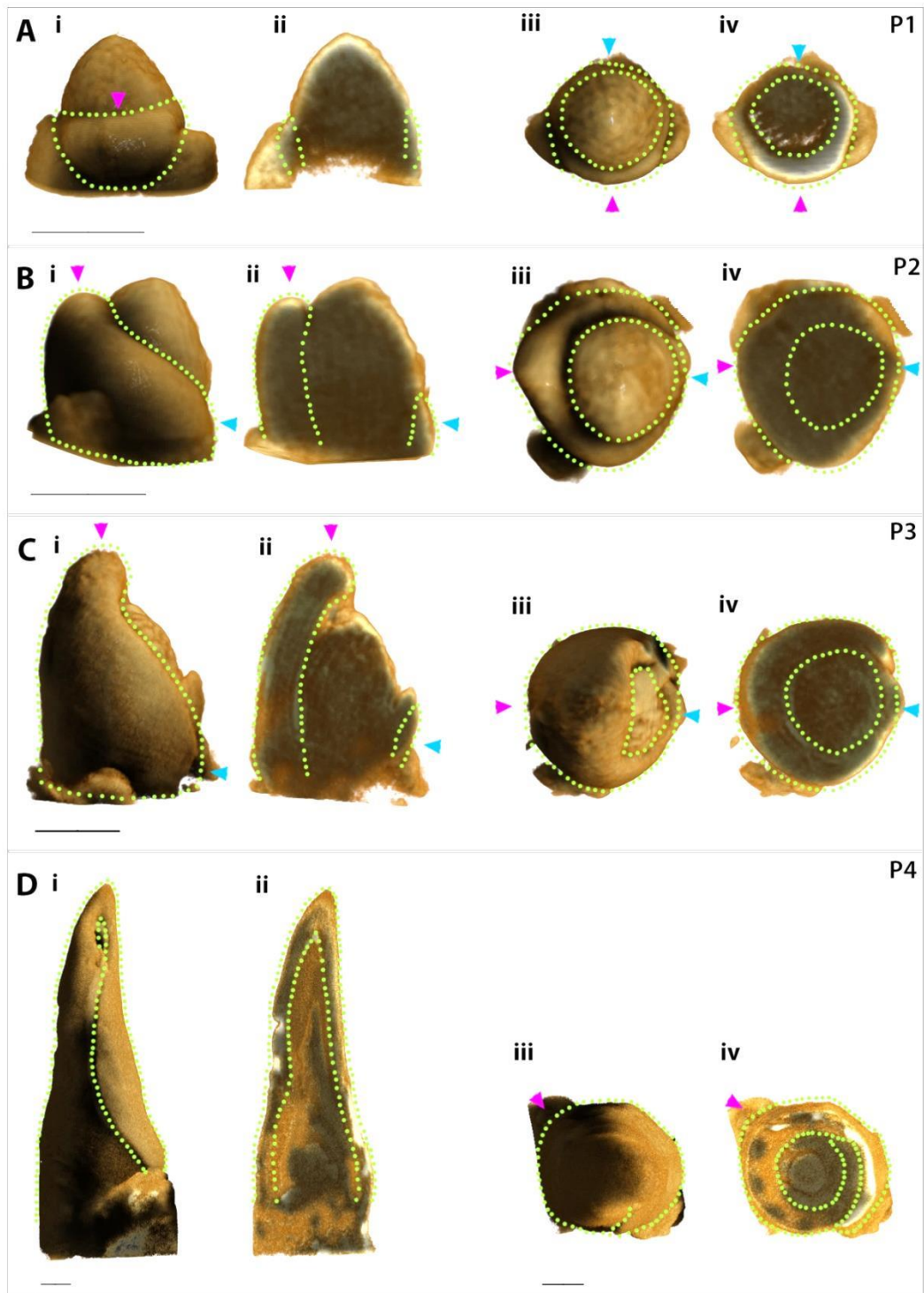


Figure 2.3 3D OPT imaging of the early stages of leaf development in B73 maize juvenile leaf 6

*A i-iv*: P1 or ring stage. *B i-iv*: P2 or hood stage. *C i-iv*: P3 or cone stage. *D i-iv*: P4 or wrapped cone stage. *i and iii*: side and top views respectively. *ii and iv*: sections through the volume to show the internal structures from the side (lateral) and the top (transverse) respectively. OPT images are 3D rendered in Drishtii software with false colouring. Green dotted lines highlight the primordium shape, pink arrowheads indicate the midvein, blue arrowheads indicate the keyhole region. All scale bars are 100µm.

I staged the OPT images by plastochron based on published studies (P1: ring stage, P2: hood stage, P3: small cone stage, P4: wrapped cone stage) and measured the different height and widths of the primordium at each stage to gain an idea of the rate of growth for different aspects of primordial leaf development. I measured leaf length (from the base of the leaf to the midvein tip, Figure 2.4.A), leaf width or diameter (the base of the primordium from the midvein to the keyhole region, Figure 2.4.B) and leaf thickness at the midvein (measured using transverse cross-sections, Figure 2.4.C). All of these dimensions increased exponentially during the primordial stages of development.

Using these measurements I generated growth curves of the natural logarithm of the dimensions against plastochron number (Figure 2.4). I then roughly approximated growth rates for each dimension, using the equations of the lines of best fit indicated in each graph in Figure 2.4. (I first converted each line equation,  $\ln Y = mX + c$ , to leaf length by raising the equation to the exponential,  $Y = e^{mX+c}$ , then calculated the derivation of this exponential equation,  $me^{mX+c}$ . To calculate the rate per day, I substituted X for 1, then divided this number by 24 to get the increase in size in micrometres per hour). If I assume that a plastochron equals 24 hours, leaf length increases at approximately 4.65µm per hour (Figure 2.4.A), leaf width increases by 1.88µm per hour (Figure 2.4.B) and leaf thickness at the midvein increases by 0.64µm per hour (Figure 2.4.C) during the 96 hours of development covering P1-P4. This means that the primordia grow more than twice the rate in length (midvein tip to base) than base width (midvein to keyhole) during the early stages of primordial growth. The increase in leaf width (from midvein to lateral edge increases beyond this rate (approximately 72 hours) is enhanced when the blade margins begin to wrap after P3.

Using the measurement data I was able to develop a set of standard measurements to describe a maize leaf during the earliest stages of development (P1-P4) (Table 2.1). These had large ranges because it is not possible to synchronise leaf development and growth is exponential.

Plastochron Stage	Mean Leaf Length (µm)	Leaf Length Range (µm)	Mean Leaf Width/ Diameter (µm)	Leaf Width/ Diameter Range (µm)	Mean Leaf Thickness (µm)	Leaf Thickness Range (µm)
P1 (ring)	48.2	35.6-60.9	111.5	86.4-136.6	18.4	7.6-29.3
P2 (hood)	136.6	109.0-162.2	144.6	134.1-155.1	44.3	41.4-47.2
P3 (small cone)	266.8	232.0-301.7	185.6	163.9-207.2	52.2	47.4-57.0
P4 (wrapped cone)	836.1	545.9-1126.3	353.8	304.3-403.2	75.5	45.6-105.2

**Table 2.1 Measurements describing a standard maize B73 juvenile leaf 6.**

The values are calculated from measurements of three independent samples for all except the P4 sample which had two samples. The range is calculated as the mean +/- 1.5 times the standard deviation. All values are in µm.

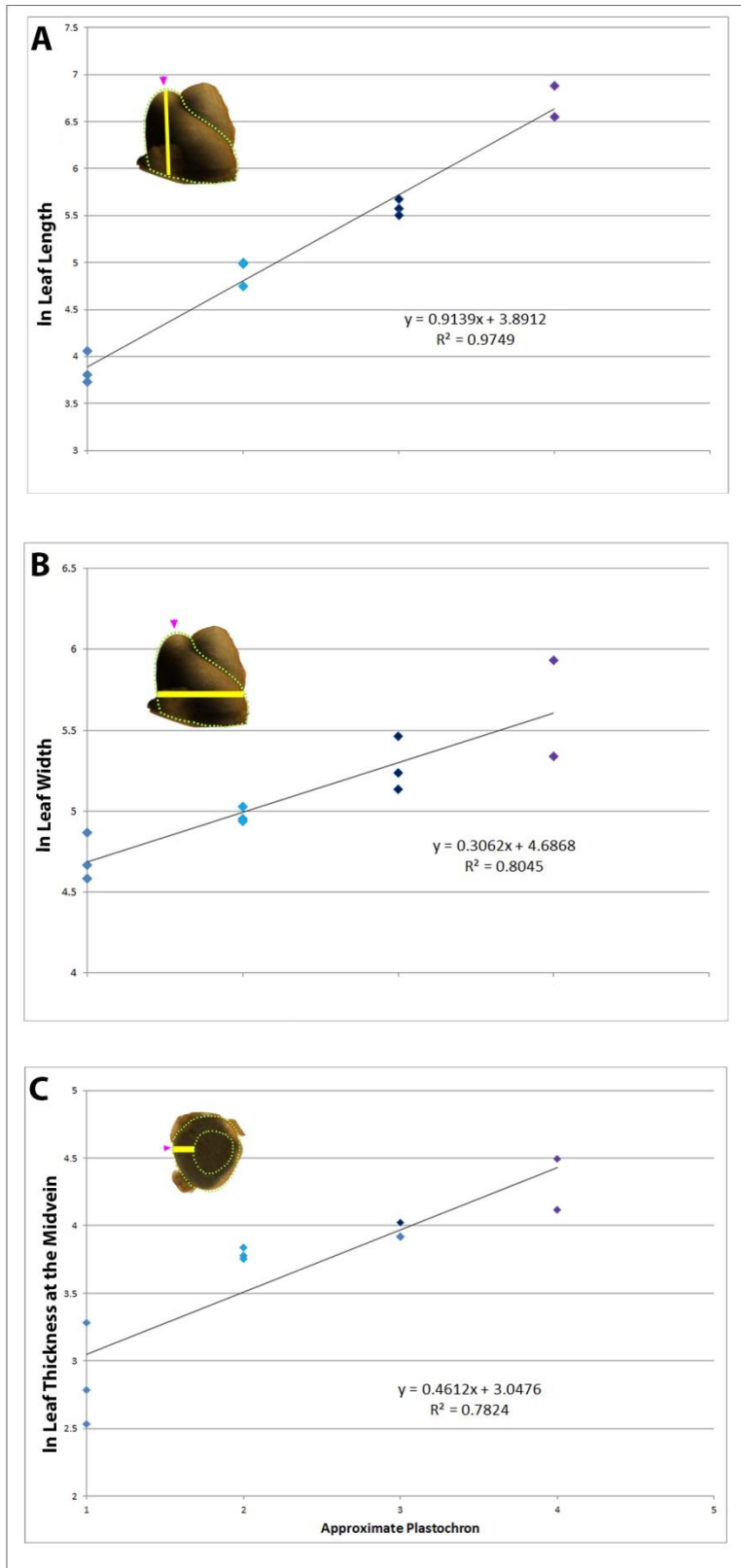


**Figure 2.4 Dimensions of B73 maize juvenile leaf 6 at P1, P2, P3 and P4**  
 All Y values are natural logarithms (ln) of the measurements, and the X axis shows the approximate plastochron (P1, P2, P3, P4.). A: In of the leaf length (from the base to the

midvein tip.) *B*: In leaf width. *C*: In leaf thickness at the midvein. Each graph shows a diagram of how the measurement was taken (yellow line), the primordium outline (green dots) and the position of the midvein (pink arrowhead). Each graph also displays the equation for the line of best fit and the  $R^2$  value which indicates how well the line fits.

Maize is a member of the subfamily *Panicoideae* in the *Poaceae* Family (Figure 2.5, the position of *Zea mays*, maize, is indicated) which diverged from other monocot families around 90-100mya [111]. I asked whether the important developmental switches in shape observed in primordial maize leaf development were common to all members of the grass family and therefore possibly important for the evolution of the grass leaf.

To address this question I used OPT imaging to analyse the early stages of leaf development in examples of different crown group grass species. (The crown group contains approximately 99% of the species in the *Poaceae* family, the subfamilies which make up the crown group are indicated by the grey box in Figure 2.5). I imaged *Brachypodium distachyon* (a member of the *Pooideae* subfamily which also includes barley, wheat and oat, the position of which is indicated in Figure 2.5), which diverged from maize around 50mya [112], and early leaves of the bamboo *Fargesia rufa* (a member of the *Bambusoideae* subfamily, position indicated on Figure 2.5) which diverged from maize around 50mya and diverged from the *Pooideae* subfamily around 40mya [112, 113]. Both *Brachypodium* and *Fargesia* have mature leaf structures which show the characteristic modular grass leaf structure, with the wrapped sheath, the ligule/auricle hinge region and the outward bending blade (Figure 2.6.D and G show macro OPT images of seedlings from *Fargesia* and *Brachypodium*.). The developing leaf primordium in both *Brachypodium* and *Fargesia* undergo the same shape transitions as seen in maize. Developing from a ring, to a hood shape (Figure 2.6.A and E) which arches over the meristem at the midvein region, (indicated by the pink arrowhead in Figure 2.6.A and E), has restricted growth in the keyhole region (blue arrowhead in Figure 2.6.A and E), and completely encircles the meristem (as seen in transverse cross-sections through the base Figure 2.6.A.iv and Figure 2.6.E.iv). Then developing from a hood, to a more cone like shaped primordium (Figure 2.6.B and F), which is taller than it is wide (Figure 2.6.B.i and ii and Figure 2.6.C.ii and ii and Figure 2.6.F.i and ii) and has leaf margins that wrap around the meristem (Figure 2.6.B.iv, and Figure 2.6.F.iv). The leaf margins wrap more as development progresses (Figure 2.6.C.iv). Like maize the base of the leaf primordium completely encircles the meristem throughout development in both *Brachypodium* and *Fargesia*, which is particularly clear in transverse cross-section images (Figure 2.6.A-F iv).

As the last common ancestor of maize, *Fargesia* and *Brachypodium* was around 50mya [112], this OPT imaging suggests that it is likely that all *Poaceae* crown group species exhibit the same developmental switches in shape from the ring to the hood to the cone shape during primordial leaf development. This indicates that the developmental switches in shape during primordial development, identified as possibly essential for final leaf shape in maize, may be common to all crown group, if not all, *Poaceae* species. Therefore the changes in growth which underlie these developmental switches in shape could be central to the evolution of the grass leaf.

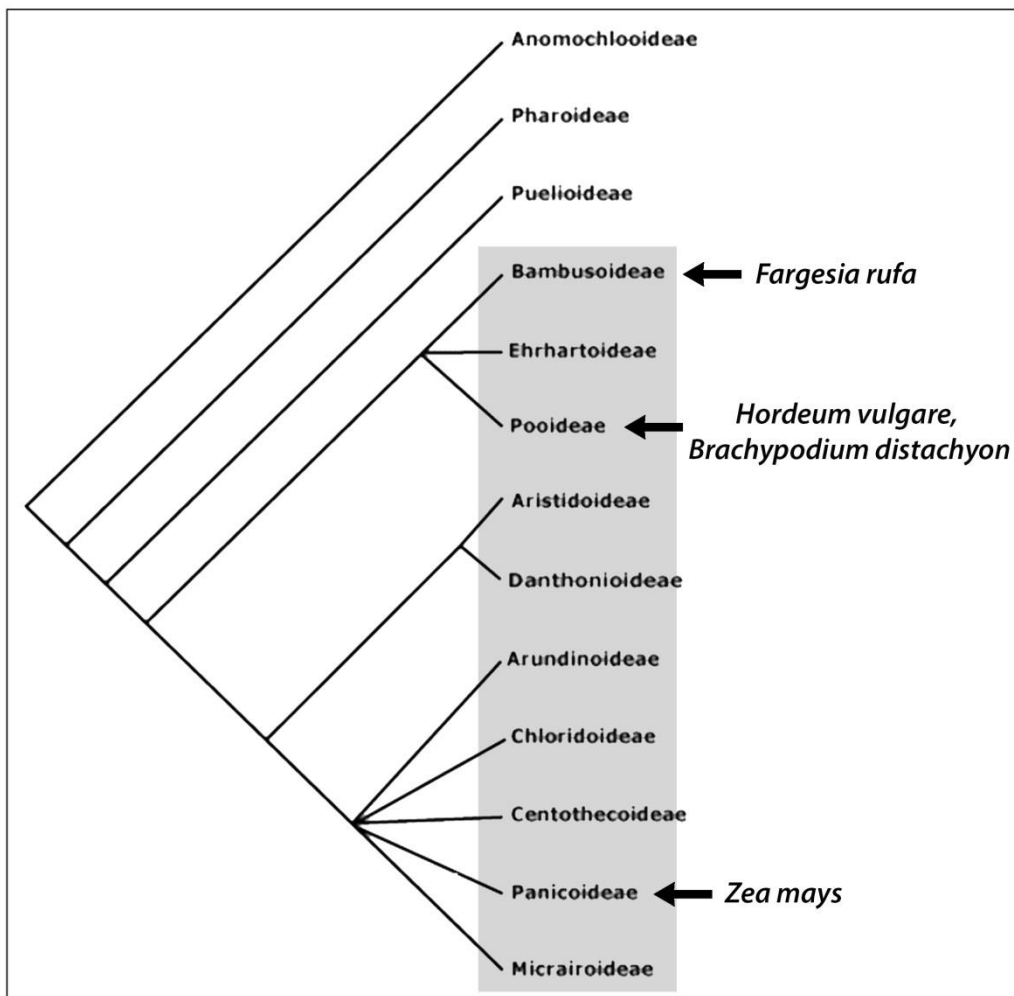


Figure 2.5 The *Poaceae* family tree adapted from the angiosperm phylogeny website <http://www.mobot.org/MOBOT/research/APweb/>. Arrows indicate the subfamily that *Zea mays* (maize), *Brachypodium distachyon*, *Hordeum vulgare* (barley) and *Fargesia rufa* belong to. Grey box indicates the *Poaceae* crown group.

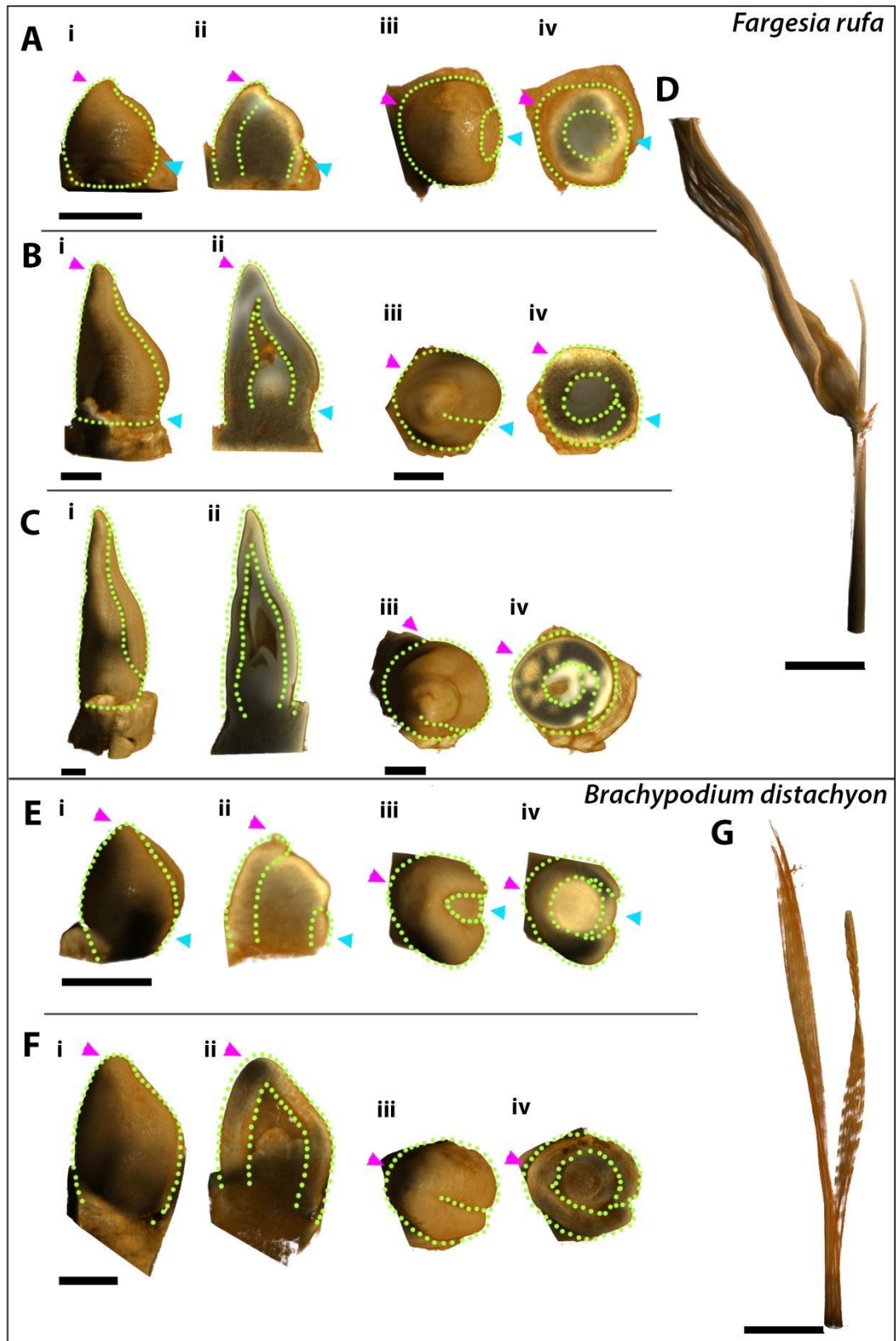


Figure 2.6 OPT images of *Brachypodium distachyon* and *Fargesia rufa*.

A-D: *Fargesia rufa* (Bamboo). A-C: primordium stages. D: mature leaf. E-G: *Brachypodium distachyon*. E-F: primordium stages. G: mature Leaf. i-ii: side image. iii-iv: top views. ii and iv: clipped images through the volume, showing internal structures. Primordial images taken

using the prototype OPT, mature leaves imaged using the Macro OPT. Volumes rendered using Drishti software. Pink arrowheads indicate the position of the meristem, blue arrowheads indicate the keyhole region. Green dotted lines highlight the shape of the primordium. Scale bars for A-C and E-F are 100µm. Scale bars for D and G are 1cm.

The grasses diverged from other monocot families around 90-100mya, which diverged from other angiosperm clades around 140-150mya [113] (Figure 2.7). Despite having diverse leaf shapes, the monocots are described as commonly having ensheathing leaf bases and parallel venation. Several monocot species also have leaf structures similar to the grass leaf. Little work has been done to characterise the primordium morphology of monocot species. Existing studies have primarily used anatomical sketches and some SEM imaging [114] which show a diverse range of primordium shapes for different monocot species. All of the published sketches and SEM images indicated that monocot primordium typically have an ensheathing base, and some seem to form hood or cone like structures similar to those observed in grass species. However these images are 2D and it is not possible to assess stage or scale, and true 3D shape is not easy to evaluate.

I therefore carried out OPT imaging of two representative monocot species outside the *Poales* (the order in which the grasses are found); *Alium ameloprasum* (leek) in the *Alliaceae* family, the *Asparagales* order (Figure 2.8.A and B) and *Acorus calamus* from the *Acoraceae* family, the *Acorales* order (Figure 2.8.C and D); at different ages, to determine whether the shape transitions identified in the grasses were common to all monocots.



Mature leek leaves appear similar in structure to grass leaves however they have a fused ensheathing base and the hinge region is not as prominent. This means that the upper region of the leaf (which corresponds to the grass leaf blade) does not bend significantly away from the main axis of the plant. OPT imaging shows that, like the grasses, the leek leaf primordium completely encircles the meristem (as shown in Figure 2.8. A.iv and B.iv transverse sections through the primordium), this is consistent with the mature leaf forming an ensheathing base. At later stages of leek leaf development (Figure 2.8.B), the leek primordium appears to form a hood or cone-like structure which may be due to the midvein region arching over (pink arrowhead in Figure 2.8.B.i indicates the possible midvein region) and restricted growth in the keyhole region (blue arrowhead), although this is a much later stage than the hood forms in the grass primordium. The earliest stage of leek leaf development captured (Figure 2.8.A) does not resemble those of grasses, instead of the ring or hood shaped primordium with a smooth margin, the leek primordium has a lobed shape (Figure 2.8.A.i). This lobed shape is due to both the midvein (Figure 2.8.A.i pink arrowhead) and the opposite keyhole region (Figure 2.8.A blue arrowhead) growing out, which contrasts with grass leaf development in which the keyhole region is severely restricted in growth. From the top transverse view (Figure 2.8.A.iii) the leek leaf primordium margin appears to have 3 lobes, which differs from the smooth margin in the grass leaf primordium. The transverse cross-section of the later stage leek primordium, in which the midvein appears to have grown up to arch over the meristem (Figure 2.8.B), is also elliptical in shape, not circular like the grass primordium. This suggests that despite some similarities between leek and grasses the leek leaf primordium does not undergo the same series of primordial developmental switches in shape as the grasses.

If the primordial shape transitions, from a ring to a hood to a cone, were important in the evolution of an ensheathing leaf base and therefore the evolution of the monocots as a whole, it would be expected that they would be found in a basal monocot family. The *Acorales* is the most basal family of monocots (Figure 2.7, blue). Therefore I imaged some early primordia samples of *Acorus calamus* using OPT (samples collected by Devin O'Connor, Figure 2.8.C-D). These images suggest that the early stages of primordium development in *Acorus* are more like that of dicots as the base does not fully fuse to encircle the meristem (Figure 2.8.C.iv for a transverse section through the primordium) and the leaf primordium is more peg like (Figure 2.8.C and D). However, it has been suggested that the shape of the *Acorus* leaf is very derived [114] and therefore it may not be the best model to use as an approximation of the last common ancestor of the monocots.

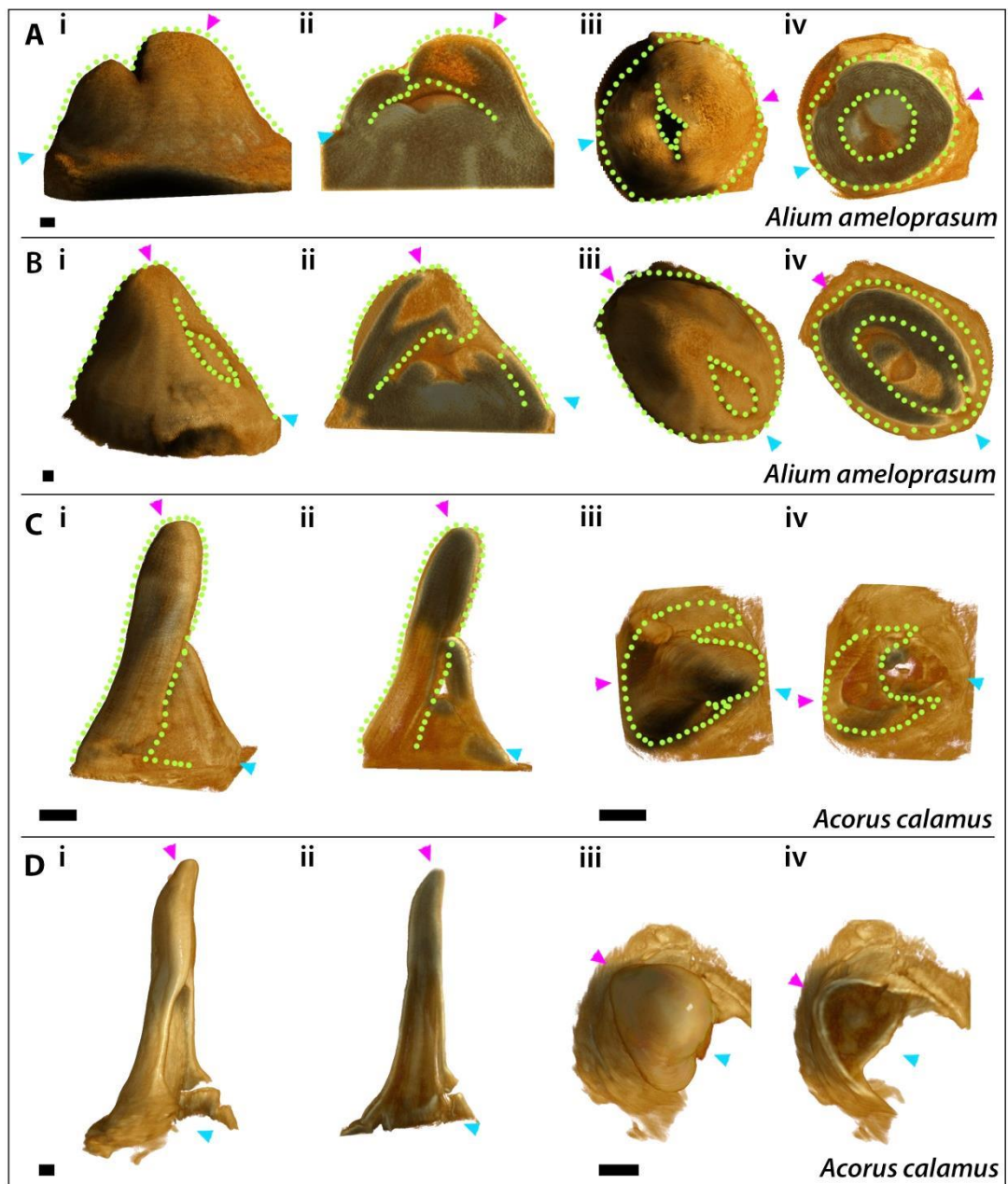


Figure 2.8 OPT imaging of leaf primordium in the monocot species *Alium ameloprasum* (leek) and *Acorus calamus*.

A-B: Leek (*Alium ameloprasum*) primordia and meristems, A is younger than B. C-D: *Acorus*, attached young leaf primordia and meristem (C), young leaf (D). i-ii: lateral views. iii-iv: top views. ii and iv: section images through the volume showing the internal structures. Pink arrowheads indicate the position of the midvein, blue indicate the keyhole region, the green dotted lines highlight the shape of the primordium. Scale bars are 100µm.

Nevertheless, this OPT imaging suggests that the developmental switches in shape from a ring to a hood to a cone may be unique to the grasses. This could indicate that these shape transitions are a central component to the evolution of the characteristic grass leaf which has contributed to their global success as a family. Therefore understanding the mechanism behind these developmental switches in shape could illustrate some of the evolutionary steps required in the formation of the grass leaf. As switches in shape are likely to arise through changes in growth, how growth rates and axiality are modulated during grass leaf development to trigger these developmental switches in shape are of particular interest.

## **2.4 The formation of the hood from a ring primordium could be accounted for by enhanced anisotropic growth towards the midvein**

To explore how changes in growth could trigger the primordial developmental switches in shape, I took a computational modelling approach. Using the Matlab based Growing Polarised Tissue framework (GPT-framework, [20-22, 24]), which models connected tissue growth based on the distribution of growth factors and growth orientations, I aimed to develop a model that could account for the observed morphological changes in early grass leaf development. The aim of this modelling was not to produce a detailed model which accounted for all aspects of maize leaf development, but instead to generate a broad model which captured the key shape transitions during primordial maize leaf development, which had been characterised using OPT; ring to hood to cone; during which blade tissue is primarily elaborated. This modelling was undertaken using the assumption that axial information within a developing plant tissue is provided by a polarity based axiality system, therefore axial information can be referred to as polarity.

The modelling framework used contains several simplifications; the first is that a plant tissue can be approximated as a connected canvas with elastic properties. This is assumed as cells within a plant tissue are prevented from moving relative to each other by the cell wall matrix, and cell walls are often modelled as elastic springs [75, 115-117]. This reduces computational complexity as it does not require cellular dynamics to be approximated and calculated. The modelling framework also simplifies the factors which influence growth, by allowing the use of single factors rather than extensive complex networks which are more likely in the

biological tissues. Again this reduces computational complexity and allows a model to be built without knowing all of the genetic components involved.

In the GPT-framework a canvas is formed from mechanically connected regions across which growth rates can be specified by the distribution of factors (specified growth rate is the rate at which that region of tissue would grow in isolation). The mechanical connection between regions in the canvas enables the deformation, created by specifying different local rates of growth, to be calculated. The resultant growth patterns (the rate at which the region of tissue grows when constrained by the connectivity within the whole tissue) and shape deformations can contain features which were not initially specified because they arise as a consequence of the constraints imposed by tissue connectedness. Each model has at least two components; an initial canvas shape with distributed factors and a growth regulatory network (KRN, a network which specifies the effect of factors on the canvas' growth rate). In models that have anisotropic growth a third component, a polarity regulatory network (PRN), which provides axial information, is required. I started with a cylindrical canvas to approximate the ring primordium (the shape of which is shown in Figure 2.9.A) and scaled it to approximate B73 maize leaf 6 ring primordium dimensions: 110 $\mu$ m in diameter and 36 $\mu$ m in height.

I first modelled the transition from a ring to a hood shaped primordium (models for this shape transition are outlined in Figure 2.9). Published data and my analysis of maize leaf development suggests that the leaf primordium initially grows preferentially in the midvein region forming a hood over the apical meristem [95]. Therefore, the initial shape transition from the ring to the hood primordium was modelled by specifying enhanced growth rates (K) in the midvein region. For simplicity, growth was initially assumed to be locally isotropic (non-directional). Isotropic growth rates were modulated with two opposing diffusible factors: MID, produced at the midvein (the graded distribution of MID is shown in Figure 2.9.A in blue), and OPP produced at the opposite side (i.e. the keyhole region, the graded distribution of OPP is shown in Figure 2.9.A in yellow). MID promotes, while OPP inhibits, the specified isotropic growth rate (K) (Figure 2.9.B.i, indicates growth rates in the ring primordium, red is high, blue is low, and Figure 2.9.Bii illustrates the KRN). This isotropic growth model led to the midvein region growing out (increase to 665 $\mu$ m which is more than four times the expected size) and curving over the meristem region to an extent (Figure 2.9.C, pink arrowhead indicates the midvein region which grew outwards). However, the circumference of the ring increased rapidly to a size much larger than seen in real

primordium (Figure 2.9.C); I would expect to see a diameter of the hood between 134-155 $\mu\text{m}$ , instead the diameter of the simulation reaches 1176  $\mu\text{m}$ , an increase by a factor of 7.5. This simultaneous increase in height and diameter resulted from high specified growth rates in all orientations due to specifying isotropic growth.

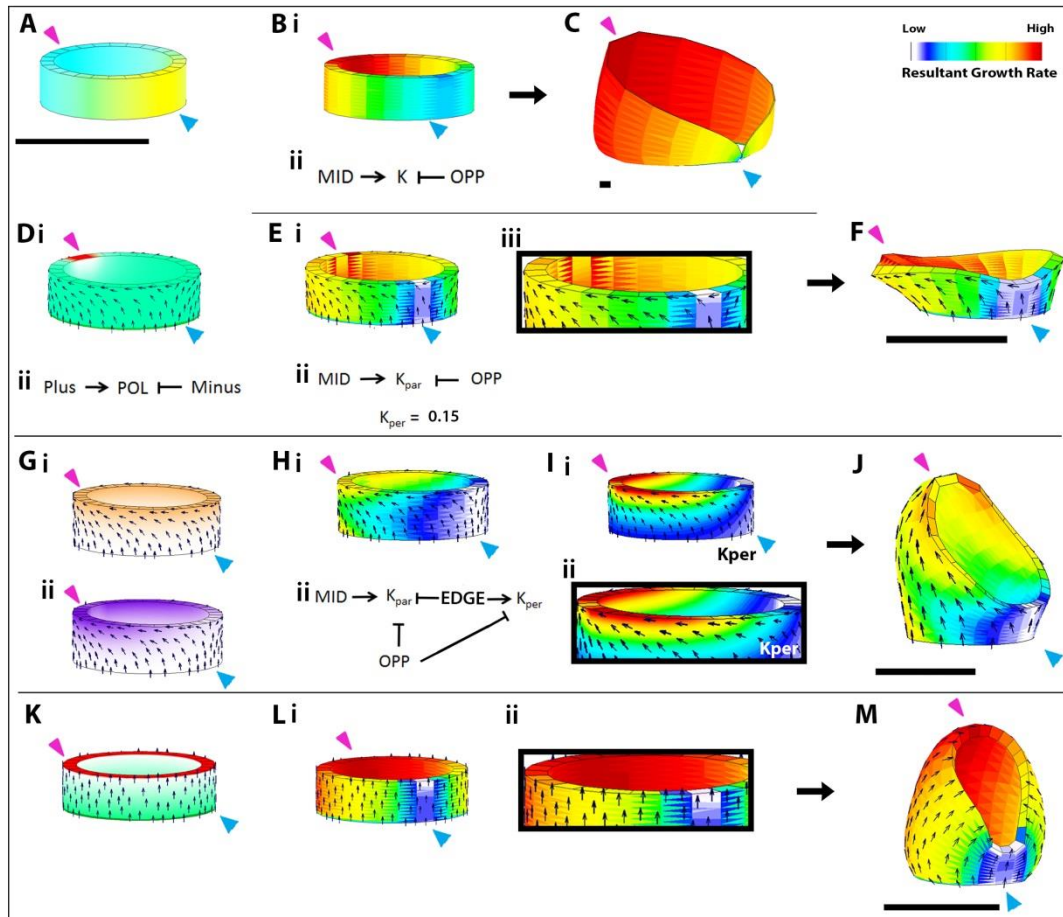


**Figure 2.9 Modelling the transition from a ring to a hood shaped primordium.** A: Initial growth factor pattern of MID (blue) and OPP (yellow) established at the start of the model, which is constant throughout all models. B – C: Isotropic growth model. B: *i*, the distribution of resultant growth rate (K) and the growth regulatory network which defines how the factors influence growth rate (*ii*, KRN). C: the outcome of the simulation. D-F: The biased anisotropic model. D: the polarity regulatory network (PRN) (*i*) set up at the start of the simulation and the distribution of minus (red) and plus (green) organisers and POLARISER (POL, turquoise green) (*ii*) which defines the axis from which the orientation of  $K_{\text{per}}$  and  $K_{\text{par}}$  are determined. E: the resultant growth map (*i*) and the KRN (*ii*), a zoomed-in image of the axial information at the margin (*iii*). F: the outcome of the simulation. G-J: Distal tip model, biased polarity field with modulated growth rate patterns. G: new identity factors added in addition to the original OPP and MID. *Gi*: MAR (orange). *Gii*: EDGE (purple). H: KRN (*ii*) for the distal tip model and the distribution of the resultant growth rate at the start of growth (*i*). I: the distribution of specified  $K_{\text{per}}$  (rate of perpendicular growth) at the start of growth, *i*: full canvas view, *ii*: zoomed-in view of the margin. J: result of the distal tip model simulation. K-M: proximo-marginal model. K: the distribution of plus, minus and POL for the PRN which is the same as in *Dii*. L: the distribution of growth determined by the same KRN as in *Eii*. *Li*:

resultant growth rate patterns set up across the canvas, *Lii*: zoomed-in image of the margin. *M*: the outcome of the proximo-marginal model simulation. Pink arrowheads indicate the midvein tip, blue indicate the opposite keyhole region. The heat maps show the resultant growth rates (red is high resultant growth rate, blue is low resultant growth rate), except where specified  $K_{per}$  is shown (red is high  $K_{per}$  and blue is low  $K_{per}$ ). Small black arrows indicate the polarity field orientation determined by the local gradient of POL. All scale bars are  $100\mu\text{m}$

Published clonal analyses in maize [10, 26] show that clones are largely elongated along the proximodistal axis of the leaf indicating that growth is strongly anisotropic during leaf development, not isotropic. I therefore incorporated anisotropic growth into the model.

To add anisotropic growth to the model, axial information was provided by a polarity field, from which local growth rates parallel ( $K_{par}$ ) and perpendicular ( $K_{per}$ ) could be defined. In the GPT-framework the PRN (Fig. 2.9.D) is defined using the local gradient of a factor called POLARISER (POL) which can propagate through the canvas. POL (Figure 2.9.D.i, turquoise green) is promoted at plus organisers (Figure 2.9.D, bright green) and is degraded at minus organisers (Figure 2.9.D.i, red, PRN is illustrated in Figure 2.9.D.ii). To decide the orientation of the polarity field I used leaf venation patterns as an indicator.

As veins develop in response to auxin and auxin may be involved in coordinating a polarity based axiality system within the tissue, vein orientation may reflect the orientation of the axial information. In mature maize leaves the veins are parallel to the long axis of the leaf and converge at the midvein tip, suggesting that the axial information could orient towards the midvein tip. I hypothesised that the polarity field in the model ring primordium would follow this pattern.

To achieve this polarity pattern in the model I added a plus organiser to the proximal base of the cylinder and a minus organiser to the distal tip of the midvein which would become the leaf tip (Figure 2.9.D.i, green and red respectively). As before I specified that growth rates were promoted by MID and inhibited by OPP (the resultant growth rates are illustrated in Figure 2.9.E.i, red being high and blue being low growth rates), restricting this effect to the growth rates parallel to the local axial information ( $K_{par}$ ) ( $K_{per}$  remained at a constant low value, the KRN used is outlined in Figure 2.9.E.ii). This results in a gradient of parallel growth rate across the ring canvas, highest at the midvein and lowest at the keyhole (Figure 2.9.E.i). The resulting shape of this model did not expand in diameter ( $135\mu\text{m}$ ) beyond the expected range ( $134\text{-}155\mu\text{m}$ ) and it grew out at the midvein region (Figure 2.9.F, pink arrowhead

indicates the midvein position). However, the canvas did not arch over the apical meristem as observed in a real primordium, instead it bent back away from the apical meristem. This backward bending of the leaf tip occurred because of the orientation of the polarity field (black arrows in Figure 2.9.E.i indicate the orientation of the model polarity field, Figure 2.9.E.iii is a zoomed-in region of the distal margin). Along the distal margin (as shown in Figure 2.9.E.iii) the model's polarity field was oriented horizontally along the margin edge. As growth was high parallel to the polarity field, the dominant direction of growth was horizontal at the margin, promoting the backward bending of the leaf tip.

There are two alternative ways to circumvent this problem. One method involves retaining the same axial information (defined in the model by the polarity field), but modifying the pattern of specified growth to compensate for the effect of the axial information at the margin. An alternative method involves retaining the same specified growth rate pattern and changing the axial information.

First I tested the hypothesis that the pattern of specified growth rate could be modified to compensate for the axial information (as defined by the model polarity field) orienting along the margin (Figure 2.9.E.iii highlights the existing model polarity field). This model is referred to as the distal tip model. The polarity field and PRN were kept the same as in the previous model (PRN outlined in Figure 2.9.D). To modify the specified growth rate pattern I introduced a new identity factor called EDGE which was promoted by a diffusible factor called MAR (produced at the margin, Figure 2.9.Gi, orange) and inhibited by the diffusible factors OPP and MID (Figure 2.9.A, blue (MID) and yellow (OPP)). This generated a gradient of EDGE near the distal margin of the ring (Figure 2.9.G.ii, purple). I then specified  $K_{par}$  to be inhibited by EDGE, promoted by MID and inhibited by OPP. Specified  $K_{per}$  was promoted by EDGE and inhibited by OPP (Figure 2.9.H.ii outlines the new KRN used and H.i shows the resultant growth gradient, the pattern of specified  $K_{per}$  is illustrated in Figure 2.9.I.i and a zoomed-in image in iii). Unlike the previous model (Figure 2.9.F), in this model the midvein side of the canvas arched over the meristem (Figure 2.9.J, midvein region indicated by the pink arrowhead) whilst the keyhole region remained inhibited, forming a hood like shape. The size of the canvas at the hood stage increased to 163 $\mu$ m in height and 138 $\mu$ m in width which was within the estimated size ranges calculated using the OPT images (Table 2.1).

I then tested the second hypothesis that the axial information in the ring primordium could begin as a uniform, proximo-marginal field (orienting from the base to the distal margin of the ring primordium), causing the parallel growth in the distal margin to be vertically oriented

(Figure 2.9.K-M). This model is referred to as the proximo-marginal model. To accomplish this proximo-marginal polarity field in the model I added a minus organiser to the entire distal margin of the cylinder (Figure 2.9.K, red). The KRN was the same as for the model in Figure 2.9.E, with high specified  $K_{par}$  at the midvein (the colour map in Figure 2.9.Li shows the resultant growth rate gradient across the cylinder, the pink arrowhead indicates the midvein) and a low constant rate of  $K_{per}$ . This resulted in the canvas arching over the apical meristem region (Figure 2.9.M), mimicking the hood shape (Figure 2.3.B) and the expected increase in dimensions to 146 $\mu$ m in height and 137 $\mu$ m in width, seen in leaf development.

These two alternative models; the distal tip model and the proximo-marginal model; provide clear predictions about growth rate patterns and the axial information in the ring primordium of the grass leaf, required for the developmental switch in shape from a ring to a hood shape. The distal tip model predicts that axial information in the ring primordium is oriented towards the midvein tip (illustrated in the zoomed-in image in Figure 2.9.iii, black arrows). In contrast, the proximo-marginal model predicts that axial information is oriented towards the margin (illustrated by the black arrows in the zoomed-in image in Figure 2.9.Lii). Both models predict that growth overall is higher at the midvein than the keyhole region. The distal tip model predicts that there are differential specified parallel and perpendicular growth rates across the primordium, with higher specified perpendicular growth rates at the margin than elsewhere in the tissue. The proximo-marginal model predicts that specified perpendicular growth rates are uniform across the primordium, but specified parallel growth rates are highest at the midvein. As specified growth rates cannot be measured, the defining differences between the two models are the predictions of axially orientation.

## 2.5 Axial information in the early grass leaf primordium

To distinguish between the models we focussed on the axially predictions. The distal tip model proposes that axial information is oriented towards the midvein tip, the proximo-marginal model proposes that the axial information is oriented towards the distal margin (model predictions are illustrated in Figure 2.10.A and B respectively; the black arrows indicate the predicted orientation of the axial information). Assuming that a polarity based axially system is active in the developing leaf primordium, PIN1 auxin transporters can be used as markers of cell polarity and the coordination of these cell polarities across the tissue (tissue cell polarity) can indicate the orientation of axially [21, 22] . Therefore we

investigated the cellular localisation of epidermally expressed SoPIN1 (SISTER OF PINFORMED1, [118]) in maize, barley and *Brachypodium distachyon* in the early ring primordium stage.

Using transgenic SoPIN1-YFP *Brachypodium* Devin O'Connor looked at the localisation of epidermal SoPIN1-YFP at the ring stage (P1) of primordial leaf development using confocal microscopy. At this stage it appeared that SoPIN1 was co-ordinately localised to the cell edge parallel with the leaf margin (Figure 2.10.C, red arrows indicate localisation of SoPIN1 in the primordium cells). This suggests that tissue cell polarity, could be oriented from the proximal base to the margin in the early ring primordium of *Brachypodium*, supporting the prediction of axiality in the proximo-marginal model.

However, this proximo-marginal orientation of tissue cell polarity is difficult to confirm as we cannot see the cell walls in this sample, definitively identifying the correct localisation of SoPIN1. Therefore I also chose to look at cellular SoPIN1 localisation using immunolocalisation techniques. I sliced FAA paraffin fixed maize apices (an OPT image with the position of the slice image shown indicated on it is illustrated in Figure 2.10.D, yellow box indicates slice position) and carried out immunolocalisation using antibodies against native ZmSoPIN1 (provided by Sarah Hake and Devin O'Connor) and combined this with the cell wall stain calcofluor to help to define the localisation of SoPIN1 in each cell (a representative image is in Figure 2.10.E, red is the cell wall calcofluor stain, green is the SoPIN1 localisation). In slices through the earliest stages of primordia collected (position of the slice is indicated in Figure 2.10.D), SoPIN1 appeared to localise to the distal end of the cells in both the first and second cell layers of the primordium (as indicated by the white arrows in Figure 2.10.E). At first glance this seems to support the prediction of the proximo-marginal model (Figure 2.10.B, black arrows). However, closer analysis of the predicted axiality pattern in the distal tip model (in which axial information is globally oriented towards the midvein tip), showed that the model predicts that at the midvein and the opposite side (the keyhole) SoPIN1 would localise to the distal side of cells (this is illustrated by the black arrows in Figure 2.10.A.i and ii, which are zoomed-in images of the midvein and keyhole regions respectively.). This means that middle tissue slices through the developing leaf primordia, may not distinguish between the two models. Using this sliced immunolocalisation technique I cannot definitively stage or position the slices imaged to recreate the 3D information, making it difficult to confirm or dismiss the model predictions.

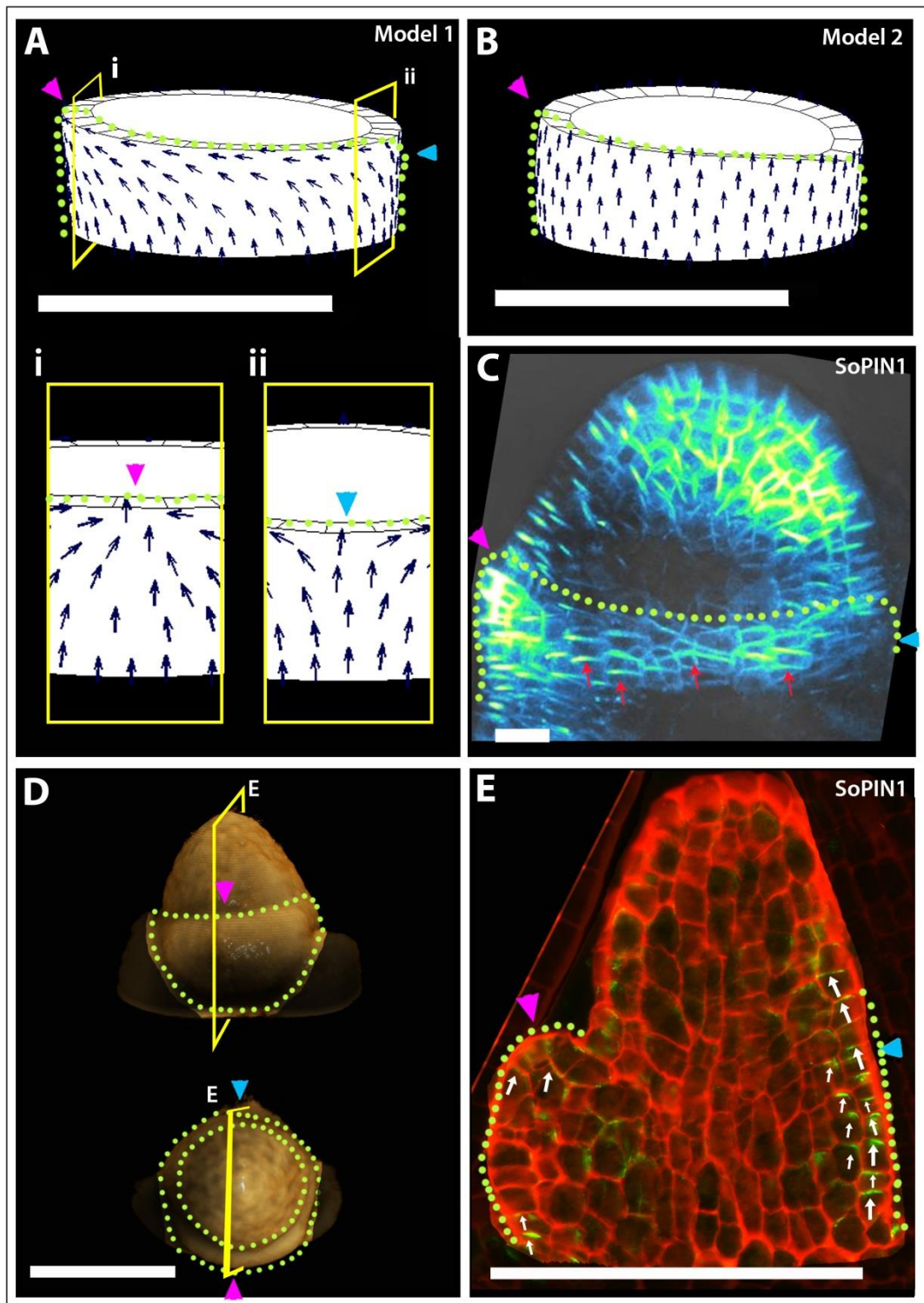


**Figure 2.10 SoPIN1 localisation in early grass leaf primordia.**

*A and B:* Model predictions for the orientation of tissue cell polarity (black arrows) during the ring stage of leaf development, suggesting the orientation of SoPIN1 localisation. *A:* The distal tip model which has polarity oriented towards the midvein tip, *i and ii:* zoomed-in images of the polarity field at the midvein (*i*) and opposite keyhole (*ii*) regions. *B:* The proximo-marginal model in which polarity is oriented proximo-marginally. *C:* The localisation of SoPIN1 in transgenic *Brachypodium* SoPIN1-YFP primordium (image from Devin O'Connor). Green is SoPIN1-YFP. *D:* OPT images of the ring stage in the maize primordium

indicating the approximate position of the immunolocalisation slice in E (yellow box). *E*: The localisation of SoPIN1 in a slice through a maize meristem and early leaf primordium using immunolocalisation (antibodies from Sarah Hake and Devin O'Connor), green is SoPIN1, red is calcofluor cell wall staining. Green dotted line highlights the outline of the primordium, arrows indicate the orientation of the SoPIN1 localisation, pink arrowhead indicates the midvein, blue indicates the keyhole region. Scale bars in *A* and *C* are 100  $\mu\text{m}$ , in *B* the scale bar is 20 $\mu\text{m}$ .

3D information about the SoPIN1 and cell wall localisation could help to distinguish between the two models. I therefore developed a protocol for whole-mount immunolocalisation in barley tissues (see Appendix A for a description of how this was developed). Using this with the ZmSoPIN1 antibody (provided by Sarah Hake and Devin O'Connor) and the cell wall stain calcofluor I probed for the localisation of SoPIN1 in the early barley leaf primordium. This whole-mount technique allowed me to investigate the pattern of axial information, indicated by the coordinated localisation of epidermal SoPIN1, in 3D at a higher sensitivity than the *Brachypodium* SoPIN1-YFP transgenics could provide. The larger size of the barley meristems also made it easier to process and explore the youngest stages of leaf development.

Preliminary results using this whole-mount technique indicated that at the earliest stage captured (illustrated in Figure 2.11), approximately half way between a ring and hood stage (P1-P2) primordium, SoPIN1 localisation was not coordinately oriented towards the leaf margin. Instead the cellular localisation of SoPIN1 in the primordium was coordinately oriented towards the midvein tip (Figure 2.11). This tissue cell polarity orientation was clear when looking at the midvein side of the primordium (Figure 2.11.A); the SoPIN1 was localised distally in each cell towards the midvein tip and the cells outside the midvein region had SoPIN1 localised more laterally towards the midvein tip (the cellular localisation of the SoPIN1 signal shown in Figure 2.11.A.i is indicated by the white arrows in Figure 2.11.A.ii). This was also clear when looking at the lateral side view (Figure 2.11.B.i) where the SoPIN1 cellular localisation was oriented towards the midvein tip throughout the primordium (this is indicated by the white arrows in Figure 2.11.B.ii). These results suggest that axial information at early stages of grass leaf development is not oriented from the proximal base to the margin as predicted by the proximo-marginal model but is instead oriented towards the midvein tip as predicted by the distal tip model.

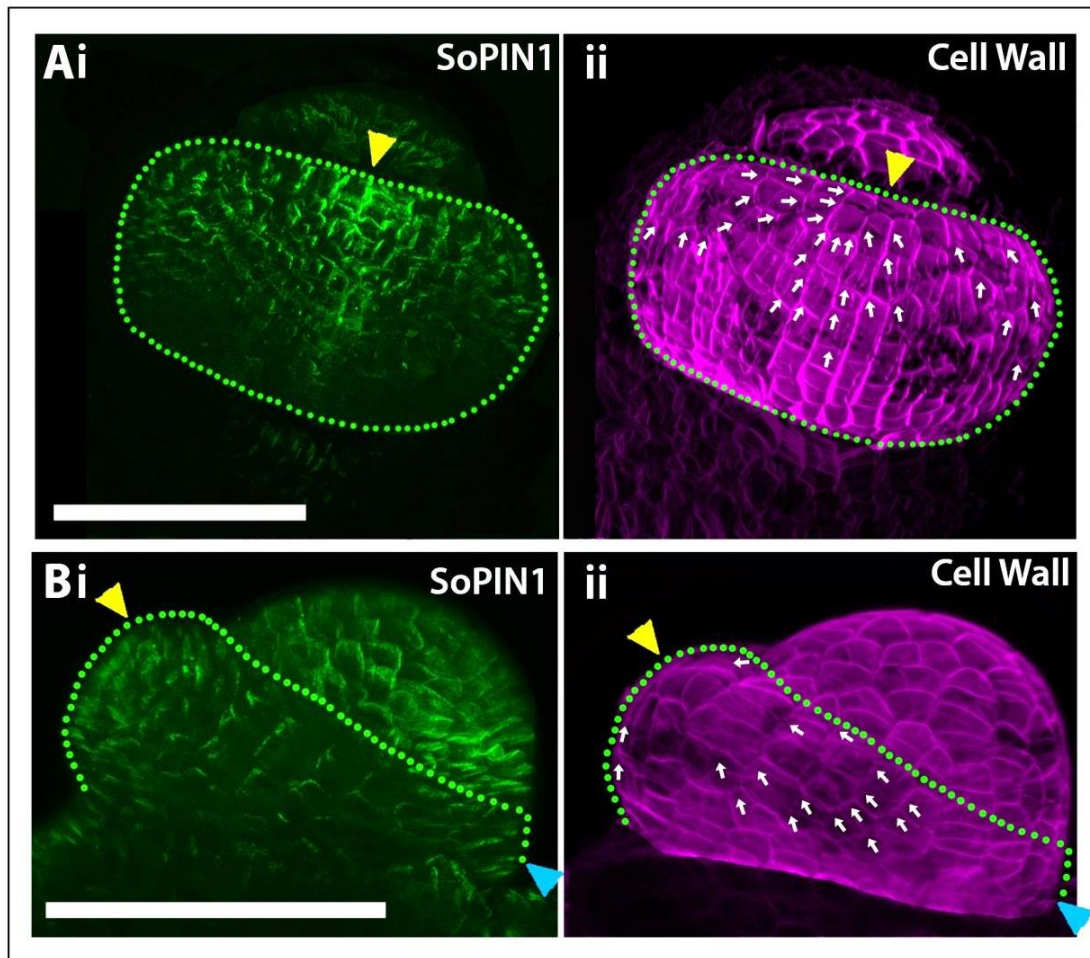


**Figure 2.11** Whole-mount immunolocalisation of SoPIN1 in early barley leaf primordia. A-B: different views of ring stage primordia (P1). A: View of the midvein region. B: Lateral side view. Images show calcofluor stained cell walls (magenta), and SoPIN1 localisation (antibody from Sarah Hake and Devin O'Connor) (green). Each panel shows the SoPIN1 alone (i) and an annotation of the cell outlines (magenta) with the orientation of the SoPIN1 (ii). Yellow arrowheads indicate the position of the midvein, green dotted line highlights the shape of the primordium, blue arrowheads indicate the position of the keyhole region, and white arrows indicate the localisation of SoPIN1 in the analysed epidermal cells. Scale bars are 100 $\mu$ m.

Combined this evidence more strongly supports the distal tip model, predicting that axial information is oriented towards the midvein tip from the start of development. However, I cannot rule-out the possibility of a very early switch in axial information from proximo-marginal, towards the midvein tip. An early axially switch may explain why the tissue cell polarity in the early *Brachypodium* ring primordium seems to be proximodistal. I cannot be sure until the whole-mount immunolocalisations are repeated and more stages of development are explored.

## 2.6 A change in axial information and/ or growth rate pattern may be required for the next shape transition from a hood to a cone

To determine whether the previous models could also account for the developmental switch in shape from a hood to a cone (based on the shape transitions outlined in Figure 2.3), I grew both models to later stages.

When the distal tip model, in which polarity was oriented towards the midvein tip from the start (Figure 2.12.A), was simulated to a later time step although it started to form a cone like shape, the midvein tip eventually arched over the meristem. The distal tip model cannot generate the shape transition from a hood to a wrapped cone (Figure 2.12.B compared to the maize leaf primordium shapes in Figure 2.3.C). This is due to the high growth perpendicular to the polarity field at the margin (zoomed-in image of the margin in Figure 2.12.C.i and ii indicates the axial information along the margin, black arrows), this means that at the margin most of the growth was horizontal not vertical (Figure 2.12.C.ii) causing the arching over. The high parallel growth at the midvein ( $K_{par}$  is illustrated in Figure 2.12.D.i and ii) also contributes to the arching over of the midvein.

Published studies have reported that at later stages of development leaf tip growth is reduced compared with the basal region of the blade [95, 97]. The distal tip model has a medio-lateral gradient of growth rate, high at the midvein and low on the opposite side. I therefore decided to manipulate the growth regulatory network (KRN) after the hood stage to try to more accurately recreate the shapes seen at the cone shape stage of maize leaf development.

I first introduced a diffusible factor called PROX (Figure 2.12. E.i, blue) produced at the base of the canvas and diffusing towards the midvein tip. Using the gradient of PROX I then introduced identity factors 'Blade', in the upper region of the canvas and 'Internode' in the lower region of the canvas below the keyhole region (Figure 2.12.E.ii, dark green and dark blue respectively). During leaf development the internode region does not elongate until later stages, therefore the internode region was defined with very low constant values of  $K_{par}$ . The blade region had higher specified  $K_{per}$  and  $K_{par}$ , and  $K_{par}$  was inhibited by OPP and promoted by PROX, whilst  $K_{per}$  was promoted by MAR and inhibited by MID and OPP (the KRN is illustrated in Figure 2.12.F). To promote edge wrapping I also introduced differential growth rates between the abaxial and adaxial surfaces, with higher growth rates on the abaxial side. This switched the growth rate pattern to a more proximodistal pattern (see

Figure 2.12.G.ii and iii for resultant growth rate patterns before and after the switch) with higher growth rates at the margin compared to the midvein. This resulted in the canvas deforming to form a wrapped cone shape, which matched the shapes seen in maize leaf development. The width of the cone was 166 $\mu$ m and height 298 $\mu$ m which was within the boundaries expected.

This predicts that if axial information is oriented towards the midvein tip from the start of leaf development, a change in growth rate only is required for the developmental switches in shape from a ring to a hood to a cone.

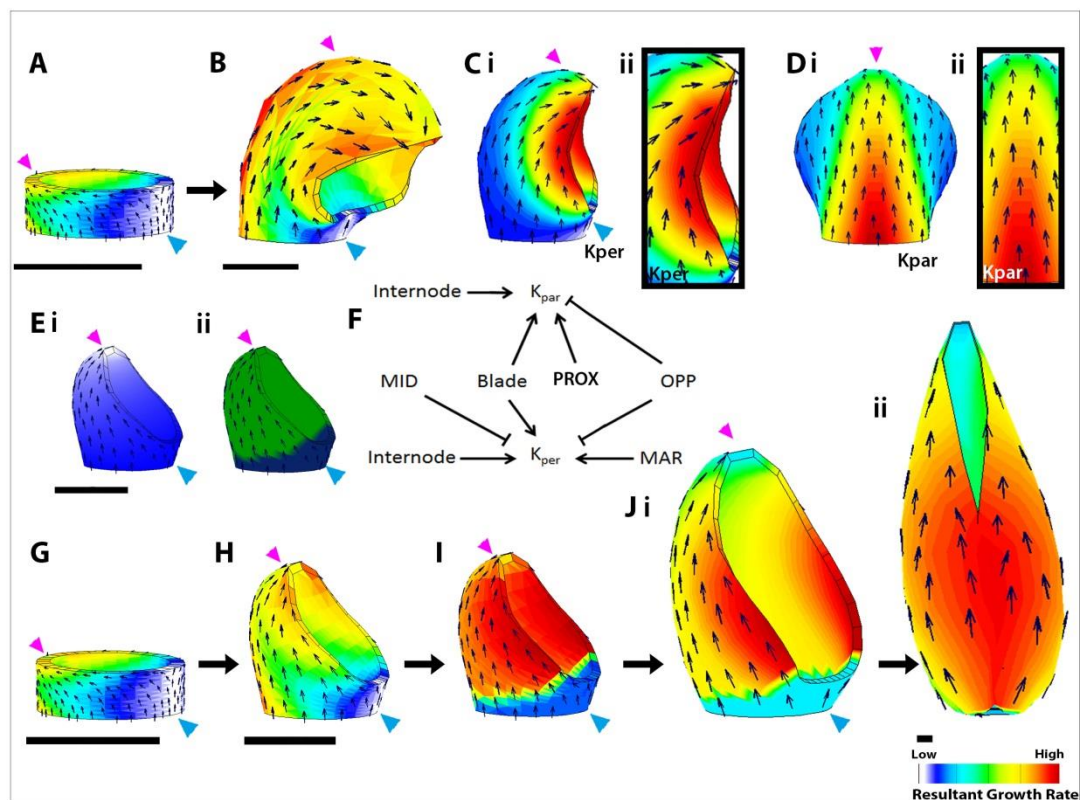


**Figure 2.12 Modelling the transition from a hood to cone shape with the distal tip model.** A: the starting pattern of resultant growth rates in the ring canvas. B: the result of allowing the original model to run to later stages of simulation, showing the resultant growth rate pattern. C: The distribution of specified  $K_{per}$  at the hood stage of the original model and the orientation of the axial information (polarity) indicated by the black arrows viewed from the side, *i*: whole canvas, *ii*: zoomed-in image of the margin. D: the distribution of specified  $K_{par}$  and the axial information at the same stage as in C, image is taken looking at the midvein, *i*: whole canvas, *ii*: zoomed-in image of the midvein region. E: New identity factors added to the canvas, *i*: gradient of PROX (blue) from the base to the tip of the hood stage, *ii*: distribution of Blade (dark green) and Internode (dark blue) determined by the gradient of PROX. F: The new KRN with the effects of PROX, Internode and Blade added. G: the initial ring canvas. H: the hood stage. I: the switch in growth rate patterns determined by the new KRN in F. J*i-ii*: The result of including the switch in growth rate pattern. The colour gradients

indicate the distribution of resultant growth (red is high, blue is low) in all images except where  $K_{per}$  and  $K_{par}$  are shown (red is high, blue is low). Black arrows indicate the local orientation of the axis (polarity) based on the local gradient of POLARISER. Midvein (pink) and keyhole (blue) are indicated by arrowheads. Scale bar is 100 $\mu$ m.

The proximo-marginal model, in which axial information was oriented from the proximal base to the distal margin of the ring (Figure 2.13.A, black arrows indicate the orientation of the axial information), also did not deform to make a cone shape when the simulation was extended. The canvas continued to curve over instead of extending vertically into a more cone like shape (Figure 2.13.B). This discrepancy between the model and the biological observations can be explained by the bending of the axial information. As the canvas deformed to form the hood shape the axial information deformed with it. This deformation resulted in the orientation of the growth (which was preferentially parallel to the axis) changing to be predominantly horizontal at the margin (shown in Figure 2.13.C and the zoomed-in image of the margin in Cii) not vertical, hence the continued curving of the canvas.

To achieve the transition to a more conical shape in the proximo-marginal model I hypothesised a switch in the axial information, reorienting towards the midvein tip, which would be consistent with the venation pattern observed in mature leaves. I restricted the minus organiser to the midvein tip by introducing a new factor called 'Tip' at the midvein tip (red in Figure 2.13. D) and removing 'Minus' after the hood stage was reached (Figure 2.13.C, red). This reset the gradient of POLARISER which re-established the polarity field to orient from the base to the midvein tip (black arrows in Figure 2.13.D). The KRN was kept the same as before with a mediolateral gradient of  $K_{par}$  across the canvas, highest at the midvein, and  $K_{per}$  kept at a low constant value (the KRN is illustrated in Figure 2.9.E.ii and the gradient of resultant growth is shown in Figure 2.13.E). The addition of this polarity switch halted the curvature of the midvein tip over the meristem and promoted a more vertical cone-like shape (Figure 2.13.E). The dimensions of this more cone-like shape were more consistent with the expected dimensions from the 3D imaging of a similar stage: expected range in height 232-301 $\mu$ m and width 163-207 $\mu$ m, model height 209 $\mu$ m and width 129 $\mu$ m.

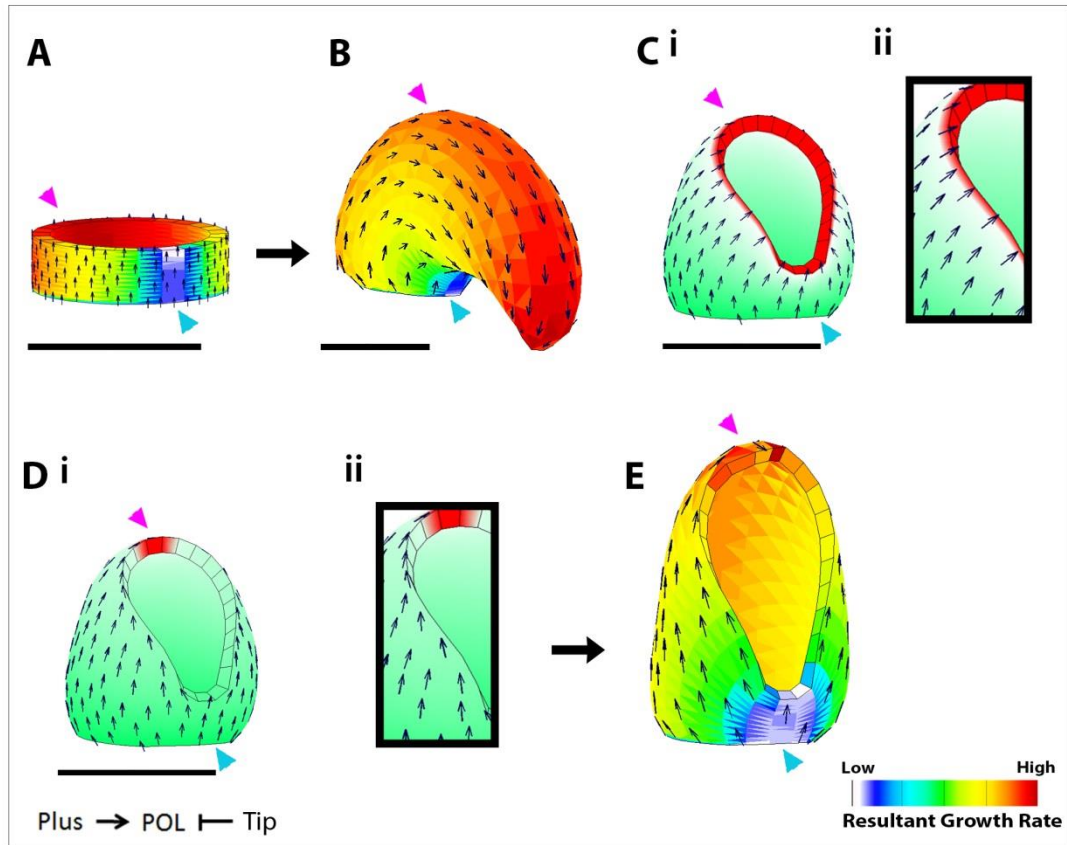


**Figure 2.13 A switch in polarity allows the transition from a hood to a more cone-like shape in the proximo-marginal model**

*A:* the starting ring shape with the proximo-marginal polarity field and mediolateral growth rate pattern. *B:* the result of the existing simulation with no changes. *C* and *D:* PRN and polarity field for the existing model (*C*) and the new model with a switch in polarity (*D*), plus organiser (green), minus (red), distribution of POLARISER (turquoise green). *Cii* and *Dii:* zoomed-in at the margin to show polarity orientation. *E:* the result of the switch in polarity model. The heat map indicates the resultant growth rate (Red is high growth rate, blue is low). The small black arrows indicate the orientation of the polarity field determined by the local gradient of POLARISER. The pink arrowheads indicate the position of the midvein tip, the blue indicate the keyhole region. All scale bars are 100µm.

As the maize primordium grows vertically the edges wrap around forming an elongated, wrapped cone shape (Figure 2.3.D). To determine whether the models could accurately recreate these changes I extended them to later stages. The distal tip model was able to form the wrapped edge cone (Figure 2.12.J.ii). However, the shapes created by the proximo-marginal model did not match those expected as the edges did not wrap and the tip extended at a fast rate, arching over the meristem (Figure 2.14.B). This was because the resultant growth rate at the midvein tip was high compared to the rest of the tissue (Figure 2.14.A-B).

I tested the hypothesis that a switch in the growth rate pattern (combined with the change in axiality) in the proximo-marginal model to a proximodistal pattern with high growth rates at the base and low at the tip could achieve the correct shape transition (the same as the growth rate switch used in the distal tip model). To enhance growth rates at the base of the blade and reduce them at the tip, I introduced a proximodistal gradient of a factor called PROX which was produced at the base of the hood primordium (Figure 2.14.C, pink). This gradient was then used to segment the canvas into different zones in the same way as the distal tip model, defining the 'Internode' and 'Blade' regions of the canvas (Figure 2.8.1.D, dark blue is Internode, dark green is Blade). As with the distal tip model, the internode region was defined with low constant values of specified  $K_{par}$ . The blade region was defined with specified  $K_{par}$  and  $K_{per}$  enhanced by PROX and OPP and restricted by MID (the new KRN is shown in Figure 2.14.F). Perpendicular growth ( $K_{per}$ ) was enhanced at the margins using the growth factor MAR which was produced at the margin of the hood (the distribution of MAR is shown in Figure 2.14.E, purple) to increase the degree of wrapping. Growth on the abaxial surface of the canvas versus the adaxial surface was increased to promote tighter wrapping. This new KRN pattern introduced a switch in the resultant growth rate pattern from a mediolateral distribution (Figure 2.14.A) to a more proximodistal pattern, with high growth rates at the base of the blade (Figure 2.14.G) at the hood stage.

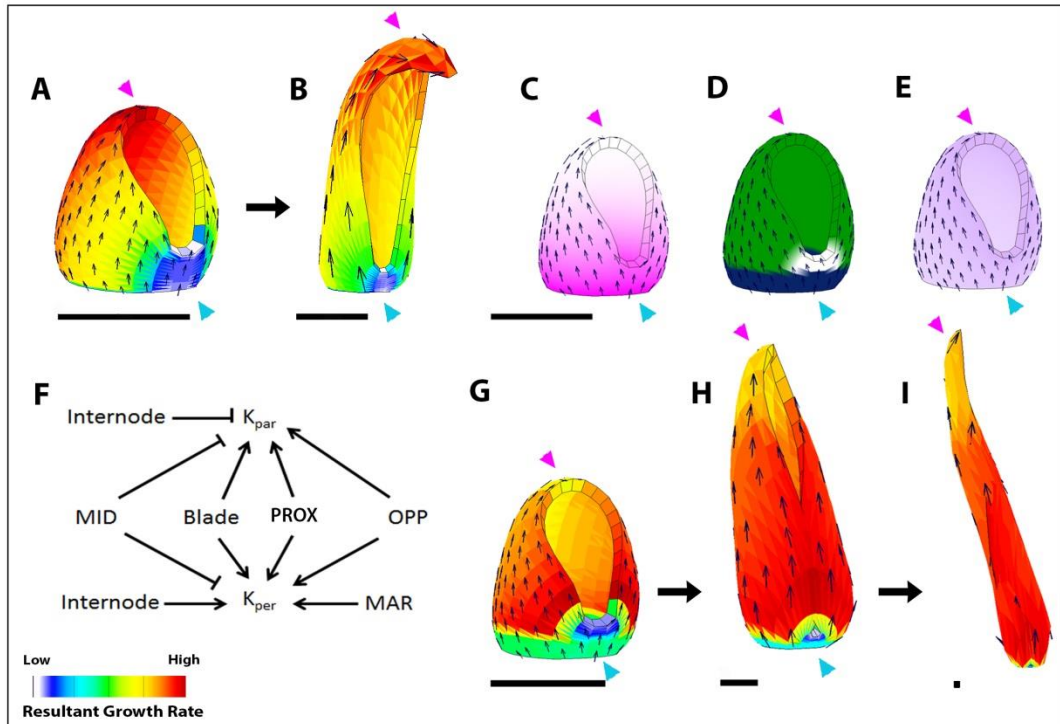


**Figure 2.14 Refining the proximo-marginal model for the transition from a hood shape to a cone like shape using a switch in growth rate pattern**

A-B: The existing model without a change in growth rate. C-E: The distributions of new factors introduced into the model at the hood stage. C: The diffusible growth factor PROX (pink). D: The identity factors Internode (dark blue) and Blade (dark green). E: The diffusible growth factor MAR (purple). F: the new KRN introduced at the hood stage. G-I: The new model, showing the new proximodistal growth rate pattern and the resulting canvas shapes. The heat maps show the resultant growth rates (red is high growth, blue is low). Small black arrows indicate the polarity field orientation determined by the local gradient of POLARISER. Blue and pink arrowheads indicate the position of the keyhole and midvein regions respectively. All scale bars are 100µm.

This switch from a mediolateral to proximodistal growth rate pattern, combined with the bias in outer surface growth resulted in the canvas growing vertically and wrapping tightly (Figure 2.14.G-I), replicating the shapes seen in the 3D imaging (Figure 2.3). The dimensions of this model all lay within the expected ranges for each stage (Table 2.2).

Stage	Expected Height ( $\mu\text{m}$ )	Model Height ( $\mu\text{m}$ )		Expected Width ( $\mu\text{m}$ )	Model Width ( $\mu\text{m}$ )	
		M1	M2		M1	M2
P1- Ring	35-61	36	36	86-136	110	110
P2-Hood	109-164	147	163	134-155	137	134
P3-Cone	232-302	288	298	163-207	170	166
P4-Wrapped	546-1126	1070	1110	304-403	305	401

**Table 2.2 Dimensions of different stages of maize leaf development and the comparable model stages**

Measurements for both the distal tip model (M1) and the proximo-marginal model (M2). P1 dimensions are defined at the start of the model, all other dimensions are emergent properties of the simulation. All measurements are in  $\mu\text{m}$ .

Both models predict that there will be a switch in resultant growth rate pattern at the hood stage, from a mediolateral to a proximodistal pattern. At the hood stage growth is predicted to switch to be at a higher rate in the lower section of the blade compared to the blade tip, and for growth rates at the blade margins to increase. It also predicts that growth rates will be higher on the abaxial side of the leaf. Both models also predict that at the hood stage of development, axiality is oriented towards the midvein tip.

Overall these final models propose two different changes in growth underlying the developmental switches in shape in primordial grass leaf development. The distal tip model proposes that only growth rate patterns are modulated. The proximo-marginal model proposes that both growth rate patterns and axial information are modulated.

## **2.7 Axial information is oriented towards the midvein tip after the hood stage consistent with both model predictions**

Both models predict that axial information is oriented towards the midvein tip after the hood stage of development. The distal tip model predicts that this reflects the existing axial information, whereas the proximo-marginal model predicts that this is the result of a change in axial information at the hood stage.

To test the model predictions that axial information is oriented towards the midvein tip after the hood stage of development (P2) we could look at the cellular localisation of SoPIN1-YFP in *Brachypodium*. However, in developing *Brachypodium* leaves we observed a loss of

epidermal SoPIN1-YFP expression and its subsequent restriction to developing veins which join at the midvein tip (Figure 2.15. A-C). Similarly the difficulty in determining the exact orientation and timing of native SoPIN1 in the sliced maize immunolocalisations made it difficult to accurately identify epidermal SoPIN1 cellular localisation at later stages.

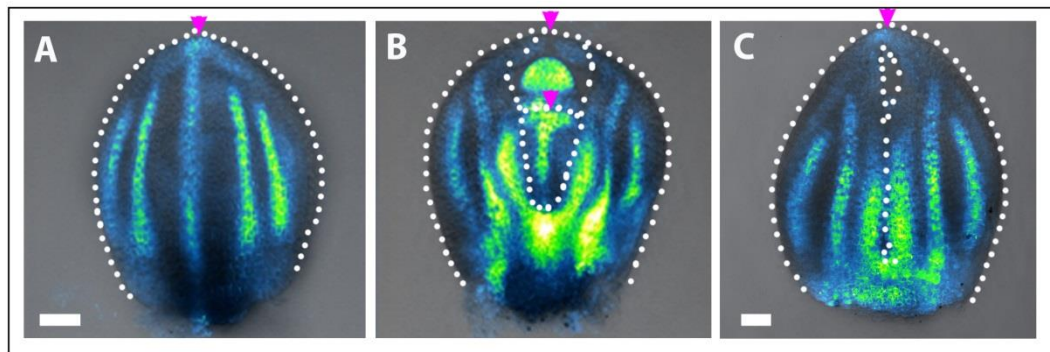


**Figure 2.15 SoPIN1-YFP in transgenic *Brachypodium* at P3 stage of leaf development.** Images from Devin O'Connor. A-B: same P3 sample, back (A) and front (B) views. C: later P3 stage viewed from the front. The white dotted line highlights the shape of the primordium. The pink arrowhead indicates the position of the midvein. Scale bar is 20 $\mu$ m.

I therefore chose to use the whole-mount immunolocalisation of SoPIN1 in barley primordia to explore the cellular localisation of SoPIN1 at this stage in leaf development. At the hood stage (P2) of leaf development in barley, much of the SoPIN1 is localised to the internal developing vasculature as seen in the stripes of SoPIN1 localisation in Figure 2.16.A.i and B.i (an example of a vein trace is highlighted by the dashed white line in Figure 2.6.A.i). However, there is still some epidermal signal, both on the adaxial and abaxial surfaces of the P2 primordium. On the abaxial surface (Figure 2.16.A) epidermal SoPIN1 is localised in each cell towards the midvein tip (as illustrated by the white arrows in Figure 2.16.A.ii). On the adaxial surface as shown in Figure 2.16.B, SoPIN1 is also localised in each cell towards the midvein tip (Figure 2.16.B.ii, white arrows). There is also extensive epidermal SoPIN1 localisation in the keyhole region (blue arrowhead in Figure 2.16.B.i). This epidermal SoPIN1 in the keyhole region may be involved in the formation of the sheath, or it could be involved in the formation of an axillary meristem. Figure 2.16.B also shows the midvein region of a younger P1 primordium inside the P2 primordium, which shows that SoPIN1 is localised within each cell to orient towards the midvein tip, supporting previous observations made in dissected samples (Figure 2.11). This suggests that tissue cell polarity is oriented towards the midvein

tip after the hood stage of development, supporting both models predictions of axial information being oriented towards the midvein tip after the hood stage.

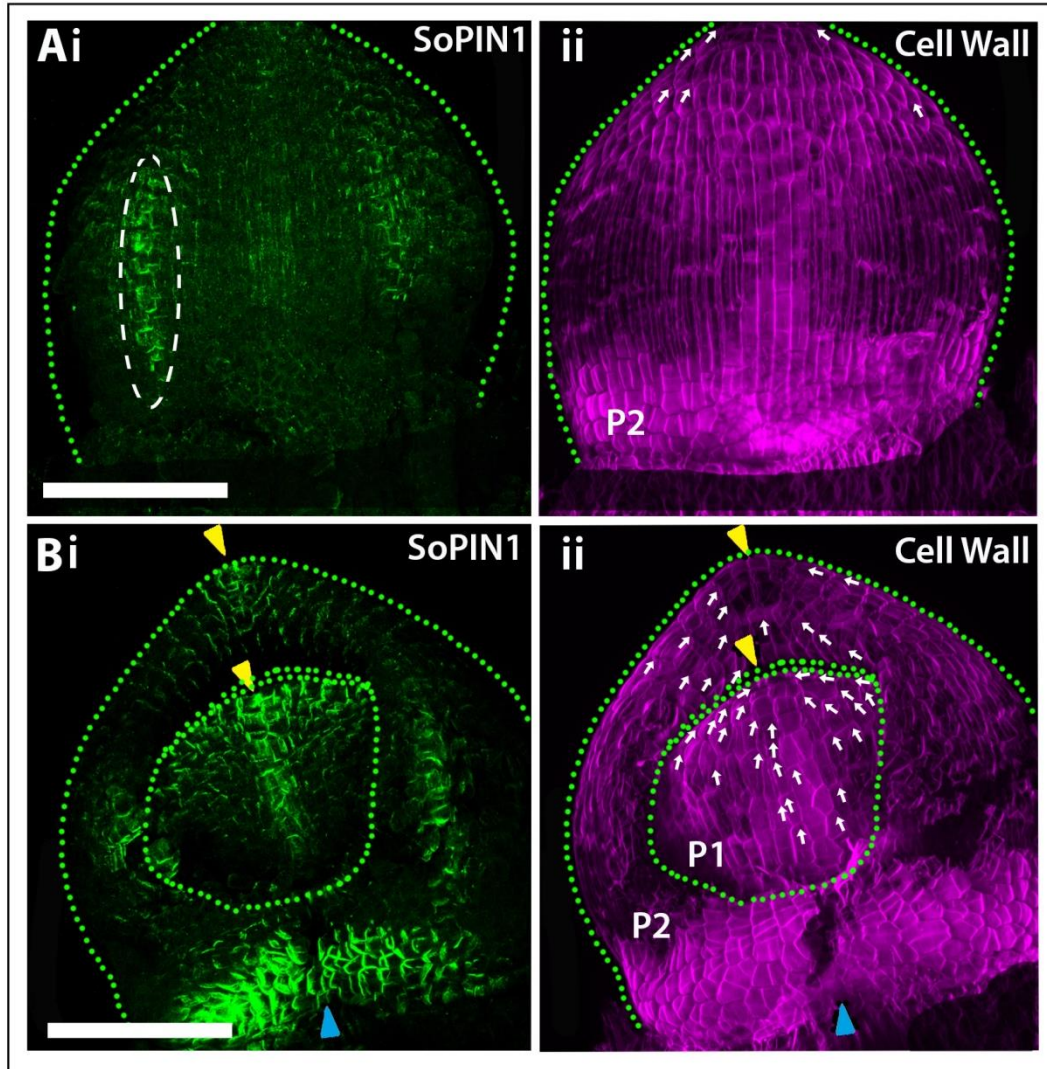


**Figure 2.16 Whole-mount immunolocalisation of SoPIN1 in P2 stage barley primordia**  
**A:** An example of the abaxial side of a P2 (late hood stage) primordium showing the midvein region, *i*: SoPIN1 localisation (green), *ii* calcofluor stained cell walls (magenta), with the orientation of SoPIN1 cellular localisation mapped on (white arrows) . The dashed white line in *Ai* highlights SoPIN1 in a developing vein. **B:** The front view of the same P2 primordium in **A**, *i*: SoPIN1 localisation (green), *ii*: calcofluor stained cell walls with the orientation of SoPIN1 mapped (white arrows). **B** shows the front adaxial view of the P2 primordium tip and the (back) abaxial view of the midvein region of a P1 primordium surrounded by the P2. The shape of the primordium is highlighted by the green dotted line. The position of the midvein and keyhole are shown by the yellow and blue arrowheads respectively. Scale bars are 100µm.

## 2.8 Exploring growth rate patterns across the grass leaf primordium

Growth is primarily due to cell expansion, however, high cell division rates generally correlate with high growth rates. It is not currently possible to measure growth rates in the early grass leaf primordium using techniques like live cell tracking and fluorescent protein clonal sector analysis due to lack of resources and the inaccessibility of the tissue. I first focussed on exploring cell division in young maize leaf primordia as a proxy for growth rate, to test the prediction, proposed by both models, that growth rates switch from a mediolateral to a proximodistal pattern at the hood stage. I labelled cells that passed through the S phase (DNA replication) of the cell cycle during a three hour incubation period with a nucleotide analogue 5-ethynyl-2'-deoxyuridine (EdU). I combined staining for EdU using click chemistry based on azide-alexa 488 with a modified pseudo-Schiff-propidium iodide protocol [119] as used by Schiessl et al 2012 [120] to label the cell walls. This method provided information about cell shape, size and number of dividing cells, acting as an indicator of growth rate.

The models predicted that for the transition between a hood and cone shaped primordium the growth rate pattern would change from a mediolateral pattern to a proximodistal pattern, with high growth rates at the base of the leaf blade (and possibly the sheath) in the cone stage primordium. This suggests that the number of cell divisions should be higher at the midvein of P1/P2 (ring/hood) stage primordium and at the base of the P3 (cone) stage primordium than the rest of the primordium.

In early leaf primordia (P1) EdU (green) staining was present in the midvein region (as seen in the views of the midvein region of P1 primordia in Figure 2.17.A and B). However, it was not clear whether there was a higher concentration of EdU stained cells in the midvein versus the rest of the primordium. Interestingly, there may have been more dividing cells (EdU stained) in the distal margin of the P1 primordium (Figure 2.17.A.ii and B.ii). This possibly suggests that in the ring primordium growth rates may be highest at the margin, which is not directly predicted by either model. Although the distal tip model does predict that specified perpendicular growth is highest at the margin when compared to the rest of the tissue.

In partial support of the model predictions that growth rates have a proximodistal gradient in later stages (P3-P4) of leaf primordium development, EdU staining in P3 stage primordium indicated that cell divisions may have been concentrated near the base of the leaf (Figure 2.17.C-F). The proximodistal pattern of EdU staining was suggested in side views of the P3 primordia (Figure 2.17.C and D) where the green nuclear signal was more concentrated in

the basal region when compared to the tip (pink arrowhead indicates the tip of the primordium). There was also a reduction in EdU signal at the tip when looking at the abaxial surface of the primordium (Figure 2.17.E and F). This suggests that there may be a proximodistal gradient in cell division across the P3 (cone stage) primordium, from high at the base of the blade, to low at the tip.

The patterns of cell division indicated by EdU labelling does provide some limited support to both models' prediction of a change in growth rate pattern after the hood shape primordium is formed. However, whether the growth rate pattern switches from mediolateral to proximodistal pattern is not clear using this technique as the data was variable, making it difficult to draw clear conclusions about growth rates.

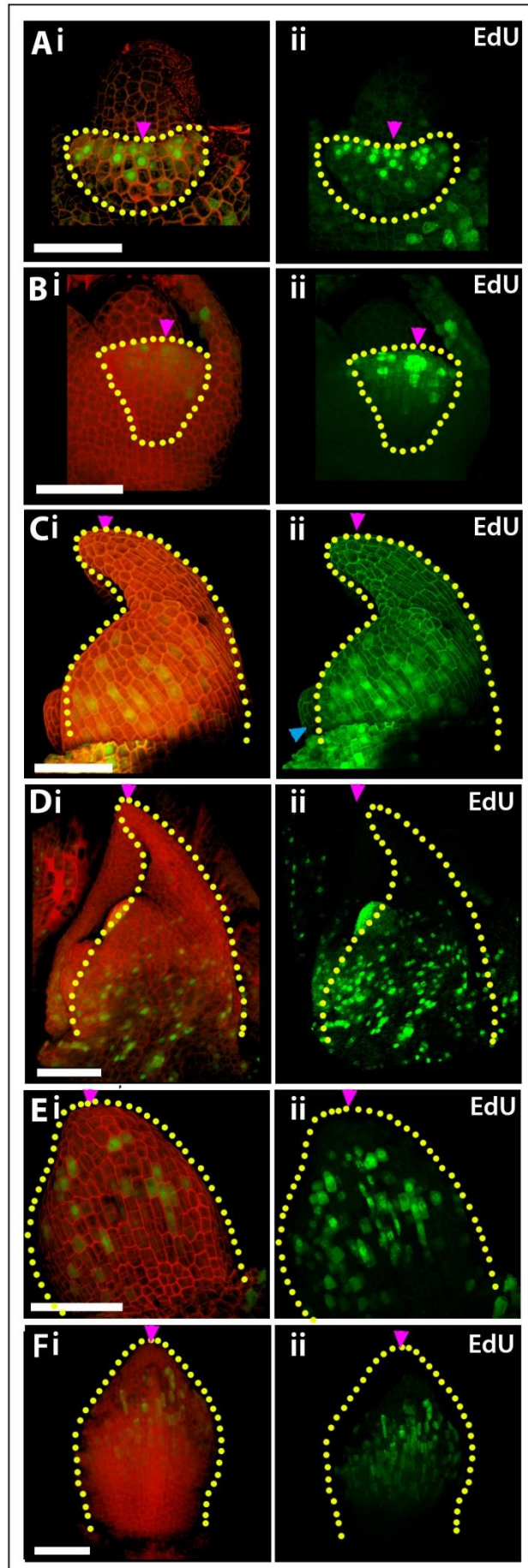


### Figure 2.17 Schiff PI and EdU staining in maize primordia

*A-B*: the midvein region of ring primordia (P1), the edges of the ring primordium are obscured by older tissue. *C-D*: the lateral sides of early cone stage primordia (P3). *E-F*: the midvein region of early cone primordia (P3). Red is the PI stained cell walls, green is the alexa-488 labelled EdU containing nuclei. Each panel shows the merged image of EdU and PI (*i*) and the EdU image (*ii*). Pink arrowheads indicate position of the midvein, blue indicate the keyhole region, yellow dotted lines highlight the shape of the primordium. Scale bars are 100 $\mu$ m.

To further investigate the patterns of growth across the leaf primordia I analysed cell size as this could indicate higher or lower regions of growth in the tissue. I used the propidium iodide stained apices from the EdU experiments and segmented the cells using MorphographX software [121] to analyse cell area in the midvein region. The results shown (Figure 2.18) are from preliminary analyses.

This initial analysis showed that in the ring primordium (P1, Figure 2.18.A) cell area was smaller in the boundary between the meristem and the primordium (this region is not shown in Figure 2.18.A), where growth rates are generally reduced (this correlates with published studies on organ boundary regions [122]). Cells at the margin also seemed smaller, however this correlated with the slightly higher rate of cell division in the margin indicated by the EdU staining pattern. The rest of the P1 primordium had a relatively uniform distribution of cell sizes. The average cell area in the P1 primordium was 407 $\mu$ m<sup>2</sup> (standard deviation of 229 $\mu$ m<sup>2</sup>). The P3 primordium (Figure 2.18.B), had more small cells at the base of the primordium, which could correlate with the higher number of cell divisions in the lower region of the primordium. The average cell area was 411 $\mu$ m<sup>2</sup> (standard deviation of 176 $\mu$ m<sup>2</sup>) which did not vary significantly from the ring primordium, suggesting that between that two stages cell expansion does not increase exponentially.

However, cell size is not an accurate measure of growth as it is a snapshot of time and I do not have dynamic data available to be able to assess 'normal' cell size which to compare our data set. Small cell size could be due to high cell division or low cell expansion, without dynamic data sets it is difficult to tell. Therefore, this data can only provide information on possible growth rate patterns until more dynamic growth data is available.

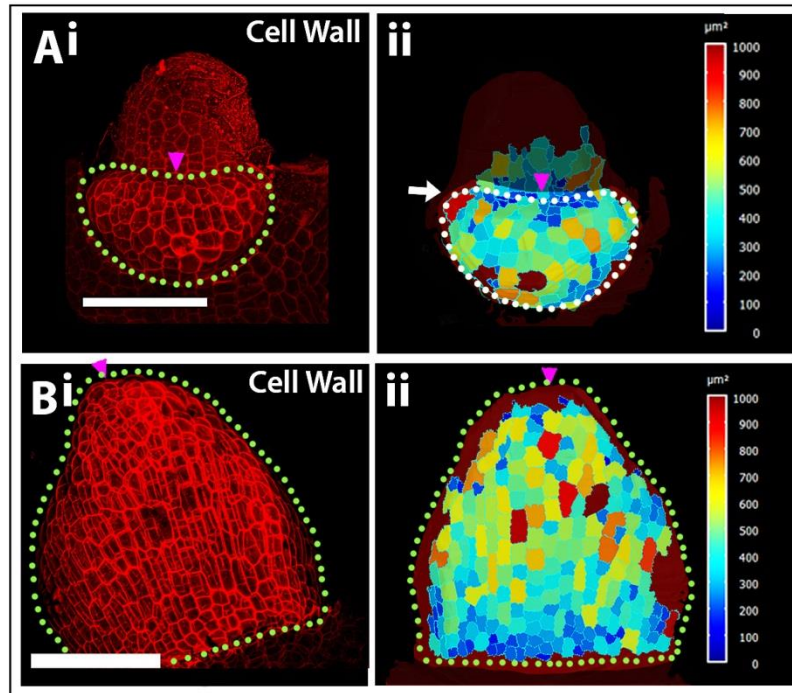


**Figure 2.18 Cell area in a P1 and P3 primordium**

Confocal images were segmented and the cell areas analysed using MorphographX [121] software. The abaxial view of the midvein region in a P1 primordium (A) and a P3 primordium (B). Both images have propidium iodide stained cell walls (red) from the EdU experiment in Figure 2.17. *i*: the original image. *ii*: the segmented MorphographX image showing cell area. The heat map indicates cell area, dark blue is less than  $100\mu\text{m}^2$ , dark red is more than  $1000\mu\text{m}^2$ . Dotted lines outline the shape of the primordium. Pink arrowheads indicate the midvein tip. White arrow indicates the margin. Scale bar is  $100\mu\text{m}$ .

The shape of cells can indicate the preferential direction of cell expansion (growth). In the early P3 primordium, the cells in the midvein region appeared to be proximodistally elongated (Figure 2.18.B.ii). The tissue cell polarity information suggests that axiality was oriented towards the midvein tip at this stage (Figure 2.16), combined with the cell shape information (Figure 2.18.B.ii) this would suggest that growth is preferentially parallel to the axis in the hood-cone stage primordium. This would support both models, which both use higher specified parallel growth rates than perpendicular growth rates at the midvein. It is difficult to use the same information in the ring primordium as the cells appear more isotropic and I do not definitively know the orientation of tissue cell polarity in this stage. The cells in the midvein region of the ring primordium may be slightly proximodistally elongated suggesting preferential parallel growth as in this region axiality is proposed to be oriented proximodistally by both models. However this is not clear.

The shape, size and orientation of cell files can also provide indications of growth patterns. Calcofluor stains cellulose in cell walls, and older cell walls in barley leaf primordia stain less than new cell walls. This allowed me to identify cell files which can indicate the preferential directions of growth, like clonal sectors. (The data shown is a preliminary analysis of these cell files.)

In the midvein region of the P1 ring primordium cell files were elongated proximodistally and were on average 2-3 cells wide (Figure 2.19.A.ii, P1 is inside the older primordia, this image shows the midvein side of the developing primordia, clonal patches are coloured differently, the midvein is indicated by the yellow arrowhead, the keyhole by a blue arrowhead.). There were very few longitudinal cell divisions in each clone (average of approximately 3) compared to the number of transverse cell divisions (average of approximately 8 per cell file). Cells also tended to be elongated proximodistally. This pattern of cell files suggests that growth is predominantly proximodistal at the midvein (supported the cell shape data). Combined with the SoPIN1 patterns discussed previously, which indicate that axial information is oriented proximodistally at the midvein, this supports both models predictions of high parallel growth rates at the midvein. (This is also supported by published clonal sector analyses [26, 96, 98])

The P2 midvein region (Figure 2.19.B) also had proximodistally elongated cell files that were on average 1-2 cells wide (clones were on average 11.61 $\mu\text{m}$  wide, 158.60 $\mu\text{m}$  long, with an average of approximately 15 cells for this sample, Figure 2.19.B), with the widest points more commonly at the base or tip of the cell file. The number of longitudinal divisions (an approximate average of 3) was also lower than the number of transverse divisions (an approximate average of 11). Combined, this suggests that growth is strongly anisotropic in the midvein region. As SoPIN1 patterns indicate that axial information in the midvein region is proximodistally oriented, this pattern of cell files suggests that there is more growth parallel than perpendicular in the midvein region. This provides some support for the growth rate patterns in both models which predict higher parallel growth than perpendicular growth in the midvein at this stage. (This is also supported by published clonal sector analyses [26, 96, 98])

The keyhole region of the P2 primordium (as shown in Figure 2.19.A, P2 labelled region, keyhole marked by blue arrowhead) had shorter, wider cell files (cell files were on average 20.36 $\mu\text{m}$  wide, 80.87 $\mu\text{m}$  long with 17.43 cells for this sample), than the midvein region, and there were a similar numbers of cells. Unlike the midvein cells, the cells in the keyhole region

appeared to be shorter in the proximodistal axis. This suggests that the keyhole region has strongly inhibited cell elongation, this again provides some support for both models as they predict that growth is strongly inhibited in the keyhole region, particularly parallel to the axial information. This again agrees with published fate map data [26, 96, 98].

Overall, this preliminary evidence supports both models' prediction that growth is strongly inhibited in the keyhole region throughout primordial leaf development, and that parallel growth rates are higher than perpendicular growth rates at the midvein during the hood-cone stage of development. However, it is not possible to conclusively tell whether the growth rate pattern switches over time. It is also not possible to distinguish between high parallel and high perpendicular growth rates at the margin in the ring primordium, which is where the two models differ in their growth rate predictions, as I have not yet confirmed the axiality patterns.

Collectively the information from EdU labelling, cell files and cell size supports some of the predictions from the model. This data suggests that growth is strongly anisotropic in the midvein and less so in the keyhole region, that growth in the internode/ sheath region may be reduced and that growth at the tip of the primordium may be reduced by the P3 stage. This provides some limited support to the broad predictions about growth rate patterns in both models.

The cell division patterns may suggest that there is a change in growth rate pattern between the ring and cone stage primordium (which is predicted by both models) but this is not clear. So far this growth rate data is not conclusive.

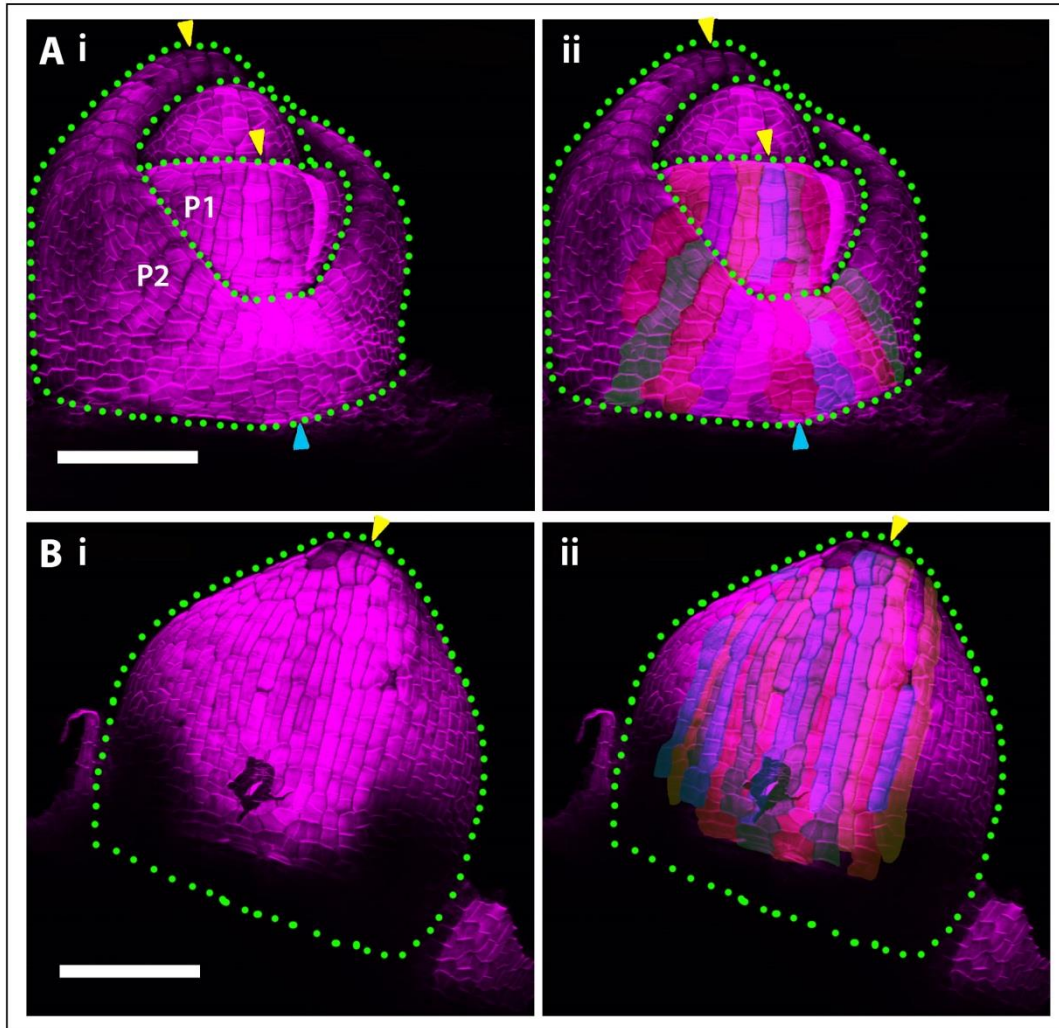


**Figure 2.19 Cell files in calcofluor stained barley primordium**

A–B: same barley P2 primordium imaged from the front (A) and back (B) with calcofluor stained cell walls. A: also shows the midvein region of a P1 primordium. *i*: original image. *ii*: coloured cell files. Yellow arrowhead indicates the midvein position, blue arrowhead indicates the keyhole position. Scale bar 100 $\mu$ m.

## 2.9 Discussion

### 2.9.1 Characterising developmental switches in shape during primordial stages of grass leaf development

Existing SEM imaging had identified the morphological transitions in primordial grass leaf development in which predominantly blade tissue is elaborated from a ring, to a hood to a cone shaped primordium. However, this data did not allow volumetric analyses of the maize leaf development and very limited SEM imaging data was available for other grass species. By carrying out OPT imaging I was able to analyse primordial leaf development of maize juvenile leaf 6 and develop a set of standard measurements to which I could compare the model simulations. I also imaged *Brachypodium distachyon* and *Fargesia rufa* primordia for the first time in 3D, identifying that the primordial shape transitions previously observed in maize also occur in these species, suggesting that these early developmental switches in shape could be common to all grass species.

This collection of data could provide a useful foundation tool for further studies on grass leaf development.

### 2.9.2 Modelling the primordial stages of grass leaf development

To explore the mechanism behind developmental switches shape in primordial grass leaf development, particularly focussing on whether growth was modulated through changes in growth rates alone, axiality alone or both combined, I used computational modelling.

To do this I made several assumptions. Firstly, I approximated the developing leaf as a single continuous canvas. This was possible because during primordial growth the ligule and the sheath region are not elaborated significantly. To include sheath and ligule development modelling of multiple tissue layers would be required, a function not currently possible with the GPT framework.

The second assumption was that a polarity based axiality system in which the gradient of a polarising factor was coordinated by the activity of organiser regions [42] could be used to define the axial information. This has been used previously to accurately predict growth orientation and organ shapes in models of the *Arabidopsis* leaf and petal, and the *Antirrhinum* flower [21, 22, 24]. (This does not exclude other methods proposed to provide

axial information, for example a stress based axiality model [37, 47], but these are not within my ability to test.)

Using this modelling framework I have generated two different models which use changes in growth to generate the key developmental switches in shape observed during primordial grass leaf development. These models may be the first examples of using computational modelling to explore the mechanism behind primordial stages of grass leaf development.

### **2.9.3 Predicted changes in growth during grass leaf development**

Modelling indicated that to achieve the developmental switches in shape which underlie primordial grass leaf development, changes in growth were necessary. These changes to growth were predicted to modulate different components of anisotropic growth based upon the starting axiality of the ring primordium.

The distal tip model predicted that the ring primordium would have axial information oriented towards the midvein tip and that a balance of perpendicular and parallel growth rate patterns across the tissue generate the shape transition to a hood shape. To transition from a hood shape to a cone like shape a change in growth rate patterns was used. This altered the resultant growth rate pattern from a mediolateral gradient (high at the midvein, low at the keyhole) to a proximodistal gradient within the blade region.

The proximo-marginal model predicted that the ring primordium would have axial information oriented towards the distal margin and a specified mediolateral gradient of parallel growth from high at the midvein to low at the keyhole. For the transition from a hood to a cone like shape, this model predicted that a change in both axial information and growth rate pattern was required. This predicted that the axial information would switch to orient towards the midvein tip and the growth rate pattern would switch to a proximodistal gradient in the blade tissue.

This then allowed the exploration of how developmental switches in shape are generated by changes in growth by testing model predictions. Gaining insight into how evolutionary important shape changes are triggered. Through this work I have evidence to suggest that during the early stages of grass leaf development only changes in growth rate patterns are required for the developmental switches in shape.

#### 2.9.4 The role of growth rate patterns in grass leaf development

Differential growth rates within a tissue have been shown to be important in forming the initial shape of entire organs [21, 22] and in elaborating the margins to make more complex shapes [77]. I have found that the change in growth, which triggers the formation of the developmental switches in shape during primordial grass leaf development, is likely to require the modulation of growth rate patterns only.

In concurrence with the model predictions, growth analyses showed that growth was anisotropic and the degree of anisotropy and the rate of growth varied across the primordium and between stages. However, the prediction of a switch in growth rate pattern from mediolateral to proximodistal was not strongly supported using the current methods. To test whether a switch in growth rate occurs, more dynamic data, such as live cell outline tracking [21], or early stage fluorescent protein clonal sector analysis, is needed. To date no one has published data of this kind. This is because most of the clonal analyses use the knockout of chlorophyll genes to generate white sectors in heterozygous plants, which although very valuable as patterns of growth can be inferred from the size and shape of clones in mature leaves, it is not possible to monitor sector size and shape during early stages of leaf development when chlorophyll is not present. Live tracking of grass leaf primordium has also not been achieved due to the inaccessibility of the tissue and because, until recently, fluorescent membrane marker lines were not available. Now with the membrane markers in maize developed by Mohanty et al [123] and the transgenic barley lines developed during this thesis work (a GFP clonal sector line and membrane marker line, described in Chapter 4) perhaps this growth data will be able to be generated. (Although this would still not distinguish between the models, it is the orientation of the axial information which forms the defining difference between the two models.)

How the growth rates are defined or a switch in growth rates in developing leaf primordia is achieved is not known.

Our model uses a field of diffusible identity factors produced by the midvein and keyhole regions to promote and inhibit growth respectively. It may be that there are real morphogens which replicate this pattern in the primordium. For example, the midvein and the keyhole regions have different genetic identities early in leaf development. In rice the gene *DROPPING LEAF 1 (DL1)* is important in the specification of the midrib region, and when over expressed the blade is curled [124]; it may be that *DL1* is able to influence growth rates in

the midvein region. Alternatively, there may be differential concentrations of hormones across the primordium which influence growth rates. For example, the balance of cytokinin and auxin are thought to be involved in elaborating the leaf margin in compound leaves [125, 126] which involves specific differential growth rates across the tissue [77].

Later in the model diffusible factors defining the margins and the basal regions of the leaf are used to switch the growth rate pattern. Again these may be influenced by concentrations of hormones across the tissue or new patterns of gene expression. There is some evidence of microRNA concentrations changing in the leaf during development, which may control the temporal expression of leaf development genes [127], perhaps they have a role in coordinating changes in growth through modulating gene expression patterns.

It was impossible to test the prediction of differential growth rates between the adaxial and abaxial surfaces as I cannot track growth rates live and I did not have clonal sector lines suitable for these early stages. However, it would be possible to define differential growth rates as the dorsoventral axis is defined very early in development by contrasting gene expression [100] and any of these genes could differentially influence growth rates. The balance of leaf curling in the mature leaf has been shown to be important for crop yield in rice [128], and it may be that these differential growth rates are important for this.

Overall the modelling and growth data suggest that changes in growth rate pattern in the primordium are central to the development of the grass leaf and the formation of the correct shape transitions. Dynamic analysis of growth focussed on the early stages of leaf development (P1-P4) would provide information on the growth rate changes. It may be that with this information and new growth rate analysis techniques, mutants could be analysed to identify the possible control mechanism behind growth rate patterns.

### **2.9.5 The role of axial information in grass leaf development**

Both models hypothesised that anisotropic growth, and therefore axial information, were central to the development of the grass leaf. Experimental evidence based upon the cellular localisation of SoPIN1 as a readout of axial information suggests that the axial information is not modulated during early stages of grass leaf development. This does not exclude the possibility that other developmental switches in shape require changes in axial information for later shape transitions. For example it may be that the development of the ligule results from a change in growth which alters axial information, as the ligule grows in a new axis from the adaxial surface of the leaf (research has shown that a reorientation of PIN is seen in the

incipient ligule region [129, 130]). Similarly, as the transgenic SoPIN1-YFP *Brachypodium* appears to have an axis oriented towards the margin not the midvein tip, I also cannot rule out a very early switch in axial information. To assess this, the axial information in early stages of barley leaf development needs to be tested using whole-mount immunolocalisation of SoPIN1. It may be that *Brachypodium* only appears to be oriented towards the margin as I cannot see the cell walls to accurately decide the cellular localisation of the SoPIN1-YFP. Or perhaps *Brachypodium* has a different, convergent method of generating the shape changes, more like the proximo-marginal model.

During this work I assumed that axiality is provided by a polarity based axiality system. There is some evidence that a polarity axial system may be involved in grass leaf development as auxin has been previously shown to be important for correct maize leaf development [82, 131]. If this is the case the models could predict the location of possible tissue cell polarity organiser regions.

The distal tip model, predicts that a plus organiser (promote high extracellular auxin) would be found in the base of the leaf primordium and that a minus organiser (promote low extracellular auxin) at the tip of the developing midvein. Plus organisers could be composed of auxin biosynthesis genes like the YUCCAs [132] and minus organisers may have a high level of auxin importers like LAXs (LIKE AUX1) [133] or veins which internalise extracellular auxin in the epidermis. The prediction of plus organiser at the base of the primordium could be supported by the expression pattern of the YUCCA gene SPI1 [55] which is expressed throughout the disc of insertion [93] at the base of the primordium. The minus organiser could be marked by the expression of auxin importers such as LAXs, although this has not been explored. Alternatively, minus organisers could be simulated by strong internal auxin transport for example, in developing veins where SoPIN1 and PIN1a are basally polarised in each cell [93] trafficking auxin away from the epidermis (as is the case in the midvein region).

### **2.9.6 Insights into the evolution of the grass leaf**

The grasses are described as having a characteristic leaf structure with a tubular ensheathing base, a hinge-like auricle/ligule region and a blade which bends away from the main axis of the plant. It follows that understanding how the grass leaf develops this characteristic modular leaf structure would indicate some of the evolutionary steps which made the grasses so successful. I aimed to contribute towards this understanding by characterising and

investigating the earliest primordial stages of grass leaf development using the crown group species maize, barley and *Brachypodium* as models.

Using 3D OPT imaging we found that all crown group grass species imaged progressed through the same key set of shape transitions during primordial leaf growth; from a ring to a hood to a cone shape. Indicating that these shape transitions are crucial to correct grass leaf development, which is further supported from mutant phenotypes in plants which fail to progress through these shape changes. Other monocot species did not appear to share these shape transitions. This suggests that the primordial shape transitions, from a ring to a hood to a cone, could be unique to the grasses and may be one of the underlying mechanisms that led to the evolutionary innovation of the grass leaf. This means that the changes in growth explored here could have been one of the evolutionary steps that led to the new shape of the grass leaf.

Given the huge diversity in primordium shape seen in the monocots it would be interesting to see if the grass leaf primordium model could be manipulated, using changes in growth rate patterns and axial information, to recreate other monocot families. Through doing this it may be possible to identify evolutionary steps which led to the development of different shapes, further highlighting the importance of changes in growth in generating novel developmental switches in shape. This work may also identify other developmental switches in shape that are triggered through different changes in growth compared to the grass leaf.

### **2.9.7 Future work and concluding remarks**

This work aimed to explore how growth was modulated to generate developmental switches in shape during early stages of grass leaf development. Particularly focussing on whether growth was altered through changes in growth rates alone, axiality alone or both combined.

Models produced provided clear predictions relating to both axial information and growth rate patterns. To distinguish between them the axial information was explored using whole-mount immunolocalisation of SoPIN1 in barley. This data supports the distal tip model in which axial information was oriented towards the midvein tip. This needs to be repeated at a range of stages to test whether there is a very early switch in axial information or whether it is fixed from the start of leaf development. It may also be useful to carry out a whole-mount immunolocalisation on *Brachypodium* to check whether axial information is oriented differently to that in barley.

As this preliminary work has suggested that the change in growth which may underlie early grass leaf development modulates growth rate patterns only, it is important that growth rate patterns are analysed in more depth. Approaches taken so far have been inconclusive. It is hoped that with the transgenic tools developed as part of this project (see Chapter 4 for a description) it may be possible to next develop live cell tracking to assess growth rate patterns across the developing grass leaf primordia dynamically for the first time. The fluorescent clonal sector line will also allow clonal sector analysis to be analysed at the P1/P2/P3/P4 stages of leaf development to provide growth data. This data, once collected, can then be used to refine the model of grass leaf development further.

Once 3D GPT framework modelling is possible, extending the model to include later stages of development such as ligule development would be interesting. As this may allow the exploration of questions such as how is a straight line drawn during leaf development (i.e. how is the ligule positioned).

Using the refined and extended model as a tool to explore different leaf development mutants, testing how they may affect growth, tissue specification or the developmental switches in shape may result in the identification of new components or mechanisms important in grass leaf development. For example, the *Kn1* mutants in maize have a range of shape phenotypes proposed to involve changes in growth rate and axial information [88, 134] . Or genes like maize *ROLLED LEAF 1* which is known to be involved in adaxial specification [100], rice mutant *rice leaf inclination 2* which has a highly angled leaf (thought to be due to higher cell division on the adaxial surface of the ligule/auricle region [135]) or rice *rolled leaf 9*, a mutant in a KANADI related GARP protein which has an inwardly rolled leaf [136]. The model could be used to make predictions about how the leaf phenotype may occur. Using model predictions, components responsible for developmental switches in shape, such as growth rate regulators and axial information organisers, could be explored by looking for genes that have a similar expression pattern to key model components. For example, exploration of the expression patterns of *LAX* and *YUCCA* genes may correlate with the predicted location of organisers of polarity (if axial information is defined by a polarity based system).

Extension of the model to explore how developmental switches in shape may have been used to generate the diverse range of shapes seen in the monocot leaves would also help answer the question of how shape diversity evolves. This could lead to the identification of new genes that allowed novel developmental switches in shape to occur.

Overall, this project has shown that developmental switches could act upon different components of growth to generate key shape transitions. Evidence so far suggests that the change in growth which generates the key shape transitions in early grass leaf development may act through altering growth rate patterns only, not affecting axial information. This suggests that one of the factors that may have led to the evolution of the grasses is the recruitment of a gene or signal which altered growth rate patterns. It may be that this is a common mechanism during evolution, in that changes to growth through the modification of growth rate patterns are used to generate new shapes.

### 3 How Can a Single Gene Induce a Developmental Switch in Shape? The *Hooded* Barley Mutant

Developmental switches in identity, which occur before organ initiation, can be triggered by single genes. It may be that developmental switches in shape, which occur during organ development, can also be triggered by single genes. These single genes may trigger developmental switches in shape through modulating the components of growth in any of three ways:

1. Axiality alone
2. Growth rates alone
3. Axiality and growth rates combined

Genes able to induce any of these changes in growth could trigger developmental switches in shape during organ development resulting in the evolution of new shapes.

To explore how single genes may be able to induce changes in growth a single gene mutation with a dramatic developmental effect on shape, like the *Hooded* barley mutant, is extremely useful.

#### 3.1 Barley floral development and the *Hooded* mutant

##### 3.1.1 Morphology of wild-type barley

The wild-type barley flower develops on an inflorescence spike (Figure 3.1.A). Each inflorescence spike can have more than ten horizontal rows of individual florets arranged along a central rachis. The barley spike can be described as six row or two row, depending on the number of mature flowers in each node. Each node has the capability of developing six mature florets, in two clusters of three, either side of the rachis. In two-row barley only the central floral meristem in each cluster of three develops further into a mature flower, while the other two abort. The floral structure is most easily described by a floral diagram. Figure 3.1.B shows a floral diagram of a transverse section through a 2-row barley spike (the position of which is shown in Figure 3.1.A by the yellow line), Figure 3.1.C shows a floral diagram of a longitudinal section through the middle of a 2-row spike of barley.

Like dicot flowers, barley flowers are made up of concentric rings of organs, the central carpel (pink) is encircled by three ventrally positioned stamen (yellow), then two ventrally positioned lodicules (blue, these are reduced organs thought to have a role in flower opening and may be analogous to petals [137]). The central floral organs (carpel, stamens, lodicules) are encircled by outer protective structures, the ventral lemma (black) and the dorsal palea (green) which cup the floral organs, protecting them (the lemma encircles more of the floral base, protecting the palea to an extent too (Figure 3.1.D)). Then there can be bract-like glumes (purple) below.

The lemma has a polarised structure with an oval shaped base that protectively cups the floral organs, and a long, thin, distal extension called the awn (Figure 3.1.A, C, and D, black). The lemma is proposed to be a bract like structure, and the awn is thought to be a modified leaf lamina. The extended shape of the lemma, suggests that growth during lemma development is strongly anisotropic (i.e. more growth along the longitudinal axis and less along the latitudinal axis). The adaxial surface of the lemma is covered in hairs, which are clear in SEM images. All of the hairs on the adaxial surface of the lemmas and the margins of the awn orient towards the proximal tip of the awn (Figure 3.1.E, red arrows indicate the orientation of the hairs, also see Appendix B for wild-type lemma SEM images). If we take hairs as an indicator of axiality within the tissue, it suggests that the axial information in the developing lemma and awn is proximodistal. This predicts that growth in the developing lemma is predominantly along the proximodistal axis. This is something that has not been previously tested in barley.

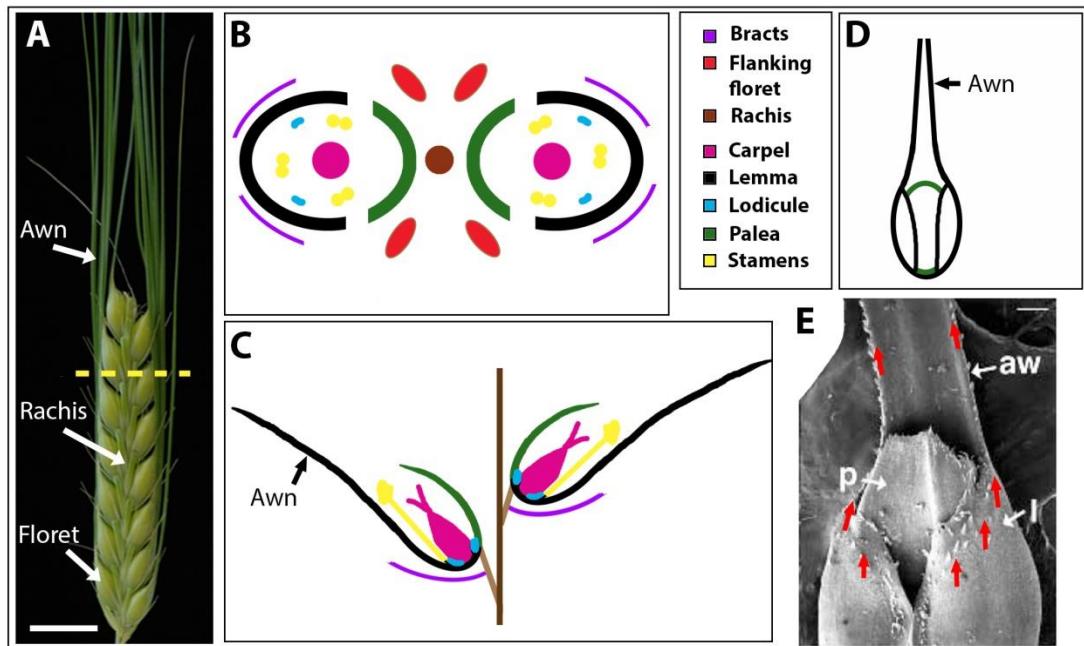


**Figure 3.1 The morphology of a wild-type barley flower**

A: Photo of an inflorescence spike of a wild-type 2-row Bowman subcultivar of barley. The position of an individual floret, the rachis, and the awn are indicated. B-D: floral diagrams of a 2-row barley inflorescence spike, the rachis (brown), aborted florets (red) and subtending bracts (purple) are indicated as well as the central floret organs; lemma (black), palea (green), lodicules (light blue), stamens (yellow) and carpel (pink). B: a floral diagram of a transverse section in a position similar to the position indicated by the yellow line in A. C: a floral diagram of a longitudinal section through 2 mature florets. D: a diagram of the lemma (black) and palea (green) shapes. E: an SEM image of the lemma awn boundary from a wild-type flower (image adapted from Williams-Carrier et al [138]), the lemma (l), palea (p) and the awn (aw) are indicated, red arrows indicate the orientation of the lemma and awn hairs. Scale bar in A is 1cm. Scale bar in E is 220 $\mu$ m.

### 3.1.2 Morphology of the *Hooded* barley mutant

The *Hooded* mutant, thought to have arisen in the Himalayas in the 1830s [89], has a clear morphological difference to wild-type barley (Figure 3.1, WT vs 3.2, HD).

The *Hooded* spike (Figure 3.2.A) develops normally, with rows of floral meristems initiated along the rachis. The arrangement of the floral organs within the mature flowers is also the same as in wild-type with organs in concentric rings (they share the same transverse cross-sectional floral diagram, Figure 3.1.B). However the development of the lemma is significantly altered.

The *Hooded* lemma does not develop a wild-type awn, instead an ectopic flower develops on the lemma and in some cases a second ectopic flower can develop above this (Figure 3.2.B, the floral diagram illustrates the new ectopic flowers which form on the original lemma) [89, 139]. The first ectopic flower (Figure 3.2.B.1) orients basipetally (i.e. upside down) as shown by the inversion of the internal organs. The second ectopic flower, if it forms, is oriented proximodistally (i.e. has the normal orientation, illustrated in the floral diagram in Figure 3.2.B.2). Figure 3.2.E shows an SEM image of the adaxial surface of a developing *Hooded* lemma, showing the ectopic flower which has fully formed floral organs and the more sparse second ectopic flower which has only formed a palea [89, 90, 139]. The second ectopic flower develops to varying degrees, this is thought to possibly be linked with resources available as the number of organs formed in both ectopic flowers correlates with meristematic region size [139]. This mutant phenotype is specific to the lemma and is relatively consistent. In the Bowman cultivar background, every mature lemma will form at least one ectopic flower when grown in greenhouse conditions (personal observation of more than 50 plants).

Imaging of the *Hooded* mutant so far has focussed on photographs at different developmental stages and SEM images. These have found that not only are the ectopic flower organs inverted, but the hairs on the adaxial surface on the lemma are inverted in the region of the first ectopic flower [89, 138-140]. In the base of the lemma, hairs orient distally as seen in the wild-type. However on the ectopic flower and just below it, the hairs orient proximally [89, 90, 139] (Figure 3.2.C) suggesting an inversion in organ polarity.

In addition to the formation of the ectopic flower, awn-like triangular outgrowths, called wings, form in the margins just below the ectopic flower (Figure 3.2.D). These wings are specific to the region below the first ectopic flower and do not form between the first and second ectopic flower. In the Bowman cultivar background these always form. It is not known whether the wings are a consequence of the global changes in growth which result in the formation of the inverted ectopic flower, or whether the wings represent a distinct developmental switch in shape triggered by changes in growth in the margins.

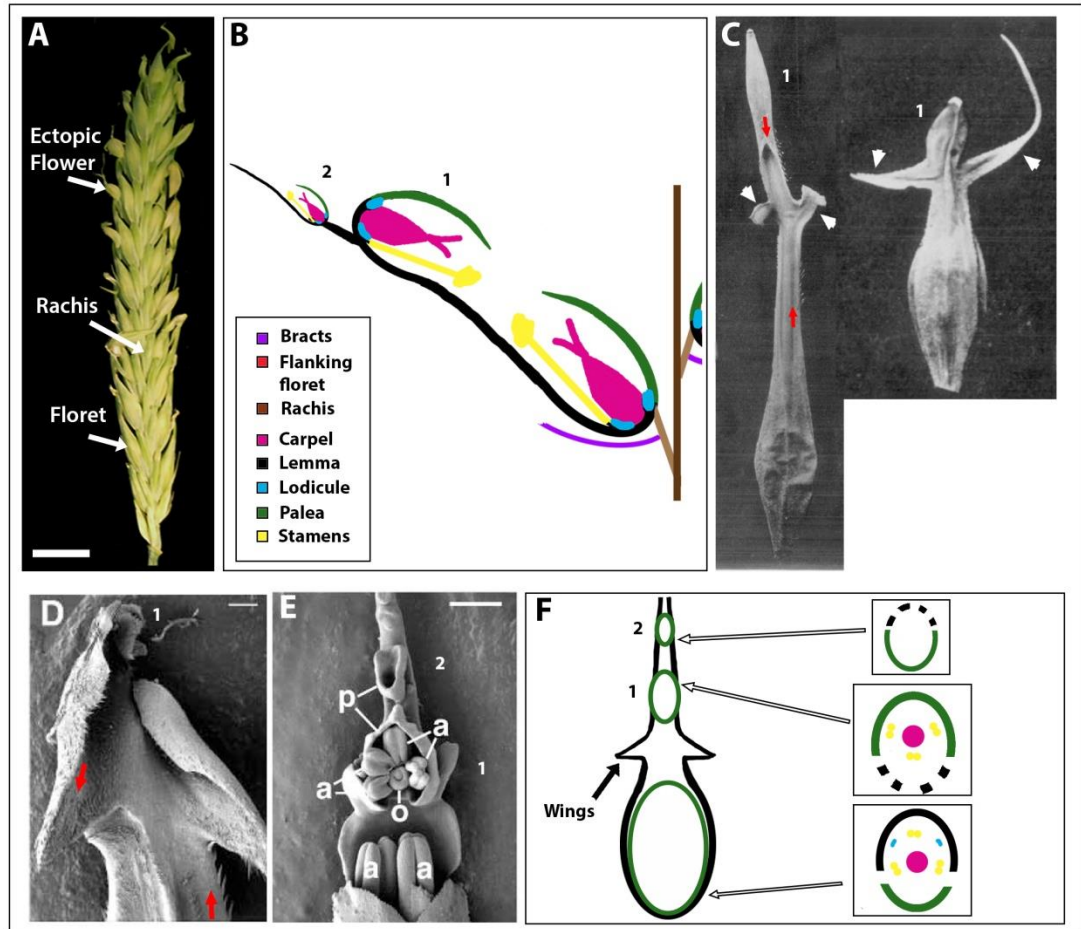


**Figure 3.2 The morphology of the *Hooded* mutant**

**A:** Photo of an inflorescence spike of a *Hooded* 2-row Bowman subcultivar of barley. The position of an individual floret, the rachis, and an ectopic floret replacing the awn are indicated. **B:** a floral diagram of a longitudinal section through a mature floret of a *Hooded* 2-row barley inflorescence spike, the rachis (brown), bract (purple) are indicated as well as the central floret organs; lemma (black), palea (green), lodicules (light blue), stamens (yellow) and carpel (pink). **C:** Photographs, adapted from Harlan 1931 [89], of *Hooded* florets, the white arrowheads indicate the wings, the red arrows indicate the orientation of the visible hairs. **D:** SEM of the wing region from a *Hooded* flower (image adapted from Williams-Carrier et al [138]), red arrows indicate the orientation of the visible hairs. **E:** SEM image of two ectopic flowers formed on the adaxial surface of the *Hooded* lemma (image adapted from Williams-Carrier et al [138]), the anthers of the basal flower (a), the ectopic paleas (p), ectopic anthers (a) and ectopic ovary (o) are indicated. **F:** Floral diagrams of the structure of the basal flower, the first and second ectopic flowers on the *Hooded* lemma, each diagram is from the perspective of a transverse section through the base of each flower, all of the colours are the same as in B, the dashed black line in the ectopic flowers indicate the position of the existing lemma. The number 1 or 2 indicates the first and second ectopic flower where relevant. Scale bar in A is 1cm. Scale bar in D is 270 $\mu$ m, E is 220  $\mu$ m.

### 3.1.3 Previous studies in the *Hooded* mutant.

The unusual inverted phenotype of the *Hooded* mutant has led to many morphological and genetic studies.

The dominant *Hooded* mutation is a 305bp tandem duplication in the fourth intron of the *KNOX* transcription factor *BKn3* which causes ectopic expression of *BKn3* in the lemma [90]. *BKn3* is the barley homologue of the transcription factor *KNOTTED1 (KN1)* in maize, and shares 90% similarity at the amino acid level [90]. *KN1* is involved in the maintenance of the shoot apical meristem [141] and is normally excluded from developing organs [134]. The normal exception to this rule is during the development of lobes and compound leaflets [5, 142] where the reactivation of *KN1* in the leaf margin is required for their formation in some species.

The ectopic expression of *BKn3* in the *Hooded* lemma has been reported to be specific to the predicted boundary between the lemma and the awn [138]. Although Muller et al reported that *BKn3* is also expressed in the lemma tip in wild-type barley [90], this was not reported in Williams et al, both at the mRNA and the protein level [138]. This mis-expression of *BKn3* in the developing lemma, has also been shown to be sufficient to induce the formation of the inverted ectopic floret and wings in barley [138]. Interestingly, when maize *KN1* is overexpressed in barley using the ubiquitin promoter (the ubiquitin promoter drives GUS expression throughout the plant) *KN1* protein is only found in the same region as *BKn3* is expressed in the *Hooded* mutant [138]. Overexpression of *KN1* in tobacco also causes ectopic meristems to form on the leaves, however they are not in an inverted orientation [90]. This suggests that *KN1* orthologues have a conserved function and additionally that there may be special regulation of *KN1/ BKn3* or unique features of boundary regions that enables *KNOX* expression. In support of this, the double *awnless (lks1)/ Hooded* mutant has an *awnless* phenotype [143] and lack ectopic flowers.

Detailed histological experiments have also shed light into the effects of *BKn3* mis-expression on lemma development. Early stages of lemma development have been reported to be the same between wild-type and *Hooded* [139, 140]. The first morphological differences arise when what is called the meristematic cushion forms on the adaxial side of the *Hooded* lemma near the distal tip [140]. This dome shape region then goes on to initiate organ primordia in the same order as a normal wild-type flower, apart from the difference that the palea is the first organ initiated as the existing lemma is used by the ectopic flower as its own [140]. Once

organ primordia have been initiated, awn-like appendages are formed below the ectopic flower called wings. However, extensive crosses into different genetic backgrounds have shown that the extent to which the phenotype develops varies significantly [89, 138, 140] and environmental factors can also influence the final phenotype [144]. At the cellular level, the first difference between the wild-type and *Hooded* lemma is the reduction in size of adaxial surface cells of the *Hooded* lemma. This is combined with the apparent deregulation of cell division orientation which is normally oriented parallel to the main axis of the lemma and awn [139].

Several hypotheses relating to how *BKn3* induces these effects on organ shape have been proposed. Through examining the number of cells going through DNA replication at different stages of development, it has been proposed that the difference in cell size and number is due to the increase in the rate of the mitotic cycle in *Hooded* (this can reach up to three times faster than wild-type). This was achieved by a reduction in the length of time spent in interphase (when elongation occurs) [144]. This has led to the hypothesis that *BKn3* induces the *Hooded* phenotype by increasing the speed of the mitotic cycle only. This makes the prediction that the developmental switches triggered by *BKn3* in the developing lemma arise through the modulation of growth rates only. However, this does not necessarily explain the consistently inverted phenotype of the ectopic flower.

Alternatively, Williams-Carrier et al hypothesised that the inverted ectopic flower arose through *BKn3* initiating a new inflorescence meristem on the developing lemma [138]. This proposes that a complete inflorescence unit is initiated on the lemma; two clusters of spikelets at 180° from each other on either side of the rachis; but only the central spikelet develops, forming ectopic flowers which are inverted relative to each other. This could be supported by previous observations that the region between the two ectopic florets (when they form) may be rachis-like [139]. However observations by Bonnett would contradict this as no glumes are formed, suggesting that the meristematic cushion cannot form an inflorescence meristem, instead it forms a floral meristem only [140].

An additional hypothesis proposes that *BKn3* may act as a secondary centre for a 'polarising gradient' which is normally produced by the main axis of the plant [139]. This 'polarising gradient' was hypothesised to be hormonal based, possibly auxin or cytokinin [139]. This could predict that *BKn3* directly affects axial information within the developing lemma in addition to the growth rate changes observed already. Stebbins et al observed that all of the

markers of polarity used, were late in development [139] and that the mechanism by which *BKn3* influences this 'polarising gradient' is unclear.

This published work highlights that *BKn3* is able to influence growth rate in the developing lemma through altering the speed of the mitotic cycle. However, although it is clear that axial information in the mature organ is likely to have been altered on the adaxial surface (as shown by hairs), it is still unclear if this change in axiality is directly triggered by *BKn3* and the precise underlying mechanism. In addition to this whether the wings are a consequence of the global changes in growth induced by *BKn3* or specific marginal changes in growth has not been explored. Therefore, the *Hooded* mutant provides an excellent system to assess how a single gene may influence growth and whether the developmental switches in shape seen in the *Hooded* mutant are due to changes in growth rate alone, or due to a combination of change in growth rate and axiality.

### **3.2 Aim of this project**

During this project, I aimed to use the *Hooded* mutant to answer the question: how can single genes modulate growth to trigger developmental switches in shape. This work also aimed to differentiate between the hypotheses that *BKn3* triggers the developmental switch in shape through modulating growth alone or a combination of growth rate and axiality changes. I also aimed to assess whether the wings were a consequence of the global change in growth in the lemma which led to the inverted ectopic flower, or whether the wings illustrate a separate developmental switch in shape triggered by specific changes in growth in the margin.

This work was done in collaboration with Dr Alexandra Rebocho, JIC. All experiments were carried out using the 2 row Barley subcultivar, Bowman. For clarity I will refer to the work I have done in the first person.

### **3.3 Characterising a developmental switch in shape in the barley flower: Staging ectopic flower development**

To assess the effects of the ectopic expression of *BKn3* on growth, the timing of events at both the cellular and tissue level during development need to be evaluated. This is

particularly important as previous studies have shown that genetic background and environmental conditions can influence the degree to which the mutant phenotype occurs [89, 138, 140, 144]. To develop a staging system for barley inflorescence development, a detailed timecourse of flower development and associated growth curves were generated. The barley subcultivar Bowman was used for all experiments as it seemed to consistently produce the full *Hooded* phenotype under greenhouse conditions.

Despite the importance of barley in agriculture, little information is available on the development of the inflorescence spike. Previous studies have mainly focussed on events in development relevant for leaf emergence and late floral development [145]. Similarly previous studies of the *Hooded* barley mutant did not include detailed and visual timecourses of floral development, making it difficult to assess the timing of morphological events. Additionally existing data on barley flower, and in particular lemma, development has been based upon scanning electron microscopy (SEM) or light microscopy which provide largely 2D information [138, 140]. I therefore chose to characterise the development of the wild-type and *Hooded* barley inflorescences over time in 3D as this would provide more detailed volumetric information about the morphogenesis of the barley flower for the first time.

To image the barley inflorescences in 3D, I used Optical Projection Tomography (OPT) [109, 110]. The data collected enabled me to digitally slice the 3D volume data, easily comparing it with 2D sliced tissue used in immunolocalisation and RNA *in situ* hybridisation protocols. The timecourse data enabled me to stage further experiments and define a timeline of events. This allowed me to test hypotheses relating to changes in growth and their effect on developmental switches in shape and explore the role of *BKn3* in modulating growth over time.

Time course samples of both wild-type and *Hooded* barley inflorescences were taken from the first developing tiller of each plant, with 2-3 replicates per time point and fixed in 100% ethanol before being imaged using OPT. Two time courses were originally collected, the first covering 240 hours of inflorescence development and the second covering 380 hours of development. Snapshot images of the OPT reconstructions were used to calculate organ sizes with Fiji [146], focussing on the morphology of the fifth floret from the base of the spike and the whole spike. Measurements included spike length and width and floret 5 width, lemma length and lemma width.

Due to flowering times varying slightly (due to growth conditions varying in the greenhouses), I first established a morphological time zero from which I could align the timecourses. Time zero morphology (T0) was based on the first timecourse before any morphological difference was observed between the wild-type and *Hooded* lemmas. T0 was defined by calculating the average size of the fifth floret in the first time point for both wild-type and *Hooded* flowers. The measurements used were floret width, lemma width and lemma length of floret 5 (see Figure 3.4 for examples of how the measurements were taken). T0 morphology was defined as a floret 5 with dimensions which lie within two times the standard deviation of the mean measurement. (See Table 3.1)

Floret Width ( $\mu\text{m}$ )			Lemma Width ( $\mu\text{m}$ )			Lemma Length ( $\mu\text{m}$ )		
Mean	Upper bound	Lower bound	Mean	Upper bound	Lower bound	Mean	Upper bound	Lower bound
115.9	129.1	102.6	36.1	46.1	26.1	184.5	197.7	171.3

**Table 3.1 Dimensions of the calculated T0 barley floret 5 morphology.**

N=4. Upper and lower bounds of T0 morphology described by the mean plus or minus two times the standard deviation.

The mean dimensions of the fifth floret in the second timecourse were then compared to the T0 morphology boundaries to see if the morphology of the first time point lay within the T0 definition. All three measurements for the first timepoint lay within the T0 morphology definition; 118.9 $\mu\text{m}$  floret width, 39.3 $\mu\text{m}$  lemma width and 186.4 $\mu\text{m}$  lemma length. This allowed me to combine both timecourses with their first time point counted as morphological T0 after which every time point could be plotted in approximate hours since T0 based on harvest time.

Once the timecourses were combined, I was able to assess morphological changes over a period of 380 hours of inflorescence development (See Appendix B for a more comprehensive set of timecourse images) in both wild-type and *Hooded* barley, particularly focussing on lemma development which had initiated before T0 . All developmental times in hours stated from now on will relate to hours from morphological T0.

Early in development both wild-type and *Hooded* inflorescence spikes have the same morphology (Figure 3.3.A and F). Spikes mature acropetally, the most mature florets at the

base and the youngest at the tip. T0 stage spikes have no mature flowers and the florets at the tip are newly emerged floral meristems (Figure 3.3.A.i and F.i). T0 spikes have 6 rows of small floral meristem domes, clustered in threes, which are formed on opposite sides of the rachis (visible in the front view in Figure 3.3.A.i, F.i and the side view in Figure 3.3.A.iii, F.iii and the transverse cross-section in Figure 3.3.A.v, F.v). In each cluster of three floral meristems, only the central one will go on to develop a mature floret, the two flanking will abort (Figure 3.3.A.v and F.v indicate a transverse cross-section through one cluster of three floral meristems showing the position of the central floret (CF) and the flanking florets which will abort (FF)). At this stage the flanking floral meristems are already smaller than the central (this is clearest in the transverse cross-section view in Figure 3.3.A.v, F.v). The central floret has a small lemma primordium forming on the proximal side of the dome (Figure 3.3.A.ii, F.ii longitudinal cross-sections through the inflorescence spike, the lemma is outlined in white). The lemma primordium curves around the proximal side of the floral meristem dome (Figure 3.3.A.iii, F.iii, white dotted line outlines the lemmas).

By 120 hours after T0, all of the floral organs have been initiated in all but the florets closest to the apex (barley inflorescence meristems are indeterminate) (Figure 3.3.B and G). By this timepoint the flanking florets are clearly distinct from the central floret, remaining very small (the difference between the florets can be seen in the transverse cross-sections in Figure 3.3.B.v, G.v) and do not develop elongated lemmas and awns (Figure 3.3.B.i, G.i). The wild-type and *Hooded* inflorescence spikes still appear to share the same morphology with similar elongation of the lemmas beyond the body of the flower (Figure 3.3.B.i and ii, G.i and ii). By 170 hours, the wild-type and *Hooded* spikes still appear similar (Figure 3.3.C and H), with the same oval shaped longitudinal cross-sections through the base of the florets (Figure 3.3.C.iv and H.iv) and the same morphology in transverse cross-sections through the spike, showing the developing central floret with multiple floral organs and the reduced, aborted flanking florets on the rachis (Figure 3.3.C.v and H.v).

By 240 hours this similarity in the shape and morphology of the cross-sections longitudinally through the base of the flower (Figure 3.3.D.iv and I.iv) and transversely through the spike (Figure 3.3.D.v and I.v) is maintained. However when looking at the morphology of the whole spike (Figure 3.3.D.i and I.i) the wild-type and *Hooded* spikes look very different. The wild-type florets have long elongated awns, giving the appearance of a 'hairy' spike (Figure 3.3.D) whereas the *Hooded* florets have shorter, wider lemmas, making them appear more compact (Figure 3.3.I). This morphology difference is due to the formation of the ectopic floret on the

lemma in the *Hooded* mutant. This difference is accentuated as the spikes develop. By 340 hours, the wild-type spikes have long thin awns, which extend beyond the tip of the inflorescence spike (Figure 3.3.E), whereas the *Hooded* spike does not (Figure 3.3.I). No other difference is seen in the cross-sectional morphology of the spikes. Both the transverse cross-section through floret 5 (Figure 3.3.E.v and I.v) maintain the same shape as before with the two clusters of 3 florets, with the central floret larger and more fully developed than the flanking ones (which have aborted fully by this stage) and the longitudinal cross-sections through the base of the central florets (Figure 3.3.E.iv and I.iv) still show an oval shaped floral structure.

Whole spike morphology over time does not vary significantly between the wild-type and *Hooded* mutant (Figure 3.3). This is supported by the growth curves for spike length and width. The natural logarithm ( $\ln$ ) of spike length, (measured from the base of the spike to the tip of the spike not the tip of the upper awns, see Figure 3.5.A for a diagram explaining how the measurement was taken), increased over time for both genotypes, but was slightly faster in the *Hooded* mutant with a rate of 0.76% per hour versus 0.58% per hour (these rates were taken from the gradient of the equation of the lines of best fit in Figure 3.5.A). However, variation in spike length was high within both genotypes possibly due to differential numbers of flower initiation along the inflorescence spikes (as barley spikes are indeterminate different numbers of florets can go on to mature) and differential internode elongation in the rachis. This variability makes it a poor measurement from which to stage other experiments.

Spike width also increased over time (Figure 3.5.B). Similar to spike length,  $\ln$  spike width also increased at a slightly faster rate in the *Hooded* mutant, 0.42% per hour versus 0.31% per hour in the wild-type spike, possibly due to the development of the ectopic flower increasing the width of the *Hooded* lemma. However again, due to the high variation in spike length and width within each genotype spike width does not provide a reliable measurement from which to stage any other experiments.

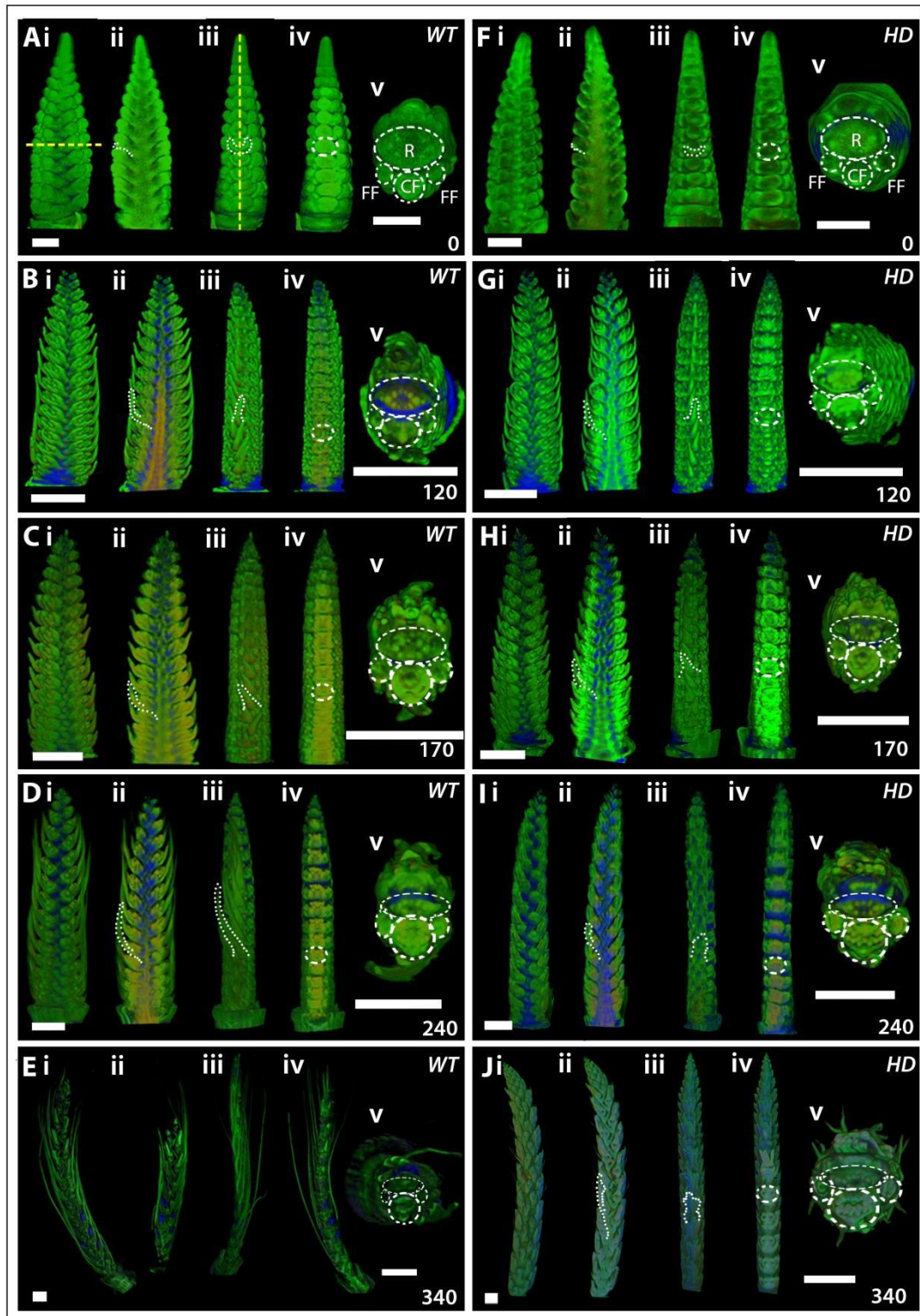


**Figure 3.3** Whole spike morphology of wild-type and *Hooded* 2-row Bowman barley over 340 hours of inflorescence development.

OPT images of developing spikes from T0 to 340 hours after T0. *A-E*: wild-type. *F-J*: *Hooded*. *i*: whole spike, front view. *ii*: longitudinal cross-section through the spike. *iii*: whole spike, side view. *iv*: longitudinal cross-section through the side of the spike at the base of the developing florets. *v*: transverse cross-section through the spike at floret 5. Numbers are

approximate hours since T0. The rachis (R), flanking florets (FF) and central florets (CF) are indicated. Scale bars are 200µm in A and F, 1mm in A-D and G-I and 2mm in E and J.

As the wild-type and *Hooded* mutants only vary in the development of the lemma and awn, I characterised the development of floret 5 (the central floret that matures, not the flanking aborted florets), focussing on lemma/awn development, over time using OPT imaging of the same samples shown in Figure 3.3.

At T0 the lemma morphology is the same in both wild-type (Figure 3.4.A) and *Hooded* (Figure 3.4.E) florets. The lemma has started to form as a proximal outgrowth from the floral meristem, with a small dome like shape (Figure 3.4.A.ii and E.ii). The rest of the floral organs have not yet initiated. 120 hours later the lemmas in both wild-type and *Hooded* samples are distally elongated (Figure 3.4.B and F). The other floral organs have also been initiated.

The first difference in lemma development between wild-type and *Hooded* florets has started before 170 hours (Figure 3.4.C and G). The lemma in the wild-type sample continues to elongate (Figure 3.4.C.ii) forming the awn. However, in the *Hooded* mutant the lemma has formed a bump on the adaxial surface (Figure 3.4.G.ii, white arrowhead). This bump is what the literature describes as the ‘meristematic cushion’ [90, 139], and is the region from which the ectopic flower will form. This is the first morphological difference which arises between the developing wild-type and *Hooded* lemmas. From this point onwards the morphology of the wild-type and *Hooded* lemmas diverge.

In the wild-type, the lemma tip differentiates to develop into the awn which rapidly elongates (Figure 3.4.D). The wild-type awn becomes increasingly thinner towards the tip (Figure 3.4.D.ii). In the *Hooded* floret this extension is not observed (Figure 3.5.H), instead the ‘meristematic cushion’ develops into a floral meristem and floral organs begin to develop. By 240 hours, many of the floral organs in the first ectopic flower have been initiated (Figure 3.4.H.ii, white arrowhead). In some cases a second ectopic flower can develop above the first, this develops to varying degrees after the first (none of the samples in Figure 3.3 or 3.4 show the second ectopic flower).

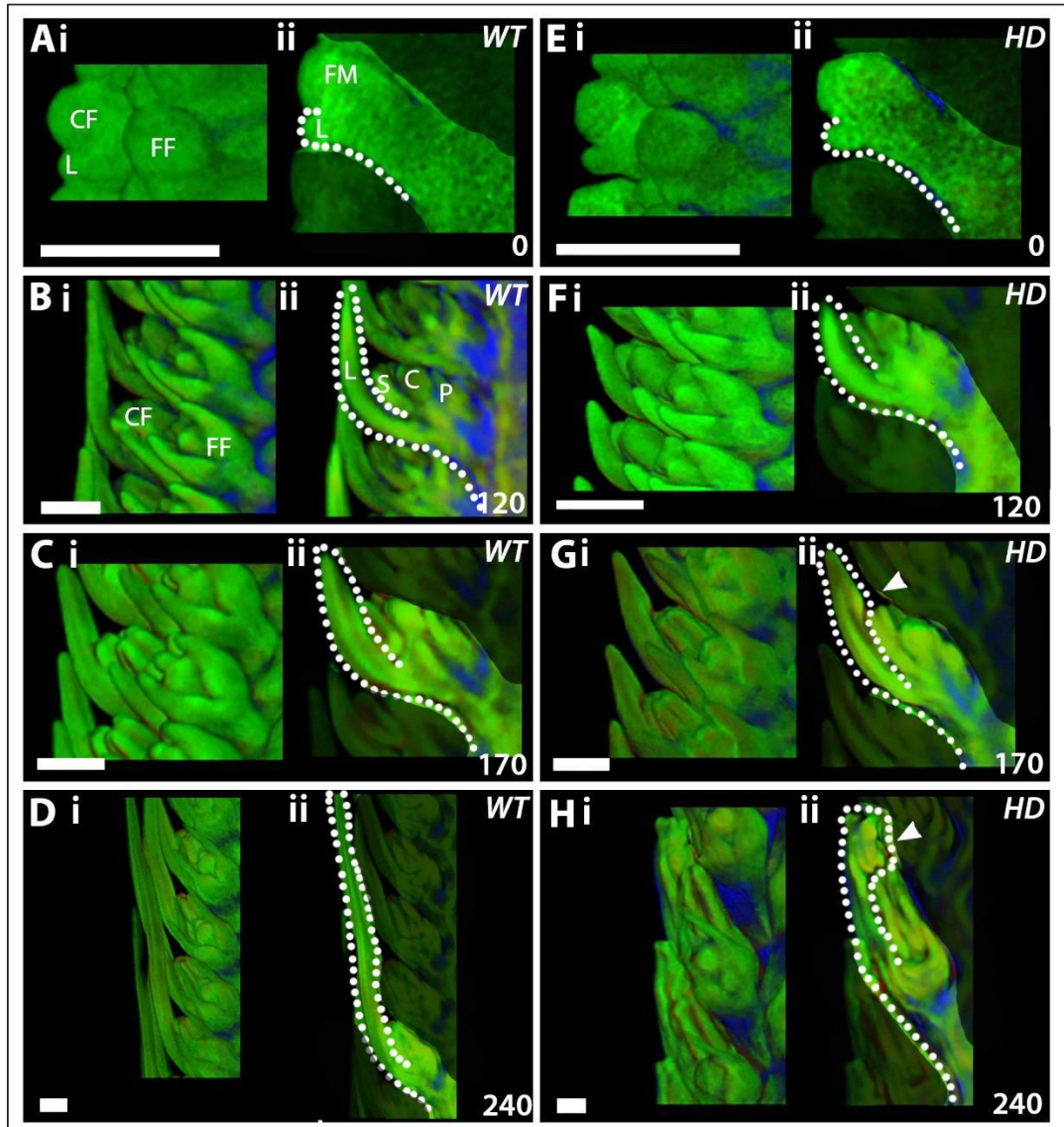


**Figure 3.4** The morphology of the floret 5 during different times in development. OPT imaging of the central floret 5<sup>th</sup> from the base of the inflorescence spike. A-D: wild-type florets. E-H: Hooded florets: *i*: whole floret view, *ii*: longitudinal cross-section through the developing florets. The outline of the developing lemma and awn is highlighted with the white dotted line in the cross-section images (*ii*). Numbers are approximate hours since T0. The central floret (CF), flanking floret (FF), lemma (L), stamen (S), carpel (C) and palea (P) are indicated. Scale bars are 200 $\mu$ m.

The *In floret width* increased linearly over time for both the wild-type and Hooded flowers at a very similar rate; 0.48% per hour for Hooded and 0.44% per hour for wild-type florets (Figure 3.5.E). In contrast to this, although the *In lemma length* for both Hooded and wild-type florets increased linearly over time, the increase in lemma length in the wild-type floret was at a faster rate of 1.06% per hour versus 0.87% per hour in Hooded (Figure 3.5.C). This

higher rate in lemma length growth in the wild-type is because of the rapid extension of the awn in wild-type flowers from around 190 hours onwards which does not occur in the *Hooded* mutant. This difference in lemma length correlates with previous studies which found that cell elongation between successive rounds of cell division in the *Hooded* mutant was reduced [139]. Conversely the increase in *ln lemma width* is faster in the *Hooded* lemma (0.55% per hour) than the wild-type (0.43% per hour). This is possibly due to the development of the ectopic flower on the *Hooded* lemma which starts at around 160 hours.

As floret width increased at a very similar rate in both genotypes over time, I selected it as the measurement from which all further experiments would be staged. The similarity in the growth rates between wild-type and *Hooded* floret width meant that I was able to combine the lines of best fit to a single line. The equation of which ( $\ln(\text{floret width}) = 0.0046(\text{time in hours}) + 4.9305$ ) would be used to calculate the approximate time of development for other samples (Figure 3.5.F) enabling cross comparisons between data sets.

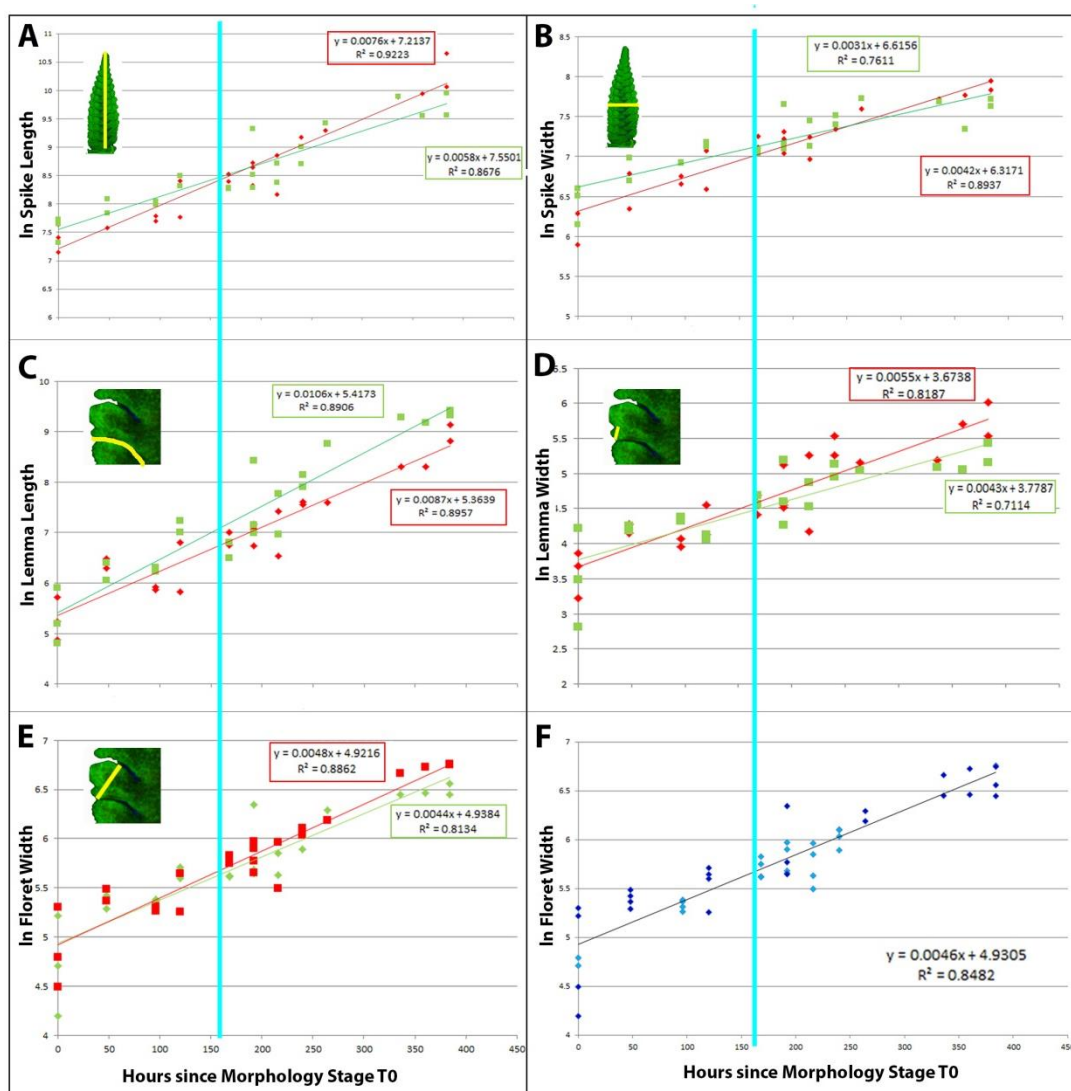


**Figure 3.5** Graphs illustrating natural logarithm (ln) of the dimensions of developing barley inflorescence spikes and floret 5 in wild-type and *Hooded* samples.

A: ln spike length. B: ln spike width. C: ln lemma length in floret 5. D: ln lemma width in floret 5. E: ln floret width in floret 5. F: combined dataset for ln floret width in floret 5 (wild-type and *Hooded*), indicating the line from which all experiments will be staged. X axis: hours since morphology T0. Y axis: ln measurement. Each line of best fit has its equation and  $R^2$  value displayed. Green: Wild-type samples. Red: *Hooded* samples. Light blue: first time course. Dark blue: second time course. Light blue lines: 160 hours when morphology starts to differ between wild-type and *Hooded*. Inset images: yellow line indicates how the relevant measurement was taken.

As the developmental switch in shape during *Hooded* lemma development occurs on the adaxial surface, to characterise developmental events further I needed to focus on this surface. However, this is not possible using OPT as the adaxial surface is close to the main axis of the spike, obscuring it from view. Therefore I imaged whole inflorescence samples using light microscopy and measured the floret width of every flower along the spike using Fiji [146]. I then dissected off the lemma of each floret, fixed them to a slide and stained the cell walls using calcofluor white. I then imaged the adaxial surface of the lemma using confocal microscopy. This developed a time series illustrating the broad morphological changes which occur on the adaxial surface of the *Hooded* lemma over time (Figure 3.6).

At 120 hours, when the *Hooded* lemma still resembles the wild-type, it has a smooth surface and a triangular shape (Figure 3.6.A). The first change to the *Hooded* adaxial lemma surface is the development of a dome of tissue in the middle of the adaxial surface which is the 'meristematic cushion' (the ectopic floral meristem, Figure 3.6.B, white arrowhead), which has formed by 170 hours. This ectopic floral meristem then begins to develop organ primordia, first initiating a semicircular primordium on the distal side of the dome (Figure 3.6.C). This curved primordium, wraps around the edges of the meristematic dome (Figure 3.6.C). Previous studies on the *Hooded* mutant have proposed that this first organ is the palea of the ectopic flower [138, 140] (Figure 3.6.C.iii illustrates an approximate floral diagram of the ectopic flower, orange is the meristematic cushion, green is the ectopic palea, yellow, the developing stamens). The next prominent organ primordia to form are the stamen primordia (Figure 3.6.C) which initially appear to fill the centre of the space enclosed by the lemma and palea. By 340 hours all of the floral organs in the ectopic flower appear to have been specified (Figure 3.6.D and floral diagram in D.iii). A second ectopic flower can form above the first (Figure 3.6.C, 2<sup>nd</sup> arrowhead), but the degree to which it matures is highly variable. If a second flower forms, a rudimentary curved palea forms on the proximal side of the meristematic region (Figure 3.6.C.ii, p and C.iii.2 green) and sometimes either reduced stamen or carpel tissues can form inside this. Previous work has found variability in the number and stage of development of different organs within the ectopic flowers, which can depend on genetic background and environment [89, 140]. Our results agree with those published; first a meristematic cushion on the adaxial surface of the lemma develops, which then goes on to form floral organ primordia distally. If a second meristematic region forms above, the organ primordia form proximally. This highlights a possible inversion of axial information within the tissue before organ primordia are initiated.

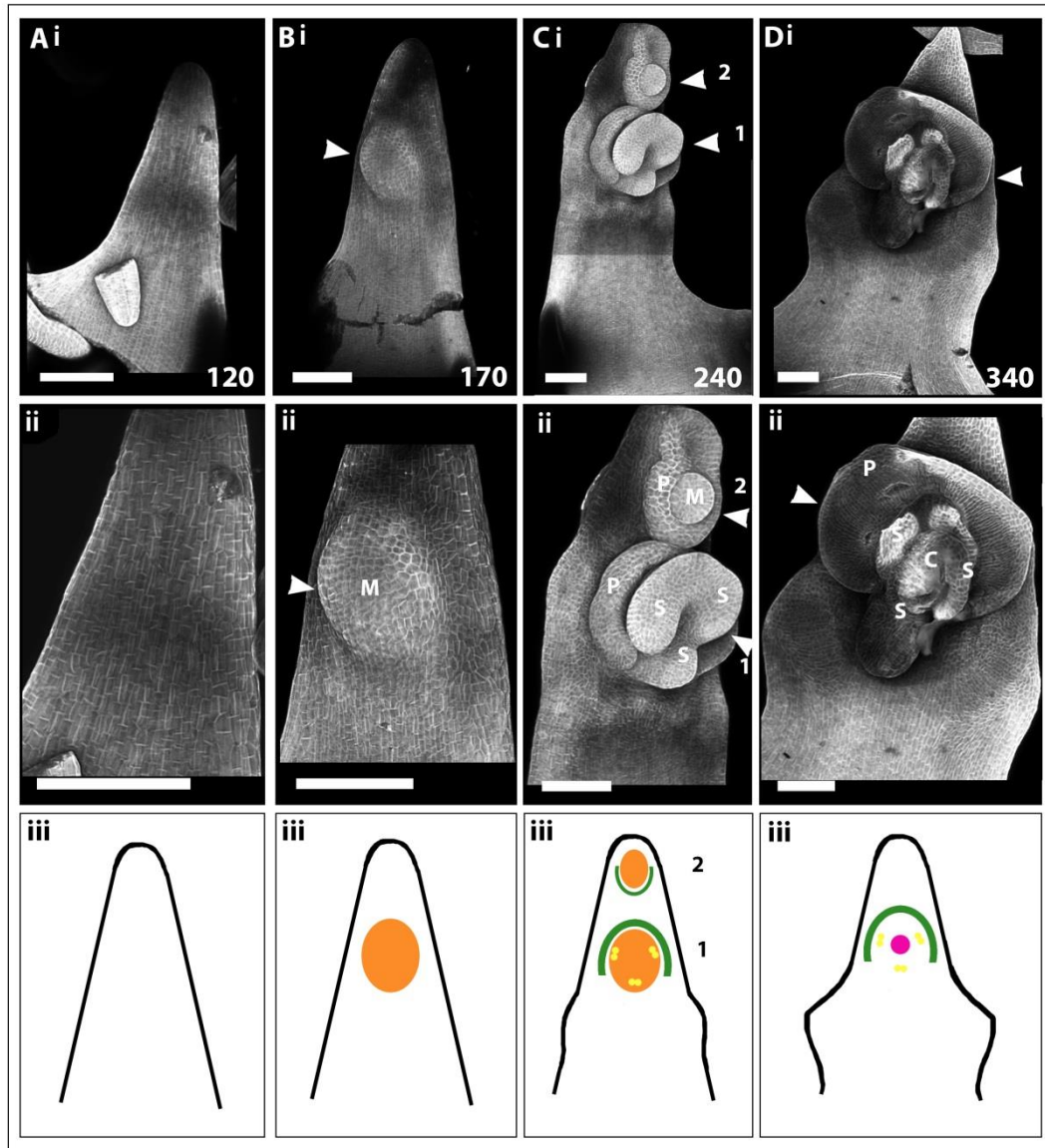


**Figure 3.6 Confocal images of the adaxial surface of calcofluor stained *Hooded* lemmas at different stages in development.**

White arrowheads indicate the first and second (only in C, 2) ectopic floral meristems. Numbers indicate approximate times since T0. Meristematic regions (M), palea (P), stamens (S) and carpels (c) are indicated. *iii*: floral diagrams explaining the morphology of the adaxial surface, the lemma shape (black), meristem tissue (orange), developing stamen primordia (yellow), palea (green) and carpel (pink) are shown. The first and second ectopic flowers are indicated by the number 1 and 2 respectively where appropriate. Scale bars are 100 $\mu$ m.

Using this timecourse of adaxial morphology markers, combined with the growth curve based upon floret width, we can now stage future experiments. The *Hooded* flower is similar to wild-type up until around 160 hours. Development of the *Hooded* lemma then diverges

from wild-type and certain key morphological changes occur. The first morphological difference is the development of the meristematic cushion on the adaxial surface by 170 hours. This morphological analysis suggests that there is a change in axial information (which may underlie the inverted flower phenotype) before 170 hours when the ectopic meristem forms.

### **3.4 Ectopic expression of *BKn3* in the *Hooded* lemma precedes the formation of the ectopic meristem**

To establish when and where ectopic expression of *BKn3* was during the development of the *Hooded* lemma and thus the earliest point at which changes in growth could occur, I chose to use RNA *in situ* hybridisation. The RNA *in situ* protocol used was based on Coen et al 1990 [147] and modified by Alexandra Rebocho for use in barley.

I used NCBI Blast services [148] of the ZmKN1 protein sequence and the construction of a basic guide phylogenetic tree to first identify the correct sequence for BKn3 in the available barley sequences. Since the barley subcultivar Bowman genome [149] was published in 2012, I have been able to add further sequences to strengthen the phylogenetic tree in Figure 3.7.A. The guide tree generated indicated the relationships between the protein sequences from *Arabidopsis thaliana* (At), *Zea mays* (Zm), *Oryza sativa* (Os), *Antirrhinum majus* (Am) and *Medicago truncatula* (Mt) and Barley (Hv) and using this I identified the sequence from barley which was most likely the homologue of ZmKN1, corresponding to the barley gene *BKn3*. In collaboration with Alexandra Rebocho, using the corresponding cDNA sequence (AK376780), I designed and made a 600bp *BKn3* specific antisense, DIG labelled probe targeting the N terminal region (318bp-STOP codon) (Figure 3.7.B shows the position of the probe sequence on the cDNA map of *BKn3*). The antisense probes hybridised with the *BKn3* mRNA in sliced, paraformaldehyde fixed tissue and the localisation of the *BKn3* mRNA was visualised through antibody recognition of DIG followed by a bcip/nbt precipitation reaction.

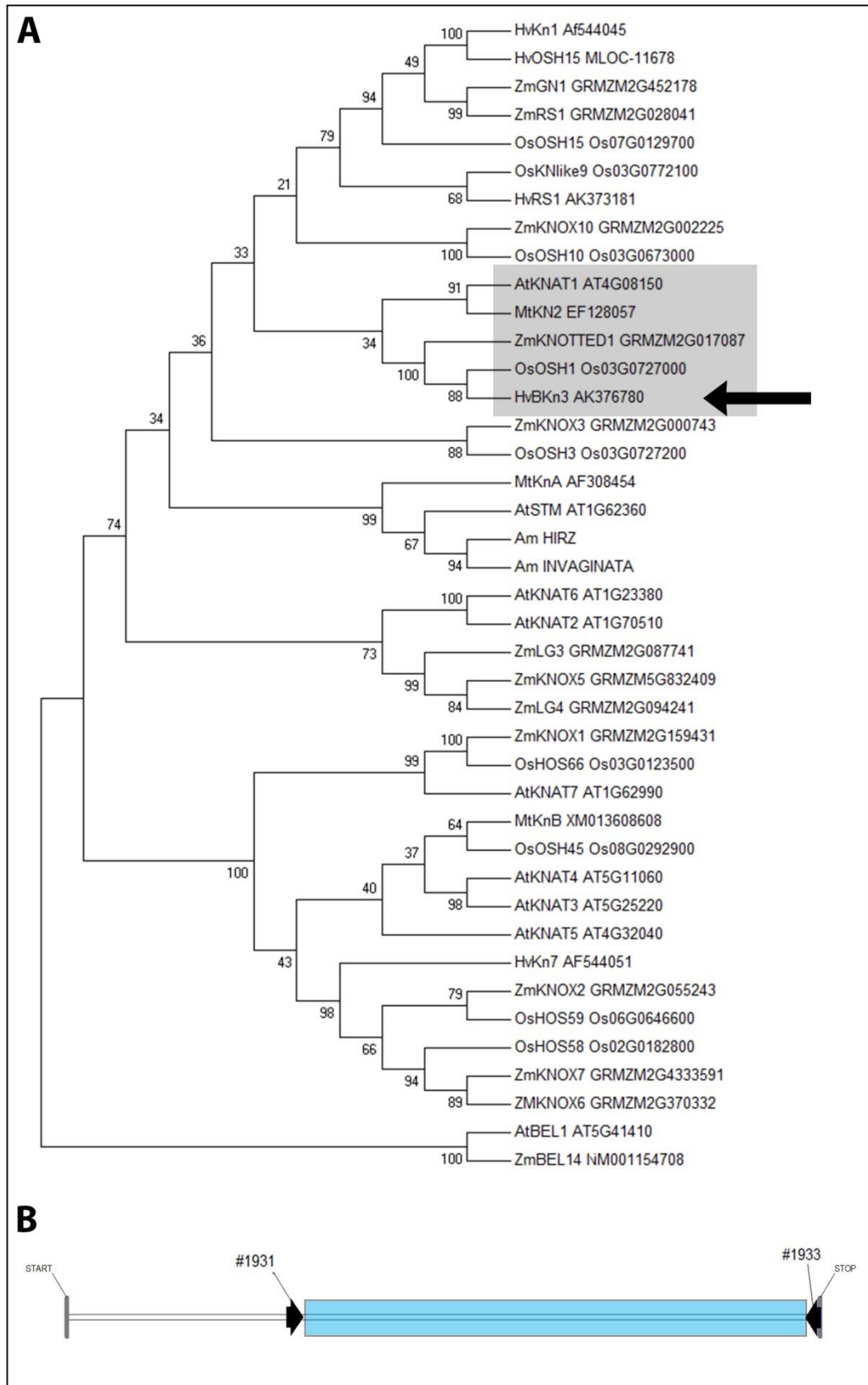


**Figure 3.7 Phylogenetic Analysis of KNOTTED1 like proteins.**

A: Phylogenetic analysis of KNOTTED1 like proteins. Protein sequences were identified using

NCBI BLAST searches of ZmKNOTTED1. Sequences are from *Arabidopsis thaliana* (At), *Antirrhinum majus* (Am, unpublished genome), *Hordeum vulgare* (Hv, Barley), *Medicago truncatula* (Mt), *Oryza sativa* (Os) and *Zea mays* (Zm). Bootstrap values for each node are illustrated. The black arrow indicates the position of barley BKn3, the grey box highlights the sequences closet to ZmKNOTTED1. B: A map of the barley *BKn3* cDNA with the position of the primers (black arrows) used to generate the RNA *in situ* probe template, the cloned region (blue) and the primer reference numbers indicated, (see Materials and Methods Table 1.9 and Table 1.10 the primer for sequences and plasmid maps).

I carried out RNA *in situ* hybridisation using the *BKn3* specific probe on multiple different stages of barley inflorescence development and staged the results using the method outlined in section 3.3 based on the OPT timecourses. All sections shown are middle longitudinal sections through the developing flower corresponding to the position shown in the OPT images in Figure 3.8.J (box *i* shows the approximate position of the slice, box *ii* shows a zoomed-in image of a single floret).

Both wild-type and *Hooded* inflorescences had *BKn3* expression in the base of the individual florets from very early developmental stages (even before T<sub>0</sub>, which is not shown). Figure 3.8 A and F show *BKn3* expression around 90 hours in single *Hooded* (A) and wild-type (F) florets. These images show that *BKn3* was localised to the central, basal region of the flower and was excluded from the lemma (white dotted line) and other developing organs (stamens, *s*, carpel, *c*, and palea, *p*). Zoomed-in images of the developing lemma (Figure 3.8.A.ii and F.ii), showed a complete absence of *BKn3* mRNA. This is consistent with the role of *BKn3* in meristem maintenance [141] and it's normal exclusion from differentiating tissues, as well as previous reports on *BKn3* mRNA and protein localisation [138] in young stages and in wild-type tissue.

Throughout wild-type development *BKn3* continued to be completely excluded from all developing organs (Figure 3.8.F-I). *BKn3* mRNA was localised to the central, basal region of the wild-type flower until maturity. There was a complete absence of *BKn3* mRNA in the lemma throughout development as shown by zoomed-in images of the developing wild-type lemmas in Figure 3.8.F-I.ii. This was as expected for a gene normally involved in the regulation of cellular meristematic identity.

Unlike in wild-type, the *Hooded* mutant had *BKn3* expression reactivated in the developing lemma. This reactivation of *BKn3* expression occurred at around 110 hours, with very faint signal in the adaxial region of the lemma (Figure 3.8.B, white arrowhead). This *BKn3*

expression region marked the site at which the ectopic flower would form. By 170 hours when the meristematic cushion had formed on the lemma, *BKn3* expression in the developing lemma was very strong (Figure 3.8.C, white arrowhead). This expression domain was very distinct from the rest of the lemma tissue, isolated to the distal, adaxial half of the developing lemma (Figure 3.8.C.ii). This was a region proposed previously to correlate with the lemma-awn transition boundary [138]. As development progressed and organ primordia were initiated in the ectopic floral meristem on the lemma, *BKn3* was excluded from the organ initiation sites (Figure 3.8.D.ii, yellow dashed regions). This exclusion from the differentiating ectopic floral organs was maintained throughout the rest of development (Figure 3.8.E) as it is in a normal wild-type flower. This indicates that *BKn3* still maintained its normal function in the ectopic floral meristem.

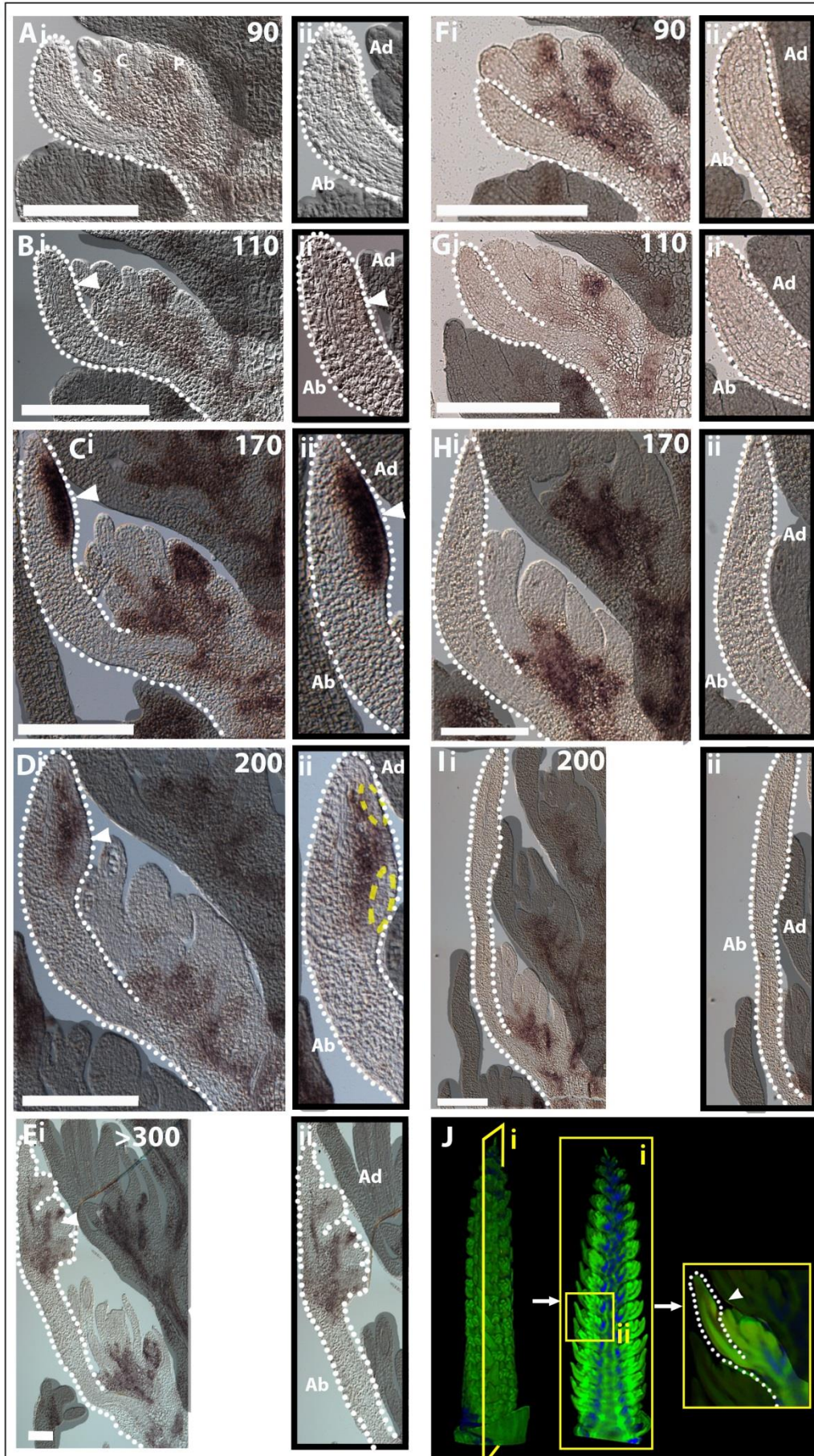


**Figure 3.8 Localisation of *BKn3* mRNA in central longitudinal sections through developing wild-type and *Hooded* barley flowers**

mRNA localisation determined by RNA *in situ* hybridisation using a specific DIG labelled antisense probe for the Bowman Barley *BKn3* cDNA sequence. Hybridised in paraformaldehyde fixed tissue, sliced longitudinally through the developing lemma and flower. *BKn3* mRNA localisation is shown by the dark brown/black staining. *A-E*: *Hooded* flowers. *F-I*: wild-type flowers. *i*: middle longitudinal section through the whole flower, a single flower is highlighted by shading out other tissues in the image. *ii*: zoomed-in image of the lemma in *i*, showing the localisation of *BKn3* mRNA in the lemma only. *J*: OPT diagram of how the images were taken. *J.i*: the yellow box indicates the orientation of the slice through the barley spike. *J.ii*: a zoomed-in image of the central slice, indicate in *i*, showing a single floret, like those shown in the *in situ* images. The outline of the lemma is indicated by the dotted white line. The position of ectopic expression of *BKn3* is indicated by white arrowheads. The yellow dashed line in *G.ii* highlights the regions where *BKn3* is excluded from developing organ primordia. *Ab*: Abaxial side of the sectioned lemma. *Ad*: Adaxial side of the sectioned lemma. The numbers indicate the approximate time from morphological T0 in hours. All scale bars are 250µm.

This expression pattern of *BKn3* differs to that shown by Muller et al 1995 [90]. They reported that *BKn3* was localised strongly in the tips of developing lemmas prior to hood emergence and in wild-type lemmas. I do not see evidence of this expression pattern in my experiments. Their RNA *in situ* hybridisation data also indicates that *BKn3* mRNA is localised to the adaxial half of the *Hooded* lemma, once hood initiation has occurred and they report that the expression of *BKn3* is downregulated as hood development progresses, this is similar to what I observed.

My mRNA localisation patterns also support data from William-Carrier 1997 [138], who used immunolocalisation of KN1 to look at *BKn3* protein distribution in the developing *Hooded* lemma and in barley plants overexpressing KN1 which replicate the *Hooded* phenotype. They reported adaxially localised *BKn3* protein in the developing mutant and transgenic lemmas which goes on to be maintained in the base of the ectopic floret and excluded from the developing ectopic organs. They also reported that they saw no localisation of *BKn3* protein in the wild-type lemma at all. This corresponds to my mRNA localisation data in *Hooded* and wild-type barley tissues.

This RNA *in situ* data shows that *BKn3* is ectopically expressed in the *Hooded* lemma before the visible development of the ectopic floral meristem on the lemma (at around 110 hours since T0) and that this ectopic expression is maintained throughout the rest of ectopic floral

development. In wild-type flowers the expression of *BKn3* is completely excluded from developing lemmas from an early stage and remains excluded throughout development. The timing of *BKn3* expression at around 110 hours provides a key timepoint in the exploration of how *BKn3* influences growth in addition to the changes to the mitotic cycle previously reported to occur before the meristematic cushion is formed at 170 hours.

### **3.5 The ectopic expression of *BKn3* in the *Hooded* lemma induces a reorientation in axial information at the cellular level**

One hypothesis is that *BKn3* expression in the *Hooded* lemma is able to induce a reorientation in axial information before ectopic flower development. Published reports have so far only looked at late stage axiality markers. I made the assumption that axial information within the developing lemma is provided by a polarity based axiality system. Therefore to explore whether *BKn3* was able to change axial information at the cellular level before the meristematic cushion was formed, I used PIN1 localisation as a marker of axiality (also referred to as tissue cell polarity in the context of the polarity based axiality system).

Within the grasses *AtPIN1* has several homologues [118], *SoPIN1*, *PIN1a* and *PIN1b*. To assess which *PIN1* family member would be the best marker of cellular axial information within the barley lemma, I first looked at the expression patterns of *SoPIN1*, *PIN1a* and *PIN1b* candidates in developing *Hooded* lemmas, focussing at around 170 hours as this is when *BKn3* expression is very strong in the developing lemma.

To identify the candidates for *PIN1a*, *PIN1b* and *SoPIN1* homologues in the published barley sequence data, I constructed a basic guide phylogenetic tree using protein sequences, taken from NCBI BLAST searches of *AtPIN1* and *AtPIN2* protein sequence, and published sequences for *Medicago truncatula* (Mt), *Zea mays* (Zm), *Oryza sativa* (Os) and *Brachypodium distachyon* (Bd) (Figure 3.9.A, the three separate clades are highlighted, grey indicates the *PIN1* family, the dashed outline boxes highlight the specific clades, *PIN1a* (green), *PIN1b* (red) and *SoPIN1* (blue)). Once identified (highlighted by the black arrows in Figure 3.9.A), the published barley cDNA sequences for *PIN1a* (MLOC12686), *PIN1b* (MLOC64867) and *SoPIN1* (MLOC293) were used to design and clone antisense probes for RNA *in situ* hybridisation. The *PIN1a* probe targeted the ATG to 426bp (Figure 3.9.B), the *PIN1b* probe targeted -116bp to 242bp (Figure 3.9.C, the probe covered the upstream 3' region because the original

published sequence used has an ATG further upstream) and *SoPIN1* targeted 165bp to 578bp (Figure 3.9.D), and each was unique to the specific PIN sequence. There was one other PIN1a like candidate (AK357068) however this was not explored as the primers used did not successfully clone it.

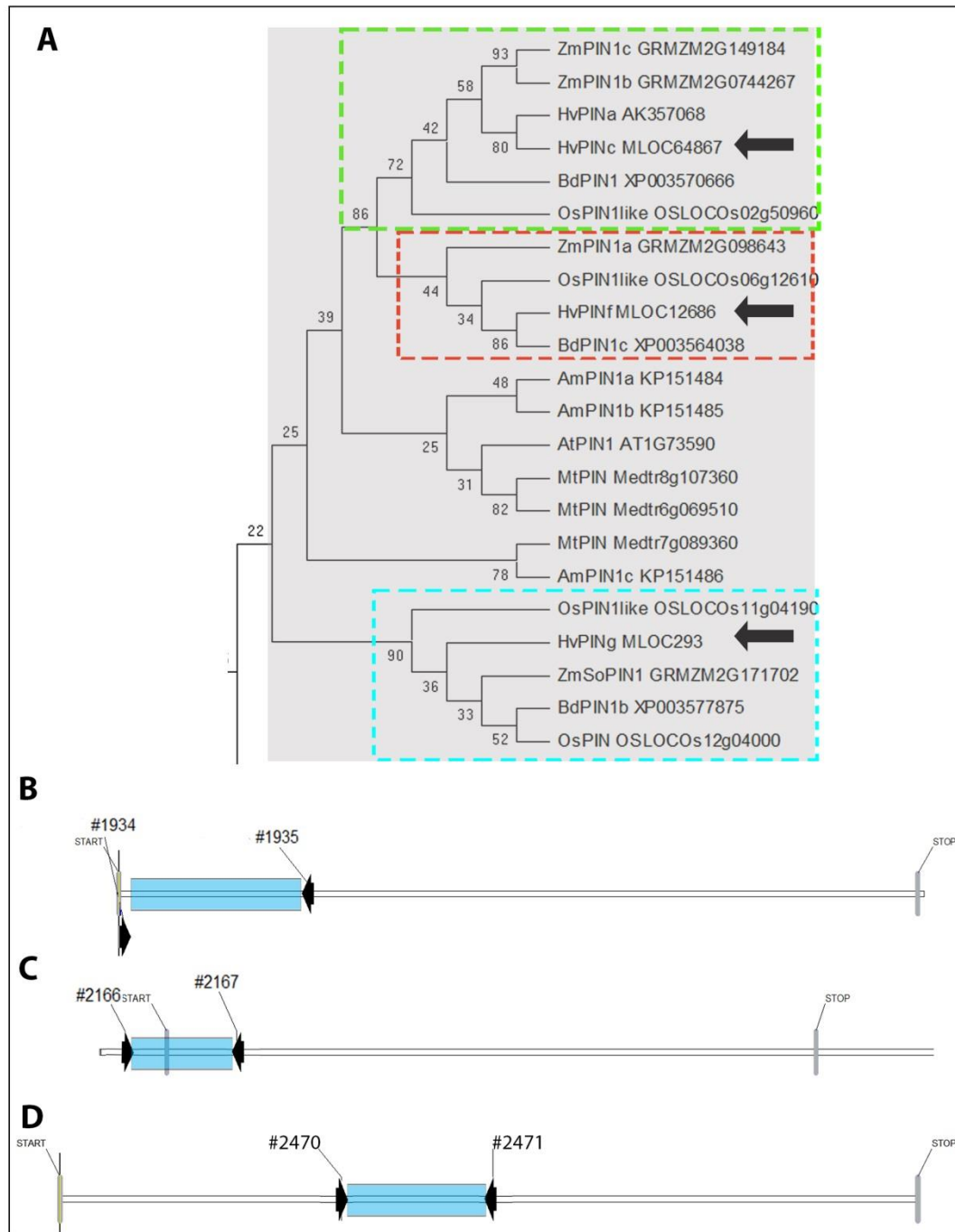


**Figure 3.9 Guide phylogeny tree of the *PIN1* family**

A: guide phylogenetic tree of PIN1 protein sequences from *O.Sativa* (Os), *A.thaliana* (At), Barley (Hv), *Z.mays* (Zm), *Antirrhinum majus* (Am) *Brachypodium distachyon* (Bd) and *Medicago truncatula* (Mt).The grey box highlights the PIN1 family. The red represents the

PIN1a clade, the green the PIN1b clade and the blue the SoPIN1 clade. The position of barley PIN1a, PIN1b and SoPIN1 are indicated by the black arrows. Codes after gene names relate to the NCBI database reference. *B-D*: Maps of the barley *PIN* cDNA sequences, indicating the region where the probe targets (blue). The start and stop codons are indicated (grey bars). The numbers of the primers (black arrows) used in generating the probe template are also labelled. *B*: *PIN1a*. *C*: *PIN1b*. *D*: *SoPIN1*.

In wild-type flowers at 170 h, *BKn3* was expressed in the base of the flower and excluded from the lemma (Figure 3.10.E). *PIN1a* (Figure 3.10.F) and *PIN1b* (Figure 3.10.G) were expressed in internal regions of the wild-type lemma, correlating with developing vasculature but not seen in the epidermal layers of the lemma. *SoPIN1* appeared to not be expressed in the wild-type lemma (Figure 3.10.H).

In contrast to wild-type, at 170 hours, ectopic *BKn3* expression was strong in the adaxial half of the *Hooded* lemma (Figure 3.10.A, white arrowhead). If *BKn3* was able to alter axial information in the tissue at the cellular level, it could be expected that *PIN1* would be expressed in the same region, particularly in the epidermis. *PIN1a* mRNA was found in the developing *Hooded* lemma (Figure 3.10.B, white arrowhead), both in the developing vasculature (the central line trace in the middle of the lemma) and in the adaxial half of the lemma. This region of *PIN1a* correlates with where *BKn3* mRNA would also be found. In contrast to *PIN1a*, *PIN1b* mRNA was restricted to the developing vasculature (Figure 3.10.C, white arrowhead) which resembled internal lines in the lemma. Like the other PIN1s, *SoPIN1* mRNA was also found in the developing vasculature. *SoPIN1* also had very strong localisation to the adaxial half of the developing *Hooded* lemma, in a similar position to where *BKn3* mRNA would be found (Figure 3.10.D, white arrowhead). This suggests that *BKn3* may influence the expression pattern of *PIN1a* and *SoPIN1*. This could link to a possible change in axial information at the cellular level.

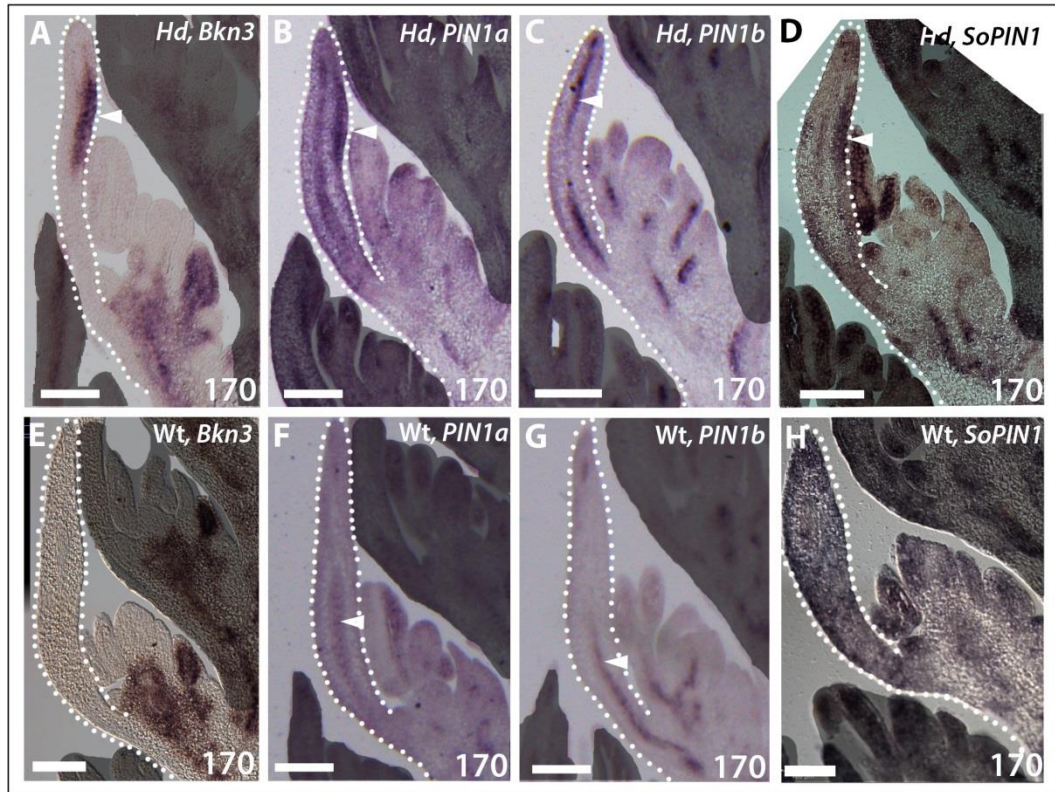


**Figure 3.10** RNA *in situ* hybridisation showing the localisation of *BKn3*, and barley *PIN1* homologues in developing barley florets.

mRNA localisation (dark staining) of *BKn3* (A,E), *PIN1a* (B,F), *PIN1b* (C,G) and *SoPIN1* (D,H) in developing *Hooded* (A-D) and wild-type (E-F) barley florets. A single floret is highlighted by shading out other tissues. The white dotted line highlights the developing lemma, the white arrowhead indicates the mRNA localisation pattern. Times are hours since T0. Scale bars are 100µm.

To explore whether *PIN1a* or *SoPIN1* was a good marker for cellular level tissue axial information, we used immunolocalisation techniques. For the detection of *PIN1a* we used Cambridge Research Biochemicals to develop an antibody which targeted 281-297 amino acids in the barley *PIN1a* protein. The antibody used in all barley *SoPIN1* immunolocalisations was raised against *ZmSoPIN1* and is from Sarah Hake and Devin O'Connor. The protocols used for immunolocalisation were based upon Conti and Bradley 2007 [150] and first modified by Alexandra Rebocho and then further modified by myself for use in barley tissue. All tissue used in immunolocalisations was fixed in FAA.

I first looked at *PIN1a* and *SoPIN1* localisation in longitudinal midsections through developing barley florets (Figure 3.11, the position of the tissue slices was the same as for the *BKn3* RNA

*in situ* hybridisation samples, Figure 3.9.J.). The stage shown in Figure 3.11 corresponds to when *BKn3* was ectopically expressed in the developing lemma. Both antibodies produced specific localisation patterns in the barley floret tissue. In *Hooded* florets, PIN1a appeared to be localised to the developing vasculature, at 170 hours (Figure 3.12.A) when the meristematic cushion had fully formed. In the *Hooded* lemma, PIN1a protein was only localised to the central developing vasculature thread (Figure 3.12.A.ii, white arrowhead). This contrasts with the RNA *in situ* hybridisation results which suggest that *PIN1a* was expressed in the epidermis of the developing *Hooded* lemma in the same region as *BKn3* and the developing vasculature. This may be due to the *in situ* probe being less specific than the antibody. In contrast to PIN1a, SoPIN1 had very little localisation signal in the developing vasculature (Figure 3.11.B) of the *Hooded* floret. Instead SoPIN1 was highly localised to the region in the *Hooded* lemma which would correspond to the *BKn3* ectopic expression zone (the meristematic cushion, Figure 3.12.B.ii, white arrowheads). This localisation of SoPIN1 was in both the epidermal and the subepidermal layers in the adaxial side of the developing lemma (Figure 3.11.B.ii).

In wild-type florets PIN1a was observed in the developing vasculature only (Figure 3.11.C) and SoPIN1 had very little signal, only in the tips of some of the developing organs and no signal in the lemma (Figure 3.11.D).

These immunolocalisation results suggest that the localisation of SoPIN1 may respond to ectopic *BKn3* expression in the *Hooded* lemma, whereas PIN1a does not.

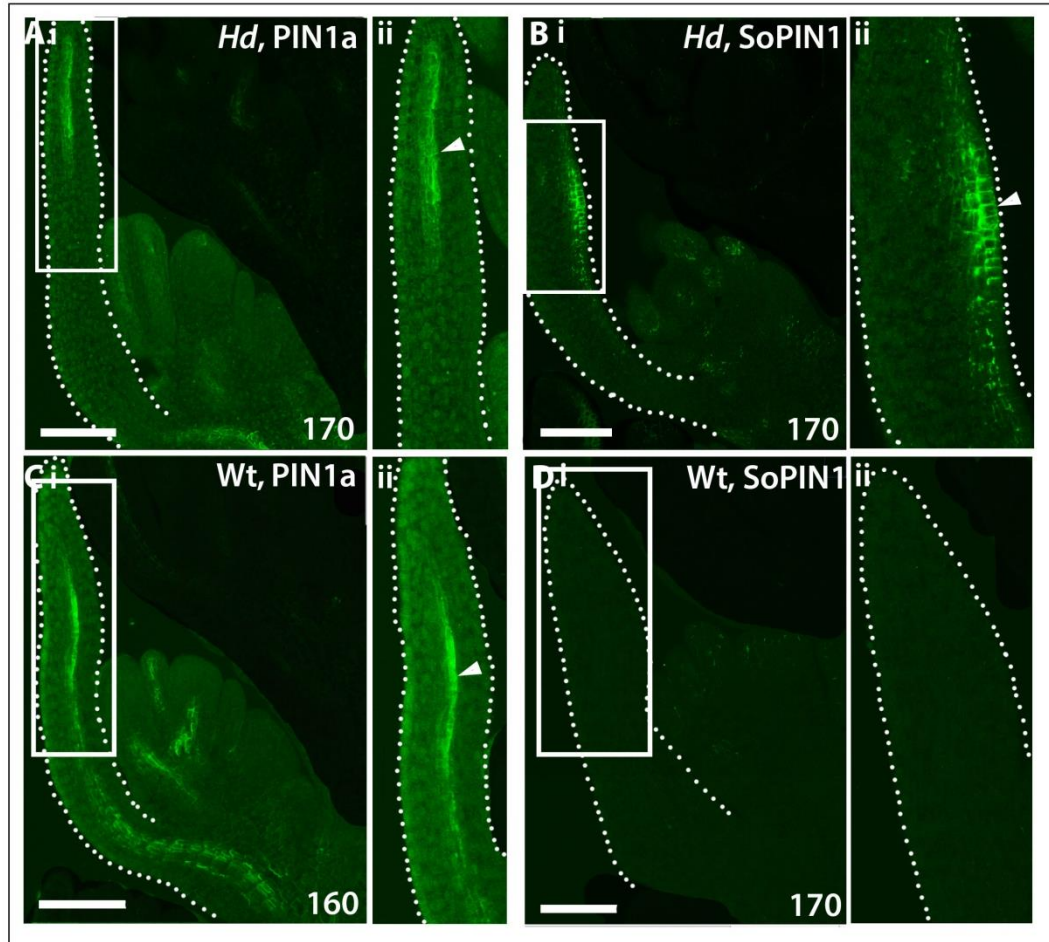


**Figure 3.11 Immunolocalisation of PIN1a and SoPIN1 in developing barley flowers.** The localisation of PIN1a (A,C) and SoPIN1 (B,D) in single *Hooded* (A-B) and wild-type (C-D) barley florets at 170 and 160 hours since T0. *i*: whole floret, *ii*: zoomed-in image of the boxed lemma region in *i*. Localisation of the protein is in green. The white dotted line highlights the lemma. The white arrowhead indicates the localisation patterns. Scale bars are 100µm.

To explore the localisation of SoPIN1 further, using it as a cellular marker of axial information within the tissue, I combined the immunolocalisation protocol with calcofluor staining to allow visualisation of the cell walls. Using this, the cellular localisation of SoPIN1 could be assessed in relation to the cell wall signal, to gain insight into the orientation of the axial information within the developing lemma.

Looking at the localisation of SoPIN1, the signal for epidermal SoPIN1 was higher in the lemma of the *Hooded* mutant (Figure 3.12.A-B, green signal) than in wild-type (Figure 3.12.C-D, green signal) from an early stage in development. In wild-type lemmas, SoPIN1 signal was very low making it difficult to assess orientation, especially at late stages (Figure 3.12.D)

when there was no epidermal SoPIN1 in the lemma (Figure 3.12.D.ii). In early stages of wild-type lemma development (localisation at 100 hours since T0 is shown in Figure 3.12.C), SoPIN1 was near the tip of the lemma (Figure 3.12.C) and appeared to be localised to the distal side of each cell (Figure 3.12.C.ii, white arrows indicate the orientation of SoPIN1 polar localisation). This suggests that axial information is oriented proximodistally towards the tip of the early wild-type lemma. As there is no epidermal SoPIN1 signal in later stage lemmas (Figure 3.12.D has an example of a wild-type lemma at 170 hours of development), it could be assumed that the orientation of axial information remains the same, and orients proximodistally.

During early stages of *Hooded* development (Figure 3.12.A illustrates an example of a *Hooded* mutant at 100 hours), before ectopic *BKn3* expression occurred, epidermal SoPIN1 was higher in the distal half of the developing lemma (Figure 3.12.A.ii) than in wild-type (Figure 3.12.B.ii). Like wild-type, SoPIN1 in the early *Hooded* lemma was also localised to the distal side of each cell (Figure 3.12.A.ii, white arrowheads). This cellular localisation of SoPIN1 was coordinated between the cells and they oriented towards the lemma tip (Figure 3.12.A.ii). This suggests that, like in wild-type lemmas, axial information is oriented proximodistally towards the lemma tip during early development. At 170 hours, when ectopic *BKn3* expression in the lemma was very strong and the meristematic cushion had formed, there was strong SoPIN1 signal in the adaxial half of the developing lemma (Figure 3.12.B). This region of high SoPIN1 corresponded to where *BKn3* would be expressed. In the epidermal cells of this region SoPIN1 appeared to be localised to the proximal side of each cell (Figure 3.12.B.ii). These cells co-ordinately localised SoPIN1 proximally. This suggests that *BKn3* may cause a reorientation of axial information compared to earlier stages of lemma development. This is also supported by the lack of SoPIN1 upregulation and localisation change on the abaxial side of the lemma where *BKn3* was not expressed (Figure 3.12.B.ii).

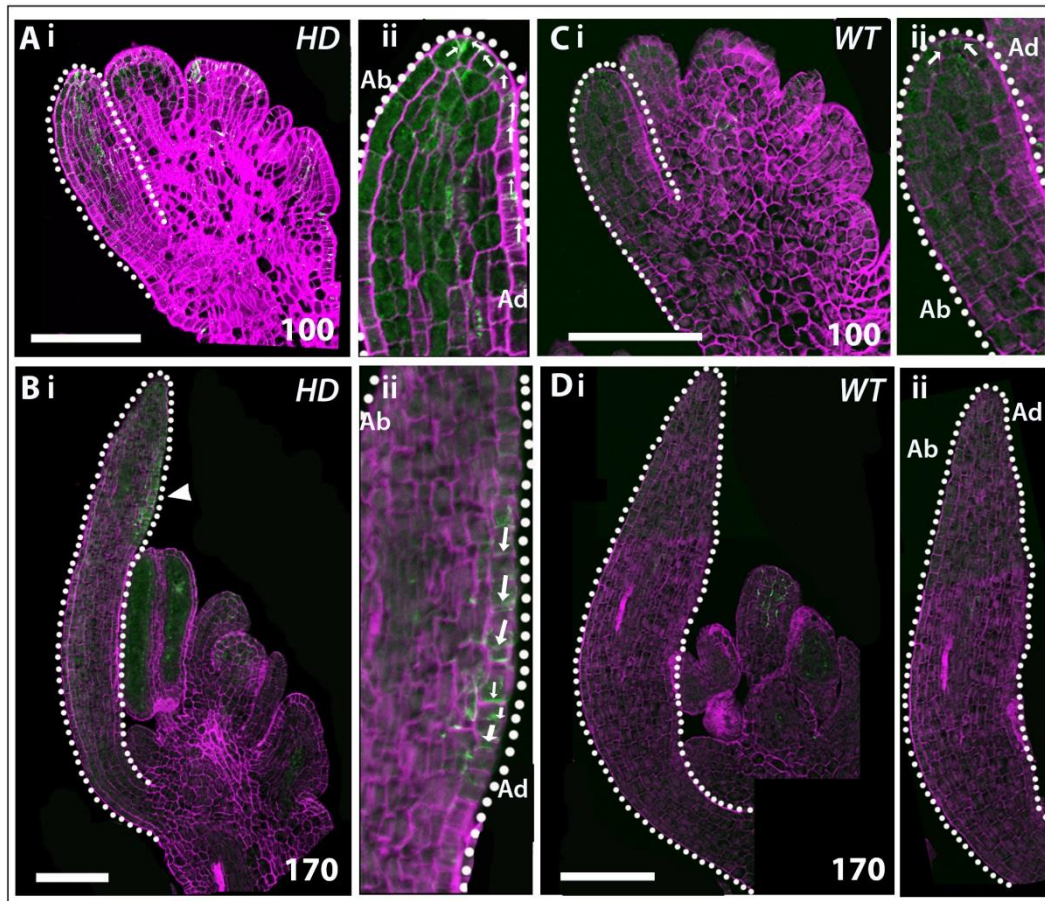


**Figure 3.12 Immunolocalisation of SoPIN1 in middle longitudinal sections of developing barley flowers.**

Immunolocalisation of SoPIN1 in FAA fixed barley inflorescences using the ZmSoPIN1 antibody. SoPIN1 localisation (green) relative to cell wall position as shown by calcofluor staining (magenta) is shown, where the localisation of SoPIN1 and calcofluor overlap the signal is white. *A and B*: Hooded mutant. *C and D*: wild-type. *i*: middle longitudinal section through a developing flower at different stages. *ii*: zoomed-in image of the lemma in *i*. Outline of the lemma is highlighted by the white dotted line. *Ad*: Adaxial. *Ab*: Abaxial. Orientation of SoPIN1 localisation within analysed cells is indicated by white arrows. Numbers indicate the approximate time from morphological T0 in hours. Staging is based upon floret width. All scale bars are 100 $\mu$ m.

As it is difficult to evaluate tissue cell polarity (co-ordinated SoPIN1 patterns across the tissue) in the whole lemma using 2D slices, I developed a new protocol for whole-mount immunolocalisation in barley tissue (See Appendix A for a description of how the protocol was developed). Using this technique, I was able to investigate the reorientation of SoPIN1 localisation (and therefore the reorientation of axial information) triggered by *BKn3* more closely in 3D in the Hooded mutant. As ectopic *BKn3* expression is confined to the adaxial

half of the lemma and SoPIN1 localisation in sliced samples reorients on the adaxial side only, SoPIN1 localisation on the adaxial surface of developing lemmas was assessed at different ages.

During early stages of wild-type lemma development, when the lemma had a triangular shape with a rounded tip (Figure 3.13.A), corresponding to around 90 hours, epidermal SoPIN1 was low (Figure 3.13.A.i). SoPIN1 was localised to the distal side of epidermal cells in early wild-type lemmas (Figure 3.13.A.ii, white arrows). This suggests that axial information is oriented towards the tip of the wild-type lemma, supporting sliced immunolocalisation data. At later stages of development, around 200 hours since T0, the wild-type lemma was more elongated in shape (Figure 3.13.B) and had very low SoPIN1 signal (Figure 3.13.B.i). Near the tip and the base of the lemma, SoPIN1 appeared to be localised on the distal side of each cell (Figure 3.13.B.ii, white arrows). This suggests that throughout development the wild-type lemma has proximodistally oriented axial information as marked by coordinated SoPIN1 cellular localisation.

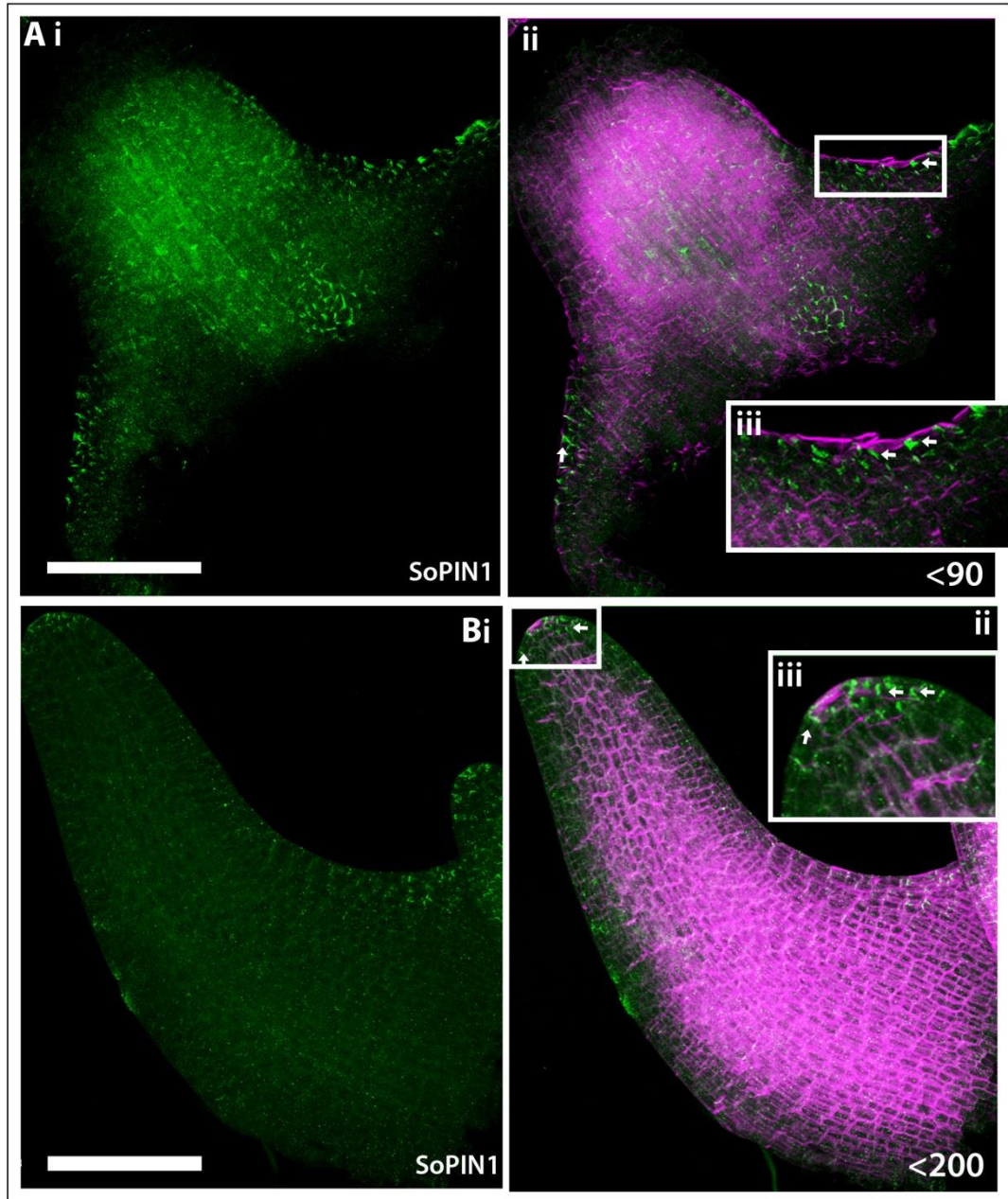


**Figure 3.13 Whole-mount immunolocalisation of SoPIN1 on the adaxial side of wild-type lemmas.**

Whole-mount immunolocalisation of SoPIN1 in wild-type FAA fixed barley lemmas using the ZmSoPIN1 antibody. SoPIN1 localisation (green) relative to cell wall position highlighted by calcofluor staining (magenta) is shown. *A*: early stage. *B*: later stage. *i*: z-projection of SoPIN1 localisation. *ii*: z-projection of both the cell wall and SoPIN1 localisation signals. *iii*: zoomed-in image of the boxed region in *ii*. White arrows indicate the orientation of the SoPIN1 signal within the representative analysed cells. Numbers indicate the approximate time from morphological T0 in hours, staging is based upon the original confocal imaging of the adaxial surface of lemmas. All scale bars are 100 $\mu$ m.

At early stages of *Hooded* development when the lemma still resembled wild-type in shape, before ectopic *BKn3* expression had been initiated (around 90 hours), SoPIN1 was polarly localised (Figure 3.14.A). Like in wild-type at the same developmental stage, SoPIN1 was localised to the distal side of lemma cells in the adaxial surface of the lemma (Figure 3.14.ii and iii). The cells co-ordinately orientated SoPIN1 to the distal side. This indicates that axial information in the early *Hooded* lemma is oriented proximodistally (Figure 3.14.A.ii). This is consistent with the pattern suggested by the sliced tissue.

After ectopic *BKn3* expression is activated in the developing lemma (at around 110 hours) the proximodistal axial information appeared to be disrupted (Figure 3.14.B). Lemmas at around 120 hours still looked wild-type in shape but the cellular localisation of SoPIN1 in the adaxial surface was altered. The cells near the tip of the lemma had SoPIN1 localised to the distal side, towards the lemma tip (Figure 3.14.B.iii, white arrows). However the cells below the lemma tip (in the distal half of the lemma), where ectopic *BKn3* expression was activated, did not have SoPIN1 localised to the distal side. Instead these cells appeared to have SoPIN1 localised to the cell side that faces towards the middle of the adaxial surface (Figure 3.14.B.iii, white arrows). This suggests that in the region correlating to where *BKn3* is expressed axial information undergoes a 90° shift to orient towards the centre of the adaxial surface of the lemma (Figure 3.14.B.ii, white arrows). This may have a role in the formation of the meristematic cushion.

As development progresses and the ectopic floral meristem is initiated where *BKn3* was expressed, the orientation of SoPIN1 localisation changed further. Once the ectopic meristem had been established the SoPIN1 localisation appeared to reorient differently across the lemma. In the ectopic meristem, SoPIN1 was oriented towards the centre of the meristem dome (Figure 3.14.C.iii, white arrows). Above and in the marginal tissues flanking the ectopic meristem, SoPIN1 was localised to the distal end of cells towards the tip of the lemma (Figure 3.14.C.ii). Immediately below the ectopic meristem, SoPIN1 was localised to the side of the cell facing the centre of the adaxial surface (Figure 3.14.C.iii). Below this SoPIN1 was localised to the proximal side of the cell away from the tip of the lemma (Figure 3.14.C.iii), which was inverted compared to earlier stages in development. Later on in development this pattern seemed to be maintained with SoPIN1 oriented towards the tip of the lemma above the ectopic meristem, towards the centre of the adaxial surface immediately below the ectopic meristem, and towards the base of the lemma below the ectopic meristem (Figure 3.14.D).

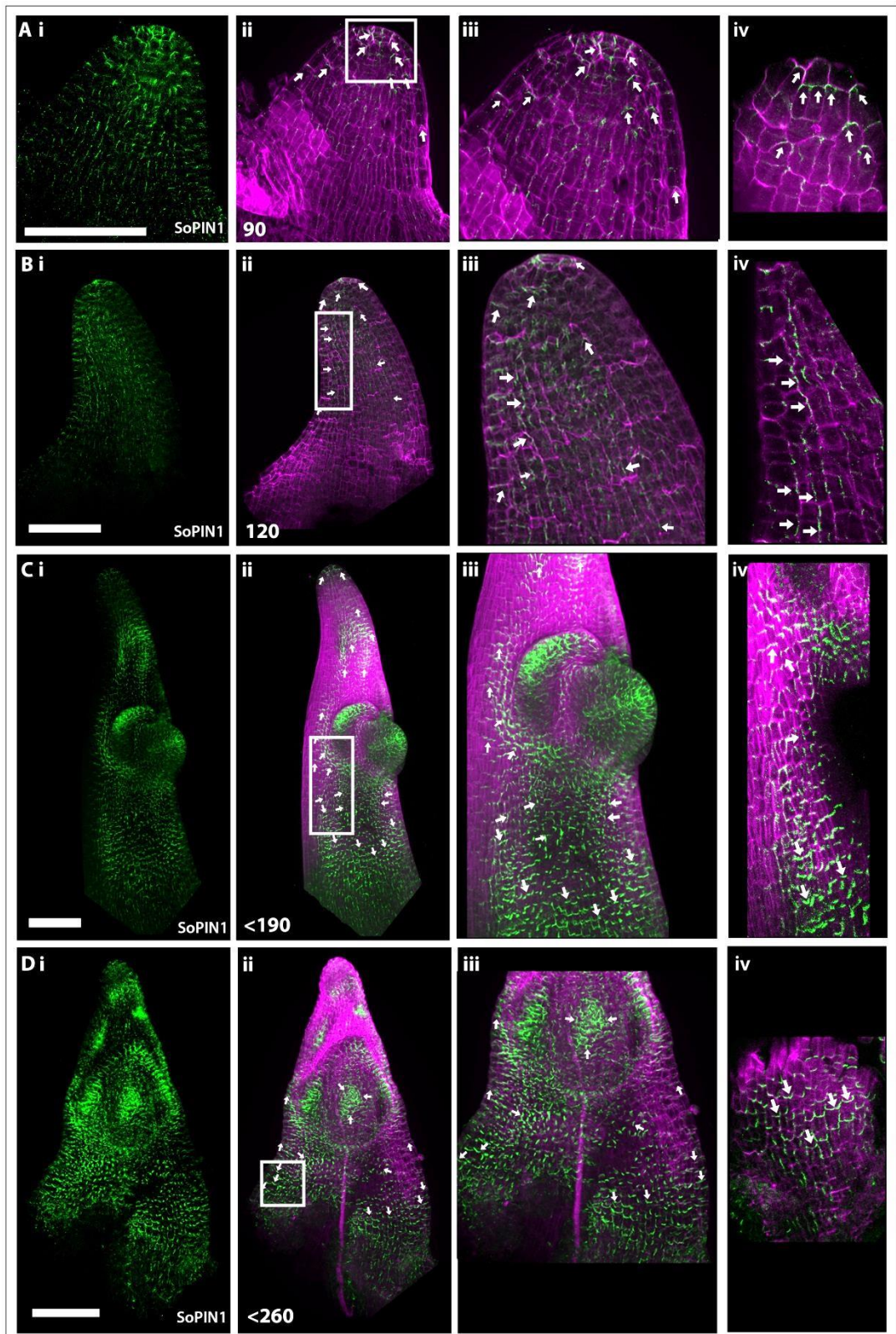


Figure 3.14 Whole-mount immunolocalisation of SoPIN1 on the adaxial surface of developing *Hooded* lemmas.

Whole-mount immunolocalisation of SoPIN1 in *Hooded* FAA fixed barley lemmas using the

ZmSoPIN1 antibody. SoPIN1 localisation (green) relative to cell wall position highlighted by calcofluor staining (magenta) is shown. *A-D*: Progressively older lemmas, showing only the adaxial surface. *i*: z projection of SoPIN1 localisation. *ii*: z projection of both the cell wall and SoPIN1 localisation. *iii*: zoomed-in images. *iv*: zoomed-in images of single z stack slices of the region highlighted by the white box in *ii*. White arrows indicate the orientation of the SoPIN1 signal within representative analysed cells. The position of the ectopic meristem is indicated by the white arrowhead. Numbers indicate the approximate time from morphological T0 in hours, staging is based upon the original confocal imaging of the adaxial surface of lemmas. All scale bars are 100µm.

Combined, the pattern of SoPIN1 localisation suggests that wild-type lemmas have proximodistally oriented axial information throughout development and that *BKn3* expression is excluded from the lemma throughout.

In the *Hooded* lemma, axial information is originally oriented proximodistally like wild-type. Once *BKn3* expression is activated at around 110 hours, axial information is then reorganised. Axial information (as marked by SoPIN1 localisation) first orients towards the centre of the adaxial surface (Figure 3.15.A, red arrows represent SoPIN1 orientation, hatched lines represent the region of *BKn3* expression) and this may be part of the formation of the ectopic meristem in the centre of the adaxial surface. Once the ectopic meristem has formed in the region where *BKn3* is expressed (Figure 3.15.B, orange indicates the ectopic meristem), axial information below the ectopic meristem switches to a basipetal orientation and above the ectopic meristem the original proximodistal pattern is maintained (Figure 3.15.B).

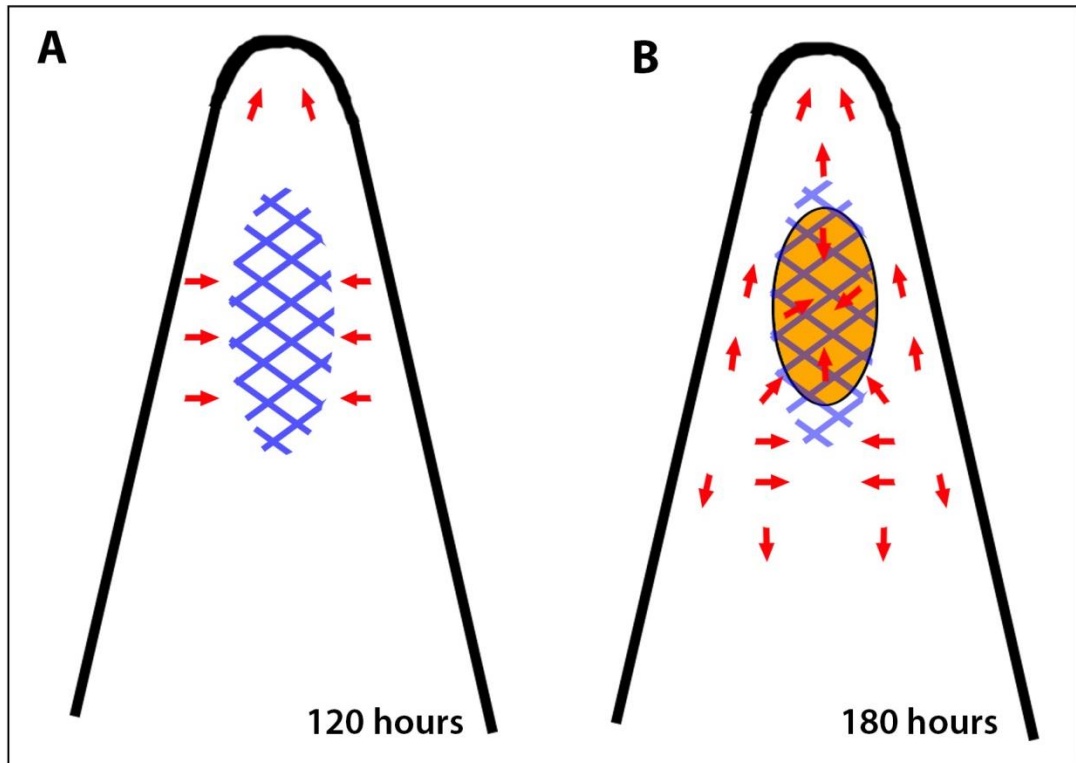


**Figure 3.15** A summary diagram illustrating the relationship between *BKn3* expression, SoPIN1 localisation and morphology.

Cartoons of the adaxial surface of *Hooded* lemmas at 120 hours (A) and 180 hours (B) since T0. Black outline represents the shape of the lemma, red arrows illustrate the localisation of SoPIN1, hatching represents the region of *BKn3* expression, orange oval represents the ectopic meristem (meristematic cushion).

This pattern of *BKn3* expression and SoPIN1 localisation, suggests that the ectopic expression of *BKn3* in the *Hooded* lemma initiates a reorientation of the axial information in addition to the effect of *BKn3* on growth rates reported in the literature. This reorientation of axial information could be activated before changes to growth rate patterns as SoPIN1 localisation reorients before the meristematic cushion is seen.

### **3.6 The ectopic expression of *BKn3* in the *Hooded* lemma induces changes in the expression pattern of candidate polarity organisers**

To assess how *BKn3* could alter axial information, I explored the expression patterns of several genes which could be part of the axially system. I based this investigation upon the assumption that a polarity based axially system was active in the developing lemma. The

polarity based axiality system proposes that the axial information within a tissue is provided by the gradient of a propagated signal across the tissue, anchored by organiser regions. This polarising signal is hypothesised to be auxin and the organiser regions may affect the distribution of auxin throughout the tissue by modulating local extracellular auxin concentrations [42]. Plus organiser regions are proposed to enhance extracellular auxin concentration due to an increase in rates of auxin export. Minus organiser regions are predicted to reduce extracellular auxin concentration due to increased rates of auxin import [42]. Possible plus organiser components could include the boundary gene *NAM* [50] and the auxin biosynthesis genes, the *YUCCAs* [53]. The auxin importer *LAX1* [133] may be a minus organiser component. These hypothesised organisers of polarity have been identified through their roles in developmental processes in *Arabidopsis thaliana* and *Antirrhinum majus* (Katie Abley, JIC, unpublished, Alexandra Rebocho, JIC, unpublished) [4]. To explore whether *BKn3* could influence organiser regions to alter axiality, I used RNA *in situ* hybridisation to define the expression patterns of the possible organiser components.

The NAC domain transcription factor *NAM* [50] (*CUC1* in *Arabidopsis*) was chosen as a possible factor involved in plus organisers as it is expressed in boundary regions which *PIN1* often orientates away from [51], and due to its role in outgrowth formation in *Arabidopsis* [4]. As with the *BKn3* probes, the barley sequence for *NAM* was identified in the published sequences available in the NCBI database using basic phylogenetic analysis of the protein sequences (Figure 3.16.A). The sequence most similar to *AtCUC1* was chosen (MLOC\_65286) for the probe and a 399bp region between the ATG and 399bp in the cDNA sequence (Figure 3.16.B, region between the two black arrows) was cloned to generate the antisense RNA probe. RNA *in situ* hybridisation was carried out on middle longitudinal sections through developing flowers.

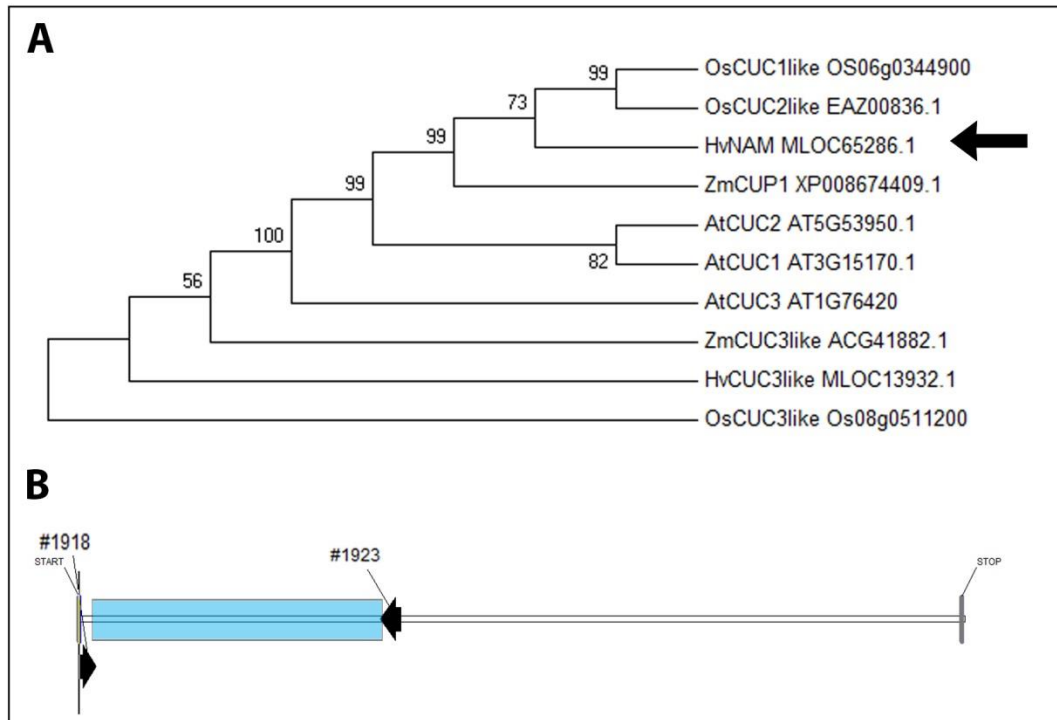


**Figure 3.16** Guide phylogenetic tree for NAM protein sequences and the map of the barley *NAM* mRNA sequence showing the region covered by the probe.

*A*: guide phylogenetic tree of NAM protein sequences from *O.Sativa* (Os), *A.thaliana* (At), Barley (Hv) and *Z.mays* (Zm). The position of barley NAM is indicated by the arrow. Numbers indicate the bootstrap value of each node. Codes after gene names relate to the NCBI database reference. *B*: Map of barley *NAM* cDNA indicating the region where the probe targets (blue). The start and stop codons are indicated (grey bars). The numbers of the primers used in generating the probe are also labelled (black arrows).

In wild-type barley flowers *NAM* expression was low but it was expressed in developing organ boundary regions during early stages of development (Figure 3.17.E, white arrowhead). *NAM* was largely excluded from the lemma throughout wild-type development, except for some expression near the base of the lemma where it joined base of the flower (Figure 3.17.F-H, white arrowhead). This expression pattern was consistent with the role of *NAM* in the development of boundary regions. It could indicate a role for *NAM* in plus organisers as the wild-type lemma has proximodistal axial information, predicting that a plus organiser would be found at the base of the lemma, where *NAM* was expressed.

Similar to wild-type, the early stages of *Hooded* flowers have *NAM* expression in organ boundary regions only (Figure 3.17.A). At early stages (Figure 3.17.A shows a *Hooded* floret at around 90 hours), *NAM* was excluded from the developing *Hooded* lemma (Figure

3.17.A.ii). However, unlike in wild-type, *NAM* expression was not excluded from the developing lemma at later stages. Around the time that ectopic *BKn3* expression was activated in the lemma (approximately 110 hours), *NAM* expression was also activated in the lemma (Figure 3.17.B, white arrowheads). Ectopic *NAM* mRNA was specifically restricted in the *Hooded* lemma to two regions in the adaxial half of the lemma, which may flank the region where *BKn3* was expressed (Figure 3.17.B.ii). As the lemma developed the expression region of *NAM* in the lemma expanded along the adaxial half of the lemma (Figure 3.17.C.ii), corresponding to the region where *BKn3* was ectopically expressed. Once organs began to initiate from the ectopic meristem, (around 190 hours) *NAM* was strongly expressed in bands indicative of developing organ boundary regions (Figure 3.17.D, white arrowheads), consistent with its role in organ boundary formation.

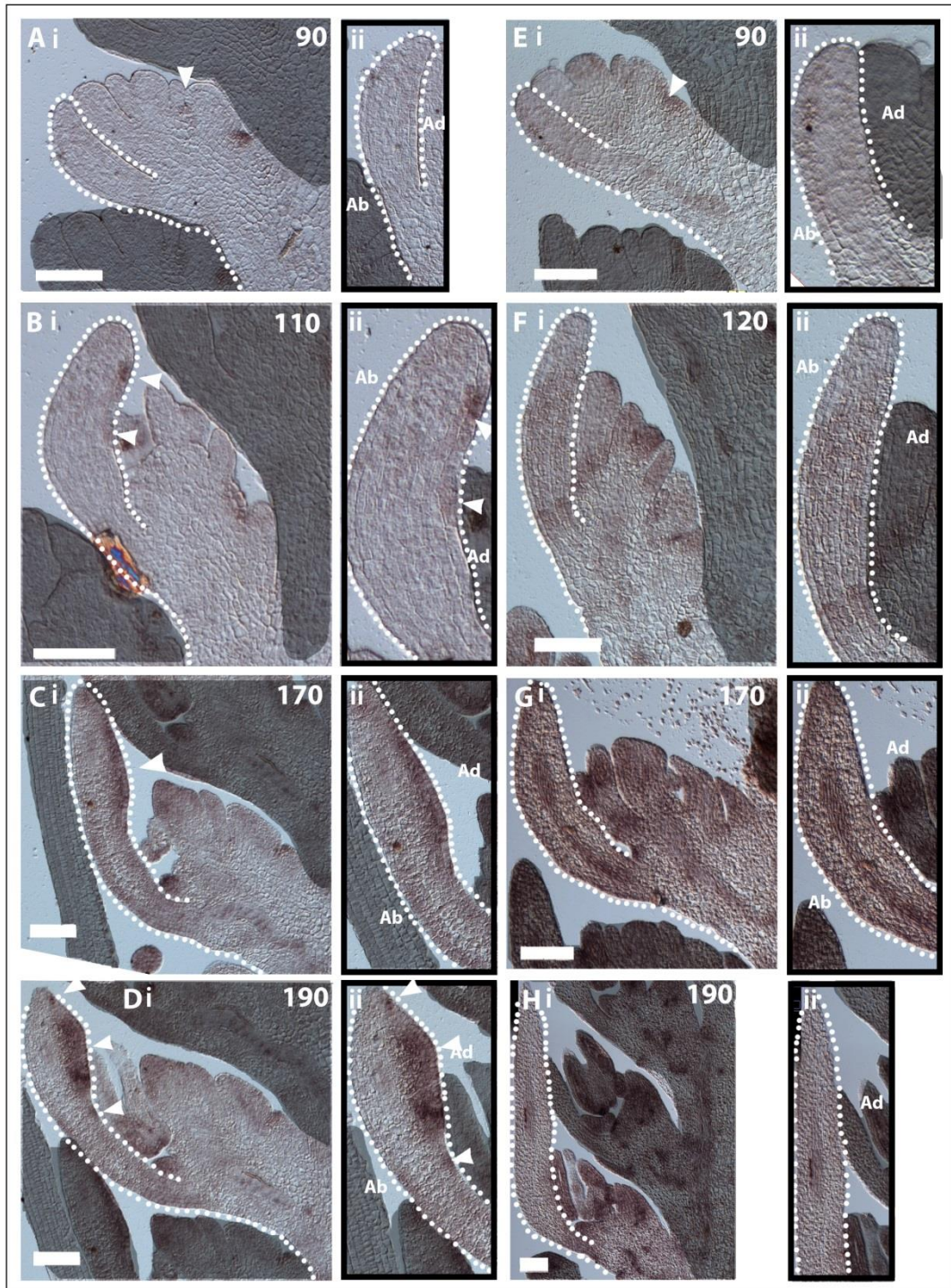


**Figure 3.17** RNA *in situ* hybridisation of *NAM* mRNA in longitudinal sections through wild-type and *Hooded* barley flowers.

*A-D*: *Hooded* flowers. *E-H*: Wild-type flowers. *i*: middle longitudinal section through the flower. *ii*: zoomed-in image of the lemma in *i*. Dotted white line highlights the shape of the lemma. *Ab*: Abaxial side of the lemma. *Ad*: Adaxial side of the lemma. The positions of *NAM* localisation (white) are indicated by arrowheads. Numbers indicate the approximate time since morphological T0 in hours. Scale bar is 100µm

Auxin biosynthesis genes such as the *YUCCAs*, could also act in plus organiser regions. Published work has identified the role of *YUCCAs* in flower development [132, 151] suggesting that they may be possible organiser components. I therefore chose to look at the expression pattern of a *YUCCA* gene in barley lemmas to see if the ectopic expression of *BKn3* affects *YUCCA* expression patterns. The *YUCCA* family is large [132] (in *A. thaliana* there are 11 different *YUCCAs*) and their expression patterns are varied. A basic guide phylogenetic tree was constructed using available barley sequences identified through NCBI Blast of the *YUCCA* proteins in *Arabidopsis* (Figure 3.18.A). The sequence used to generate an antisense RNA probe was AK364489, which clustered with the family containing *AtYUCCA5* and *9* (from here on referred to as *YUCCA*). (This gene was originally identified before the barley genome was published. Since the publication of the barley genome [149] many more candidates were added to the phylogenetic tree. The candidate *YUCCA*, AK364489, was chosen as it was the first to amplify successfully, it may be that this is not the best candidate to have used as it does not cluster with *YUCCA1* genes shown to be expressed in the developing *Antirrhinum* flower (Alexandra Rebocho, JIC, unpublished.)) The probe covered the region from 152bp to 630bp of the *barley YUCCA* mRNA sequence (Figure 3.18.B). This was used to probe middle longitudinal sections through barley flowers at different developmental stages to visualise *YUCCA* mRNA localisation.

In early developmental stages of wild-type flowers (Figure 3.19.D shows a flower at 90 hours, when all organ primordia have been initiated), *YUCCA* mRNA was localised to the tips of the developing floral organs (Figure 3.19.D, white arrowheads). This is consistent with previous reports of some *YUCCA* gene expression patterns in other species [132]. In the lemma *YUCCA* mRNA appeared to be throughout the developing organ (Figure 3.19.D.ii). This pattern of mRNA localisation in the lemma was maintained until after 120 hours (Figure 3.19.E). As development progressed the region within the lemma where *YUCCA* mRNA was localised seemed to reduce and become largely localised to developing vasculature (Figure 3.19.F), although some expression appeared to remain at the base of the lemma (Figure 3.19.F) possibly consistent with a role as a plus organiser component.

In early stages of *Hooded* flower development *YUCCA* was also expressed in the tips of developing organs (Figure 3.19.A, shows a flower at 90 hours, white arrowheads indicate the tips of organ primordia). Unlike *NAM*, the expression of *YUCCA* in the *Hooded* lemma around the time of the activation of ectopic *BKn3* expression (110 hours) seemed to remain similar to wild-type. *YUCCA* mRNA seemed to be throughout the developing *Hooded* lemma at early

stages in development (Figure 3.19.B.ii). However as development progressed, and around the time the ectopic meristem had started to grow out of the adaxial surface of the *Hooded* lemma (170 hours since T0), *YUCCA* expression was activated strongly on the adaxial half of the lemma (Figure 3.19.E.ii, white arrowhead). This region corresponded to where the ectopic meristem was developing and *BKn3* was ectopically expressed. There was also some expression at the base of the lemma (Figure 3.19.C) similar to the pattern in wild-type. This suggests that the expression of *YUCCA* may respond slowly to the ectopic expression of *BKn3* but it is activated downstream of the expression of *BKn3* and possibly *NAM* in the *Hooded* lemma.

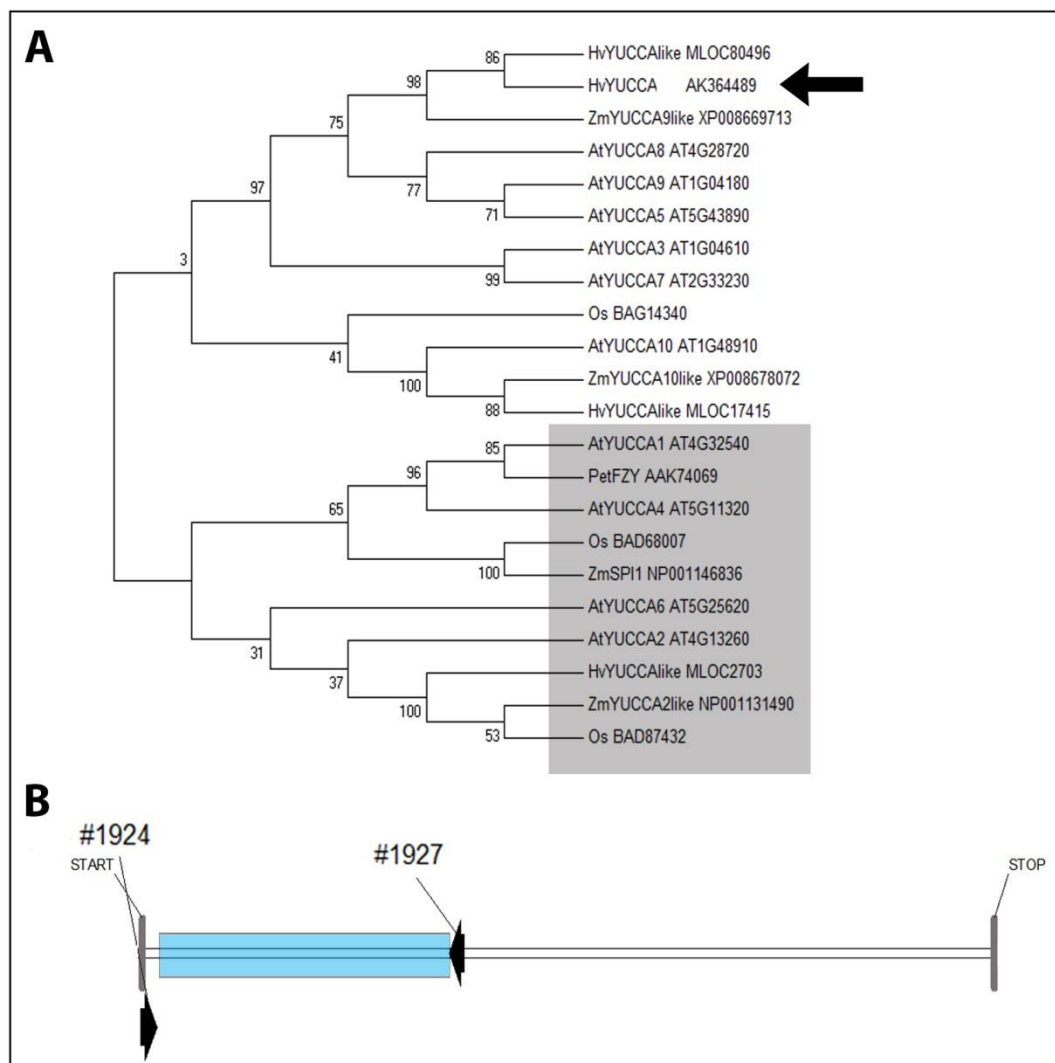
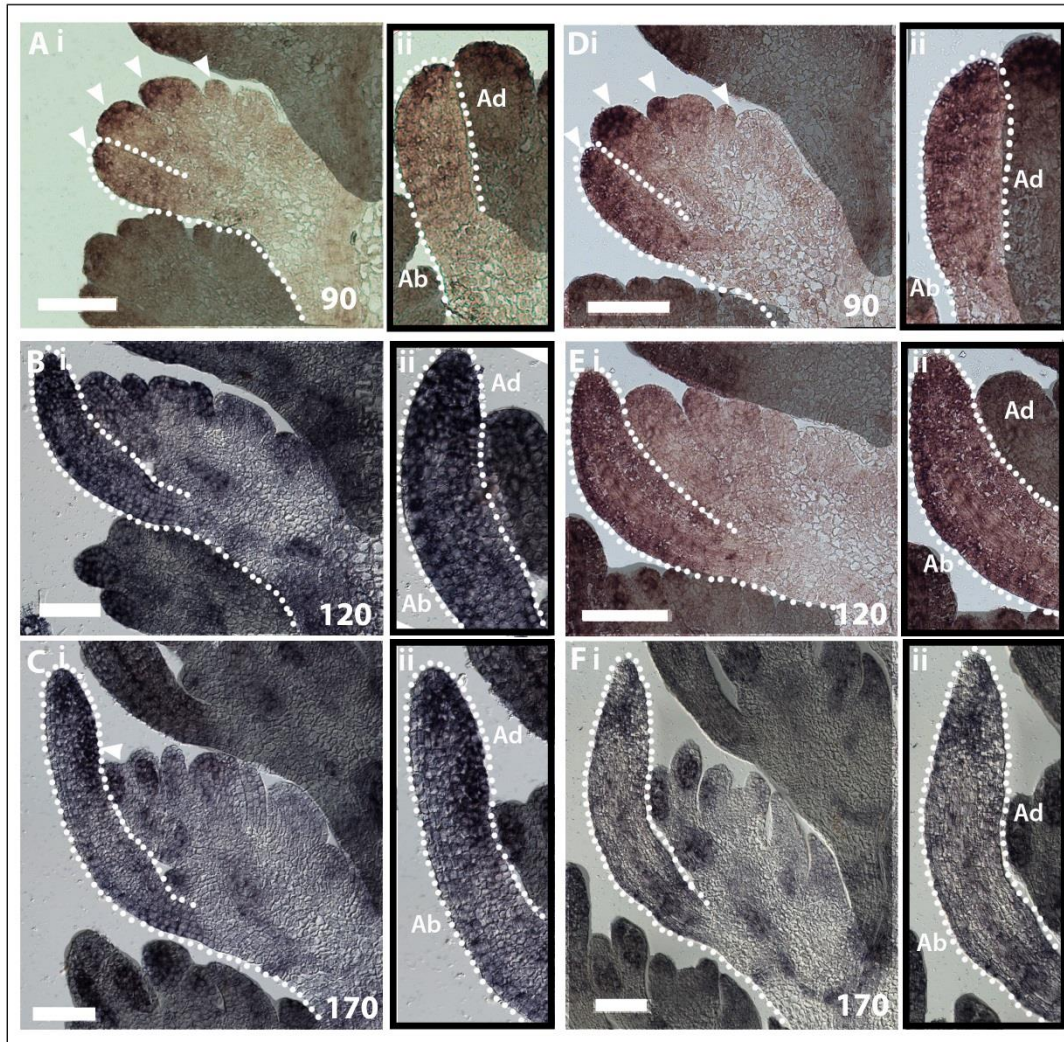


Figure 3.18 Guide phylogenetic tree for *YUCCA* protein sequences and the map of barley *YUCCA* cDNA showing the region covered by the probe.

A: guide phylogenetic tree of *YUCCA* protein sequences from *O. Sativa* (Os), *A. thaliana* (At),

Barley (*Hv*), *Petunia hybrida* (*Pet*) and *Z. mays* (*Zm*). The position of barley *YUCCA* is indicated by the arrow. Numbers indicate the bootstrap value of each node. Codes after gene names relate to the NCBI database reference. *B*: Map of barley *YUCCA* cDNA indicating the region where the probe targets (blue). The start and stop codons are indicated (grey bars). The numbers of the primers used in generating the probe are also labelled (black arrows).



**Figure 3.19** RNA *in situ* hybridisation of *YUCCA* mRNA in longitudinal sections through wild-type and *Hooded* barley flowers.

*A-C*: *Hooded* flowers. *D-F*: Wild-type flowers. *i*: longitudinal section through the flower. *ii*: zoomed-in image of the lemma in *i*. Dotted white line highlights the shape of the lemma. *Ab*: Abaxial side of the lemma. *Ad*: Adaxial side of the lemma. The positions of regions of *YUCCA* localisation are indicated by white arrowheads. Numbers indicate the approximate time since morphological T0 in hours. Scale bar is 100µm.

Minus organiser regions are proposed to promote low extracellular auxin concentration [42], therefore auxin importers such as *AtAUX1* and *AtLAX1* could be a component. I chose to focus on the expression pattern of the homologue to *AmLAX1*, as *AmLAX1* is expressed at the tips of developing organs (Alexandra Rebocho, JIC, unpublished) suggesting a possible role as a minus organiser. The homologue of *AmLAX1* in the published barley sequence was identified using guide phylogenetic analyses of LAX protein sequences from a range of species (Figure 3.20.A). The corresponding cDNA to the most similar barley protein sequence to *AmLAX1* was selected for further analysis by cloning the cDNA of AK369583 as an *in situ* probe. The probe clone was 530bp long and covered a unique region in the barley *LAX1* cDNA sequence from 305bp to 835p (Figure 3.20.B, region between the black arrows).

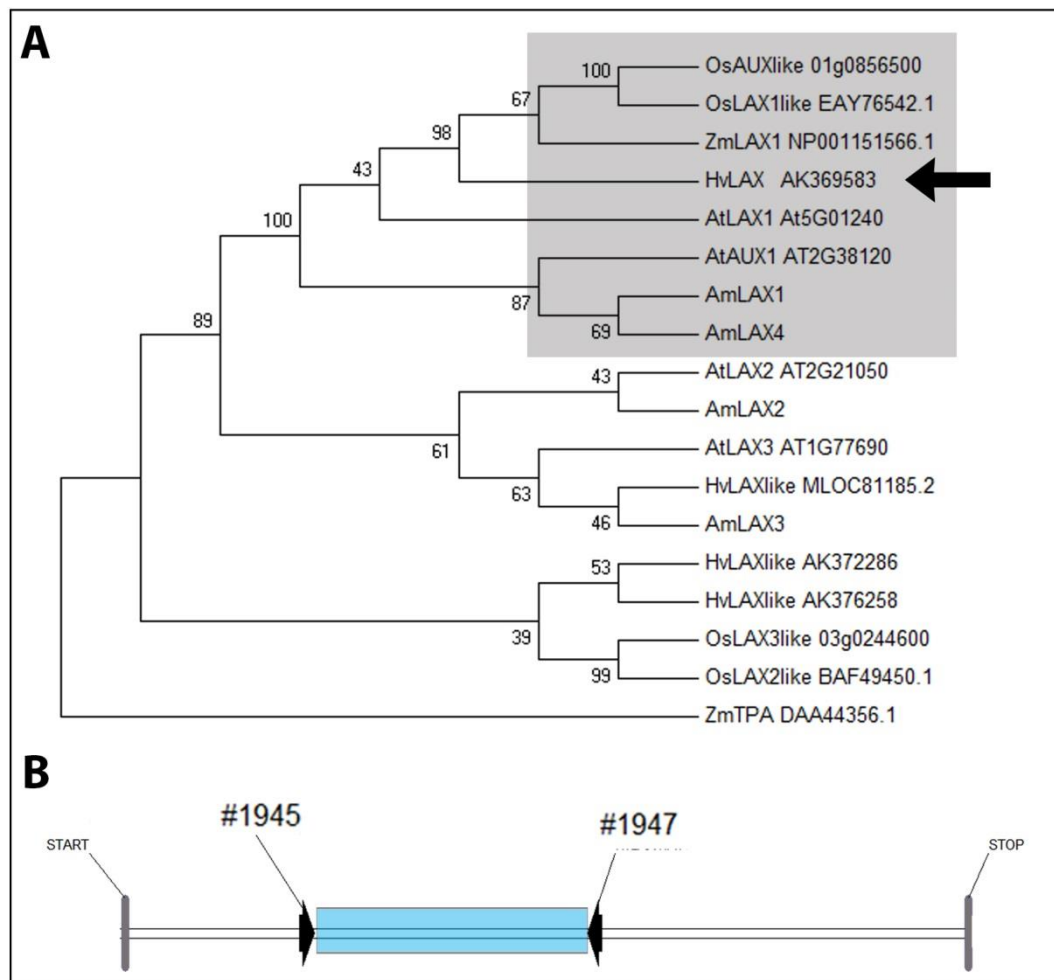


**Figure 3.20** Guide phylogenetic tree for LAX protein sequences and the map of barley *LAX1* cDNA showing the region covered by the probe.

A: guide phylogenetic tree of LAX protein sequences from *O. Sativa* (Os), *A. thaliana* (At), Barley (Hv), and *Z. mays* (Zm). The position of barley *LAX1* is indicated by the arrow. Numbers indicate the bootstrap value of each node. Codes after gene names relate to the NCBI

database reference. *B*: Map of barley *LAX1* cDNA indicating the region where the probe targets (blue). The start and stop codons are indicated (grey bars). The numbers of the primers (black arrows) used in generating the probe are also labelled.

As reported in other species, *LAX1* mRNA was localised to the tips of developing organs and the developing vasculature during early stages of flower development in both wild-type and *Hooded* barley flowers (Figure 3.21.A and D). At 90 hours *LAX1* mRNA was not localised to the developing lemma in wild-type or in the *Hooded* mutant (Figure 3.21.A.ii and E.ii).

In wild-type barley flowers, as development progressed *LAX1* expression was absent from the lemma (Figure 3.21.E and F) and it was only localised to some developing vasculature in the body of the flower (Figure 3.21.E and F, black arrowheads) and the tips of some of the developing floral organs (Figure 3.21.E and F, white arrowheads). In contrast to this, at 140 hours in the *Hooded* lemma, after ectopic *BKn3* expression had been activated (110 hours), *LAX1* mRNA was localised specifically to the adaxial L1 layer in a region corresponding to where *BKn3* was expressed (Figure 3.21.B.ii). At 140 hours this expression was very weak. As development progressed and the ectopic meristem formed on the *Hooded* lemma (around 170 hours), *LAX1* expression increased in the adaxial L1 layer in a region corresponding to the L1 of the ectopic meristematic cushion (Figure 3.2.C.ii). This expression of *LAX1* on the surface of the meristematic cushion could be due to it being a new outgrowth from the lemma, and *LAX* is typically found at the tip of new outgrowths like organ primordia.

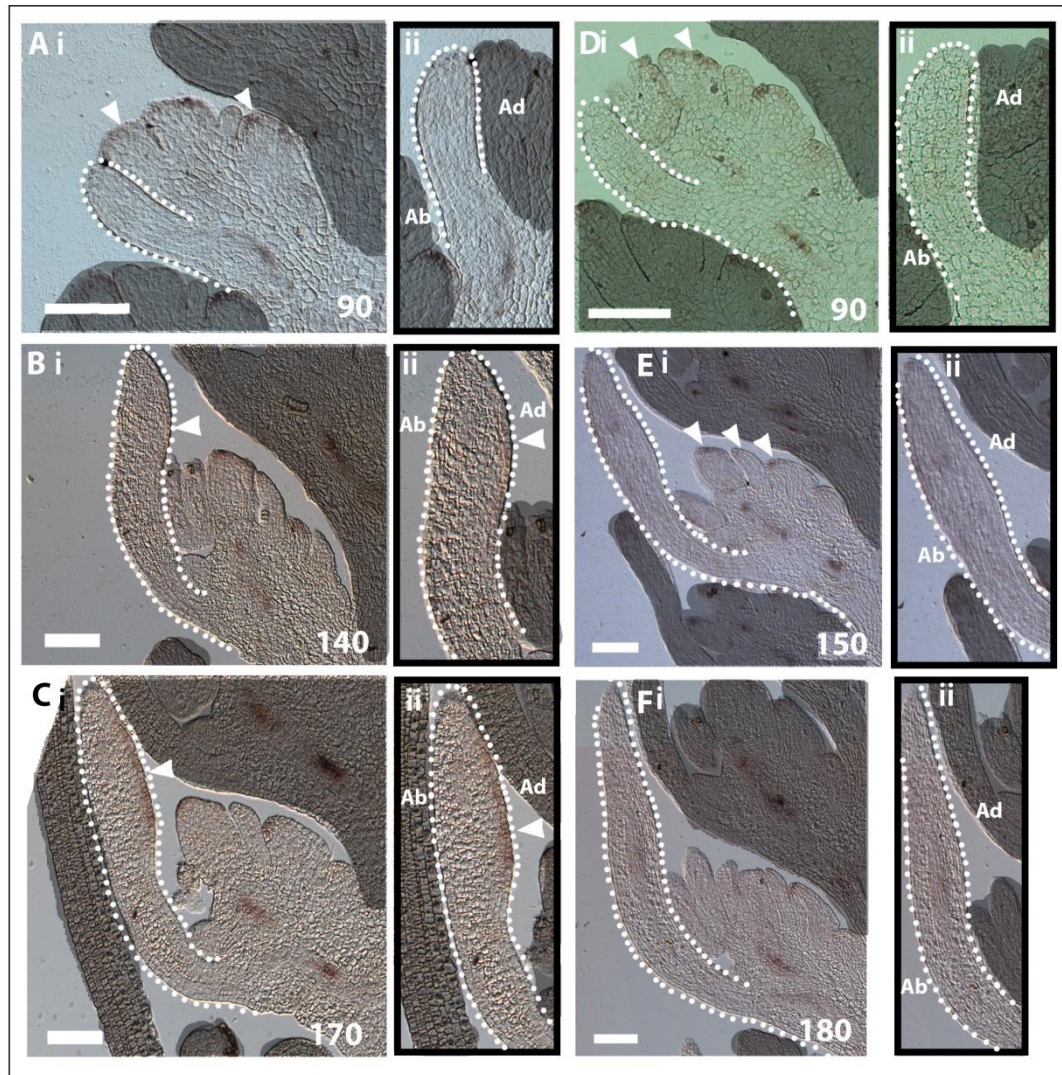


**Figure 3.21** RNA *in situ* hybridisation of *LAX1* mRNA in longitudinal sections through wild-type and *Hooded* barley flowers.

*A-C*: *Hooded* flowers. *D-F*: Wild-type flowers. *i*: longitudinal section through the flower. *ii*: zoomed-in image of the lemma in *i*. Dotted line highlights the shape of the lemma. *Ab*: Abaxial side of the lemma. *Ad*: Adaxial side of the lemma. The position of *LAX1* localisation are indicated by white arrowheads. Numbers indicate the approximate time since morphological T0 in hours. Scale bar is 100 $\mu$ m.

The mRNA localisation patterns of *NAM*, *YUCCA* and *LAX1* suggest that the ectopic expression of *BKn3* in the *Hooded* lemma, initiated at around 110 hours, can cause the ectopic expression of possible genetic components of organisers of polarity. Some genes, like *NAM* and *LAX1* are expressed ectopically in the *Hooded* lemma soon after ectopic *BKn3* expression is initiated, whereas the expression pattern of *YUCCA* is modulated later in development.

*BKn3* is initially excluded from the developing lemma (Figure 3.22.A.i). At around 110 hours, ectopic *BKn3* expression is activated in the adaxial side of the lemma, near the distal tip (Figure 3.22.A.ii) and this expression is maintained until the meristematic cushion (ectopic floral meristem) forms by around 170 hours (Figure 3.22.A.iii). It is between the activation of *BKn3* expression at 110 hours and the formation of the ectopic meristem (formed by 170 hours) that axial information, as marked by SoPIN1 localisation, reorients. This reorientation starts at around 120 hours. During this time period *LAX1*, *NAM* and *YUCCA* expression patterns are altered in the *Hooded* lemma.

Like *BKn3*, *LAX1* and *NAM* are excluded from the developing *Hooded* lemma during early stages of development (Figure 3.22.B.i, *LAX1* and Figure 3.22.C.i *NAM*). Once ectopic *BKn3* expression is activated in the lemma, both *NAM* and *LAX1* are also ectopically expressed in the lemma in the same adaxial region. *LAX1* mRNA is localised to the L1 of the region where *BKn3* is expressed (Figure 3.22.B.ii), and remains in this region until the ectopic meristem forms (Figure 3.22.B.iii). *NAM* is initially expressed in regions flanking the zone of *BKn3* expression (around 110 hours, Figure 3.22.C.ii). The expression of *NAM* then expands to be expressed in the meristematic cushion region which forms by 170 hours (Figure 3.2.C.iii). *YUCCA* is expressed throughout the developing lemma (Figure 3.22.D.i and ii) until around 170 hours. In *Hooded* lemmas at 170 hours, *YUCCA* mRNA is localised to the meristematic cushion region where *BKn3* is expressed (Figure 3.22.D) whereas at the same time in the wild-type *YUCCA* expression is lost from the lemma.

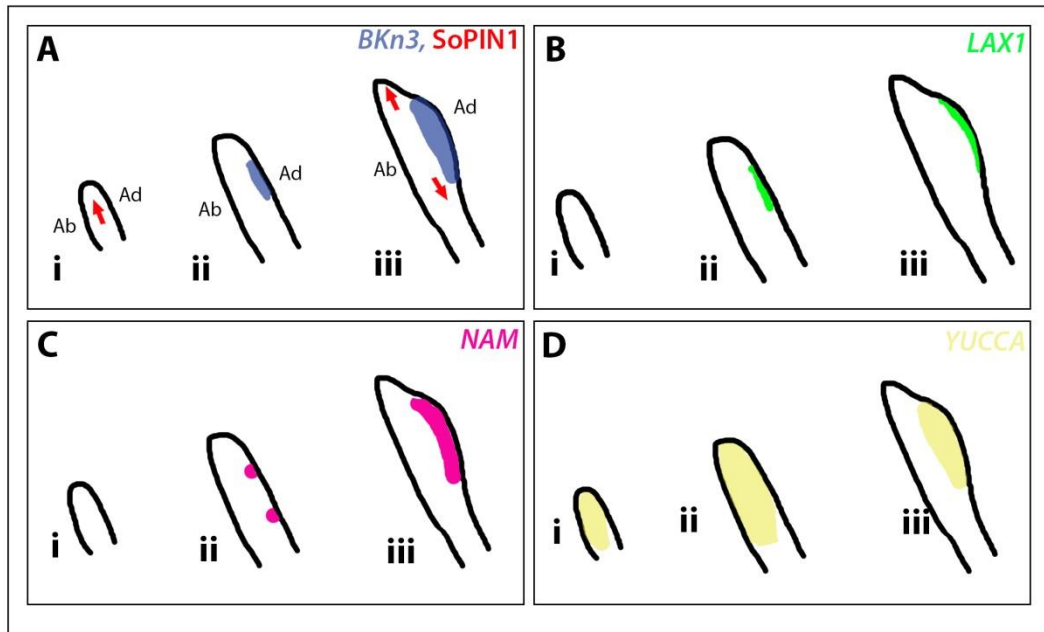


**Figure 3.22** Summary cartoon of the localisation of *BKn3*, *LAX1*, *NAM* and *YUCCA* mRNA and the pattern of SoPIN1 localisation in longitudinal midsections through *Hooded* lemmas at different stages in development.

All of the panels show cartoon representations of middle longitudinal sections through developing lemmas at 90 hours (*i*), 110 hours (*ii*) and 170 hours (*iii*) since T0, the outline of the lemma is shown by the black line. A: mRNA localisation of *BKn3* (blue). B: mRNA localisation of *LAX1* (green). C: mRNA localisation of *NAM* (pink). D: mRNA localisation of *YUCCA* (yellow). Red arrows indicate the pattern of SoPIN1 localisation in 2D slices through the middle of the lemma.

Overall, taking gene expression and SoPIN1 localisation patterns into account, *BKn3* may induce a reorientation of axial information through inducing the expression of organisers of tissue cell polarity in the developing lemma. It could be that the ectopic expression of *NAM*, soon after *BKn3* expression is activated, in the lemma (110 hours) signals the formation of a new plus organiser in the adaxial surface, possibly triggering the start of the axiality reorientation as marked by SoPIN1 (120 hours). This pattern may be reinforced later on with the increased localisation of *YUCCA* to the same region (although the expression of other *YUCCA* genes may provide a clearer picture). *LAX1* expression in the L1 layer of the meristematic region may indicate the position of a minus organiser in the dome of the meristematic region, promoting the orientation of SoPIN1 towards the centre of the meristematic dome. This could then lead to the formation of the inverted ectopic flower. However whether this is the case is not clear, as these patterns of expression could be related

to the formation of a new meristem. 3D expression patterns of *NAM*, *LAX1* and *YUCCA* may generate a clearer picture of the relationship between axial information and the organiser regions. Similarly the expression pattern of other members of the *YUCCA* and *LAX* families could provide better markers of organiser regions.

### **3.7 Specific changes in growth in the lemma margin trigger the developmental switch in shape responsible for wing formation**

The ectopic expression of *BKn3* in the *Hooded* lemma leads to the formation of wings in the margin of the lemma below the inverted ectopic flower (Figure 3.23, white arrowheads). It may be that the wings are a consequence of the change in growth rates and axiality that lead to the formation of the ectopic flower, i.e. are an indirect effect of *BKn3* expression in the developing lemma. Alternatively the wings could be the result of a separate change in growth specifically induced in the margin, i.e. a direct effect of *BKn3* (similar to how the diverse morphological effects of *KN1* expression in the maize leaf are dependent on where it is expressed [88, 152]). This separate change in growth could act through altering growth rates alone, axiality alone or both growth rates and axiality combined.

If wing formation is a distinct developmental switch in shape from the formation of the ectopic flower, *BKn3* could act in two different ways to change growth. *BKn3* may act non-cell autonomously over a long range to trigger the change in growth in the margin (i.e. the expression of *BKn3* does not match where the phenotype occurs), or *BKn3* could be ectopically expressed in the lemma margin and act cell autonomously to induce the change in growth (i.e. *BKn3* is expressed wherever a change in shape occurs).

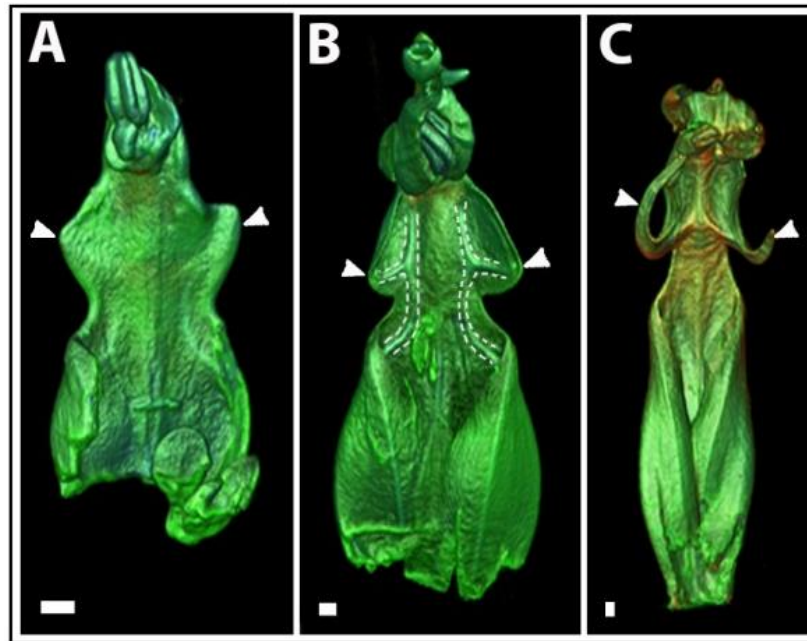


**Figure 3.23** OPT images of *Hooded* lemmas showing the wing outgrowths at different stages of development.

A-C: OPT images of the adaxial surface of *Hooded* lemmas at different late stages of development. The position of the wings is indicated with white arrowheads. An example of the branching of veins into the developing wing is highlighted by the dashed white line in B. Scale bar is 100 $\mu$ m.

### 3.7.1 Characterising a possible second developmental switch in shape in the *Hooded* mutant

To explore whether the formation of the wings is a separate developmental switch in shape from ectopic flower formation, I first generated an image timecourse to stage when different morphological events occurred. Using the developmental timecourse previously described (section 3.3), I was able to construct an OPT image timecourse focussed on wing development.

At the earliest stage in lemma development captured (T0), the lemma formed an upward crescent shaped primordium on the distal side of the floral meristem in both wild-type (Figure 3.24.A) and *Hooded* (Figure 3.24.E). By 170 hours, when the ectopic floral meristem had started to form on the adaxial side of the *Hooded* lemma, the abaxial side of the lemma in both wild-type and *Hooded* were an elongated triangular shapes (compare Figure 3.24.B.i to Figure 3.24.F.ii respectively). The cross-section through the base of the developing lemma showed that the insertion point of the lemma into the flower base shared the same shape

between wild-type and *Hooded*, forming an upward curving crescent (Figure 3.24.B.ii and Figure 3.24.F.ii).

By 240 hours (when the adaxial ectopic flower was developing organ primordia) the abaxial shape of the lemma diverges between wild-type and *Hooded*. The wild-type lemma continued to elongate, forming an extremely elongated triangular shape due to awn development (Figure 3.24.C.i). This elongation of wild-type continued throughout the rest of development (Figure 3.24.D.i). In contrast to this the *Hooded* lemma did not elongate greatly. At 240 hours, small bumps formed in the margin on opposite sides of the *Hooded* lemma (Figure 3.24.G.i, white arrowheads) below where the ectopic floral meristem was on the adaxial surface. By 340 hours these small bumps formed into triangular shaped outgrowths, the wings, (Figure 3.24.H.i) resulting in the *Hooded* lemma developing a star like shape. Despite this dramatic change in shape of the lemma, the cross-sectional shape of the lemma base where it inserts into the flower base remained the same as in wild-type, forming an upward crescent (Figure 3.24.C-D.ii, wild-type and Figure 3.24.G-H.ii *Hooded*). This shows that the shape change resulting from the outgrowth of wings from the *Hooded* lemma margins only affects the shape of the upper region of the lemma, not the lower region.

The wings form late in development (around 240 hours), after the ectopic expression of *BKn3* is activated (110 hours) and the inversion of axial information marked by *SoPIN1* localisation (starts at around 120 hours) has occurred. At this stage the ectopic floral meristem is established and has initiated organ primordia. This could suggest that the wings form as a consequence of the change in growth which led to the formation of the ectopic floral meristem as the wings form after these events. However, the long delay (around 120 hours between the change in axiality and wing development) between these events and the formation of the wings could indicate that the formation of the wings is a distinct developmental switch in shape.

As the timing of the different morphological events does not clearly distinguish between the hypotheses that the wings are either an indirect consequence of ectopic flower formation or they are a separate developmental switch in shape specific to the margin, other approaches are needed. If the formation of the wings is a separate developmental switch in shape specific to the margin of the lemma, it would be predicted that there would be specific expression of *BKn3* and organiser components in the margin, distinct from the expression patterns in the ectopic flower region. Alternatively using computational modelling, it may be

possible to test the hypothesis that distinct changes in growth occur specifically in the margin to generate the wings.

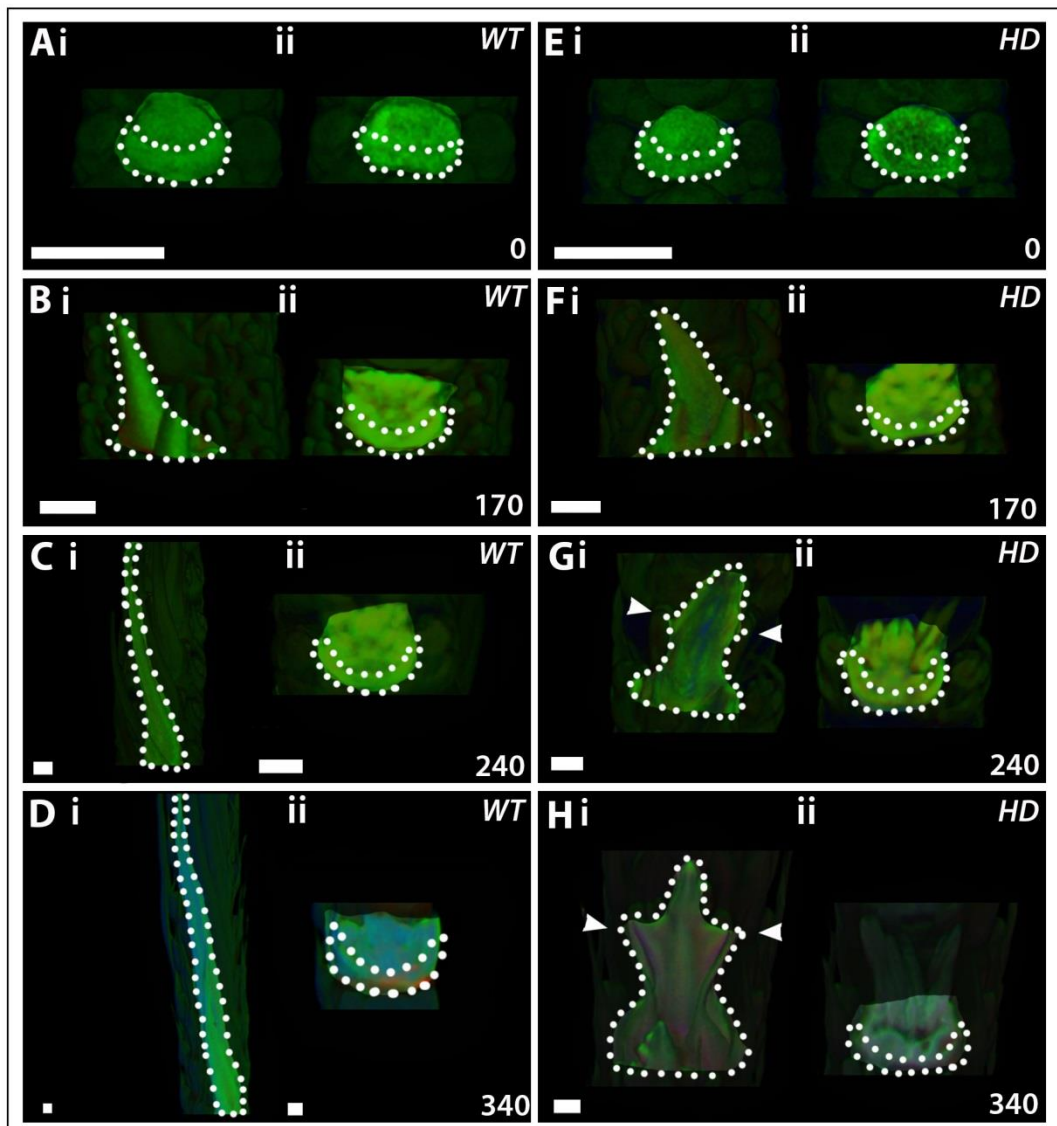


**Figure 3.24** The development of lemma shape in floret 5 of wild-type and *Hooded* inflorescence spikes over time.

OPT images of floret 5 at different stages in development, looking at the abaxial side of the lemma (the adaxial side is obscured by the rest of the inflorescence spike). *A-D*: wild-type lemmas. *E-H*: *Hooded* lemmas. *i*: the abaxial side of the lemma. *ii*: cross-sectional view through the base of the floret, showing the shape of the lemma at the insertion point with the base of the flower. White dotted lines highlight the shape of the lemma. White arrowheads indicate the position of the developing wings. Scale bars are 200 $\mu$ m.

### 3.7.2 Modelling *Hooded* lemma wing development as a consequence of changes in growth

To try to distinguish between the hypothesis that the wings form as a consequence of the global change in axiality and growth rates in the lemma and the hypothesis that the wings form in response to a specific change in growth in the margin, I developed some simple GPT framework based models to explore how outgrowth formation might be induced or controlled. The models focus on what conditions may be like in the lemma region where wings form below the ectopic flower.

Each model has a polarity regulatory network (PRN) from which growth orientations can be specified and a growth regulatory network (KRN) which specifies growth rates within the connected canvas. The axis of growth is determined by the local gradient of a diffusible factor called 'POLARISER' (POL, set up in the PRN), and growth can be defined parallel ( $K_{par}$ ) and perpendicular ( $K_{per}$ ) to this axis. All simple models were based on a square starting shape 0.1mm by 0.1mm and 1000 finite elements.

The whole-mount immunolocalisations of barley lemmas indicate that the axial information, as marked by SoPIN1 localisation, diverges below the ectopic meristem to orient towards the base of the lemma where the wings will form (Figure 3.14.D). Therefore, I first explored whether a diverging polarity field would be sufficient to initiate outgrowth formation. I introduced a polarity field which diverges in the middle of the rectangle. To do this I specified a source of POL in the middle of the canvas using the localised activity of a factor called 'Plus' (Figure 3.25.A.i, green is the plus organiser, the PRN is illustrated in Figure 3.25.B) and a sink of POL at the proximal and distal ends of the canvas through the local activity of a factor called 'Minus' (Figure 3.25.A.i, red and Figure 3.25.B shows the PRN). This generated a gradient of POL which was high in the middle of the canvas and low at the proximal and distal ends, giving rise to a diverging polarity field (Figure 3.25.A.i, POL is turquoise, the local orientation of axial information is indicated by the black arrows). A low constant rate of  $K_{per}$  and a higher constant rate of  $K_{par}$  was also introduced (KRN is outlined in Figure 3.25.C) (chosen because wild-type lemma development appears to be very anisotropic parallel to the proximal-distal axis of the lemma). This model developed small outgrowths in the middle of the canvas at the point of polarity divergence. However, as the simulation progressed the outgrowths did not elongate (Figure 3.25.Aii). This morphology is unlike the shape of the wing outgrowths in the *Hooded* mutant (Figure 3.23) which can be longer than the width of the lemma.

This simple model suggested that small outgrowths could be initiated from global reorientations in axial information although this model does not replicate the shapes seen in the developing *Hooded* lemma. This may indicate that the changes in growth that trigger the formation of the wings may be independent of those responsible for the formation of the ectopic meristem. The small size of the outgrowths formed may be due to the local effects of a plus organiser (Figure 3.25.A.ii, resultant growth is lower than the surrounding canvas, as shown by the yellow colour). This led me to test whether high growth rates specifically in the margin could be key to generating wing outgrowths independent of the global changes in growth.

I introduced a uniform proximodistal polarity field (Figure 3.25.Di and the PRN in Figure 3.25.B) with patches of high perpendicular growth in the margins of the canvas. The polarity field was set up by activating 'Plus', which promoted the production of POL, at the proximal end of the canvas and 'Minus', which promoted the loss of POL, at the distal end of the canvas (Figure 3.25.Di). A new diffusible factor called 'PROMOTE' was introduced in patches in the margin of the canvas (Figure 3.25.Di, pink) which enhanced  $K_{per}$  in these regions,  $K_{par}$  remained constant as before (the KRN used is in Figure 3.25.E). This model produced rounded outgrowths in the regions where growth was specified to be high (Figure 3.25.Dii). However, the increase in  $K_{per}$  also influenced the rest of the canvas meaning that the canvas did not elongate as before, producing a short, squat model with rounded outgrowths (Figure 3.25.D.ii). This resultant model shape does not match the shapes seen in the wing development.

If axiality is oriented towards the wing tip in the margin before wing development, it could be that the outgrowths form through reorientation of axiality specifically at the margin, similar to the way serrations form in *Arabidopsis* [4]. To test this hypothesis, I used a proximodistal polarity field with POL produced at the base of the canvas and introduced two additional regions in the canvas margin called 'Tip', which acted as additional minus organisers and inhibited POL (PRN in Figure 3.25.G, canvas set up in Figure 3.25.F.i).  $K_{per}$  and  $K_{par}$  were kept constant (see KRN in Figure 3.25.C). The result of this simulation (Figure 3.25.F.ii) developed outgrowths that were larger and pointier than the model with a broad polarity field change (Figure 3.25.A.ii) and which were wider in the lower half of the outgrowth. This was due to the growth being higher parallel to the polarity field and the polarity field orienting specifically towards the tip of the outgrowths. This resultant shape

was more like the shapes seen in the early stages of wing development (Figure 3.23.A) although they were still quite small.

During lobe development in *Arabidopsis lyrata* growth rates are predicted to be higher in the outgrowth region than the flanking areas [4]. If the wings on the *Hooded* mutant develop like leaf lobes it could be that the addition of a localised increase in specified growth rate at the margin may more accurately recreate the shape of the wings seen in OPT imaging (Figure 3.23). To test this, I used the same model as before which had specific polarity reorientations in the margin (see Figure 3.25.G for the PRN, Figure 3.25.H for the canvas set up) and added the diffusible factor PROMOTE in the same region (Figure 3.25.Hi) which promoted both  $K_{per}$  and  $K_{par}$  (See figure 3.25.I for the KRN). The resulting shape of this simulation generated larger wings with a broad base and rounded tips which were shifted distally, more accurately replicating the shape of the wings in Figure 3.23.A and those imaged in Figure 3.24.G-H. The specific shape changes during wing development illustrated in Figure 3.23.A-C may occur through changing the balance of growth rates parallel ( $K_{par}$ ) and perpendicular ( $K_{per}$ ) to the axial information over time.

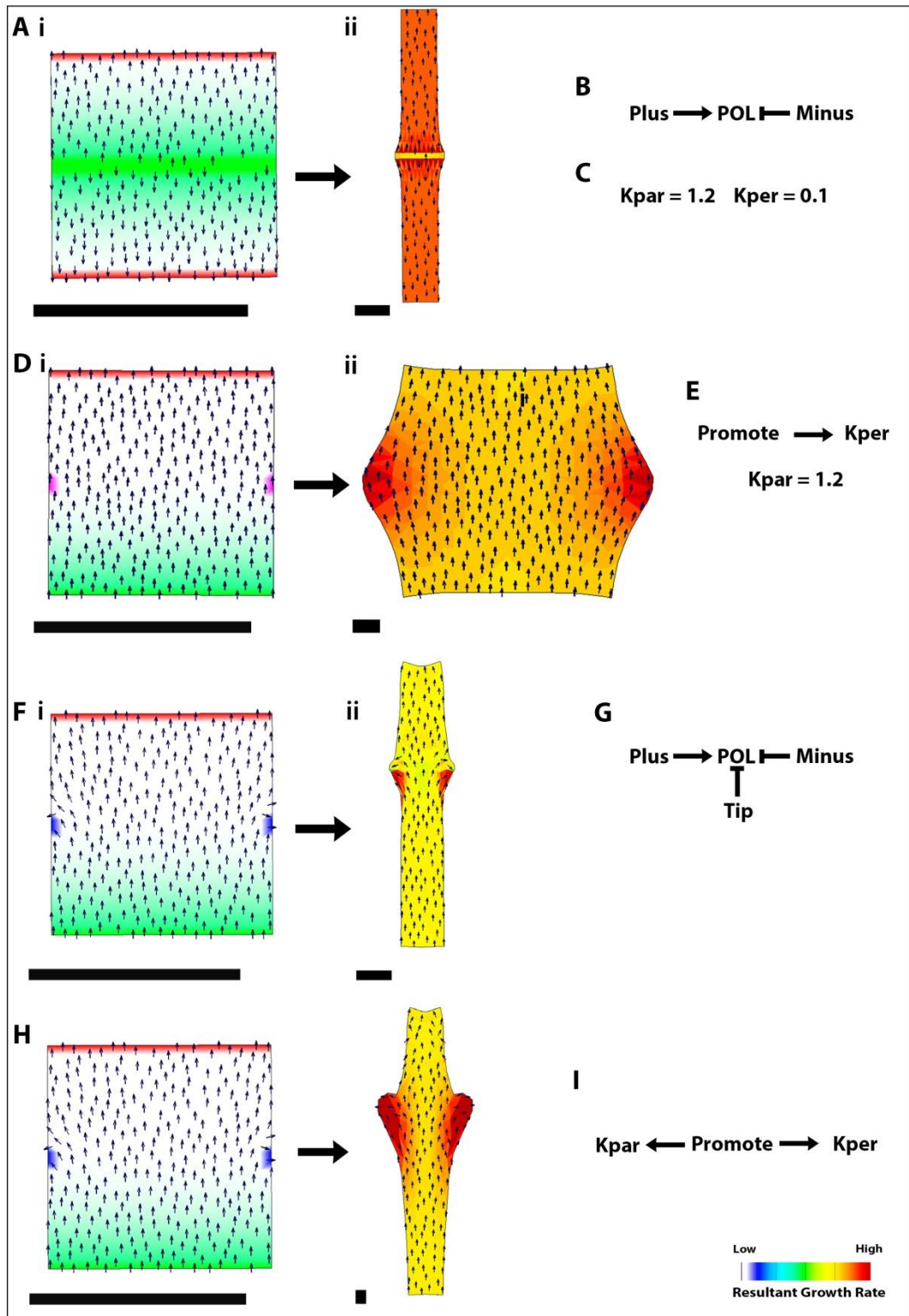


Figure 3.25 GPT framework modelling of outgrowths.

*i*: Set-up of the canvas, indicating POLARISER gradient (turquoise), Plus (green), Minus (red), Tip (blue) and Promote (pink) regions where relevant. *ii*: result of the simulation, indicating the resultant growth rate (colour scale, red high growth rate, blue low growth rate). A: Global polarity divergence model. B: Polarity regulatory network (PRN) for the models in A and D. C: Growth Regulatory Network (KRN) for the model in A. D: Enhanced marginal growth rate

model. *E*: KRN for the model in D. *F*: Margin polarity reorientation model. *G*: PRN for the models in F and H. *H*: Combined enhanced growth rate and modified polarity field in the margin model. *I*: KRN for the model in H. Scale bars are 100µm.

This modelling suggests that the wings of the *Hooded* mutant may be a second developmental switch in shape in the *Hooded* lemma, independent of the formation of the inverted ectopic flower. This developmental switch in shape may be triggered by changes in growth specifically in the marginal tissues of the developing lemma, after the ectopic flower has started to form. The change in growth could be the result of alterations in both growth rates and axial information in the margin. The modelling predicts that the axial information in the wing in the *Hooded* mutant is oriented towards the wing tip (rather than towards the base of the lemma or tip of the lemma) and that growth rates will vary in the wing region compared to the rest of the lemma. This could also predict that either *BKn3* is acting non cell autonomously at a distance to generate the wing outgrowths (as these form below the ectopic meristem region where *BKn3* is expressed) or that *BKn3* is also expressed in the margin of the developing lemma, which has not been shown by previous studies.

### **3.7.3 Axial information may specifically reorient at the margin of the *Hooded* lemma**

To test the prediction that axial information reorients specifically in the margin of the lemma, I looked at markers of axiality at later stages of *Hooded* lemma development.

I first looked at late stage indicators of axial information to test the prediction that the axial information orients towards the wing tip. One indicator of axial information is hair orientation. To assess the orientation of hairs in the mature wings I carried out SEM imaging of the wings in mature *Hooded* lemmas (in collaboration with Elayne Barclay at JIC Bioimaging Services). The abaxial surface of the wild-type lemma did not have any distinct hairs (SEM images of wild-type lemmas are shown in Appendix B), therefore I focussed on the hairs on the adaxial surface of the lemma. In mature *Hooded* lemmas the hairs above the point where the wings form, oriented towards the base of the lemma (Figure 3.26.i, red arrows). As imaging progressed along the wing, the hairs appeared to orient towards the tip of the wing (Figure 3.26.ii, red arrows), rather than towards the base of the lemma or the bottom edge of the wing which would be expected if the wings maintained the same inverted orientation of the axial information as the margins. At the tip of the wing the hairs all

oriented towards the tip of the wing (Figure 3.26.iii, red arrows), indicating that the axial information was oriented towards the tip of the wing during development.

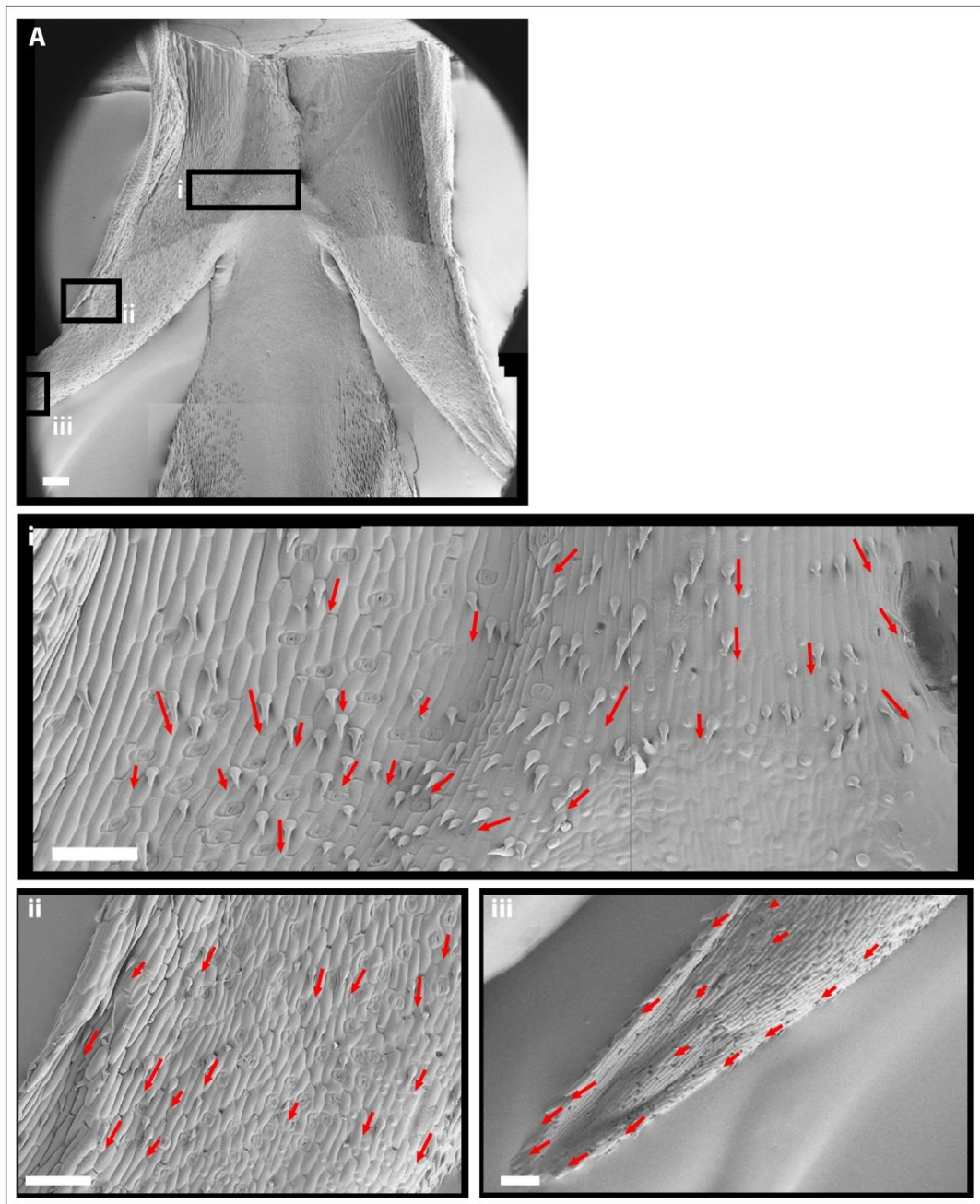


**Figure 3.26** SEM images of the adaxial wing region in a mature *Hooded* lemma  
Cryo SEM images of the adaxial surface of the wing region, just below the ectopic flower in a mature *Hooded* lemma (Images taken by Elayne Barclay, JIC Bioimaging service). **A**: a zoomed out image of the whole region imaged. *i-iii*: zoomed-in images of the boxed regions in **A**. *i*: the region just below the ectopic flower. *ii*: top of the wing. *iii*: the tip of a wing. The red arrows indicate the orientation of the hairs. Scale bars are 100 $\mu$ m.

Another read out of tissue cell polarity may be vein orientations as they develop in response to auxin and auxin is hypothesised to be a coordinator of axial information [42]. In the OPT images of *Hooded* lemmas, fully developed veins were visible (Figure 3.23.B and C, an example is outlined with a white dashed line). In the base of the lemma the veins were parallel, and they then appeared to specifically form new branches which lead into the wing tips (Figure 3.23.B, an example is shown by the white dashed line). This branching suggests that the axial information may be oriented towards the wing tips.

To explore axial information at earlier stages in development than hairs and veins provide, I analysed the orientation of cell files in developing wings. To visualise the cell files in developing wings, I stained *Hooded* lemmas with the cell wall stain calcofluor and imaged the adaxial surface using confocal microscopy. Cell files were then highlighted by colouring individual cells which share the same cross-walls. In *Hooded* lemmas before the wings started to develop (170 hours, Figure 3.27.A.i) cell files in the margin of the lemma were relatively straight and oriented proximodistally (Figure 3.27.A.ii).

In the central region of *Hooded* lemmas at later stages (Figure 3.27.B.i) the cell files were oriented proximodistally and were relatively straight (Figure 3.27.B.ii). This suggests that growth is predominantly along the proximodistal axis in the centre of the lemma. In the regions near the wings, these orderly straight cell files were disrupted, bending towards the tip of the developing wings (Figure 3.27.B.ii). This strongly suggests that the growth orientation (and therefore the axial information) in the margin of the developing lemma is specifically altered where the wings form.

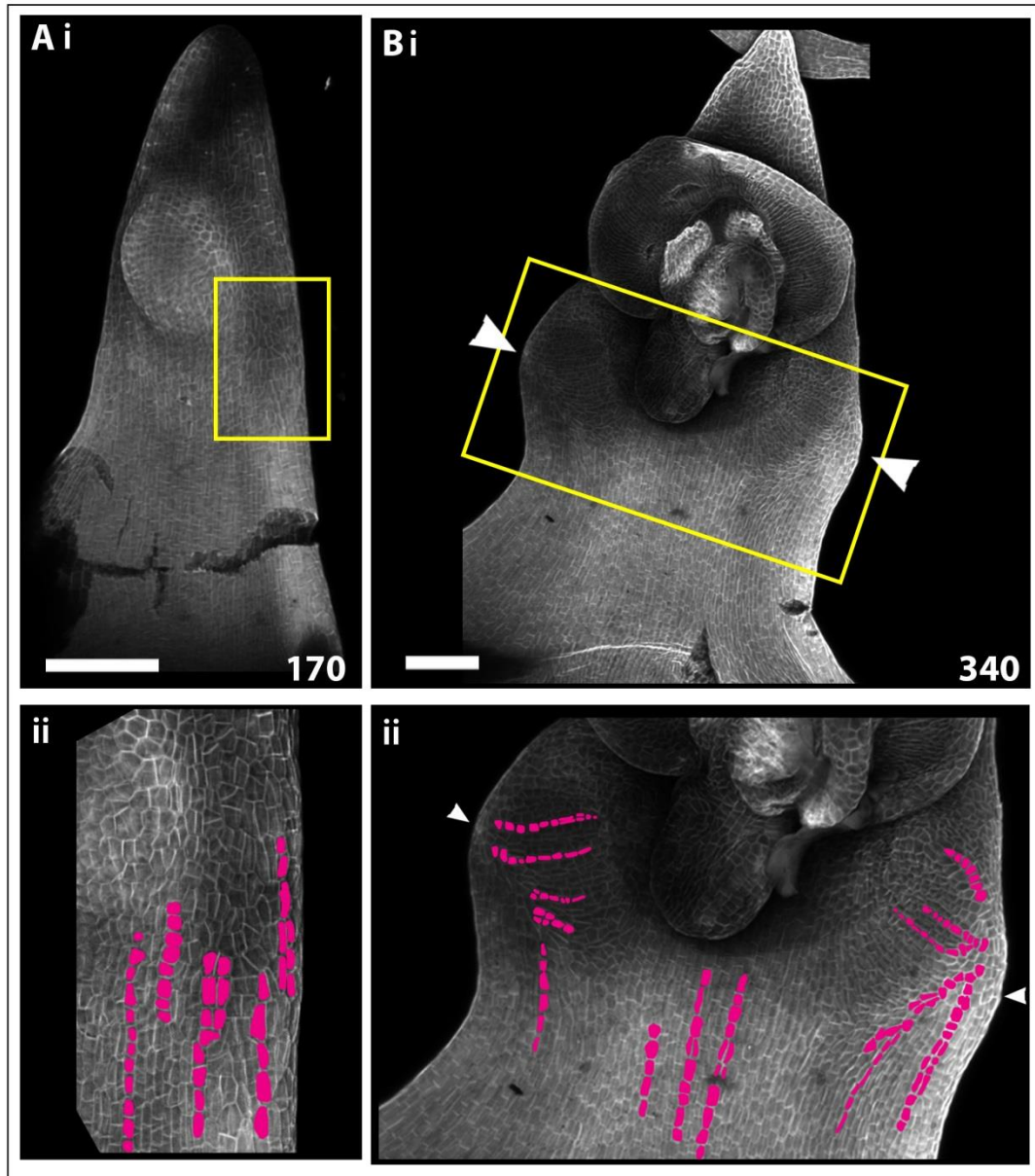


**Figure 3.27** Cell file patterns in the adaxial surface of *Hooded* lemmas. Adaxial views of developing *Hooded* lemma at approximately 170 (A) and 340 (B) hours since T0. *i*: image of the whole lemma at each time stage. *ii*: zoomed-in image of the yellow boxed region in *i*. Wing tips are indicated by white arrowheads. Cell files are coloured pink. Scale bars are 100 $\mu$ m.

I have not yet been able to explore SoPIN1 localisation in the margin of the developing lemma, as it is hard to image the margins, to test whether SoPIN1 localisation patterns are specifically altered in the wings.

These markers of axiality all suggest that the axial information may reorient in the margin, specifically where the wings form. This provides some support for the hypothesis that the wings are a developmental switch in shape independent from the formation of the inverted ectopic flower. This may also support the model prediction that the wings are formed by a specific change in growth activated in the margins of the developing *Hooded* lemma. The modelling also predicts the involvement of a specific change in growth rate pattern in the margin however I have not yet been able to test this. This evidence so far is not definitive, it may be that with dynamic data such as information on axiality or growth rates over time, or over more timepoints it may be possible to explore the independence of wing formation from the other changes in the lemma.

#### **3.7.4 *BKn3* may act cell autonomously in the margins to form the wings in the *Hooded* mutant**

As the wings may be a second independent developmental switch in shape triggered by *BKn3* expression in the *Hooded* lemma, it raises questions about how *BKn3* induces changes in growth in different spatial and temporal patterns. Work so far has shown that *BKn3* is specifically expressed in the region relating to the ectopic meristem. This would suggest that perhaps *BKn3* is acting non-cell autonomously to trigger changes in growth in the margin, forming the wings. KN1 protein has been shown to be mobile [153], however the distance between the ectopic meristem and wings is large making it unlikely that the protein moves to the margins to trigger the formation of the wings. Alternatively *BKn3* could be expressed specifically in the margin of the lemma later in development where it triggers the developmental switch in shape.

To explore this I carried out RNA *in situ* hybridisation in the *Hooded* lemma at later stages of development (Figure 3.28 shows slices through flowers at 300 hours since T0, wings start to form at 240 hours). In these late stage samples there does not appear to be *BKn3* expression in the regions below the ectopic flower. *BKn3* mRNA appears to be specifically localised to the base of the ectopic flower and the base of the normal flower (Figure 3.28.A, white arrowheads). This would suggest that *BKn3* is not expressed as a collar around the lemma, below the ectopic flower, although it does not exclude that it is only expressed in the marginal edges which I have not been able to capture using this slice technique.

If *BKn3* was inducing a specific change in axial information in the wing region it may be that the possible components of polarity organisers are also ectopically expressed in the wing

region. In late developmental stages, there does appear to be a very faint band of *NAM* expression in the region where wings would develop, just below the ectopic flower (Figure 3.28.B, white arrowhead). Similarly there appears to be an indication of possible localised *YUCCA* expression in the L1 on the adaxial and abaxial surfaces of the lemma in the region where the wings would develop (Figure 3.28.C, white arrowhead). These patterns of mRNA may be consistent with the formation of a possible new plus organiser at the base of the wings although they are not clear. There is no evidence of *LAX1* overlapping with these bands of expression (Figure 3.28.D) below the ectopic flower, instead *LAX1* mRNA is localised to the tip of the developing organs and vasculature. It may be that a new minus organiser is formed at the tip of the wing, however I have been unable to get a slice through the tip of a developing wing to assess whether *LAX1* is expressed here.

This expression data suggests that *BKn3* may be able to non-cell autonomously trigger a change in growth in the margins, through influencing the expression pattern of possible components of organisers of polarity to alter the axial information. However this data is only 2D making it difficult to truly assess the 3D pattern of gene expression in relation to wing development. This makes it difficult to conclude whether *BKn3* acts cell autonomously.

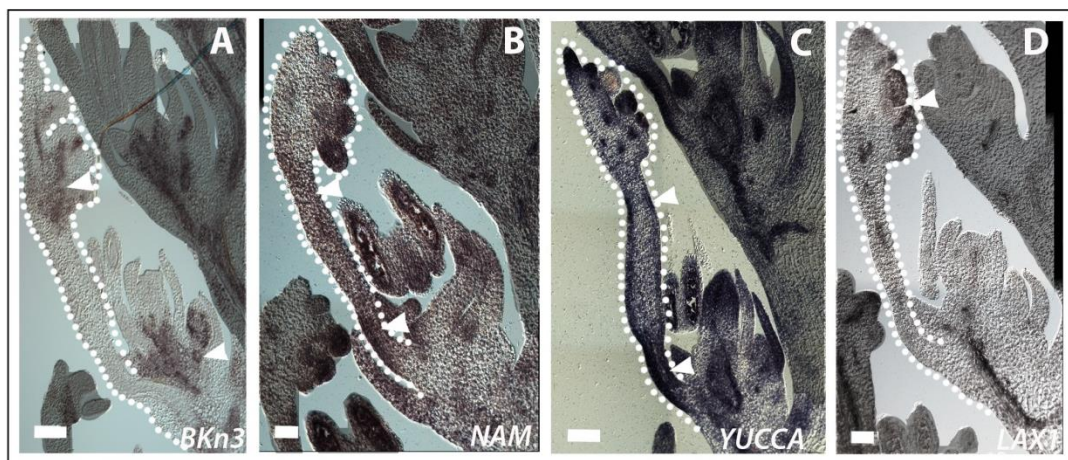
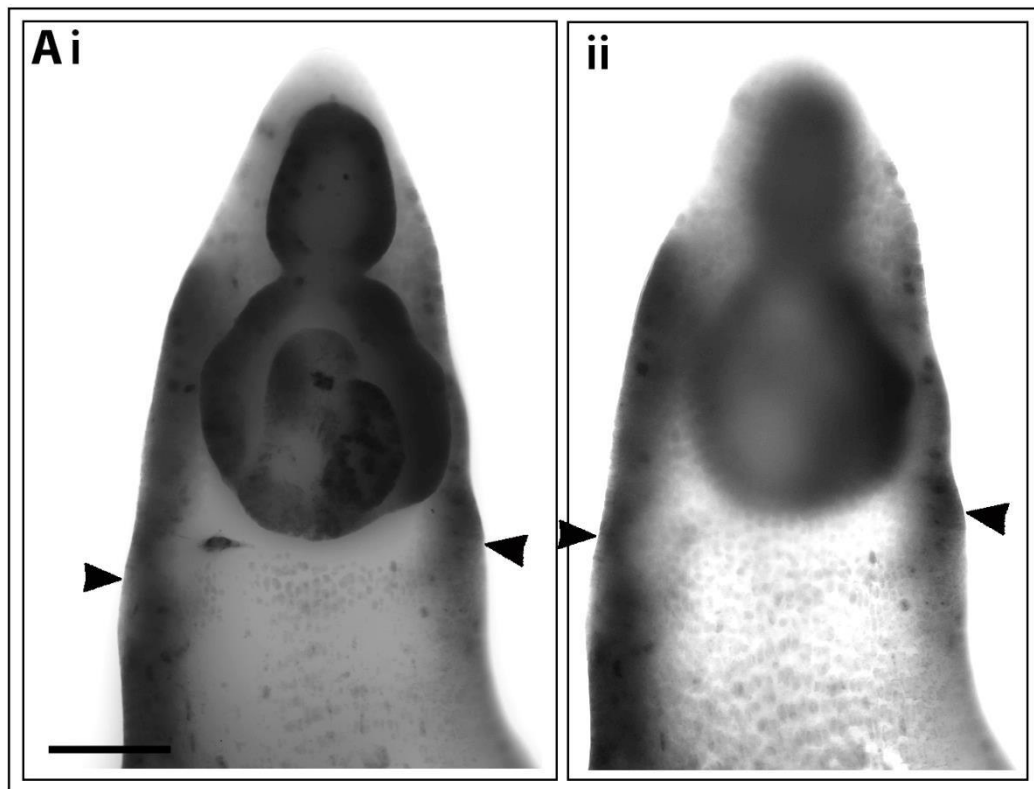


Figure 3.28 RNA *in situ* hybridisation patterns of *BKn3*, *NAM*, *YUCCA* and *LAX1* in longitudinal sections through *Hooded* flowers at late stages in development. Longitudinal middle sections through *Hooded* flower at around 300 hours since T0. A: *BKn3*, B: *NAM*, C: *YUCCA*, D: *LAX1*. Position of the expression regions of the genes are indicated (white) with arrowheads. Scale bars are 100µm.

As it is difficult to evaluate what the expression pattern of each of these genes is in 3D in relation to wing development, I trialled using the whole-mount immunolocalisation protocol to visualise the localisation of BKn3. Using this 3D information about BKn3 localisation in the *Hooded* lemma I hoped to assess whether BKn3 truly was acting non-cell autonomously or whether BKn3 was ectopically localised in the margins of the *Hooded* lemma. To do this I used an antibody which recognises all KNOX1 proteins from Sarah Hake. I used a modified precipitate DAB staining protocol to visualise the localisation of the KNOX1 antibody. Preliminary results using this whole-mount protocol suggest that BKn3 protein may be localised in the margins of the developing lemma, although it is not specific to the wing region only (Figure 3.29, dark staining indicates the localisation of KNOX proteins including BKn3, possible ectopic localisation of BKn3 in the margin is indicated by the black arrowheads).



**Figure 3.29** Whole-mount immunolocalisation of BKn3 in a developing lemma at approximately 260 hours.

DIC light image of the adaxial surface of a *Hooded* lemma at approximately 260 hours since T0. Whole-mount immunolocalisation of KNOX proteins using a DAB staining protocol. KNOX (including BKn3) protein localisation is indicated by the black precipitate. Possible localisation of BKn3 in the margin where wings form is indicated by the black arrowheads. *i*: z projection of the whole lemma image stack. *ii*: z projection of the slices which contain the lemma margins only. Scale bar is 100 $\mu$ m.

This preliminary evidence suggests that *BKn3* may not act non-cell autonomously to trigger the formation of the wings in the margin. Instead *BKn3* may be ectopically expressed in the margin of the lemma during later stages of development where it acts cell-autonomously to change growth and trigger the formation of the wings. These changes in growth may be through local modulation of both growth rates and axial information. To confirm this finding more whole-mount immunolocalisations of SoPIN1 and BKn3 and studies of growth dynamics in the wing region would be required. Although unlikely, this protein localisation pattern does not exclude the possibility that *BKn3* protein moves to the margins, therefore more *in situ* hybridisation is also required to establish the expression pattern of *BKn3* during later stages of development.

## **3.8 Discussion**

### **3.8.1 Characterising the morphology of the wild-type and *Hooded* spike during development**

Existing studies of wild-type barley development have predominantly focussed on late stage leaf and flower development. Many of the images available for developmental studies on the barley flower (particularly for *Hooded* barley) are based upon SEM and light microscopy [89, 138, 140] which, although valuable do not provide 3D volumetric information. By carrying out 3D OPT imaging of wild-type and *Hooded* barley spikes over a period of 380 hours of inflorescence development, I have developed a detailed 3D image resource covering early inflorescence development which was not previously available in the literature.

This timecourse data has enabled me to approximately describe the relative timings of important morphological events during barley inflorescence development. I have also been able to develop sets of descriptive measurements and growth curves for barley inflorescence and individual floret development. Although the exact timings and measurements may vary depending on growth conditions and genotype, this data provides an approximate baseline to which other studies can be compared. The volumetric nature of the OPT images also enabled me to develop a technique to stage data collected using 2D slices of tissue.

This morphology data has corroborated existing literature which reported that very early stages of development in the *Hooded* mutant resembles wild-type [139, 140] and has identified key morphological events which occur during *Hooded* development. From 0-160

hours during the period observed, lemma development in the *Hooded* mutant resembles that of wild-type, both morphologically and in estimated growth rates. From 160 hours onwards the development of the *Hooded* lemma diverges from that of wild-type (wild-type continues to elongate). By 170 hours the 'meristematic cushion' reported in the literature, has developed. By 180-200 hours organ primordia begin to differentiate in the ectopic meristem. By 240 hours the wings below the ectopic meristem begin to develop. This detailed information enables targeted questioning of events that lead to these morphological changes both by myself and for future studies.

### **3.8.2 There may be two independent developmental switches in shape in the *Hooded* mutant**

Through characterising morphological and growth changes I have identified two possible developmental switches in shape during the development of the *Hooded* lemma.

The first developmental switch in shape occurs soon after ectopic *BKn3* expression is detected in the lemma and results in the formation of the inverted ectopic flower. This developmental switch in shape is located on the adaxial surface of the lemma and starts at around 160 hours with the formation of a 'meristematic cushion' (ectopic meristem) towards the distal tip of the lemma (formed by 170 hours). The ectopic meristem then goes on to develop distally positioned organs. The second developmental switch in shape occurs later in lemma development forming wing outgrowths in the lemma margin. The wings begin as bulges from the lemma margin, below the ectopic flower at around 240 hours. These then develop into large triangular, awn like outgrowths.

Both of these developmental switches in shape are induced by the same gene, *BKn3*. The different response of the tissue shape dependent on the region in which *BKn3* is expressed is similar to the effects of *KNOTTED1* overexpression in maize leaves. When *KN1* is expressed in association with veins, knots form, while when it is expressed in the margin, leaf flaps form, and in the tip of the leaf a forked leaf forms [88, 152]. This difference in phenotype which appears dependent on the location of ectopic expression suggests that the precise shape triggered by a gene can depend upon the tissue context where the growth change is initiated.

It may be that wing formation is analogous to the formation of leaf flaps in the *Knotted1* mutant in maize [88] and lobe or leaflet formation in *Arabidopsis* relatives [5, 77]. In the elaboration of *Arabidopsis* (and its relatives) leaf margins both growth rates and axiality

changes have been found to have roles. Serration, lobe and leaflet formation are preceded by specific reorientations of PIN1 in the leaf margin to form regularly spaced convergence points suggesting changes in the axial information [4]. This is then followed by changes in growth rate patterns. For example, *Arabidopsis* leaf serration development may arise through slightly enhanced growth [5]. In transgenic *Arabidopsis* plants which produce lobes instead of serrations, it is proposed that the growth of the region distal to the lobe is reduced [77].

Through elucidating the precise change in growth that generates the wing outgrowth in the *Hooded* mutant, it may be possible to shed light on how other developmental switches in shape in marginal tissues may be regulated.

### **3.8.3 Single genes are able to trigger developmental switches in shape through modulating growth rates and axiality**

Both of the identified developmental switches in shape are triggered by the specific ectopic expression of *BKn3* in the developing lemma. I have found that *BKn3* is likely to act cell autonomously to alter growth separately in the middle of the lemma generating the ectopic flower and in the margin to form the wings. In both of these cases *BKn3* may act to modulate both growth rates and axiality.

Previous work in the *Hooded* mutant had identified that *BKn3* enhanced the rate at which the mitotic cycle occurred in the adaxial surface of the lemma, suggesting that *BKn3* was able to modulate growth rates in the barley lemma [139]. I have shown that *BKn3* is able to induce a reorientation of axial information at the cellular level, changing SoPIN1 localisation. Both the change in growth rate and the change in axiality occur before any change in morphology suggesting that these *BKn3* induced changes in growth trigger the formation of the inverted ectopic flower (the developmental switch in shape). Through modelling the development of wings, I have also predicted that it is likely *BKn3* is able to modulate growth rates and axiality in the lemma margin to trigger the formation of the wings (although the growth changes are yet to be confirmed in this case).

This suggests that *BKn3* and possibly other class 1 *KNOX* transcription factors are able to induce changes in axial information and growth rates during development. This would correlate with the involvement of class 1 *KNOX* genes in several different developmental switches in shape in other systems, such as leaf knot formation in *Knotted1* mutants in maize [88, 152], compound leaf formation in tomato [142] and petal spur formation in the

*Antirrhinum Hirz* mutant [154]. All of these developmental switches in shape involve the reactivation of class 1 *KNOX* genes in the developing organs.

Class 1 *KNOX* genes may be able to induce such dramatic developmental switches in shape due to their ability to modulate both growth rates and axial information. This ability could be due to their role as master regulatory nodes in transcriptional networks. For example ChIPseq work on *KNOTTED 1* gene in maize has identified 643 genes which are possibly regulated by KN1 in different tissues [155]. Many of the genes modulated by KN1 are transcription factors. This work also identified that KN1 was able to influence elements within auxin, cytokinin, gibberellic acid and brassinosteroid biosynthesis and signalling pathways. This ability of KN1 to influence transcriptional networks and hormone regulation may explain how the mis-expression of a single gene is able to modulate both axial information and growth rates. (The ability of a single gene to influence so many diverse aspects of development was a highly debated feature of the *Hooded* mutant before the *BKn3* gene was cloned [140], however this wide ranging influence of *KNOX* class 1 genes now explains this.)

It may be that during evolution the reactivation of genes able to influence growth in developing organs has been used to trigger novel developmental switches in shape altering final morphology. This reactivation of genes able to induce changes in growth could arise through cis-regulatory changes in the gene itself (as is the case of *BKn3* in *Hooded* [90]), or through changes in trans-acting regulatory elements (as is the case in miRNA control of leaf polarity in maize and *Arabidopsis* [156, 157]). The relative contribution of trans-acting and cis-acting regulatory changes in the induction of new developmental switches in shape is an interesting question which remains to be answered. Interestingly, many of the changes induced by class 1 *KNOX* mis-expression are due to cis-regulatory changes [88, 90, 154].

#### **3.8.4 *BKn3* may influence axial information through modulating the expression of organiser components**

Based on the assumption that axiality within a developing plant tissue is provided by a polarity based axiality system, I explored how *BKn3* may influence axial information in the developing lemma through the modulation of organisers of polarity. Through assessing the expression patterns of candidate components of organisers of polarity I found that *BKn3* was able to induce the ectopic expression of all candidate components tested so far specifically in the adaxial region of the lemma. This suggests that *BKn3* could influence axiality through

modulating the distribution of organiser components in the developing lemma. In particular the formation of a new plus organiser in the region of the ectopic meristem may contribute to the reorientation of polarity markers in the developing lemma. The ability of *BKn3* to induce the expression of possible organiser components is also supported by previous studies which have shown that *KN1* homologues in different species can influence the expression levels of possible components; *STM* binds the *CUC1* promoter directly in *Arabidopsis* [126], *KN1* upregulates *PINs* and auxin biosynthesis genes and downregulates *LAXs* in maize leaves [155]. If *BKn3* induces new organisers of polarity in the *Hooded* lemma, generating changes to axial information, this could be the mechanism behind the ‘source of new polarising gradients’ proposed by Stebbins et al [139].

However, the patterns of induced organiser gene expression in the *Hooded* lemma do not immediately provide a clear picture of how the polarity field is influenced by *BKn3* (the expression patterns may be more consistent with the formation of a meristem). It is possible that the correct components of organisers of polarity have not been identified and assessed. For example, in *Antirrhinum majus* (Alexandra Rebocho, JIC, unpublished) and *Arabidopsis*, *YUCCA1* is thought to be a key player in defining polarity and the maize homologue *SPI1*, essential for inflorescence development [55], is highly expressed in the inflorescence. The *YUCCA* analysed in this study so far was not in the *YUCCA1* clade, therefore its expression pattern may be misleading with respect to organiser localisation. Using the more detailed microarray expression data now available on the IPK barley database it may be possible to identify better candidates for organisers active in developing tissues. It may also be that *BKn3* itself is able to act as a plus organiser component.

If the formation of wings in the lemma margin is due to a *BKn3* induced change in marginal axial information, and is independent of the formation of the inverted ectopic meristem, this could be evidence in support of the hypothesis that *BKn3* is able to influence the axiality mechanism.

Alternatively, the formation of the inverted ectopic flower may be due to an independent level of axial information (i.e. not determined by the axial information provided by the distribution of organiser regions and auxin). For example, *BKn3* could induce the formation of an inflorescence meristem (rather than a floral meristem) on the lemma, conferring a proximal, rachis like identity to the region where *BKn3* is most highly expressed [138]. This would trigger the formation of two opposing florets on the *Hooded* lemma, recapitulating the distichous patterning in the wild-type inflorescence and vegetative meristems. Another

hypothesis, could be that the ectopic meristems form in the lemma/ awn boundary and it is the identity of the underlying tissue that determines whether the palea forms proximally or distally (e.g. palea could form furthest from the lemma/awn boundary which may have a different identity to the rest of the lemma tissue).

This work was based upon the assumption that a polarity based axiality system was active in the developing lemma. However this does not exclude the possibility that a stress based axiality system may be functional in the developing lemma instead. How the effect of ectopic *BKn3* expression on a stress based axiality system could be tested remains unclear.

Clarifying how *BKn3* is able to influence axial information within the developing *Hooded* lemma may ultimately provide insight into how other mutant phenotypes arise. For example ectopic expression of *KN1* in the maize leaf results in the formation of knots, which have swirled patterns of venation, and marginal outgrowths which disrupt the parallel venation of the leaf [152]. If *BKn3* is able to directly influence a polarity based axiality system which is centred around auxin, this may explain the vein patterns, as veins form in response to auxin [49]. However, whether *BKn3* can directly affect a polarity based axiality system is yet to be confirmed.

### **3.8.5 Future work and concluding remarks**

This project aimed to test how single genes were able to trigger developmental switches in shape through modulating growth, as well as testing whether the formation of the wings was a developmental switch in shape distinct from the formation of the ectopic flower.

Modelling combined with preliminary whole-mount immunolocalisations of BKn3 in the *Hooded* lemma suggests that the formation of the wings may be a separate developmental switch in shape to the formation of the ectopic flower. However to confirm this, more detailed whole-mount immunolocalisations of BKn3 are required to confirm whether BKn3 is specifically in the margin where the wings form. RNA *in situ* hybridisation of the margin region in *Hooded* lemmas may also contribute to testing this localisation pattern. The exploration of SoPIN1 localisation patterns in the lemma margin at stages relevant for wing development would also be required to confirm the hypothesised specific reorientation of axial information in the lemma.

Published work, in combination with work carried out during this project has found that BKn3 is able to induce changes in both axiality and growth rates during the formation of the ectopic

flower. This dual effect is also predicted to occur during the formation of the wings, however this is yet to be confirmed. In particular growth in the wing region is yet to be explored. Through using new tools developed during this thesis work, such as the adapted EdU staining protocol (used in maize to assess the pattern of cell divisions) and the transgenic fluorescent protein clonal sector line (developed in barley), it may now be possible to assess growth rates within the developing lemma.

How BKn3 influences axiality information remains unanswered. My exploration of the expression pattern of candidate components of polarity organiser regions has indicated that BKn3 is able to induce changes in their expression pattern. However the relationship between these regions and the polarity patterns predicted by the SoPIN1 localisation patterns is yet to be clarified. Through exploring the expression pattern of other members of the gene families and other possible components of polarity organisers, the role of BKn3 in the modulation of axiality may become clearer. 3D information about the distribution of possible organiser regions throughout the developing *Hooded* lemma would be of most use, however attempts so far at whole-mount RNA *in situ* hybridisation in *Hooded* barley have yet to be successful, perhaps development of antibodies against some candidate polarity organiser genes will be valuable. Exploration of the expression of organiser regions in the wing region would also provide insight into how BKn3 may influence axiality. It would be predicted that *LAX1* may be expressed at the tip of the wing, and that *NAM* and *YUCCA* at the base.

If the formation of the *Hooded* phenotype is due to changes in auxin dynamics, perhaps external application of synthetic IAA or auxin transport inhibitors like NPA could disrupt lemma formation, inducing different developmental switches in shape. Some work has already been reported in the literature where injection of IAA into developing *Hooded* spikes reduced the strength of the *Hooded* mutant slightly [158]. The effects of these treatments on changes in axiality and growth rates as well as overall morphology of both wild-type and *Hooded* lemmas may help dissect the relationship between BKn3 and growth.

Once a candidate mechanism for how BKn3 influences growth has been identified it would be particularly interesting to test whether the same mechanism is active in other model systems where class 1 *KNOX* genes are overexpressed. For example the leaf flaps in the maize *Knotted1* mutant may be analogous to the *Hooded* wings and the maize leaf knots may be analogous to the ectopic *Hooded* floral meristem.

One of the major unanswered questions relating to the *Hooded* mutant is why *BKn3* is only expressed in the region predicted to be the boundary between the lemma and awn. Exploration of why *BKn3* is expressed in this boundary region may provide insight into why *KN1* expression in the maize leaf is not ubiquitous [88] and why transgenic tobacco overexpressing *KN1* seems to form ectopic meristems on the adaxial surface only [159]. This specific control of *BKn3* may be due to the distribution both spatially and temporally of *KNOX* inhibitors, like *ROUGH SHEATH 2* [160, 161] within developing tissues. It may be that where *BKn3* is ectopically expressed these inhibitors are not present. This could be assessed through RNA *in situ* hybridisation of candidate regulators, or through RNAseq of different regions in the wild-type and *Hooded* lemmas to assess which genes are differentially expressed spatially and temporally. Through using the inducible *BKn3* over-expression line developed as part of my thesis work, it may be possible to identify a region in time when the tissue is able to express *BKn3* and to respond to the effects of *BKn3* on growth to generate the *Hooded* phenotype. This could highlight specific temporal regulation of ectopic *BKn3* expression and tissue responsiveness.

Overall this work has found that a single gene (*BKn3*) is able to influence the pattern of growth by modulating both axiality and growth rates, leading to developmental switches in shape. It may be that depending on where *BKn3* is expressed in the developing organ different developmental switches in shape are triggered. Novel organ shapes may have arisen during evolution through the mis-expression of genes within developing organs that are able to modulate growth. The genes responsible for these changes may be able to influence multiple genetic and hormonal pathways, like the *KNOX* class 1 family.

## 4 Developing a Transgenic Toolkit in Barley

### 4.1 Tools available in other species

For shape development studies, information on growth rate and orientation, and cell polarity is essential to test hypotheses. Several tools have been developed in different systems to collect this data using both non-transgenic and transgenic approaches. The most extensive transgenic toolkit has been developed in the model plant *Arabidopsis thaliana*.

*Arabidopsis* has been widely used as a model system in plant development to explore how shape is defined in leaves, flowers and fruits. Central to this is the availability of extensive mutant and transgenic lines. The combination of both the mutant and transgenic lines in *Arabidopsis* enables the rapid testing of hypotheses, as well as live imaging and cell tracking, which is not as accessible in model systems with fewer resources.

Particularly useful in *Arabidopsis* are cell membrane markers, such as fluorescent protein tagged membrane proteins, like aquaporins [162], which when combined with live imaging, can permit the tracking of division and expansion of epidermal cells, providing accurate information on resultant growth rate, cell volume and shape [21, 77]. Cell membrane markers have been extensively used in different tissues in *Arabidopsis* for both tracking and cellular localisation studies, showing that a stable membrane marker is a valuable tool in any transgenic toolkit.

Clonal analysis is another method of assessing growth rate and orientation. Clonal analysis can be carried out using both non transgenic and transgenic methods. The process involves the induction of an irreversible change in a random set of cells, then leaving the tissue to grow for a period of time. The resulting cell clones (i.e. the descendants of the original labelled cells) are analysed. The shape, size and orientation of each clonal sector can provide information about growth rate and orientation which are central to exploring how shape develops [96]. Original, non-transgenic methods use X-ray induced chromosome breakage, disrupted spindle organisation, or the movement of endogenous transposons to generate labelled cells. In maize for example, X-ray chromosome breakage has been extensively used to carry out clonal analyses and it has provided information about the development of the maize leaf and flowers [27, 96, 98, 163]. For example, the number of founder cells initially recruited into the ring primordium from the meristem were estimated using clonal analyses [96]. However, X-ray induced chromosome breakage in maize is often based upon the disruption of the non-mutant chromosome in a heterozygous plant for a pigment mutation,

such as chlorophyll [98]. This means that clonal sectors are only visible once pigment production has started and it is not suitable for use in tissues that do not produce the pigment, including early stages of leaf development. Therefore, we can gain only limited information about growth rate and orientation changes during early leaf development. The methods which involve the induction of polyploid cells using microtubule disrupting drugs [164, 165] are suitable for all tissues to which the drug can be applied, however they are difficult to analyse as the method relies upon identifying larger polyploid nuclei versus normal nuclei. The transposon method, which uses the activation of mobile transposons to label cells through inserting into colour genes for example, has been used extensively in species such as *Antirrhinum* [166]. However, it requires the model system to contain transposons that are easily activated in a controllable fashion, for example by heat shock. All of these traditional methods involve permanent damage to the DNA of the clone cells, sometimes with large scale changes like chromosome breakage and genome duplication, which carries the risk of modifying the cell's behaviour with respect to their neighbours.

An alternative, transgenic approach to clonal analysis has been developed and extensively used in *Arabidopsis* [21, 22, 167]. Transgenic clonal analysis constructs are based upon the *CRE lox* site system from the *P1 Enterobacteriophage* [168]. The system is based upon two separate constructs. One uses a constitutive promoter upstream of two consecutive marker genes, with their own STOP codons and terminators, the first marker gene is flanked by *lox* sites. The second construct contains an inducible promoter driving the expression of *CRE* (Figure 4.1). Under normal conditions, *CRE* is not expressed, and only the first marker gene is expressed throughout the tissue. Under induced conditions (either through heat shock or chemical treatment) *CRE* is expressed, acting to generate the recombination of the *lox* sequences, excising the sequence between the *lox* sites, i.e. marker gene 1, this means that now only marker gene 2 is expressed in induced cells. This is an irreversible reaction. The descendants of the marked cells all express marker 2, forming a clonal sector [167] (see Figure 4.1). Normally, the inducible *CRE* and the marker genes are transformed into separate plants and then crossed, which is suited to *Arabidopsis* due to the short generation times. This transgenic clonal sector method has been used with multiple different marker genes to explore meristem [167], leaf [21], flower [22, 169] and fruit development (Tilly Eldridge, JIC, unpublished) in *Arabidopsis*. The use of fluorescent proteins as the marker genes can enable imaging of the tissue of interest multiple times during development, gaining more dynamic information about growth. This clonal sector technique can be modified to induce clonal sectors of a gene of interest [167], allowing the subsequent downstream effects to be

monitored. The use of inducible sector lines provide information about resultant growth and allow testing of hypotheses relating to the function of genes of interest, following localised expression, proving to be a valuable tool in a transgenic toolkit.

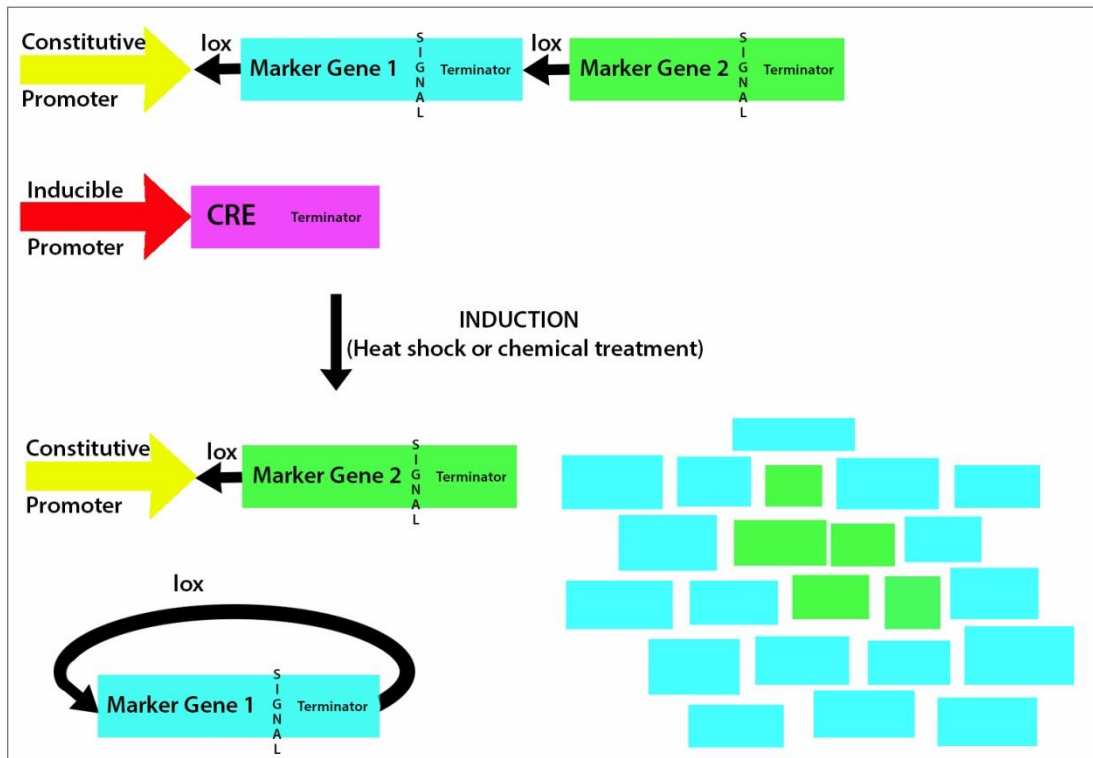


**Figure 4.1** Diagram illustrating the *CRE lox* clonal sector technique.

The *CRE lox* system consists of two separate constructs. The first contains a constitutive promoter upstream of a *lox* flanked 'marker gene one' which has its own associated signal peptide and terminator, and 'marker gene two' with its own signal peptide and terminator. The second construct contains the inducible promoter and the coding sequence of *CRE*. After *CRE* expression is induced, *CRE* causes the recombination of the direct repeats of the *lox* sites, excising 'marker gene 1', causing the expression of 'marker gene two' in induced cells. The progeny of these marked cells all express 'marker gene two' forming a clonal sector.

Auxin is a key regulator of plant growth and development and its distribution within the tissue is therefore of particular interest to development studies. An auxin reporter which has been extensively used is the *DR5* enhancer element [170]. The *DR5* reporter for auxin highlights where intracellular auxin maxima are within the tissue and has been used in many studies. The *DR5* reporter is often combined with the auxin exporter *AtPIN1* reporter as this provides information on the cellular localisation of the *PIN1* protein and thus the direction of auxin transport. Assuming that a polarity based axiality system determines axial information within the developing tissue, the localisation of *PIN1* also provides information

about the cellular polarities within the tissue and their coordination across the tissue, indicating the orientation of tissue cell polarity (axiality). The combination of the DR5 and the PIN1 reporters allows investigation of the tissue cell polarity proving a useful tool in the *Arabidopsis* toolkit.

With the extensive transgenic toolkit available in *Arabidopsis* many hypotheses relating to the development of its relatively simple leaf, petal and fruit shape have been developed and tested ([21, 22], Tilly Aldridge, JIC, unpublished). If elements of this toolkit could be transferred to other systems, the study of more complex shapes, like the grass leaf and flower, could be advanced further.

## 4.2 Aim of this work

Cereals present many fascinating developmental problems, especially as there are largely untapped mutant collections. However, the transgenic toolkit readily available in model species such as *Arabidopsis thaliana*, which have contributed to much of the understanding of plant development, do not exist in most cereals (with the exception of maize which has recently had several transgenic lines created for developmental studies [123]).

Given recent advances in cereal transformation efficiencies, particularly in barley (*Hordeum vulgare*) [171], and the publication of the barley genome [149] it is the ideal time to try to develop the barley transgenic toolkit. Barley has the further advantage of extensive mutant collections [172, 173]. I aimed to generate a basic toolkit of transgenic barley plants to test the expression of different fluorescent proteins, the possibility of heat shock inducible gene expression, and the stacking of multiple genes in single constructs.

I focussed on a core set of six transformation constructs designed to assess the aforementioned questions and to provide more information for investigation into developmental switches in shape in the *Hooded* barley mutant and grass leaf development. These constructs included a plasma membrane marker (*HvPIP2.5*, an aquaporin), a *HvPIN1a* marker with a *DR5* reporter, a heat shock inducible CRE/lox system for the generation of *eGFP* clonal sectors and an inducible system for the generation of *HvBkn3* sectors (see Table 4.1).

The design and construction of the transformation constructs was carried out in collaboration with Samantha Fox (Coen Lab, JIC) and ENSA (Engineering Nitrogen Symbiosis

for Africa group at JIC). Some resources were provided by Nicola Patron (TSL SynBio). The transformation of barley was carried out by BRAC (Biotechnology Resources for Arable Crop Transformation, based at JIC).

### **4.3 Spectral scan of barley flowers**

Before designing the constructs a spectral scan on barley leaf and flower tissue was carried out to check for endogenous autofluorescence which would interfere with any possible fluorescent protein tag signals. By carrying out the scan I aimed to identify the best candidate fluorescent proteins to use in the marker lines.

Leaf and inflorescence tissue of different ages was harvested from wild-type Bowman barley and imaged using the SP5 II Leica confocal laser microscope. Native fluorescence when excited with different wavelengths appropriate to CyPET, eGFP and mCHERRY was assessed. When imaging the tissue using the x20 water immersion lens the gain was increased until signal could be seen in each of the fluorescent marker channels (CyPET: 449-508nm, eGFP: 518-565nm, mCHERRY: 586-644nm). In all wild-type tissues this was very high (gains used were around 700 for the PMT detector and 400 for the HyD detectors, fluorescent protein signal would be visualised at gains of around 100). (Figure 4.2)

All three fluorescent proteins (mCHERRY, eGFP and CyPET) are suitable for use in transgenic barley as the signal from any autofluorescence would be too weak to interfere with signals from fluorescent proteins in the tissues tested (see Figure 4.2.A lemma, 4.2.B older blade tissue and 4.2.C young leaf tissue shown in each condition). However, mature leaf tissue (Figure 4.2.B) does have a high level of endogenous fluorescence which will need to be taken into account when screening mature leaf tissue.

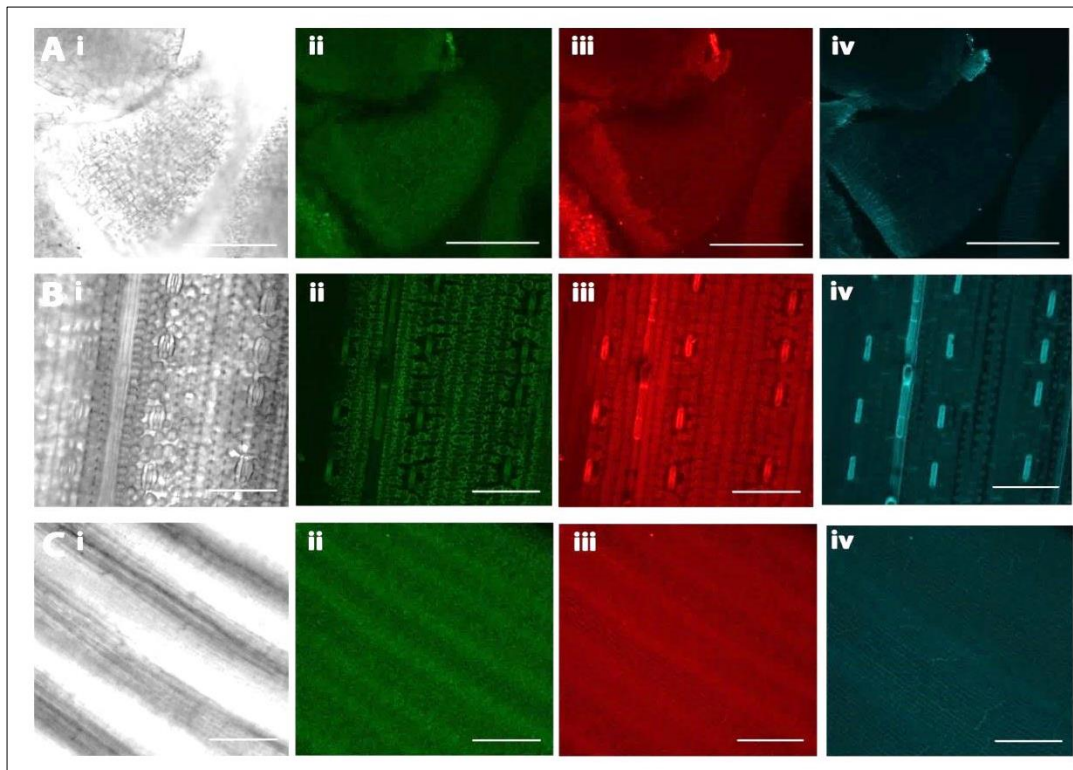


**Figure 4.2 Screening of wild-type barley tissue for endogenous fluorescence.**  
*A-C.i*: bright field channels. *ii*: eGFP channel. *iii*: mCHERRY channel. *iv*: CyPET channel. *A.i-iv*: images of a young wild-type barley lemma. *B i-iv*: images of mature barley leaf tissue (blade) and *C i-iv*: images of young barley leaf tissue. Scale bars are 100 $\mu$ m.

#### 4.4 Design of the transformation constructs

I chose to use hierarchical modular goldengate cloning [174] to develop constructs for transformation as it enables flexibility and easy stacking of large gene constructs into a single binary transformation vector. Cloning progresses from L0 constructs (synthesised components), combined to make L1 constructs (transcriptional units), which are then combined to make L2 constructs (multigene units), the method for this process is outlined in the paper by Weber et al [175]. Goldengate cloning exploits the ability of the bacterial type IIS endonuclease restriction enzymes BsaI, BpiI and Esp3I to cut downstream of a specific recognition site. The design of different specific overhangs (also referred to as fusion sites, Table 4.1) allows fragments cut by the same type IIS endonuclease to be linearly ligated by T4 ligase in a pre-designed order. This is combined with a library of pre-designed, standardized modules (L0) to allow rapid and highly efficient assembly of transcriptional units (L1), which are later combined to generate large multicomponent constructs (L2) for transformation. The standardization of the different modules means that a library can be

built up which can generate many different combinations. I used the standardised nomenclature and overhangs described by Weber et al [175] (Table 4.1). This nomenclature will be used for each level of cloning from now on.

Module Name	Sequence Feature	3' Overhang	5' Overhang	Flanking Enzyme Site
L0-P	Promoter	GGAG	TACT	Bsal
L0-U	UTR	TACT	AATG	Bsal
L0-PU	Promoter and UTR	GGAG	AATG	Bsal
L0-SP	Signal Peptide	AATG	AGGT	Bsal
L0-C	Coding Sequence	AGGT	GCTT	Bsal
L0-SC	Coding +/- signal peptide	AATG	GCTT	Bsal
L0-T	Terminator	GCTT	CGCT	Bsal
L1-Position 1	Transcriptional unit	TGCC	GCAA	Bpil
L1-Position 2	Transcriptional unit	GCAA	ACTA	Bpil
L1-Position 3	Transcriptional unit	ACTA	TTAC	Bpil
L1-Position 4	Transcriptional unit	TTAC	CAGA	Bpil
L1-Position 5	Transcriptional unit	CAGA	TGTG	Bpil
L1-Position 6	Transcriptional unit	TGTG	GAGC	Bpil
L1-Position 7	Transcriptional unit	GAGC	TGCC	Bpil

**Table 4.1** The different components for golden gate cloning with their related overhangs and endonuclease enzyme recognition sites as described by Weber et al 2011 [175].

#### 4.4.1 Selecting sequences

Previous work in collaboration with BRACCT and in published literature highlighted possible components for use in the generation of the transgenic barley lines. Work in collaboration with the BRACCT group had shown that maize ubiquitin promoter (ZmpUbi) driven free *eGFP* expressed well in barley (Figure 4.3). *CRE* has previously been used to remove extra transgene copies in wheat [176]. The barley Hsp17 promoter (*HvpHSP17*) had been previously used to drive a reporter gene in wheat [177]. For the plasma membrane marker,

the aquaporin *HvPIP2.5* was selected based on sequence similarity to the maize aquaporin used by Mohanty et al 2009 [123] (Figure 4.4).

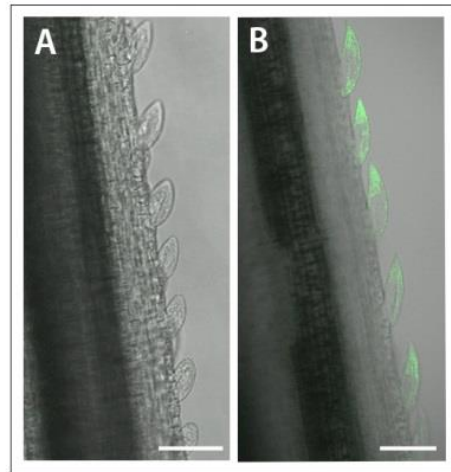


**Figure 4.3** *eGFP* expression in *pZmUbi::eGFP-T* barley lemmas.

A: wild-type lemma. B: the *pZmUbi::eGFP-T* transgenic lemma from BRAC. Scale bars are 100 $\mu$ m.

Combining the information gained from the spectral scan of barley tissues and previous and published data I designed six different goldengate constructs for transformation into barley (see Table 4.2 and below) using , where possible, monocot specific sequences. The six constructs were:

1. ***pHvPIN1a::HvPIN1a-eGFP-T/ DR5:mp35S::mCHERRY-T***, to act as a PIN1a and auxin reporter line.
2. ***pHvPIP2.5::HvPIP2.5-eGFP-T***, to be used as a plasma membrane marker line.
3. ***pHvHSP17::CRE-T***, for heat shock induced *CRE* expression to be used to cross into sector line plants.
4. ***pZmUbi::lox mCHERRY-HDEL-Tlox/eGFP-HDEL-T***, a sector line for the induction of *eGFP* sectors when crossed with the heat shock inducible *CRE* line.
5. ***pHvHSP17::CRE with U5 intron- T/ pZmUbi::loxmCHERRY-HDEL-Tlox/eGFP-HDEL-T***, a combined heat shock inducible *CRE* with an *eGFP* sector line, to explore whether I could stack both components
6. ***pHvHSP17::CRE with U5 intron-T/ pZmUbi::loxCyPET-HDEL-Tlox/HvBKn3-mCHERRY-T/ pHvPIN1::HvPIN1a-eGFP-T***, a heat shock inducible *CRE* with a *HvBKn3*

sector line and *HvPIN1a* marker line, to induce *HvBkn3* sectors upon heat shock and see the response of PIN1a.

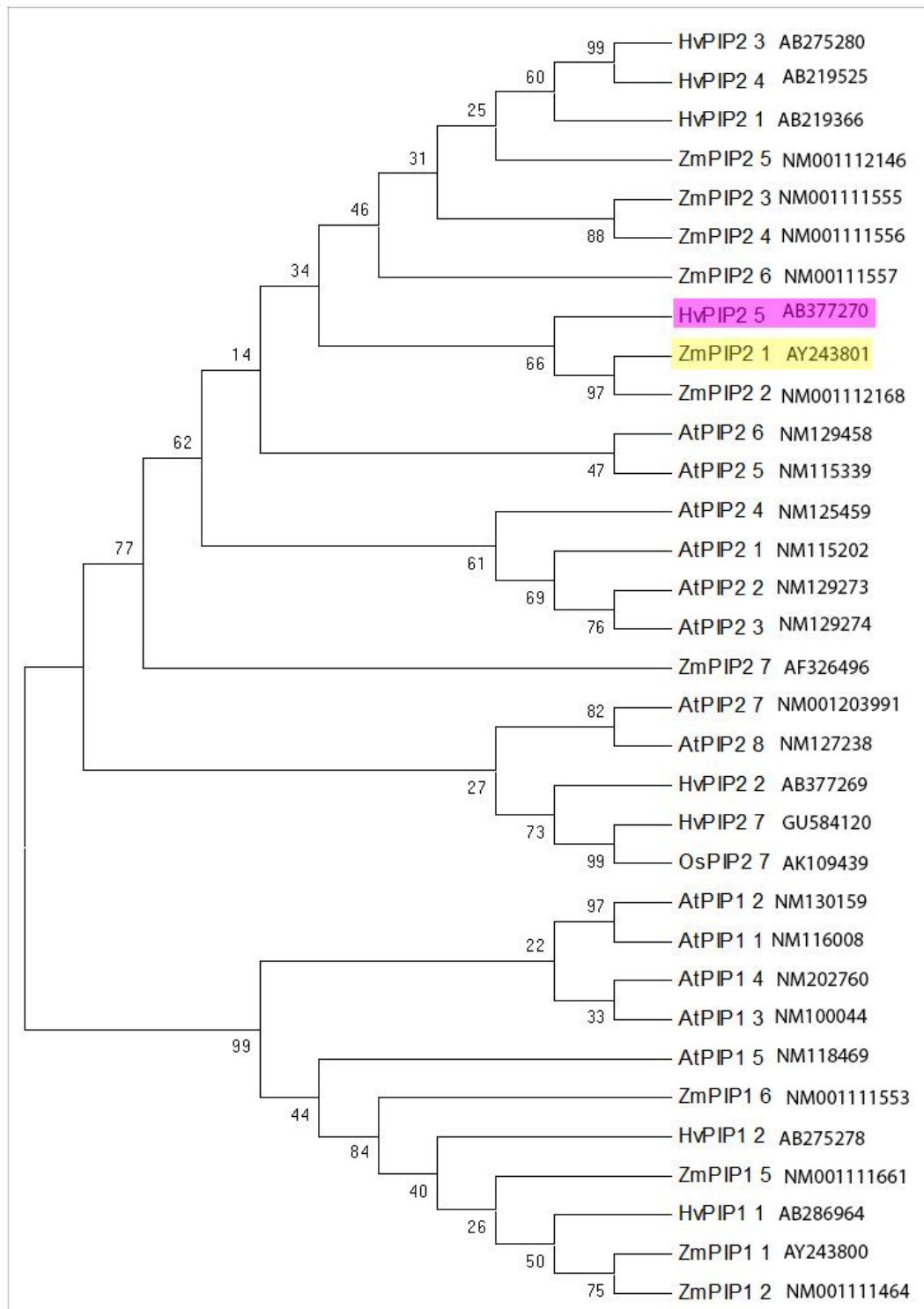


**Figure 4.4** Phylogenetic tree showing the relationship between the PIP aquaporin proteins. Protein sequences are from *Arabidopsis thaliana* (At), *Zea mays* (Zm) and barley, (Hv). Yellow highlights the maize aquaporin (ZmPIP2.1) used by Mohanty et al 2009 [123], pink highlights

the barley aquaporin most similar in sequence to ZmPIP2.1 and therefore chosen to be used as the plasma membrane marker line. Numbers indicate the bootstrap score for each node.

Some L0 components were already available through the ENSA library at JIC these included the domesticated sequences for *eGFP*, *mCHERRY* and *CyPET*, the *DR5* and the minimal *35S* promoter and the *Arabidopsis* actin terminator. The other L0 components required were designed and then synthesised using Invitrogen Gene Systems (See Table 4.3 for L0 modules synthesised). For barley specific sequences phylogenetic analyses were used to identify the appropriate sequences and the sequence was then domesticated by removing all existing Bsa1, Esp3I and Bpi1 enzyme sites using, where possible, neutral base pair changes. As the barley genome is not extensively annotated at least 1.5kb upstream of the START codon and 1kb downstream of the STOP codon were selected when designing native promoters and terminators.

The sequences for *CRE* (Genbank GeneID: 2777477) and the *lox* site sequences were taken from the genome sequence of *Enterobacteria Phage P1*. The *lox* site sequence was “GACCTAATAACTTCGTATAGCATA CATTATACGAAGTTATATTAAGGGTTG” (*loxP* sequence).

For the plasma membrane marker line, I chose to use the same aquaporin (an intrinsic plasma membrane protein which transports water and solutes across the plasma membrane) as used by Mohanty et al [123], *ZmPIP2.1*. The homologue in barley was identified using phylogenetic analyses (Figure 4.4) as *HvPIP2.5* (AB377270.1, GenBank). I designed the plasma membrane marker, as used in Mohanty et al, with an N terminal *eGFP* fusion instead of *CFP* (as *eGFP* is one of the brightest and most stable fluorescent proteins) with a double glycine linker. The native promoter and terminator for *HvPIP2.5* was also selected, taking a region 1965bp upstream of the transcriptional START site, and the terminator was chosen by selecting 1100bp downstream of the STOP codon.

The *PIN1a* gene was identified in the barley genome using phylogenetic analyses as previously described (Chapter 3, Figure 3.9, *SoPIN1* was not selected at the time as its role as an epidermal marker of tissue cell polarity in barley had not yet been identified). I selected to internally tag *HvPIN1a* with *eGFP* at the 218<sup>th</sup> amino acid with a seven alanine linker, as this had previously been successfully used to tag *ZmPIN1a* by Gallavotti et al 2008 [81]. I selected 3.13kb upstream from the START codon and 1.4kb downstream of the STOP codon to use as the native promoter and terminator respectively.

For the inducible expression constructs I decided to use the barley heat shock protein 17 promoter (*HvpHSP17*) which I had identified in the literature [177]. The sequence of *HvpHSP17* was taken from the BRAC T plasmid pHSPdGUS.

For the inducible *HvBKn3* sector construct, I used the genomic coding sequence of *HvBKn3*, identified in phylogenetic analyses described in Chapter 3 (Figure 3.7). This was then C terminally fused to *mCHERRY* using a seven alanine linker, based on previous work in *Arabidopsis* in which *KNOTTED1* was C terminally tagged [178].

Each sequence was first domesticated for goldengate cloning by editing out all BsaI, BpiI and Esp3I enzyme sites. This was done by creating silent nucleotide substitutions *in silico*. These sequences were used to design each level of construct, allocating standard goldengate overhang sequences to each L0 appropriate to their position in the L1 transcriptional units as described in Weber et al [174]. These sequences were the ones sent for gene synthesis.

L2 construct ID	pL2 Vector	Position 2	Position 3	Position 4	Linker	Experiment
EC71117	EC15027 pL2iV-1	EC71173 HvHSP17: CRE-U5-CRE	EC71128 UBqP-Loxp-ER-Targ-CYPET-HDEL-Loxp-BKn3-mCHERRY	EC71145 HvpPIN1a-PIN1-eGFP-PIN1	EC41780 pL1M-ELE-4-41780	<i>BKn3</i> activation system, PIN1a marker, modified <i>HsCRE</i>
EC71118	EC15027 pL2iV-1	EC71108 HvpPIN1a-PIN1-eGFP-PIN1	EC71129 DR5-mCHERRY	N/A	EC41766 pL1M-ELE-3-41766	reporter line (mCHERRY), PIN1a marker
EC71121	EC15027 pL2iV-1	EC71113 HvpPIP2-GFP	N/A	N/A	EC41744 pL1M-ELE-2-41744	membrane marker line for tracking
EC71165	EC15027 pL2iV-1	pICH54022-Dummy pos 2	EC71167 UBqP-Loxp-ER-Targ-mCHERRY-HDEL-Loxp-eGFP	N/A	EC41766 pL1M-ELE-3-41766	sector line, for crossing
EC71172	EC15027 pL2iV-1	EC71099 HvHSP17: CRE	N/A	N/A	EC41744 pL1M-ELE-2-41744	Unmodified <i>HsCRE</i> for crossing
EC71174	EC15027 pL2iV-1	EC71173 HvHSP17: CRE-U5-CRE	EC71167 UBqP-Loxp-ER-Targ-mCHERRY-HDEL-Loxp-eGFP	N/A	EC41766 pL1M-ELE-3-41766	modified <i>HsCRE</i> with clonal sectors

**Table 4.2** The L2 constructs transformed into barley and their component parts. Each construct is given an ID number to record it in the database, each position is the L1 module required to stack in the vector backbone to make the final construct. Position 1 is already occupied by the hygromycin resistance cassette (contained in the pL2 vector). Blue boxes highlight L1 components that I made during the project (outlined in Table 4.3).

L1 construct ID	Standard name	L1 cloning vector	P/PU	U	S/SC/SC1	C1	C/C2	T
EC71099	pL1M-R2-pHvHSP17-CRE-tHSP	EC47811 pL1V-R2-47811	EC71100 PU-pHSP17	N/A	EC71102 pL0M-SC-CRE	N/A	N/A	EC15320 T-AtHsp
EC71108	pL1M-R2-HvpPIN1a-PIN1-eGFP-PIN1	EC47811 pL1V-R2-47811	EC71109 PU-HvpPIN1	N/A	EC71110 pL0M-S-HvpPIN1-71110	EC71103 pL0M-C1-L-eGFP-L-71103	EC71111 pL0M-C2-HvpPIN1-71111	EC71112 T-HvpPIN1
EC71113	pL1M-R2-HvpPIP2-GFP-PIP2-t	EC47811 pL1V-R2-47811	EC71126 PU-HvpPIP2.5	N/A	EC15094 pL0M-S-eGFP-15094	N/A	EC71131 pL0M-C-HvpPIP2-71131	EC71132 T-HvpPIP2
EC71128	pL1M-R3-UBqP-Loxp-ER-Targ-CYPET-HDEL-Loxp-BKn3-mCHERRY	EC47822 pL1V-R3-47822	EC71139 P-pZmUBI-intron	EC71019 U-LoxP-CyPET-HDEL-t35S-LoxP	EC71125 pL0M-SC1-BKn3	N/A	EC71093- pL0M-C2-L1- mCHERRY- 71093	EC44300 T-Act2
EC71129	pL1M-R3-DR5-mCHERRY	EC47822 pL1V-R3-47822	EC71059 PU-DR5-35S	N/A	EC15071 pL0M-SC-mCHERRY-15071	N/A	N/A	EC41414 T-35S
EC71145	pL1M-R4-HvpPIN1a-PIN1-eGFP-PIN1	EC47831 pL1V-R4-47831	EC71109 PU-HvpPIN1	N/A	EC71110 pL0M-S-HvpPIN1-71110	EC71103 pL0M-C1-L-eGFP-L-71103	EC71111 pL0M-C2-HvpPIN1-71111	EC71112 T-HvpPIN1
EC71167	pLM-R3-UBqP-Loxp-ER-Targ-mCHERRY-HDEL-Loxp-eGFP	EC47822 pL1V-R3-47822	EC71139 P-pZmUBI-intron	EC71022 U-LoxP-mCHERRY-HDEL-t35S-LoxP	EC71090- pL0M-S- ER-Targ- 71090	EC71088 pL0M-C1-eGFP-71088	EC71020 pL0M-C2-HDEL-71020	EC44300 T-Act2
EC71173	pL1M-R2-pHvHSP17-CRE-U5-CRE-tHSP	EC47811 pL1V-R2-47811	EC71100 PU-pHvHSP17	N/A	EC71171 pL0M-SC-CRE-U5-CRE	N/A	N/A	EC15320 T-AtHsp

**Table 4.3 L1 components made for L2 construction**

All L1 components designed and made to make the final L2 constructs, each L1 construct is separated into vector backbone, and parts of the transcriptional unit (L0 modules, P/PU, U, S/SC/SC1, C1, C/C2, T). All other L1 constructs outlined in Table 4.2 were already available from the ENSA and TSL SynBio databases. Yellow boxes highlight L0 modules which I had synthesised during the project; the red box indicates an L0 module that was modified during the project. All other L0 modules were already available in the ENSA library.

## 4.5 Goldengate cloning of constructs

The final constructs were made as outlined by Weber et al [175]. The identity of each stage was verified using colony PCR and sequencing and the final constructs transformed into *Agrobacterium tumefaciens* were tested using restriction digestion and sequencing. The maps of the final constructs are provided in Appendix D.

At the start of the project, the existing goldengate cloning method was not amenable for generating the constructs for clonal sector analysis. The existing method allowed the combination of the L0 components; promoter (P), upstream coding region (U), coding sequence (C), signal peptide (S) and terminator (T); to make an L1 construct (illustrated in Figure 4.5.A). This format did not allow the addition of *lox* sites to a fluorescent protein coding region and terminator (C-S-T 1, marker gene 1), and then allow the addition of a promoter (P) upstream and another gene with its terminator (C-S-T 2, marker gene 2) downstream of this. To solve this problem, in collaboration with Sam Fox, JIC and Cristian Rogers, ENSA, I designed an additional cloning step before the formation of the L1 constructs to allow the combination of *lox* units with fluorescent protein 'C-S-T' unit making an 'L0.5' construct. This involved the creation of a 0.5 level of cloning to first combine the flanking *lox* sites with the first fluorescent protein coding region, signal peptide and its terminator (C-S-T 1). This was made possible through synthesising a backbone vector which contained the *lox* sites, the overhangs for assembly and two additional restriction enzyme sites (specific for Esp3I) flanking both *lox* sites (Figure 4.5). This allowed the assembly of L1 constructs in the format 'P-*lox*-C1-S1-T1-*lox*-C2-S2-T2' using a two-step reaction. First the Bsa1 enzyme was used to combine the 'C1', 'S1' and 'T1' L0 units with the *lox* backbone to make the L0.5 '*lox*-C1-S1-T1-*lox*' construct, the specific overhangs for this made it equivalent to a 'U' unit in the normal goldengate format. Then a second reaction with Bsa1 and Esp3I enzymes was used to combine the L0.5 '*lox*-C1-S1-T1-*lox*' module and the 'P', 'C2', 'S2' and 'T2' L0 units to make the 'P-*lox*-C1-S1-T1-*lox*-C2-S2-T2' L1 construct. This could then be used to make the L2 multigene constructs.

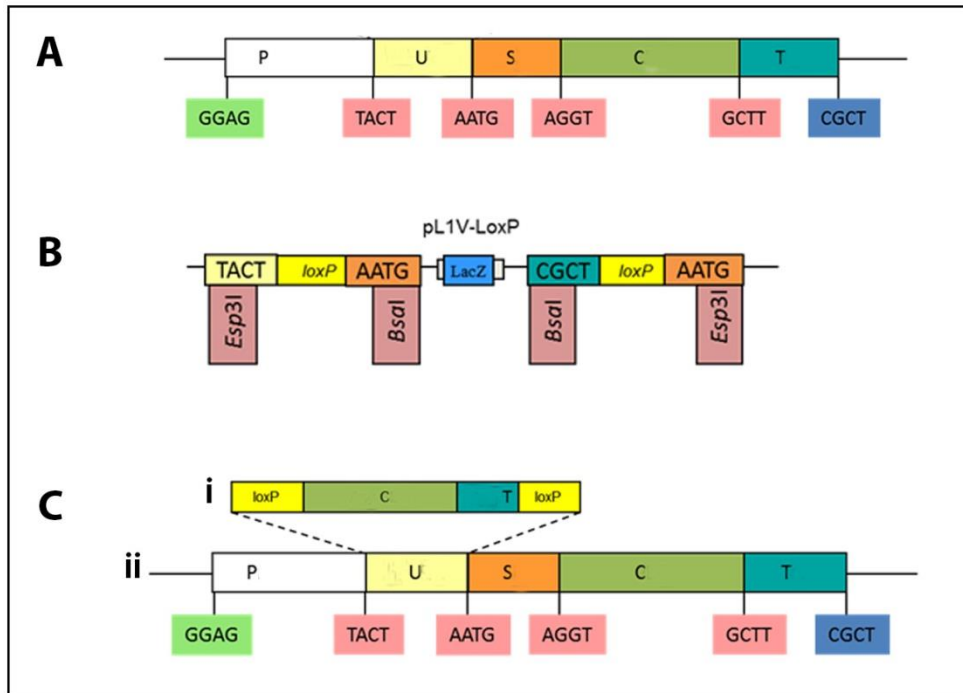


**Figure 4.5** The modification of the goldengate method to make clonal sector lines  
**A:** The original format of an L1 construct in goldengate cloning. The position of the promoter (P), UTR (U), signal peptide (S) and coding sequence (C), terminator (T) L0 units are labelled. The specific overhangs on each L0 module needed for the ligation assembly are also indicated.  
**B:** The structure of the synthesised, modified vector, designed to allow the formation of the L0.5 level construct with *lox* sites flanking the marker gene coding sequence, signal peptide and terminator. The enzyme sites are indicated by the pink boxes. The overhangs are written in capital letters. The *LacZ* is a selectable marker which is removed during the cloning process, this is replaced by marker gene 1 coding sequence, signal peptide and terminator.  
**C:** The final *lox* flanked gene 1 (with signal peptide and terminator) L0.5 construct acts as a U module in the cloning of the L1 construct which adds the constitutive promoter and marker gene 2 coding sequence (with a signal peptide) and terminator.

As part of the project I chose to stack the heat shock inducible *CRE* transcriptional unit with the *lox* containing units on the same plasmid, which has not been used before in plants. This approach was taken as it removes the need to cross the transgenic plants to combine these constructs at a later time, removing a generation from the process. During cloning I identified problems with the activation of the heat shock promoter during the heat shock transformation of *E. coli*, and the subsequent excision of the coding sequence between the *lox* sites. To combat this I introduced an intron into the *CRE* coding sequence to prevent bacterial expression, based on a previous study in mice which added an intron at 254bp [179]. The intron used was from the *A. thaliana* U5 small nuclear ribonucleoprotein component [174], provided by Nicola Patron, TSL SynBio (the method used is outlined in

section 6.3.1.4). The introduction of the intron into the *CRE* coding sequence successfully inhibited the expression of the *CRE* in *E.coli* during cloning as shown by sequencing results of cloned constructs. However, I would not know if the introduction of the intron disrupted the functionality of the *CRE in planta* until the transgenic plants were analysed, therefore I also chose to make separate heat shock inducible *CRE* lines suitable for crossing at a later date if needed.

The constructs were transformed into *A. tumefaciens* and then these stock cultures were given to BRAC for transformation into barley callus tissue.

## 4.6 Screening of plants

The T0 plants generated by BRAC were grown in CER conditions to prevent accidental activation of the heat shock promoters. Samples from four plants from each batch were sent for copy number analysis by iDNA genetics, allowing me to identify single copy lines. The seeds from the T0 constructs with single copies were sown and the T1 seedlings were again assessed for copy number to identify homozygotes and hemizygotes. These were then analysed for fluorescent expression in the leaf and inflorescence tissue using confocal microscopy. The best expressing lines with minimal copy numbers for the *pHvPIP2.5::HvPIP2.5-eGFP-T*, *pHvPIN1a::HvPIN1a-eGFP-T/DR5:35Smp::mCHERRY-T* and *HvHsp17::Cre/loxmCHERRY-HDEL-Tlox/eGFP-HDEL-T* constructs were taken forward to cross into *Hooded* Bowman barley for analysis.

The *pHvHSP17::CRE* transgenic plants were only assessed for copy number as they did not contain a fluorescent marker for screening. Homozygous plants were selected to cross with the appropriate *pZmUbi::loxmCHERRY-HDEL-Tlox/eGFP-HDEL-T* plants.

Expression of *HvPIP2.5-eGFP-T* was strong and uniform in all tissues from all T1 lines tested (illustrated in Figure 4.6.B inflorescence spike, 4.6.D young leaf tissue, 4.6.F mature blade tissue, 4.6.H mature sheath tissue) when compared to the null, wild-type siblings (Figure 4.6.A,C,E,G). Little evidence of silencing was observed even in multi-copy plants. Given the strength of expression, homozygous lines with two copies of the transgene were selected for crossing into the *Hooded* mutant.

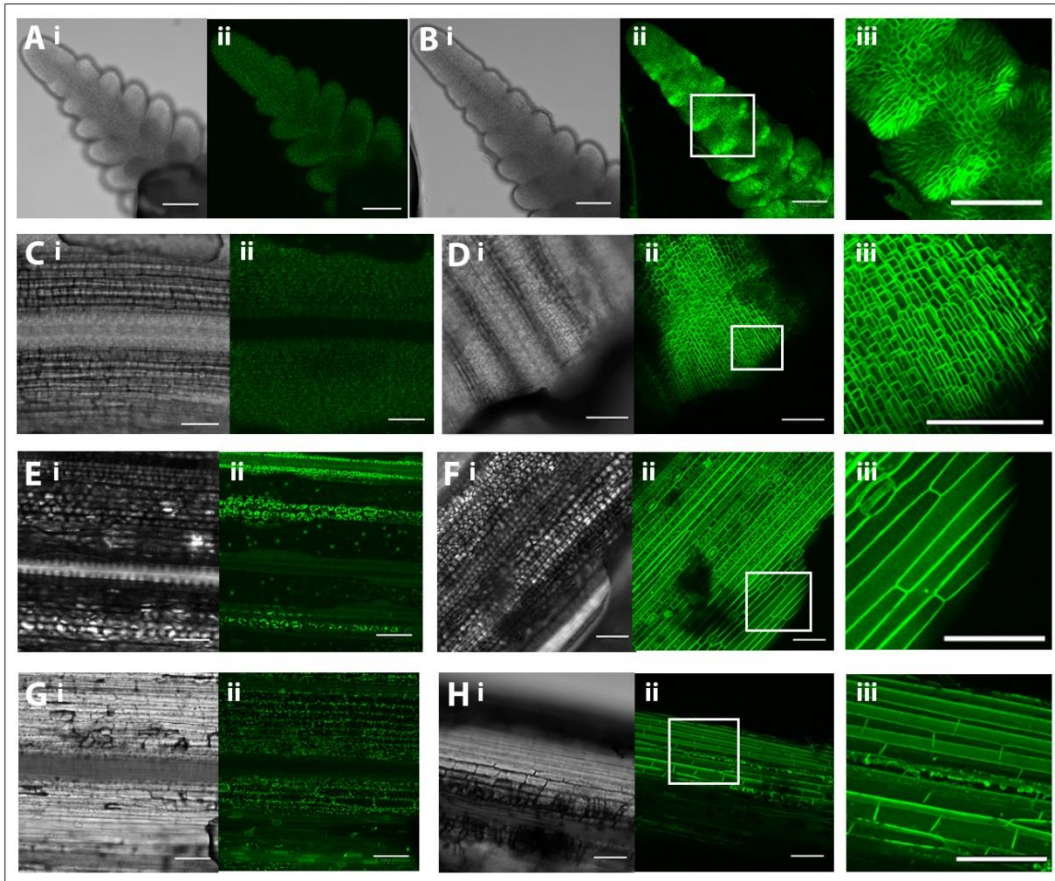


**Figure 4.6 Expression of *HvPIP2.5-eGFP-T* in T1 barley plants.**

*A, C, E* and *G*: tissue from a null (wild-type) sibling. *B, D, F* and *H*: a homozygous transgenic plant carrying two copies of the transgene. *i*: bright field images of the tissue. *ii*: eGFP settings. *iii*: zoomed-in views of the boxed region in *ii*. *A-B*: inflorescence spikes. *C-D*: young leaf tissue. *E-F*: mature blade tissue. *G-H*: mature sheath tissue. Scale bars are all 100µm.

The expression of the marker gene in the two different *eGFP* sector lines (the *pZmUbi::loxmCHERRY-HDEL-Tlox/eGFP-HDEL-T* for crossing and the combined *pHvHSP17::Cre/pZmUbi::loxmCHERRY-HDEL-Tlox/eGFP-HDEL-T* construct) was strong and uniform in all tissues from all hemizygous and homozygous T1 lines tested.

Example images for the *pZmUbi::loxmCHERRY-HDEL-Tlox/eGFP-HDEL-T* lines are illustrated in Figure 4.7. The expression of *mCHERRY* is strong (Figure 4.7.C-E, C is blade tissues, D is auricle tissue, and E is sheath tissue) and specific to the ER in the homozygous plants (illustrated in the zoomed-in images (iv) of the white boxed regions in Figure 4.7.ii). There is little signal in the *mCHERRY* or the *eGFP* conditions for the null siblings (Figure 4.7.A and B). The low non-specific signal in the *eGFP* imaging conditions shows that there is no read through into the *eGFP* reading frame (Figure 4.7 C-E. iii).

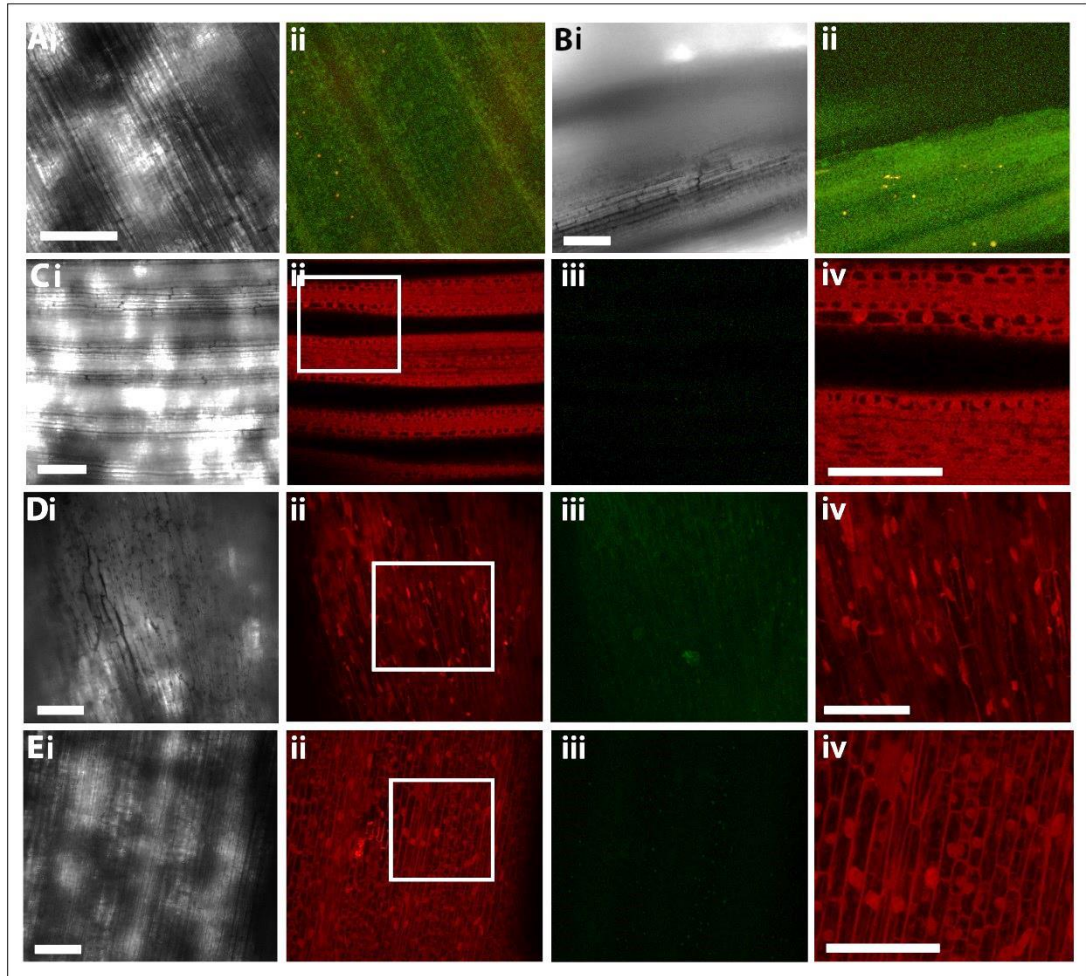


**Figure 4.7** Expression and localisation of the *pZmUbi::loxmCHERRY-HDEL-Tlox/eGFP-HDEL-T* construct in T1 barley plants.

*A-B*: tissue from a null (wild-type) sibling. *A*: blade. *B*: sheath. *i*: bright field image of the tissues, *ii*: combined image of the eGFP and mCHERRY settings. *C-E*: a homozygous transgenic plant carrying two copies of the transgene. *i*: bright field images of the tissue. *ii*: mCHERRY settings. *iii*: eGFP settings. *iv*: zoomed-in views of the boxed region in *ii*. *C*: young blade tissue. *D*: mature auricle tissue. *E*: mature sheath tissue. Scale bars are all 100 $\mu$ m.

Example images for the *pHvHSP17::Cre/pZmUbi::loxmCHERRY-HDEL-Tlox/eGFP-HDEL-T* lines are illustrated in Figure 4.8. The expression of mCHERRY is strong as in the previous line (Figure 4.8.C-F, C is auricle tissue, D is awn tissue, E is blade tissue, and F is sheath tissue) and specific to the ER in the homozygous plants (the localisation is illustrated in the zoomed-in images (iv) of the white boxed regions in Figure 4.8.ii). There is also little signal in the mCHERRY or the eGFP conditions for the null siblings as before (Figure 4.8.A and B). As was

the case for the crossing line, the low non-specific signal in the eGFP imaging conditions also shows that there is no read through into the eGFP reading frame (Figure 4.8 C-F. iii).

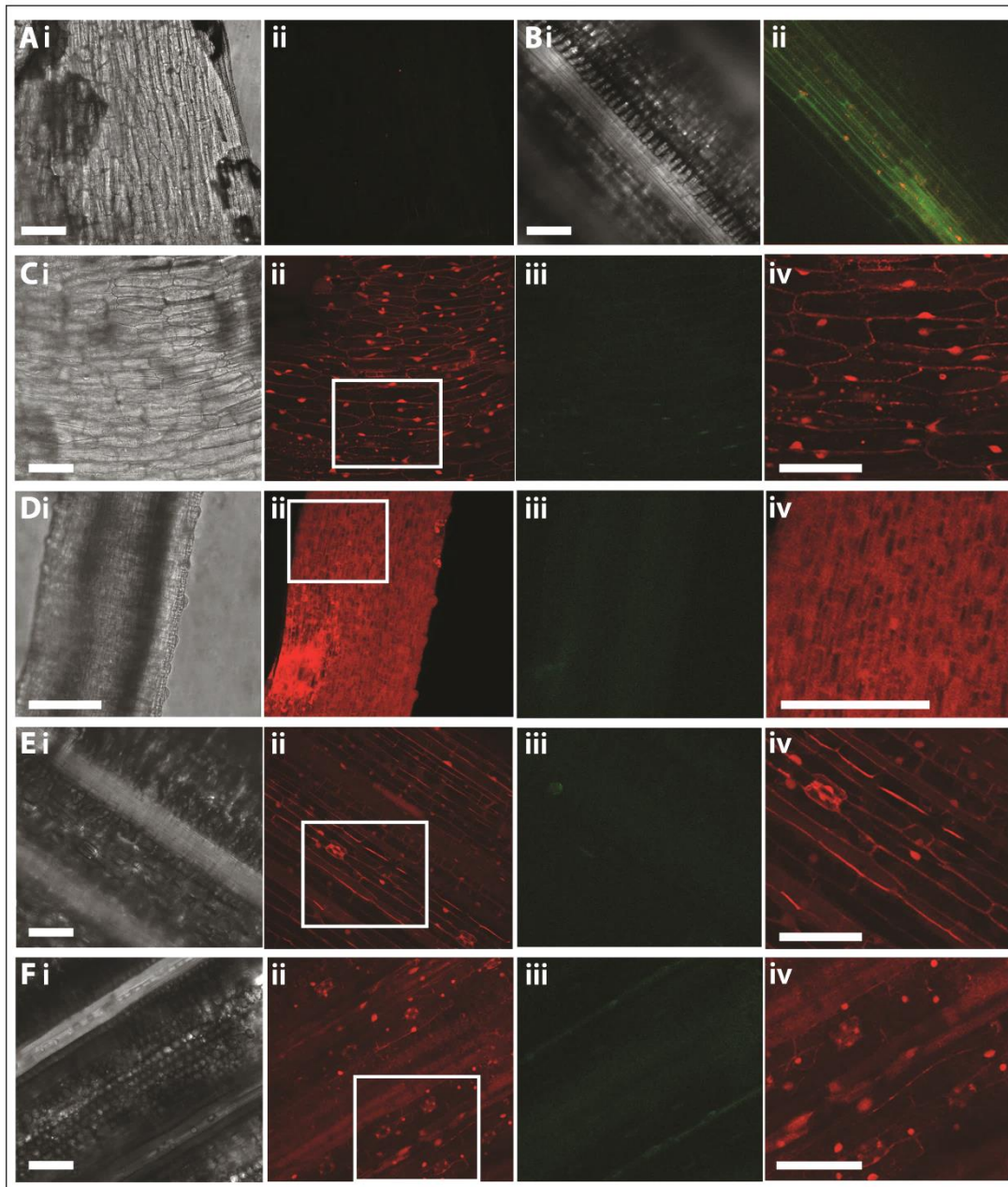


**Figure 4.8** Expression and localisation of the *pHvHSP17::Cre/pZmUbi::loxmCHERRY-HDEL-Tlox/eGFP-HDEL-T* construct in T1 barley plants.

A-B: tissue from a null (wild-type) sibling. A: auricle tissue. B: blade tissue. *i*: bright field image of the tissues, *ii*: combined image of the eGFP and mCHERRY settings. C-F: a homozygous transgenic plant carrying two copies of the transgene. *i*: bright field images of the tissue. *ii*: mCHERRY settings. *iii*: eGFP settings. *iv*: zoomed-in views of the boxed region in *ii*. C: mature auricle tissue. D: awn tissue. E: mature blade tissue. F: mature sheath tissue. Scale bars are all 100µm.

The expression of the *CyPET* marker gene in the *BKn3* sector lines (*pHvHSP17::Cre/pZmUbi::loxCyPET-HDEL-Tlox/BKn3-mCHERRY-T/pHvPIN1a::HvPIN1a-eGFP-T construct*) was slightly weaker than the mCHERRY in the clonal sector lines but was still clear and uniform in all the hemizygous and homozygous T1 lines imaged so far. Example images for the *pHvHSP17::Cre/pZmUbi::loxCyPET-HDEL-Tlox/BKn3-mCHERRY-T/pHvPIN1a::HvPIN1a-eGFP-T* lines are illustrated in Figure 4.9. The expression of CyPET is specific to the ER in the homozygous plants (Figure 4.9.C-E, C is blade tissues, D is sheath tissue, and E is lemma tissue). There is some autofluorescence from the hairs on the surface of the mature blade in Figure 4.9.C.ii. The specific CyPET signal is not seen in the null siblings (there is autofluorescence of xylem elements and stomata, Figure 4.9.A.ii and B.ii). In all samples imaged there is low signal in the mCHERRY range, the signal that is there is likely to be due to autofluorescence, this suggests that there is no read through into the *BKn3* reading frame in the absence of heat shock. There is little signal in the mCHERRY or the eGFP conditions for the null siblings (Figure 4.9.A and B). There does not appear to be any strong *PIN1a-eGFP* expression, but this may be because the tissues imaged so far are older and may not be expressing *PIN1a*(Figure 4.9 C-E. iii).

The *PIN1a*, DR5 auxin reporter line (*pHvPIN1a::HvPIN1a-eGFP-T/ DR5:mp35S::mCHERRY-T*) was difficult to assess in mature tissue, therefore I imaged young leaf and inflorescence tissues. The *PIN1a-eGFP* signal was strongly localised to the cell membrane in young tissues of homozygous plants (Figure 4.10.B-C, young lemma and young lead tissue respectively, green signal in ii and iv) when compared to the null siblings (Figure 4.10.A). However, the mCHERRY DR5 signal, if present at all, is very weak in the samples imaged so far (Figure 4.10.B-C,iii). This lack of DR5 signal may be because the correct stage in development when there are high peaks of auxin have not been imaged yet, or it could be due to silencing of the construct. Alternatively it may be that the minimal 35S promoter is not functional in barley.

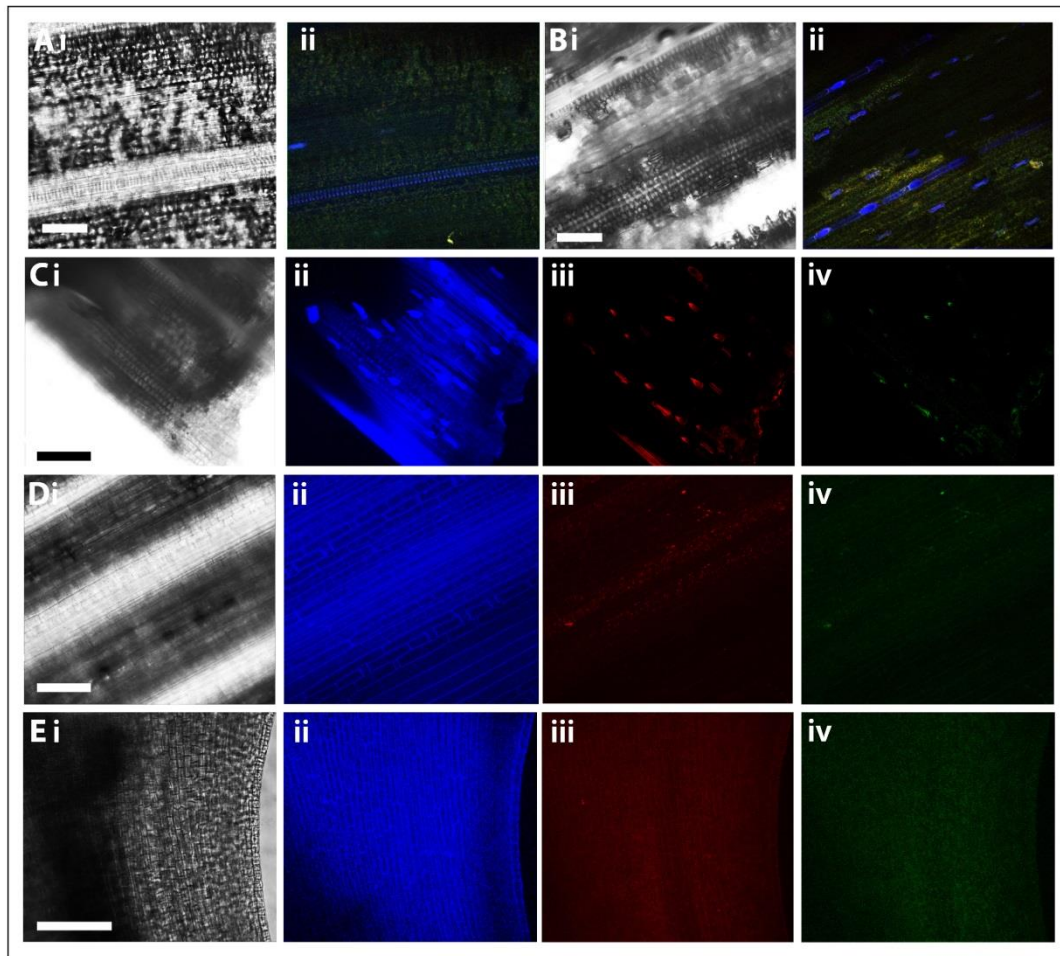
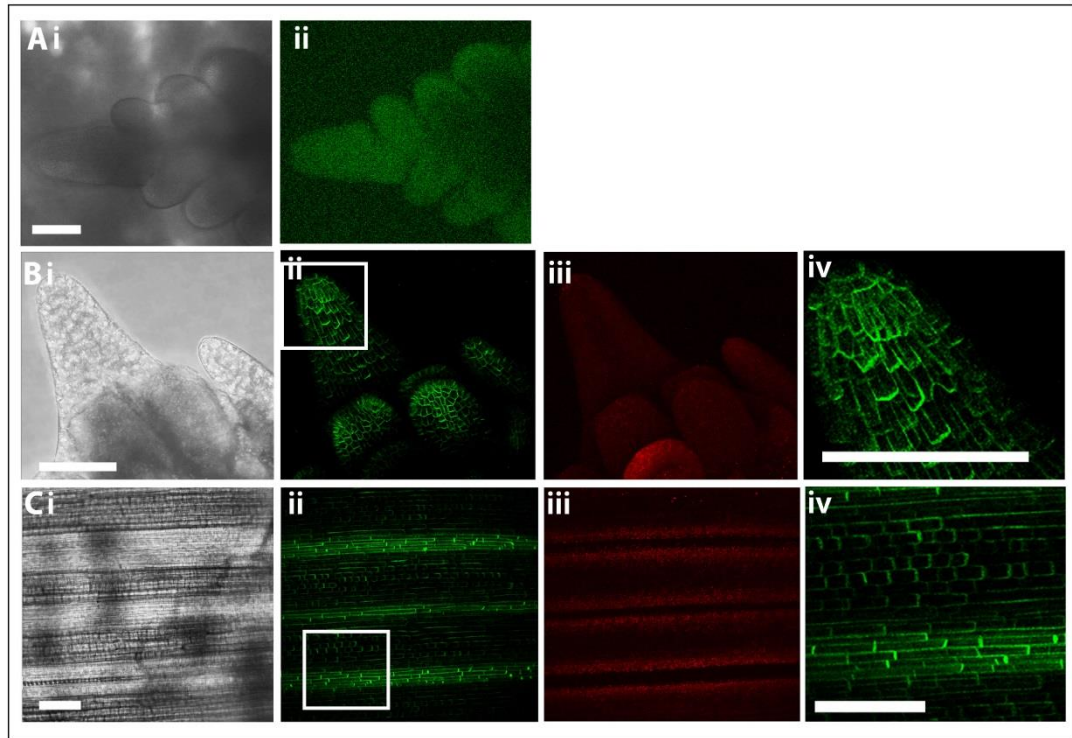


Figure 4.9 Expression and localisation of the *pHvHSP17::Cre/pZmUbi::loxCyPET-HDEL-Tlox/Bkn3-mCHERRY-T/ pHvPIN1a::HvPIN1a-eGFP-T* construct in T1 barley plants. A-B: tissue from a null (wild-type) sibling. A: sheath tissue. B: blade tissue. *i*: bright field image of the tissues, *ii*: combined image of the CyPET, eGFP and mCHERRY settings. C-E: a homozygous transgenic plant carrying two copies of the transgene. *i*: bright field images of the tissue. *ii*: CyPET settings. *iii*: mCHERRY settings. *iv*: eGFP settings. C: mature blade tissue. D: mature sheath tissue. E: developing lemma tissue. Scale bars are all 100 $\mu$ m.



**Figure 4.10** Expression and localisation of the *pHvPIN1a::HvPIN1a-eGFP-T/DR5:mp35S::mCHERRY-T* construct.

A: a developing inflorescence spike from a null sibling (wild-type). *i*: brightfield image. *ii*: combined mCHERRY and eGFP settings. B-C: homozygous transgenic sibling. B: young lemma. C: young leaf tissue. *i*: brightfield image. *ii*: eGFP settings. *iii*: mCHERRY settings. *iv*: zoomed-in image of the boxed region in *ii*, showing the cellular localisation of the PIN1a-eGFP. Scale bars are 100µm.

This initial screening of the segregating T1 plants, suggests that all of the constructs have been transformed successfully and that the marker genes are expressed. The imaging also indicates that there is no read through into the inducible gene open reading frame in the clonal sector lines.

#### 4.7 Testing the heat shock inducible lines

To test whether the heat shock inducible clonal sector line, *pHvHSP17::Cre/pZmUbi::loxmCHERRY-HDEL-Tlox/eGFP-HDEL-T*, was functional I used conditions used by Freeman et al [177] to test whether the second marker gene (*eGFP*) could be induced. After 30 minutes heat shock at 38°C, samples (seedlings and whole, detached

spikes) were left to grow in normal conditions for three days before they were imaged using confocal microscopy.

In control samples treated in the same way but not heat shocked, *mCHERRY* expression after 3 days is still strong in the tissue and specific to the ER in both blade tissue (Figure 4.11.A.ii) and leaf primordia (Figure 4.11.C.ii). In control samples there was no activation of specific ER targeted *eGFP* signal (Figure 4.11.A.iii and Figure 4.11.C.iii). In contrast the heat shocked samples had specific ER targeted *eGFP* induced throughout the tissue in both blade tissue (Figure 4.11.B.iii and zoomed-in iv) and leaf primordia tissue (Figure 4.11.D.iii and zoomed-in in iv). There was no loss of *mCHERRY* signal in these samples (Figure 4.11.B.ii and Figure 4.11.D.ii), however this may be because the lines are homozygotes with two copies of the transgene and not all copies of the transgene have been activated by the heat shock. This suggests that heat shock at 38°C can induce the expression of the *CRE* which then recombines the *lox* sites flanking the *mCHERRY* region, removing it and allowing the expression of the *eGFP* reading frame.

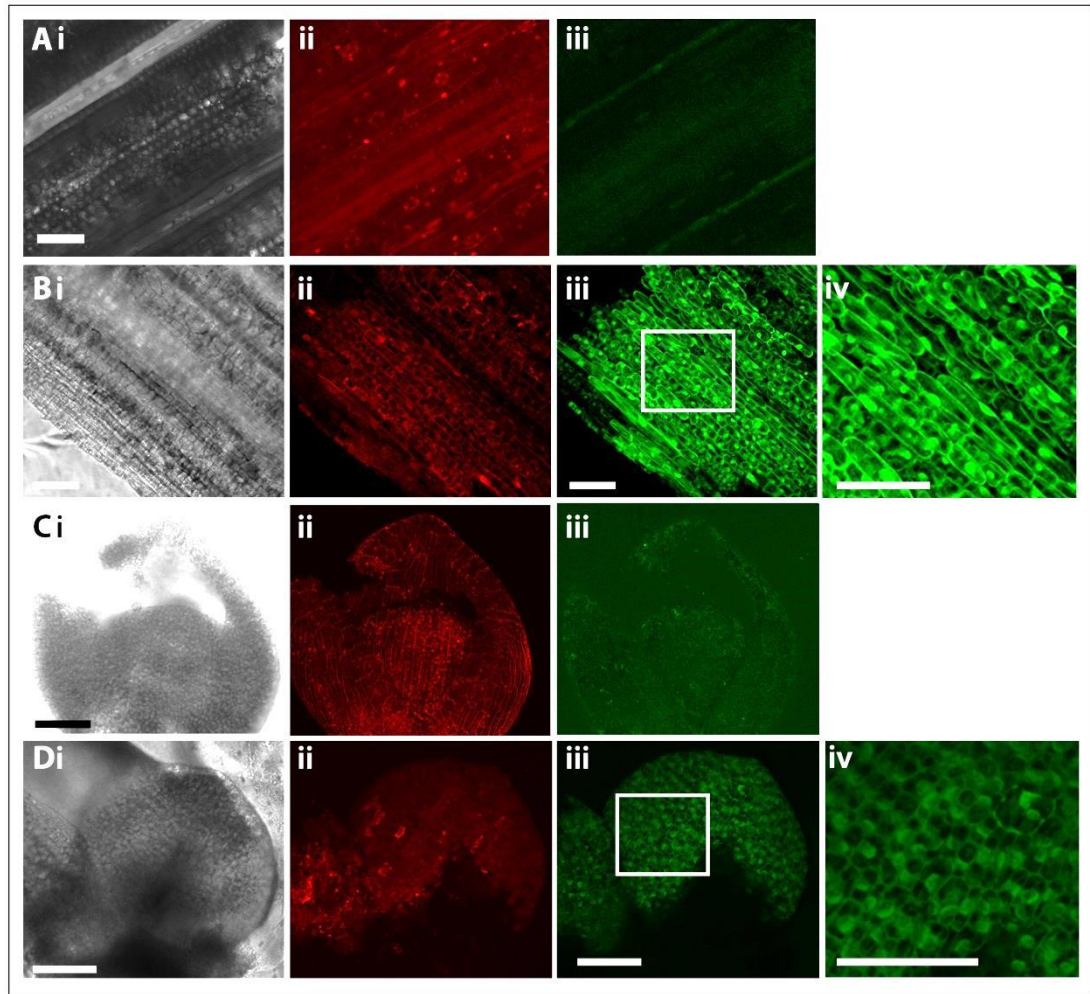


**Figure 4.11 Heat shock test on the expression and localisation of *mCHERRY* and *eGFP* in *pHvHSP17::Cre/pZmUbi::loxmCHERRY-HDEL-Tlox/eGFP-HDEL-T* T1 barley plants.**

*A and C*: control tissue from a non- heat shocked sibling. *A*: blade tissue. *B*: developing leaf primordia. *B and D*: tissue samples from heat shocked (30 minutes at 38°C) plants. *B*: blade tissue. *D*: developing leaf primordia. *i*: bright field images of the tissue. *ii*: mCHERRY settings. *iii*: eGFP settings. *iv*: zoomed-in image of the boxed region in *iii*. Scale bars are all 100µm.

The inducible *BKn3* sector lines are yet to be tested as, based on previous published results by Williams-Carrier et al [138] who used ZmUbi promoter to overexpress *KN1* in barley, *BKn3* is only expected to be induced in developing lemmas. Therefore to test these lines I need to wait until the T2 generation to maximise the seed collected from the T1 generation.

## 4.8 Discussion

### 4.8.1 Development of a barley transgenic toolkit

I have developed a small transgenic toolkit in barley using goldengate cloning for use in developmental studies. Through developing this toolkit I have answered several questions about barley transgenics.

Firstly I have added *mCHERRY* and *CyPET* to the list of fluorescent proteins suitable for use in barley, as shown by the clonal sector lines which use ER targeted *CyPET* and *mCHERRY* as marker genes. *mCHERRY* seems to have particularly strong expression in all barley tissues tested so far.

I have also shown that it is possible to stack the heat shock inducible *CRE* module with the *lox* modules in the same construct, by adding an intron into the *CRE* to prevent bacterial expression, something so far only shown in mammalian tissues [179]. This means that only one transformation is needed and no further crosses are necessary to generate functional clonal sector lines. The *CRE* construct containing an intron, developed in this project, has already been used in both *Arabidopsis* (Sam Fox, JIC, unpublished) and in *Utricularia gibba* (Claire Bushell, Chris Whitewoods and Sam Fox, JIC, unpublished) clonal sector constructs and shown to be fully functional in both.

I have also illustrated the use of heat shock inducible *CRE* clonal sector constructs in monocots for the first time. The protocol for induction will now be optimised to allow the induction of single clonal sectors rather than complete activation across the tissue. I am yet to test the induction of *BKn3*. This is because of the need to generate as much T1 seed as possible, as based on previous published work [138], I only expect *BKn3* to be activated in developing lemmas, which would require the entire plant to be heat shocked. I hope that this line will illustrate the first example of inducible *BKn3* expression in barley.

### 4.8.2 Future work

Homozygous plants (Golden Promise background) with good expression and localisation are now being crossed with the *Hooded* mutant (in a Bowman background) to generate lines for testing the growth rate predictions made by the computational models outlined in chapter 3.

The plasma membrane marker line developed will be useful in testing some of the existing predictions about growth during both lemma and leaf development (outlined in Chapters 2

and 3). I hope to develop live imaging techniques to enable tracking of cell outlines to calculate resultant growth rates, cell division rates and growth orientations as done previously for the *Arabidopsis* leaf [21]. With this data I would be able to test predictions and contribute dynamic growth data relating to leaf and inflorescence development to the field of monocot developmental biology.

I can also use the *mCHERRY/eGFP* clonal sector lines to test growth predictions in both the leaf and the lemma. By optimising the conditions required for the induction of single cell clones in barley tissues I hope to generate clonal sector maps as previously carried out for *Arabidopsis* and *Antirrhinum* [22, 24]. The size and shape of the clonal sectors will be able to provide indications of the rate and direction of growth. Once crossed into the *Hooded* mutant I will be able to compare growth in the wild-type lemma and the *Hooded* lemma, testing the model predictions.

It would also be interesting to cross the clonal sector lines and the plasma membrane lines into other barley mutants such as the *calcaroides* mutants [180, 181]. This would allow exploration and comparison of growth rate patterns in a range of different mutants. Ultimately exploring how changes in growth are able to generate a wide range of developmental switches in shape.

The *PIN1a* and *DR5* marker line, will be used to explore the orientation of PIN1a and the peaks of intracellular auxin during different developmental processes. Unfortunately I am yet to see any *DR5* signal in samples tested, this may be due to silencing in the young tissues of interest. I will need to screen these lines carefully to find a line which stably marks auxin maxima and PIN1a orientations. Unfortunately my work and recent work by Devin O'Connor has shown that SoPIN1 is the predominantly epidermally expressed homologue of AtPIN1 in monocots. Devin O'Connor's work has shown that PIN1a acts differently to SoPIN1, in that although it can be expressed in the epidermis, it is usually restricted to developing vasculature, possibly through posttranslational modifications (Devin O'Connor, The Sainsbury Laboratory, Cambridge University, unpublished). This means that I may not be able to use the PIN1a marker lines to dynamically track the reorientations of axial information during development as hoped. However, tracking of these lines will still provide valuable information about vein development and auxin dynamics during development. It would be of interest to now develop SoPIN1 marker lines to track changes to axial information (tissue cell polarity) during development.

I hope to optimise the activation of the *BKn3* clonal sector line, allowing the exploration of the effect on morphology of different positions of the *BKn3* sectors within the developing lemma. It may be that activation of *BKn3* in sectors near the margin will only generate the wing outgrowths for example. Using this line I will also be able to explore the possibility of a window of responsiveness in the lemma/awn boundary tissue. This would also allow the exploration of the effect on morphology of different times of *BKn3* induction as the effect of *BKn3* may be dependent on temporally regulated partners.

Once fully characterised I hope that these constructs will be able to be easily translated for use in other monocot systems, such as maize and rice, contributing to the field of monocot developmental biology.

Overall, I hope that this basic transgenic toolkit will be of use to others as well as current studies and advance the field of monocot developmental biology by enabling dynamic data collection about growth and cell dynamics, which has advanced *Arabidopsis* developmental biology so far.

## 5 Discussion

### 5.1 Summary of this work

During this work I have explored how developmental switches in shape arise from changes in growth and how single genes can modulate growth. I focussed on the role of alterations to growth, composed of axiality and growth rates, in triggering developmental switches in shape using a wild-type case (the grass leaf) and a mutant case (the *Hooded* mutant). Through doing this I have tested the following alternative hypotheses for how growth could be manipulated:

1. Axiality alone is altered
6. Growth rates alone are altered
7. Both axiality and growth rates are altered

To test these hypotheses I made three assumptions, first that axiality is provided by a polarity based axiality system, second that PIN localisation patterns can be used as a marker of this axiality information and third that the developing organ can be treated as a whole (different tissues do not have different properties). With these underlying assumptions, I used a combination of 3D imaging, computational modelling, protein localisation and gene expression analysis to test the different hypotheses for how growth could be modulated.

Using this multidisciplinary approach I have found that growth can be altered through changing growth rates alone (the grass leaf), or through altering both axiality and growth rates (the *Hooded* mutant) to generate developmental switches in shape. However, there is no evidence, so far, that growth can be altered through changing axiality alone. I have also found that single genes can induce developmental switches in shape through influencing growth rates and axial information (the *Hooded* mutant).

Through this project I have also generated a set of tools which will help in the advancement of monocot developmental studies. I have developed a set of 3D image records of monocot leaves, not previously available in the published literature. I have also developed a detailed 3D timecourse of barley inflorescence development, which will help others in defining morphology changes in mutants and in the initiation timing of different organs. A transgenic toolkit has also been developed, which will hopefully be of use for future developmental studies and illustrates the use of inducible sector lines in a monocot species.

## 5.2 Developmental switches in shape arise from changes to growth rates alone and from changes in growth rates and axiality combined

Through exploring developmental switches in shape, during early grass leaf development and *Hooded* barley lemma development, I have found that growth can be manipulated through changing growth rate alone, or growth rate and axiality combined, but not necessarily through changing axiality alone.

This apparent inability of axiality to be altered alone may be due to the diverse range of roles that auxin plays during development. Auxin is proposed to play a central role in a polarity based axiality system. This is supported by many examples of auxin underlying different developmental processes [4, 33], as well as auxin influencing the polar distribution of markers such as root hairs [65, 68] and PIN proteins [182]. This suggests that axiality could be altered through changing auxin dynamics within a tissue. Auxin has also been proposed to act on growth rates. It is well established in the literature that auxin induces cell elongation [183]. This could be through influencing hydrogen ion concentration in the cell wall [184] or through inducing the expression of cell wall modulating enzymes such as expansins [57]. The interconnected nature of the phytohormone pathways could mean that auxin is able to influence growth rates more indirectly through modulating other hormone signalling pathways. For example, cytokinin and brassinosteroids have both been shown to influence cell wall properties [185, 186]. This dual function of auxin in axiality and growth rate modulation could explain why separate regulation of axiality is not possible. Whereas growth rate alone can be altered as there are many auxin independent pathways able to modulate cell wall properties. Alternatively, it could be possible that axiality can be modulated alone, although this may not have been used extensively during evolution.

These findings predict that other changes in organ morphology, which arise through developmental switches in shape during organ development, would involve either changes to growth rates alone or changes to both growth rates and axiality.

Changes in growth rates and axiality may act during serration development in *Arabidopsis*. One of the first indications of an incipient serration is the formation of a PIN1 convergence point in the margin of the developing leaf [4], indicating a change in the axial information. The formation of lobes in *Arabidopsis lyrata* leaves has also been found to involve a change in growth rate pattern (RCO is proposed to restrict growth in the sinus of each developing lobe)[77]. Modelling of the *Antirrhinum* flower also predicts that precise changes in growth

rate patterns and axial information are required for the formation of the mouth, which is central for selecting specific pollinators [24]. These predictions in *Antirrhinum* are currently under investigation. Preliminary research suggests that changes in growth rate patterns are more central to the formation of the *Antirrhinum* flower palate shape than changes in axial information (Alexandra Rebocho, JIC, unpublished), similar to my findings in grass leaf development.

It may be that axial information is only altered when new axes of growth are defined, for example, perhaps this is true in the formation of the ligule in grass leaves in which new PIN1 orientations are observed [129, 130]. Published work has also indicated that during ligule development many of the genes involved in organ outgrowth are activated [130], suggesting that changes in growth which trigger developmental switches in shape, may be redeployed organ initiation networks.

These incidences of axial information changes are restricted, implying that developmental switches in shape can occur in a localised manner through specific changes in growth to generate small and precise alterations to final organ shape.

### **5.3 Single genes can trigger developmental switches in shape through modulating growth rates and axial information**

Using the barley *Hooded* mutant as a model system, I have also found that single genes can alter growth during organ development (therefore triggering developmental switches in shape) through changing growth rates and axially.

The *BKn3* gene, the barley homologue to maize *KNOTTED1* [187] and *Antirrhinum* *HIRZ* [154], is able to induce both a reorientation of the axial information within the developing lemma and a change in growth rate. This action is likely to happen both globally across the lemma (forming the inverted ectopic flower) and locally in the lemma margin (forming the wing outgrowth later in development). *KN1* is a transcription factor which is normally involved in the maintenance of the shoot apical meristem [156]. Its mis-expression due to cis-regulatory element changes commonly causes changes in shape. For example, the ectopic expression of *KN1* at the tip of the midvein in developing maize leaves results in the formation of a forked leaf [152], and *Hirz* mutants in *Antirrhinum* form spur like structures on the petals [154]. Work had previously suggested that *KN1* may have an influence in organ polarity due to the formation of new vein patterns in *Kn1* maize mutants, which predicted a local change

in axial information at the cellular level. Others have also proposed that KN1 is able to influence the orientation of growth [152, 188]. My results support these predictions, as I have shown that BKn3 is able to induce a reorientation in axial information, as marked by SoPIN1, at the cellular level resulting in organ level changes in morphology.

KN1 is a transcription factor that is able to influence many different target genes involved in a wide range of hormonal and developmental pathways [155]. It may be that KN1 is unique in the ability to alter both growth rates and axiality, generating developmental switches in shape, as it is a key regulatory node in many transcriptional networks. KN1 has a role in several different developmental switches in shape, for example, expression of *KN1* in the margin of the developing tomato leaf allows the formation of a wild-type compound leaf [189], and it is also involved in compound leaf formation in *Cardamine hirsuta* [190]. However other *KNOX* genes can also induce shape changes. For example, other class 1 *KNOX* genes like *KNAT1* in *Arabidopsis* can severely alter leaf morphology when over expressed. In the case of *KNAT1* overexpression in *Arabidopsis*, leaves become deeply lobed [191].

It is unlikely that *KNOX* genes are unique in their ability to trigger developmental switches in shape through modulating growth, as there are many examples of new morphologies generated independently of *KNOX*. For example, the Fabaceae family also develops compound leaves (an example is the *Pisum* genus) but uses a mechanism independent of the characterised *KNOX* pathway [192]. Interestingly they utilise a homologue of *LEAFY* instead of *KN1* [193]. In *Arabidopsis* *CUC2*, a NAC domain transcription factor, is necessary for serration development and is independent of *KNOX* expression patterns [4, 5]. Although in this case, the change in growth involves a reorientation of cell files and change in growth rates, which is dependent on auxin [4, 5]. Lobe formation in *Arabidopsis lyrata* uses the existing PIN and auxin patterns set up for serration development (therefore does not alter existing axial information), but the additional expression of *RCO*, a homeodomain transcription factor, in the sinus of each region inhibits growth and promotes lobe formation [77].

Although the gene that triggers the change in growth can vary, some common elements, such as auxin and PIN1 patterns, are involved in causing many developmental switches in shape.

## 5.4 Modulating axial information with organiser regions

Through RNA *in situ* hybridisation I found that BKn3 induced the ectopic expression of several candidate organiser components in the *Hooded* lemma. It may be that through inducing the formation of new organiser regions (plus and minus organisers, which are able to modulate auxin concentration locally) BKn3 generated a change in the axial information in the developing lemma, triggering the developmental switch in shape. If this is the case, it could provide support for the polarity based axiality system, which was assumed to be active in defining axial information in developing organs during this project. In support of BKn3 inducing new polarity organiser regions, which may involve auxin dynamics, published ChIPseq work on KN1 targets in maize suggest that KN1 is able to upregulate auxin synthesis and recognition components [155]. It could also be that *KNOX* class 1 proteins are able to directly influence axial information through defining a new organiser of polarity themselves. The observation that *KNOX* genes are expressed in the base of the maize leaf primordia [79] and the involvement of *Arabidopsis* *KNAT6* (class1 *KNOX* related to *STM* and *KNAT1* [194]) in boundary formation would support the idea that *KNOX* could act as a plus organiser.

If axial information is provided by a polarity based axiality system, my results would predict that other developmental switches in shape generated by changes in axial information and growth rates, would also involve the ectopic expression of candidate organiser components (e.g. *YUCCAs*, *NAM*, *LAXs*). For example, serration development in *Arabidopsis* involves reorientation of PIN1 patterns in the margin, suggesting a change in axiality. Serration formation in *Arabidopsis* requires the ectopic expression of *CUC2*, a possible component of a plus organiser, in the serration region [4]. In grass ligule development this hypothesis would predict that possible candidate organiser components like *YUCCAs* and *NAM* would be ectopically expressed in the region between the sheath and blade. Work by Johnston et al found that during ligule formation genes associated with organ initiation are activated in maize, and this includes expression of a *CUC2* homologue (a *NAM* homologue) in the preligule band [130] which becomes restricted to the ligule cleft (the base of the ligule). This may support the hypothesis that new organiser regions are also involved in the formation of the ligule.

This work does not exclude the possibility that a stress-based axiality system may define the axial information within developing organs. However, as the components involved are unknown, it is difficult to test whether a stress based model could account for the changes in growth and shape observed. It may be that until possible components of the stress based

axiality hypothesis are characterised, it is unlikely that we can conclusively decide which axiality system is active during plant development.

## 5.5 The contribution of different tissues

To explore the role of growth changes in developmental switches in shape in the grass leaf and in the *Hooded* mutant, I made the assumption that the entire organ could be treated as a continuum, with no specific contribution of each tissue within. This enabled me to generate simplified models of both grass leaf development and lemma wing development. The models generated a set of predictions which were then testable *in planta*, indicating that the use of this simplified assumption in exploring the development of shape is valuable.

The model predictions, particularly those relating to axial information, were tested using epidermal markers of polarity, like SoPIN1 localisation and hair orientations. The models predicted that the patterns of axial information were required for the development of shape in both systems. As the experimental data taken from epidermal markers correlated with the model predictions, it could be that the epidermis is able to influence the growth of subepidermal tissues, influencing overall organ shape. However, as I have not explored the axial information and growth rates in subepidermal tissues I cannot exclude the possibility that this axial pattern is shared throughout the tissue. Similarly, as vascular development is concurrent with the organ shape development, it would be difficult to distinguish whether veins have a driving role in defining final organ shape. Although at the stages in development in which I have been interested, veins are not fully formed, suggesting that they may not be mechanically distinct from the rest of the tissue, questioning whether they would be able to drive shape development at these stages. Later stages of development do seem to be influenced by different properties of component tissues. For example, altering the properties of the midrib region in the grass leaf is able to change leaf curvature [124], which can have a significant impact on productivity [128].

Perhaps at very early stages in development it is a valid assumption to approximate the entire tissue as a continuum, but at later stages differential properties arise between the component tissues, influencing growth and shape.

My work in the *Hooded* mutant may indicate that expression of *BKn3* in different regions of the developing organ (rather than different tissue layers) could trigger different developmental switches in shape. This suggests that the induction of specific developmental

switches in shape may be based upon the tissue context of the ectopic gene. The effect of ectopic *KN1* expression on shape may also be tissue context dependent. I have preliminary evidence that *Hooded* wing development may be due to ectopic expression of *BKn3* specifically in the margin of the developing lemma, whereas the ectopic flower forms due to expression of *BKn3* in the middle of the lemma. This is a phenomenon previously observed in the *Kn1* mutants of maize which form tissue knots when *KN1* is expressed in the middle of the leaf and leaf flaps (reminiscent of the barley wings) when it is expressed in the leaf margins. This could provide evidence that developmental switches in shape are not only influenced by the ectopic expression of 'master regulators', but also the genetic and tissue context that it is found in. This differential response, suggests that specific tissues could influence final shape. This predicts that the expression of other genes able to trigger developmental switches in shape, like the *Arabidopsis CUC* genes, in different tissue contexts could result in different shapes.

## 5.6 Monocots as developmental models

To explore the role of changes in growth in defining developmental switches in shape, I chose to use monocot model systems which covered floral and leaf development. Through using these I identified three distinct developmental switches in shape: one that may underlie a key step in grass leaf development and two which were triggered by the ectopic expression of *BKn3* in the developing barley lemma. Using these models I have been able to separate out the effects on growth based on axiality and growth rates. As well as develop information on monocot development to allow future comparisons between monocot and dicot development.

This has partly been made possible by the very distinct change in axiality in the *Hooded* mutant lemma, which I was able to show was related to cellular level changes in axial information using immunolocalisation of SoPIN1. This change in axiality, induced by ectopic *BKn3* expression, may be unique to this system as in dicots overexpression of *KN1* homologues have not been reported to generate macro changes in axial information, although ectopic meristems are formed [90, 159]. In addition to this, the localised ectopic expression of *BKn3* in the *Hooded* lemma is very consistent, making it easier to target experiments. This contrasts with dicot systems, where ectopic expression of *KN1* homologues is often spread through the developing leaf tissue, making it difficult to target specific areas of the developing leaf and to stage developmental events.

Another advantage of using monocots to explore the role of changes in growth in defining developmental switches in shape, is that the development of the grass leaf has very distinct series of whole organ shape transitions during early development. These developmental switches in shape seem to be essential in forming the correct mature leaf shape (as shown by the *hoja loca* mutant (Sarah Hake and Aaron Sluis, UC Berkeley, unpublished)) and may be one of the characteristics that underlie the evolution of the distinctive grass leaf. This allows the dissection of evolutionary important developmental switches in shape which affect the shape of the mature organ and influence growth habit. This differs from existing dicot models like *Arabidopsis* which do not have complex developmental switches in whole organ shape early in development. This also differs to dicot models like the *Antirrhinum* flower which undergo an intricate series of shape transitions throughout development, making it difficult to dissect out changes due to different components of growth.

One of the drawbacks of using these monocot models is the difficulty in assessing growth rates. Most methods used to analyse growth rates in very young organs have been developed in the dicot system, *Arabidopsis*. These include clonal sectors using fluorescent proteins and live cell tracking. Without easy access to these tools in my monocot systems, it was difficult to assess growth rates. In addition to this, the concealed nature of the lemma and the leaf as they develop makes it difficult to carry out live imaging of samples to allow live cell tracking. However, with the development of the transgenic toolkit in barley, I hope to be able to resolve at least some of these problems, particularly by optimising the use of the fluorescent protein clonal sector lines to assess growth patterns in the developing leaf and lemma at early stages (current clonal sector lines in monocots use X-ray induced chromosome breakage in heterozygous mutants for chlorophyll genes and are therefore not suitable for use in tissues without strong chlorophyll gene expression).

The distinct differences between final monocot and dicot organ shapes, means that it is valuable to explore development in both systems, as this highlights evolutionary innovative steps which led to the divergence of the monocots and dicots. Similarly there are several examples where monocot and dicot development differ making it important that both systems are explored. This is valuable as it will hopefully lead to the identification of common mechanistic principles underlying shape development in plants. For example, common mechanisms such as the use of an axiality system, possibly based on auxin, and the role of changes in growth in triggering developmental switches in shape may be active. Comparisons between monocot and dicot development would also highlight key changes in the common

mechanism that contributed to the evolutionary divergence of such distinct groupings within the plant family.

## **5.7 Developmental switches in shape are involved in the evolution of new organ morphologies**

Developmental switches in shape can form the basis of fundamental shape transitions during development, determining the final form of the mature organ. Through exploring the developmental switches in shape during the early stages of grass leaf development, which appear to be central to the formation of the mature leaf, I identified a change in growth essential for the crucial shape transitions. It may be that this change in growth could be one of the underlying features which led to the evolutionary innovation of the grass leaf.

During evolution new developmental switches in shape may have been recruited to generate the huge diversity in final organ shape now seen. These new switches will all be underpinned by novel changes in growth during organ development. It could be that over evolutionary time, changes to growth, either through modulating growth rates alone or through changing growth rates and axiality, have been repeatedly used to generate new shapes.

For example, the formation of spurs in flowers, which can have a significant impact on pollination syndrome [195], has been repeatedly lost and gained throughout evolution [196]. This may be due to loss and recruitment of changes in growth required for the developmental switch in petal shape. Ectopic expression of genes able to influence both growth rates and axiality could underlie the formation of petal spurs. This could be related to the ectopic expression of the *KN1* homologue, *HIRZ*, in the *Antirrhinum* mutant which develops petal spurs due to the ectopic expression of *HIRZ*. If *HIRZ* acts like *BKn3*, it may induce a developmental switch in shape by modulating growth rates and axiality.

These new developmental switches in shape could be achieved through the ectopic expression of single genes like *KN1* resulting from mutations in cis-regulatory elements. Every over expression mutant of *KN1* is due to a mutation in a cis-regulatory region. For example, insertions in intron IV in *Hooded* [90] and in intron 1 in *Hirz* [154] are responsible for the ectopic expression and morphology changes. Cis-regulatory element changes are rapidly being realised as key drivers of evolutionary change rather than mutations in gene coding regions [78, 190, 197-201]. This could be due to cis-regulatory elements ability to introduce new changes in growth in different temporal or spatial positions during organ

development, triggering developmental switches in shape. The central role of changes in cis-regulatory elements in evolution is also a key research area in animal biology [202].

Alternatively existing changes in growth could have also been modulated during evolution to have different effects on shape. For example, the changes to growth could be as small as expanding or reducing the size of the region the change acts upon, such as is the case in the development of the animal limbs [8, 9]. This may be what is responsible for determining how closed a flower mouth is in close relatives of *Antirrhinum*. The closed mouth shape is proposed to involve significant changes in growth rate patterns in the pallet of the flower. *CUP* (the homologue of *CUC* in *Arabidopsis*) is expressed in the pallet region and its expression domain is expanded in *Antirrhinum* whereas it is smaller in *Mimulus* which has a more open mouth (Alexandra Rebocho, JIC, unpublished). This suggests that *CUP* could influence growth rates either directly or indirectly, and the expansion of the domain allowed the increase in growth rates required to generate the closed *Antirrhinum* flower. Similarly modelling of the development of broad leaves suggest that modulation of the position of PIN1 convergence points in the developing leaf margin and the degree of growth induced in that region, can generate a diverse range of lobed and serrated broad leaves (Przemysław Prusinkiewicz, University of Calgary, seminar talk, unpublished). This indicates that the modulation of an existing change in growth during organ development can produce a diverse range of shapes.

Through the introduction of novel changes in growth and altering existing changes, new developmental switches in shape could have arisen, allowing the evolution of a diverse range of organ shapes which all develop from similar, simple peripheral outgrowths.

## **5.8 Computational modelling allows exploration of shape development at different scales**

Computational modelling used in this project did not aim to build comprehensive models of shape development, instead they were simplified models used as tools to provide a series of testable predictions. These predictions allowed me to focus experiments to test hypotheses relating to how shape is determined during development. The results from these tests could then be fed back into the models to refine them further if desired.

The models generated were based upon a deforming tissue, and did not consider cellular level dynamics. This was done to save computational power, and to reduce the number of

parameter assumptions needed (as I do not have dynamic data available to calculate precise cell division patterns and cell behaviours). However, this simplification did not prevent the model from making clear predictions at the cellular level. The models made predictions about the coordinated cellular localisation of SoPIN1 proteins and predictions about where more cell elongation (i.e. growth), and possibly cell division, would occur in the tissue. These cellular level predictions were then experimentally testable. The tissue level model was also able to make predictions at the organ level, by predicting the overall shape of the organ under certain conditions, these are yet to be tested through looking at mutant samples.

The ability of the tissue level models to provide clear predictions at all developmental scales; cellular, tissue and organ; makes them a powerful tool for exploring hypotheses relating to how shape forms during plant development.

## **5.9 Future directions**

Through this project I have begun to explore how changes in growth may influence key developmental switches in shape, through modulating axial information and growth rate patterns, and their importance in the development and evolution of shape.

Through computational modelling I have explored the role of axiality and growth rate changes in triggering different developmental switches in shape. These found that either growth rates alone were altered or both axiality and growth rates were changed. The predictions of the models have been tested, although much of the experimental work shown is preliminary. Therefore these preliminary results first need to be confirmed through more whole-mount immunolocalisations in early stages of barley leaf and lemma development. The patterns of growth dynamics in early stages of grass leaf and lemma development are also yet to be established. This may now be possible using the new transgenic tools developed as part of this work. A detailed dynamic description of growth during early stages of leaf and lemma development would contribute to the field of monocot development, as so far very early stages of development have not been described using dynamic growth data. This growth rate data could then be used to refine the model of primordial grass leaf development in particular. The development and use of other tools such as transgenic gene expression reporters and graded hormone reporters, like those developed by the Weijers lab [203], would also provide more detailed analysis of leaf and lemma development. In addition

to this these future transgenic tools could help in assessing possible genetic or hormonal triggers of the developmental switches in shape identified during this work.

Refinement of the leaf model specifically, would allow it to be extended further to investigate the role of axial information and growth rate changes later in development. This would test the hypothesis that growth rates alone are altered during grass leaf development, or whether a combination of changes to growth rate alone, and combined with axially are used to generate the final form of the grass leaf. For example, the ligule/ auricle region is an essential feature of the grass leaf acting as a hinge region. The ligule grows out from the main axis of the leaf, predicting that a new axis of growth may need to be defined for ligule development. This is supported by the expression of genes involved in lateral organ formation, such as PIN1, in the preligule band region [130]. It could also be hypothesised that the auricle region arises separately from the ligule through modulation of growth rate patterns, generating the wedge-shaped region of tissue. This may be supported by a mutant in rice which has increased leaf angle, possibly due to enhanced growth on the adaxial surface of the auricle[105]. The grass ligule can also have outgrowth elaborations which are used in botanical classification [204] and it may be that changes in growth are deployed to develop these switches in shape as well. Possibly mirroring leaf serration and lobe development which elaborate leaf margins. The ligule/auricle region is also of agronomic interest as it controls the extent to which the blade bends from the main axis of the plant, influencing productivity [63, 205]. Another feature of the grass leaf important to yield is the degree of leaf rolling as shown in rice studies [128]. Leaf rolling could be a simple feature to explore using the model. Extension of the model to explore how the grass leaf may have evolved from other monocots would also highlight the role of changes in growth, which modify axial information and growth rate patterns, in the evolution of new shapes.

The model of early grass leaf development could also be expanded to explore how mutant phenotypes develop. This would be useful to both validate the model using well-studied mutants and provide insights into how mutant phenotypes involving distinct developmental switches in shape may occur. A mutant of particular interest is the dominant *KN1* overexpression mutant in maize which has a range of different phenotypes depending on the strength of the allele and the spatiotemporal pattern of expression [88, 152]. If *KN1* is expressed associated with veins in the blade, knots form, if it is expressed in the margin, leaf flaps which resemble sheath or auricle tissue form. One hypothesis suggests that *KN1* induces proximal identity which causes outgrowth of these knot and leaf flaps [152], another

could propose that KN1 influences the axial information or growth rate patterns to cause the phenotype. Regions of 'proximal' identity could be induced within the blade in the extended model to test these hypotheses, providing insight into the relationship between KN1 and axial information. The DL mutant allele of the *Kn1* mutant also develops forked leaf tips [152]. Again there are several hypotheses about how this phenotype develops. One hypothesis suggests that KN1 inhibits growth rates at the midvein tip causing the forking. Alternatively, KN1 could suppress the 'midvein' identity which could then cause lateral veins to take on 'midvein' identity and extend deforming the tissue. Another hypothesis is that KN1 could alter the axial information at the tip of the developing primordium possibly through inducing a new polarity plus organiser (either directly or indirectly) which causes the shape change. Modelling this mutant phenotype would contribute to the understanding of the relationship between KN1 and growth which I have started to address using the *Hooded* mutant in barley.

Another question to explore further is the contribution of different regions of tissue to morphology. My preliminary work in the barley *Hooded* mutant indicates that the expression of *BKn3* in different regions of the lemma tissue triggers different developmental switches in shape (consistent with observations in the maize *Kn1* mutant.). These differences could arise through mechanical constraints of the surrounding tissue, or the genetic context in which the ectopic *BKn3* expression is initiated. For example *KNOX* genes are proposed to act in heterodimers [206], therefore the change in growth could be due to different dimer partners already expressed in the tissue, influencing downstream effects. Alternatively, the different developmental switches in shape could arise from differential plasticity of the tissue, in that certain regions are less restricted in the shapes they are able to form. For example, perhaps boundary regions are more able to respond than the margin resulting in the formation of the ectopic floret versus simple outgrowths.

The *Hooded* mutant is a particularly good system to test the idea of differential plasticity within an organ as it is specific to the lemma and *BKn3* expression is predictable. It has also previously been shown that overexpressing *ZmKN1* using the ubiquitin promoter in barley, results in precise ectopic expression in the predicted boundary between the lemma and awn [138], not throughout the tissue as would be expected. This indicates that there is a special property of the lemma/awn boundary which may make it more responsive to the expression of meristem identity genes. This is also evident in the fact that there are a number of mutations which developmentally affect this region, for example, the *Calcaroides* group of mutants form sac like structures in the lemma/awn boundary [180, 181, 207]. Why *BKn3* is

only expressed at the boundary between the lemma and awn is not known (*KN1* overexpression in maize occurs in clonal sectors across the leaf [88]). The small ectopic expression region may be due to the availability of other partner *KNOX* proteins in the region as *KNOX* proteins act as heterodimers [206]. It has been suggested that without an interacting partner *KNOX* proteins may be rapidly degraded [141], although this would not necessarily affect the mRNA localisation, but it would affect the protein localisation. On the other hand, *KNOX* could be expressed in this boundary region due to the absence of the normal class 1 *KNOX* repressors present in differentiated tissues, like the MYB transcription factor *RS2* [160]. This may correlate with the observation that some shape elaborations occur at boundary regions like the ligule. Alternatively, the 305bp insertion in intron IV of *BKn3* might affect the chromatin structure or insulators present on the *BKn3* gene, making it accessible for transcription only under certain conditions, which happen to be present in the lemma awn boundary in barley (this has been proposed as a mechanism for explaining *KN1* overexpression in maize [206]). This would also correlate with the finding that all gain of function *KNOX* class 1 mutants so far studied are due to changes in cis-regulatory elements [90, 152, 154]. Using the heat shock activation line of *BKn3* it would be interesting to test the window of responsiveness for ectopic *BKn3* expression in the lemma/awn boundary. Coupling this with laser dissection RNA sequencing of different regions in the lemma, including the lemma/awn boundary region, at different stages may also highlight partner factors to *BKn3* that enable this responsiveness. This work would contribute to understanding of *KNOX* class 1 protein regulation and in developmental plasticity of tissues, as it may highlight why the lemma/awn boundary retains the ability to respond to *KNOX* overexpression. It has been suggested that the lemma/awn boundary is analogous to the ligular boundary region between the sheath and blade in the leaf, which develops in response to the expression of the *LIGULELESS* genes [104, 208]. Similarly, tobacco plants which over express *KN1* predominantly only form ectopic shoots at the junction between the petiole and lamina [134], suggesting that boundary regions may have special ability to respond to *KNOX* expression. Therefore, studying the effects of *BKn3* on the lemma/awn region in detail could provide insights into the plasticity of other boundary regions. This could also contribute to the understanding of morphological diversity due to secondary morphogenesis of specific regions.

With this future work it may be possible to contribute further to the wider field of developmental biology, beyond the questions I have asked here. For example, the control of developmental plasticity is currently a key area of investigation in developmental biology as

this also relates to how plants respond developmentally to environmental conditions. Similarly, whether different regions within a tissue contribute differently to development is a key debated area within developmental biology and extension of this work may contribute towards this debate, if the causative factors behind different responses to the same gene can be identified. This may also lead to the identification of key regulatory elements and dynamic growth rate patterns central to grass leaf development, providing foundational knowledge for current projects designed to model a developing crop plant and its responses to abiotic and biotic factors [117, 209, 210].

### **5.10 Concluding remarks**

This work is the starting point for further investigation into the role of changes in growth which trigger developmental switches in shape, resulting in the formation of new organ morphologies. It has aimed to contribute to the existing knowledge relating to this subject area and to provide useful resources for future study, including 3D image timecourses and a transgenic toolkit for developmental studies in barley. It is hoped that this work has laid a foundation for further study using monocots as model developmental systems. This work has also contributed to the larger question of how does diversity in organ shape arise in both plant and animals from simple bud like starting shapes.

## 6 Materials and methods

### 6.1 General Methods

#### 6.1.1 DNA extraction

Amelia's DNA extraction method was used to extract gDNA from barley and maize seedlings. Two young seedlings were dissected out of the coleoptile and removed from the seed before being ground in liquid nitrogen; 1mg of tissue was transferred to a 1.5ml Eppendorf tube. 750  $\mu$ l Extraction buffer (100mM Tris pH8, 1.4mM NaCl, 20mM EDTA, 2% CTAB 2g/100ml and 0.2%  $\beta$ -mercaptoethanol 2  $\mu$ l/ml) was added before incubating at 65°C for 30 minutes. The solution was cooled for 2 minutes, and a half volume of chloroform was added and the sample was vortexed before being centrifuged at 13,000rpm (using an Eppendorf Centrifuge 5415D) for 5 minutes. The supernatant was transferred to a new DNase free Eppendorf tube and 2/3 volume of isopropanol was added before centrifuging for 10 minutes at 13,000rpm. The supernatant was discarded and 70% ethanol was added to wash the pellet and then centrifuged at 13,000rpm for 5 minutes. The ethanol was removed and the pellet was air-dried for 15 minutes before being re-suspended in 50  $\mu$ l TE, pH8.6. The DNA sample was checked using gel electrophoresis and the sample stored at -20°C.

#### 6.1.2 RNA extraction

RNA was extracted from one to two seedlings ground in liquid nitrogen and extracted using the RNeasy® Plant Mini Kit (Qiagen, 74904) using the manufacturer's instructions with on column DNase digestion (Qiagen). RNA was eluted with 50  $\mu$ l RNase free water, and then eluted a second time with 30 $\mu$ l RNase free water to give a final RNA volume of 80  $\mu$ l.

#### 6.1.3 cDNA synthesis

Reverse transcription was carried out using the Invitrogen Superscript III First strand synthesis system for RT-PCR (cat 18080-051) according to the manufacturer's instructions. The temperature cycles were carried out on a G-STORM® Thermocycler (GT40361).

A 10  $\mu$ l reaction containing 1 $\mu$ g RNA, 0.5  $\mu$ l b26 (#1222) primer, 1 $\mu$ l 10mM dNTPs, and DEPC-treated water was incubated at 65°C for 5 minutes then transferred to ice for 1 minute. Once this step was complete 2 $\mu$ l of 10x RT buffer, 4  $\mu$ l of 25mM MgCl<sub>2</sub>, 2  $\mu$ l of 0.1M DTT, 1  $\mu$ l of RNaseOUT (40U/  $\mu$ l) and 1  $\mu$ l of Superscript III RT (200 U/  $\mu$ l) were added to bring the reaction volume to 20  $\mu$ l. This reaction mix was incubated at 50°C for 50 minutes and the reaction as

then terminated by incubating at 85°C for 5 minutes. 1 µl of RNase H was added to the reaction and incubated at 37°C for 20 minutes. Once complete 200 µl water was added and the cDNA was stored at -20°C.

#### **6.1.4 PCR and colony PCR**

PCR reactions normally used the Qiagen Taq DNA Polymerase kit and generally contained 0.5 µl Taq DNA Polymerase, 2 µl 10x CoralLoad Buffer, 5mM primers, 1mM dNTPs, 1-2 µl DNA, plasmid or cDNA with a final volume of 20 µl. Colony PCR used the same reaction mix without the addition of DNA instead a small amount of colony was transferred to the PCR tube and mixed. PCR reactions were carried out using a G-STORM® Thermocycler (GT40361) and amplified products were analysed by 1% agarose gel electrophoresis.

The typical PCR program used was as follows; 98°C for 30 seconds, then 35 cycles of 98°C for 10 seconds, 58°C for 30 seconds and 72°C for 60 seconds. Followed by 72°C for 10 minutes, and held at 12°C. The annealing temperature and elongation time were altered according to primer melting point and length of target respectively.

#### **6.1.5 Sequencing reactions**

Sequencing reactions for low concentration plasmids were carried out using the BigDye® Terminator v3.1 Cycle sequencing kit (Life Technologies). The reaction mix contained 2 µl of BigDye® Buffer, 1 µl of BigDye® Reaction Mix, 1 µl of 5mM primer, 1-2 µl of plasmid with a final volume of 10 µl. The sequencing reaction was then amplified using the G-STORM® Thermocycler (GT40361) with the following program; 96°C for 60 seconds, then 35 cycles of 96°C for 10 seconds, 55°C for 10 seconds and 60°C for 4 minutes, followed by a hold step at 12°C. These reactions were then sent to Eurofins Genomics for sequencing. For higher concentration plasmids, 15 µl of 100mg/ µl plasmid and 2 µl of 5mM primer was sent to Eurofins Genomics for value read sequencing.

#### **6.1.6 Heat shock transformation of *E.coli***

For transformation Maximum Efficiency One Shot® OmniMAX™ 2 T1 Phage-Resistant Chemically competent *E.coli* (Invitrogen Life Technologies) or Library efficiency DH5α chemically competent *E.coli* (Invitrogen Life Technologies) were used. Competent cells were thawed on ice for 15 minutes and 1-5 µl of plasmid or DNA-ligation was added and mixed gently and incubated on ice for 5 minutes. The cells were then heat shocked at 42°C for 20 seconds, followed by a minute incubation on ice. 250 µl of SOC medium (Invitrogen Life

Technologies, 2% Tryptone, 0.5% Yeast Extract, 10mM NaCl, 2.5mM KCl, 10mM MgCl<sub>2</sub>, 10mM MgSO<sub>4</sub>, 20mM glucose) was then added and incubated at 37°C for 1 hour. Transformed cells were plated on selective LB (lysogeny broth) media and incubated at 37°C overnight.

### **6.1.7 Heat shock of inducible transgenic lines**

Seedlings and dissected tillers (kept with the cut base in water) were heat shocked at 38°C for 30 minutes. These were then left to grow at 25°C for 3 days before being dissected and imaged using confocal microscopy (SP5 II confocal) with standard settings for GFP, mCherry and brightfield imaging.

### **6.1.8 Electroporation transformation of *Agrobacterium tumefaciens***

AGL1 electro-competent cells were used for transformation. 20 µl of electro-competent cells were defrosted on ice for 15 minutes, then mixed with 100ng of plasmid and incubated on ice for 30 minutes. The cell-plasmid mixes were transferred to pre-chilled cuvettes and pulsed for 4.4-4.8ms using the BioRad GenePulser<sup>®</sup> II (125V, capacitance 25 µF, resistance 200Ω). 250 µl of SOC was added to the cuvette before transferring the cells to fresh 1.5ml Eppendorf tubes. The cells were incubated at 28°C for 1 hour before plating on selective media (LB with 25:50:20 rifampicin: carbenicillin: kanamycin) and incubating at 28°C for 48 hours.

### **6.1.9 Plasmid extraction from bacterial cultures**

Plasmids were extracted from 6ml of overnight selective media liquid cultures using the QIAprep<sup>®</sup> Spin Miniprep kit (Qiagen, 27104) according to the manufacturer's instructions. Plasmid DNA was eluted in 50 µl of 80°C elution buffer twice to produce a total volume of 50 µl. The concentration of plasmid was assessed using Thermo Scientific NanoDrop 1000 spectrophotometer according to the manufacturer's guidelines.

### **6.1.10 PCR purification**

PCR reactions were purified using the QIAquick PCR Purification kit (Qiagen) according to the manufacturer's protocol, and were eluted in 30 µl of 80°C elution buffer twice to produce a total volume of 30 µl. Concentrations of purified PCR were checked using the Thermo Scientific NanoDrop 1000 spectrophotometer according to the manufacturer's guidelines.

### **6.1.11 Restriction digest**

Restriction digests were carried out to check the sequence of large plasmid constructs (in addition to sequencing checks). First appropriate enzymes were identified using Vector NTI Advance™ 11.0 © Invitrogen and virtual gels were generated. The digest reaction mix typically contained 1µl of each restriction enzyme, 2µl of compatible buffer, 3µl of plasmid and H<sub>2</sub>O to a total volume of 20µl. The reaction was incubated at 37°C for 1 hour and the results analysed using agarose gel electrophoresis.

### **6.1.12 Propidium iodide staining**

Maize and *Brachypodium* vegetative meristem samples were stained with propidium iodide for prototype OPT imaging.

The protocol used was as published by Truernit et al 2008 [119] with the following modifications. Samples were fixed in 100% ethanol for at least overnight, the samples were then rehydrated to 80% ethanol and boiled at 80°C in a waterbath for 12 minutes. Rehydration was completed (60%, 40%, 20% ethanol, 2x H<sub>2</sub>O) and the samples were incubated for at least 12 hours with alpha-amylase solution (20mM Sodium phosphate buffer, (pH7), 2mM NaCl, 0.25mM CaCl<sub>2</sub>, 0.3mg/ml alpha-amylase from *Bacillus licheniformis* (Sigma Aldrich A4551)) at 37°C. The samples were then washed (3x H<sub>2</sub>O) and incubated with 1% periodic acid (Sigma Aldrich, 3951) for 1 hour in the fumehood. Once completed the samples were washed (3x H<sub>2</sub>O) and incubated in Schiff Reagent (PI) (100mM sodium metabisulphite and 0.15M HCl; propidium iodide to a final concentration of 100 mg/mL was freshly added) for 2 hours and then washed (3 x H<sub>2</sub>O).

### **6.1.13 Maize seed sterilisation**

B73 maize seeds from Sarah Hake (UC Berkeley) were sterilised using the following protocol.

Seeds were washed for three minutes in 70% Ethanol, then wash three times in sterile water, and transferred to in 6% parazone bleach with one drop of SDS for 10 minutes with shaking. The bleach was removed by washing 10 times in sterile water.

Once the bleach had been completely removed the seeds were plated on damp sterile filter paper, under sterile conditions, in a flow hood and sealed with micropore tape.

#### **6.1.14 Optical projection tomography**

The protocol used for OPT imaging [110] was as is used in Lee et al 2006 [109] and is as follows.

##### ***6.1.14.1 Sample preparation***

Samples for OPT imaging were fixed for at least overnight in 100% ethanol. They were then gradually rehydrated through an ethanol series (90%, 80%, 70%, 60%, 50%, 20%) to sterile water. They were then mounted in aqueous 1% low melting point agarose (UltraPure™ LMP Agarose, Invitrogen) and left to set at 4°C. Once set, the samples were mounted on metal cylinder mounts using superglue (Loctite) and cut to a prism. Once the glue had set the samples were stored in 100% methanol in the dark for at least overnight. 24 hours before imaging the mounted samples were transferred to benzyl alcohol benzyl benzoate (BABB) (2:1 benzyl benzoate: benzyl alcohol) to clear the tissue.

##### ***6.1.14.2 Sample preparation for PI stained samples***

The preparation of PI stained samples was as for unstained samples however the PI staining occurred after the rehydration step, before the mounting in LMP agarose. Immediately after the PI staining was complete the samples were mounted in LMP agarose and kept in the dark once transferred to methanol.

##### ***6.1.14.3 Imaging***

Prepared samples were imaged either on the Prototype OPT scanner [109] (up to 1cm sample), the Commercial Scanner Bioptonic 3001 (SkyScan) (up to 1.5cm samples) or the prototype Macro OPT scanner (up to 4cm samples) in BABB depending on sample size. All samples collected were imaged 400 times on an x/y rotation. Depending on which scanner was used, different lights and filters were used to collect the image data. On the prototype scanner white light through the gfp1 filter, UV light through the TXR filter, and UV light through the gfp1 filter were used. On the commercial scanner white light through an infrared filter, and UV light through a GFP1, GFP+ or Cy3 filter were used. On the Macro scanner white light through a GFP filter, or UV light through a GFP or TXR filter were used.

##### ***6.1.14.4 Image reconstruction***

Images collected using the prototype scanner first needed to be converted to tif files using a python code. Images from the commercial and the Macro scanners could be processed in

their original form. Images from each collection channel were first aligned using NRecon software (NRecon Version 1.6.3.3 © SkyScan, 2010) and saved as tif sequences. Once aligned each channel image sequence was separately edited in the freely available Volviewer software (<http://cmpdartsvr3.cmp.uea.ac.uk/wiki/BanghamLab/index.php/VolViewer#Description>) and converted to png image sequence files. Once all channels were edited and converted they were combined using Volviewer. These combined 3D images were then explored and imaged using the Volviewer. Alternatively images were viewed after reconstruction in NRecon using the freely available Drishti v2.5.1 software (developed by Ajay Limaye <https://github.com/AjayLimaye/drishti>).

## **6.2 Plant Growth Conditions**

### **6.2.1 Timecourse samples**

#### **6.2.1.1 Barley**

(Grown either June/ August 2014 or September/ October 2013) Wild-type (WT) and *Hooded* Bowman Barley seeds (BW341) were plated on damp filter paper and then transferred to 4°C for 48 hours of stratification, the plates were then transferred to room temperature to germinate. 5 days after coleoptile emergence seedlings were planted out in 15 well trays in John Innes Cereal Mix (1 seedling per well) and grown in the greenhouse. Barley inflorescence samples were taken from 17 days after germination.

#### **6.2.1.2 Brachypodium**

Seeds of BD21-3 (WT) were dissected out of the lemma and palea and plated on damp filter paper, then left for 5 days at 25°C to germinate. Seedlings were then transferred to 15 well trays in John Innes Cereal Mix (1 seedling per well) and grown at 25°C in long day conditions (18 hours light, 6 hours dark, in a Sanyo growth cabinet (SANYO Versatile Environmental Test Chamber)). Vegetative meristem samples, targeting leaf 6 development were taken from when leaf 4 emerged.

#### **6.2.1.3 Maize**

Maize (B73) seeds were sterilised, and then plated under sterile conditions on damp filter paper. Seeds were left to germinate at 25°C in the dark for 4 days, and then transferred to

long day light conditions (25°C, 18 hours light, 6 hours dark, in a Sanyo growth cabinet (SANYO Versatile Environmental Test Chamber)) to continue to grow. Samples of maize vegetative meristems, targeting leaf 6 development were taken from 7 days after germination.

## **6.2.2 *In situ* hybridisation and immunolocalisation samples**

### **6.2.2.1 *Barley***

Seeds were germinated and seedlings grown as for the timecourse samples (see above) throughout the year, with the modification of cutting the main stem after 3 weeks of growth to encourage tillering. Inflorescences were harvested at varying stages of development.

### **6.2.2.2 *Maize***

Seeds were germinated and seedlings grown as for the time course samples (see 6.2.1.3).

## **6.2.3 Transgenic barley**

T0 plants were grown in CER (controlled environment room, Gallen Kamp) conditions with 75% humidity, 16hours light at 15°C, 8 hours dark at 12°C. T1 seeds were grown as for the barley samples for the timecourse (see above).

## **6.3 Generating transgenic barley lines:**

### **6.3.1 Goldengate cloning**

I used the modular cloning technique Goldengate cloning [175] to rapidly make the plasmid constructs for the barley transformations.

#### **6.3.1.1 *Level 0 module synthesis***

The full constructs were designed using Vector NTI Advance™ 11.0 © Invitrogen, I then used the plasmid maps to identify the component level 0 (L0) modules required and the appropriate adaptor sequences needed. The existing database of L0 constructs available through ENSA (Engineering Nitrogen Symbiosis for Africa) at JIC (John Innes Centre) was searched for relevant L0 constructs and the sequences of the L0 modules that were not available were sent for synthesis with Invitrogen.

### **6.3.1.2 Level 1 module cloning**

Using the synthesised L0 module plasmids, the level 1 constructs, broadly described as transcriptional units (including a combination of promoter, coding sequences, tag and terminator) were cloned using the following method. For most L1 constructs, 100ng of L1 vector backbone was combined with 100ng of each assembly piece, 1.5 µl of 10 x NEB (New England Biolabs) T4 Buffer, 1.5 µl of 10x BSA (NEB), 1 µl of BsaI enzyme(NEB), 1 µl of NEB T4 ligase and H<sub>2</sub>O to a total volume of 15µl. For L1 constructs containing a *lox* component, the 1 µl of BsaI was replaced with a mixture of 0.5 µl of BsaI and 0.5 µl of Esp3I (NEB, also called ESp3I). The reaction was then incubated in a G-STORM<sup>®</sup> Thermocycler (GT40361) with the following program: 3 minutes at 37°C and 4 minutes at 16°C for 40 cycles followed by 1 cycle of 5 minutes at 50°C and 5 minutes at 80°C. Once completed the ligation was transformed into library efficiency DH5α *E.coli* using heat shock and plated on selective media (100µg/ml IPTG, 40µg/ml X-gal, 100µg/ml ampicillin) to grow at 37°C. Colony PCR was used to check for successful transformants. Plasmids were extracted using a miniprep kit and the plasmid was sequenced to check the identity.

### **6.3.1.3 Level 2 module cloning**

The L1 transcriptional units were then built into the final construct for transformation into barley. For most L2 constructs the following protocol was used. 100ng of L2 vector backbone and 100ng of each assembly piece combined with 1.5 µl of 10 x NEB T4 Buffer, 1.5 µl of 10x BSA (NEB), 1 µl of BpiI enzyme(NEB), 1 µl of NEB T4 ligase and H<sub>2</sub>O to a total volume of 15µl. When an L2 vector with position one already filled (e.g. EC15027) was used a mixture of 0.5 µl of BsaI and 0.5 µl of BpiI was used. The reaction was then incubated in a G-STORM<sup>®</sup> Thermocycler (GT40361) with the following program: 3 minutes at 37°C and 4 minutes at 16°C for 40 cycles followed by 1 cycle of 5 minutes at 50°C and 5 minutes at 80°C. Once completed the ligation was transformed into library efficiency DH5α *E.coli* using heat shock and plated on selective media (50µg/ml kanamycin) to grow at 37°C. Colony PCR was used to check for successful transformants. Plasmids were extracted using a miniprep kit and the plasmid was sequenced to check the identity.

### **6.3.1.4 Modification of CRE level 0 module**

To correct problems with the activation of the heat shock promoter and subsequent expression of the *CRE* in *E.coli* when stacked on the same plasmid I introduced an intron into the *CRE* sequence at 254bp, based on studies in mammalian systems [179].

To select which intron to use I first used Vector NTI Advance™ 11.0 © Invitrogen to make virtual plasmids containing the available introns at a CAGG site (plant introns start sites are MAG.G, where “M” is an A or a C and “.” symbolises the cut site) 254bp into the *CRE* sequence. I then compared the GC content of the available introns using freely available software GC-Profile (<http://tubic.tju.edu.cn/GC-Profile/>) to check that they had a very strong difference between GC and AT content from the sequence to the intron (i.e. that the intron was very AT rich compared to the sequence). I then used Vector NTI to virtually translate the full sequence to check for frame shifts and to look for stop codons within the intron which would ensure that the *CRE* sequence would not be expressed in *E.coli*. I chose to use the U5-intron from the pICSL80006 plasmid from TSL SynBio (<http://synbio.tsl.ac.uk/>) as it did not introduce a frameshift, it had many stop codons, and the GC/ AT difference was very strong.

Primers were designed to amplify the *CRE* in two fragments and to amplify the U5 intron. All sets of primers were designed with custom overhangs that would allow them to be cut by the *Bpil* restriction enzyme and then religate in the correct orientation in the vector backbone pICH41308. These primers followed the general template of: NGAAGACNN + 4bp overhang + 18-30bp of the target sequence. The primers were synthesised by Sigma Aldrich.

The fragments were amplified using PCR, checked by 1% agarose gel electrophoresis and purified using the Qiagen PCR purification kit. The fragments were then digested and ligated in a Goldengate reaction using the following components; 1µl of pICH41308 vector, 2µl of each PCR fragment, 1.5 µl of 10x BSA, 1 µl of T4 ligase buffer, 1 µl of *Bpil* enzyme, 1 µl of T4 DNA ligase, 3µl of water. This reaction was then run on G-STORM® Thermocycler (GT40361) with the following program: 3 minutes at 37°C and 4 minutes at 16°C for 40 cycles followed by 1 cycle of 5 minutes at 50°C and 5 minutes at 80°C. Once completed the ligation was transformed into library efficiency DH5α *E.coli* using heat shock and plated on selective media (50µg/ml spectinomycin) and grown at 37°C. Colony PCR was used to check for successful transformants. Plasmids were extracted using a miniprep kit and the plasmid was sequenced to check the identity.

### **6.3.2 Barley transformation, crossing and screening**

*Agrobacterium* transformed with the Goldengate L2 plasmids were sent to BRAC (Biotechnology Resources for Arable Crop Transformation, <http://www.bract.org/>) for transformation into the barley subcultivar Golden Promise using callus culture. Leaf tissue

was harvested from selected T0 plants for copy number analysis by iDNA Genetics (<http://www.idnagenetics.com/>). Self-seed was harvested from the T0 plants and sown in batches for expression analysis. Expression was assessed by first looking at fluorescence in the leaf tissue using confocal microscopy using the Zeiss EXCITER Laser Confocal Microscope and then the early flower stages. If suitably expressing lines were not found in the first batch for which the copy number had been assessed, leaf samples from T1 seedlings were sent for copy number analysis and the expression screened in these plants.

Selected T1 lines were then crossed with both WT and HD Bowman barley.

#### **6.4 Tissue fixation and preparation for *in situ* hybridisation and immunolocalisations on sliced tissue**

Samples of barley inflorescences and maize vegetative meristems were collected in glass vials on ice in either 4 % Paraformaldehyde (PBS pH7, Water and 16% Paraformaldehyde solution (Electron Microscopy Sciences)) with 4% DMSO and 0.1% Triton X or FAA (100% ethanol, acetic acid, water, 37% Formaldehyde solution (Sigma Aldrich, F8775)) with 1% DMSO and 0.5% Triton X, for use in *in situ* hybridisation or immunolocalisation respectively. Samples were then placed under vacuum pressure for three rounds of 10 minutes, until the samples dropped to the bottom of the collection tubes. They were then transferred to 4°C to fix further overnight.

The paraformaldehyde was removed and the samples washed in cold 0.85% saline for 30mins at 4°C. The saline was then replaced with cold 50% ethanol/ 0.85% saline for 3 hours at 4°C, and this was then replaced with 70% ethanol/ 0.85% saline for a further 3 hours. The solution was refreshed with 70% ethanol/ 0.85% saline and stored at 4°C.

The FAA was removed and replaced with cold 50% ethanol and left for 3 hours at 4°C. This solution was replaced with cold 70% ethanol and left for another 3 hours at 4°C. The solution was refreshed with cold 70% Ethanol and stored at 4°C.

Once enough samples have been collected and fixed, all samples were transferred to labelled Tissue-Tek® mesh biopsy cassettes (Sakura) in 70% ethanol. These were then loaded into the Tissue-Tek® TEC VIP vacuum wax infiltrator (Sakura) with the following program:

Step	Solution	Percentage (%)	Time (hours)	Temperature (°C)	P/V	Agitation
1	EtOH	70	4	35	On	On
2	EtOH	80	4	35	On	On
3	EtOH	90	4	35	On	On
4	EtOH	100	4	35	On	On
5	EtOH	100	4	35	On	On
6	EtOH	100	4	35	On	On
7	Xylene	100	4	35	On	On
8	Xylene	100	4	35	On	On
9	Xylene	100	4	35	On	On
10	Paraffin wax	100	4	60	On	On
11	Paraffin wax	100	4	60	On	On
12	Paraffin wax	100	4	60	On	On
13	Paraffin wax	100	4	60	On	On

Table 6.1 VIP machine program for paraffin embedded samples

Once the program was complete, the samples were transferred to hot paraffin in the Tissue-Tek® TEC (Sakura) embedding machine and embedded in paraffin within 5 days. Once the paraffin blocks had set they were removed from the moulds and stored at 4°C.

Blocks were selected and sliced in 8µm thick ribbons using the Reichert-Jung 2030 microtome. The tissue slices were then mounted on Polysine™ microscope slides (VWR, 631-0107) with water, the water was not removed, instead the slides were left to dry on a 37°C hotplate for 2 days to ensure that the slices are flat and dry. Dry slides were stored at 4°C.

## 6.5 *In situ* hybridisation

### 6.5.1 Probe design

I used phylogenetic analysis to first identify the appropriate target genes in the published *Hordeum vulgare*, subcultivar Bowman, genome [149]. Protein sequences were identified using local BLAST of published genomes sequences from *Arabidopsis*. A range of dicot and monocot published genomes were searched to make the tree more robust.

Once identified the sequences were converted into a FASTA format and aligned using MUSCLE (EMBLI-EBI). The aligned sequences were then used to generate a phylogenetic tree using MEGA 6 [202] which could be used to identify the correct target sequences in barley.

Once the target gene sequence was identified, we designed primers to amplify unique approximately 500bp fragments of the gene in varying positions. Each primer was tested for off targets by blasting the primer sequences against the genomes, only primers that had a top hits for the gene of interest were chosen. The uniqueness of each fragment was assessed by running blast searches of the sequence against the published barley genome to check for off target matches.

### **6.5.2 Probe preparation**

Primers were used to amplify the 500bp fragments from purified Bowman barley cDNA using PCR. This PCR reaction was then used to clone the fragment into the pCR<sup>®</sup>4-TOPO<sup>®</sup> vector using the Invitrogen Life Technologies TOPO<sup>®</sup>TA Cloning<sup>®</sup> kit according to the manufacturers guidelines. The resulting ligation product was transformed into Maximum Efficiency One Shot<sup>®</sup> OmniMAX<sup>™</sup> 2 T1 Phage-Resistant Chemically competent *E.coli* (Invitrogen Life Technologies) using heat shock and the cells were plated on selective media (50µg/ml kanamycin). Colonies were checked using colony PCR and the identity of extracted plasmids were checked using sequencing.

RNA probes were then made using the protocol published in Coen et al 1990 [147] with the following modifications. Instead of plasmid linearization, PCR was used to first amplify the T7 or T3 transcription start site and the probe coding sequence, the PCR product was then purified first using a QIAGEN PCR purification kit, then using phenol-chloroform extraction. Approximately 1µg of purified PCR was then used to make the digoxigenin-UTP labelled RNA using T7 or T3 RNA polymerase.

### **6.5.3 *In situ* hybridisation protocol**

The protocol was as published in Coen et al 1990 [147] with the following modifications. 80µl of hybridisation buffer plus 2-4µl of RNA probe were used per slide (depending on probe strength), slides were covered with HybriSlip<sup>™</sup> Hybridization Covers (Grace Bio-Labs). Slides were washed with 0.2% SSC at 50°C before washing in NTE (0.5M NaCl, 10mM Tris-HCl pH7.5, 1mM EDTA) at 37°C and the RNase treatment. These were then washed in NTE buffer and then Buffer 1 (100mM of Tris-HCL, 150mM of NaCl) at room temperature before incubating

with blocking reagent (Roche) for 1 hour. Anti-digoxigenin-AP (Roche) were used at 1:3000 dilution in 1% BSA, 0.3% Triton-X, Buffer1 and incubated for one and half hours. Subsequent washes were with Buffer 1 with and without 0.3% Triton-X. Localisation of the anti-digoxigenin was then visualised incubating with 0.15mg/ml NBT (Nitro blue tetrazolium, Promega) and 0.075mg/ml BCIP (5-bromo-4-chloro-3-indolyl-phosphate, Promega) in 100mM Tris-HCl pH9.5, 100mM NaCl, 50mM MgCl<sub>2</sub> at room temperature overnight.

#### **6.5.4 Imaging**

Stained *in situ* slides were imaged in water on the Leica DFC495 Stereomicroscope under bright field light conditions and on the Leica DM600 microscope under DIC light. Imaged slides were then dried and mounted with VectaMount™ AQ (Aqueous mounting medium, H-5501) Vector Laboratories and stored at room temperature in the dark.

## **6.6 Immunolocalisation**

### **6.6.1 Antibody information**

Three different primary antibodies were used in immunolocalisation of SoPIN1, PIN1a and BKn3. The SoPIN1 primary antibody was provided by Devin O'Connor (The Sainsbury Laboratory, Cambridge University) and was raised in guinea-pig against 188-407 purified residues of the maize SoPIN1 protein tagged with 6-His and purified on a GST column bound to the GST tagged protein of the same residues. The primary antibody made for HvPIN1a, was made by Cambridge Research Biochemicals in rabbit and targeted the sequence "TGATPRPSNYEEDAPKP" (281-297amino acids) in the protein sequence. The primary antibody used to detect the localisation of Bkn3 protein was provided by Sarah Hake (UC Berkley) and was raised in rabbit against the whole KNOTTED 1 protein (KN1) and purified against the full length protein, and was previously shown to detect multiple members of the KNOX 1 protein family [211] .

The KNOX antibody was detected using biotinylated horse anti-rabbit antibodies (Vectastain Elite ABC kit). Standard anti-guinea-pig Alexa 488, anti-rabbit-Alexa 488, and anti-rabbit-HRP conjugated secondary antibodies from Life Technologies.

## **6.6.2 Immunolocalisation protocol for sliced tissue**

The protocol used was as published by Conti and Bradley 2007 [150] with the following modifications.

All tissue was fixed in formaldehyde acetic acid solution (FAA) and embedded in paraffin wax. All blocking solutions contained 3% BSA (Bovine Serum Albumen, Sigma Aldrich) instead of 5% milk. Blocking was carried out for 3 hours not overnight in 3% BSA in PBS with 0.3% Triton X. All antibodies were used at 1:200 dilution in 3% BSA in PBS and the primary was incubated overnight at 4°C, the secondary was incubated for 3 hours at room temperature. As the secondary antibodies used were fluorescently tagged the final BCIP/NBT staining steps used in the Conti et al protocol were not used. The slides were additionally stained with 0.1% calcofluor for 20 minutes.

### **6.6.2.1 Imaging**

Samples were mounted on dip slides with 1% DABCO and imaged on the Leica SP5 II confocal microscope. To visualise the calcofluor staining the 405nm laser with PMT detectors set to 400nm-480nm. To visualise the SoPIN1 localisation highlighted by AlexaFluor 488 the 488nm laser with PMT detectors set to 500nm-575nm. To image both calcofluor and alexa-488 at the same time we use sequential line scans.

## **6.6.3 Whole-mount immunolocalisation of barley**

### **6.6.3.1 Tissue preparation**

As for normal immunolocalisation, dissected barley spikes and meristems were fixed in FAA and stored at 4°C. 48 hours before immunolocalisation fixed samples were transferred to labelled Tissue-Tek® mesh biopsy cassettes (Sakura) in 70% ethanol. These were then loaded into the Tissue-Tek® TEC VIP vacuum wax infiltrator (Sakura) with the following program:

Step	Solution	Percentage (%)	Time (hours)	Temperature (°C)	P/V	Agitation
1	EtOH	70	4	35	On	On
2	EtOH	80	4	35	On	On
3	EtOH	90	4	35	On	On
4	EtOH	100	4	35	On	On
5	EtOH	100	4	35	On	On
6	EtOH	100	4	35	On	On
7	Xylene	100	4	35	On	On
8	Xylene	100	4	35	On	On
9	Xylene	100	4	35	On	On

Table 6.2 VIP program for non-wax embedded samples

### 6.6.3.2 Protocol

The same method as for normal immunolocalisation on sliced tissue was used with the following modifications.

Samples were taken straight from the completed VIP machine program and were washed in 100% ethanol and then passed through the ethanol rehydration series. Samples were treated with a solution of 2% Driselase and 1% Pectolyase Y-23 for 30 minutes at 37°C and washed in PBS before continuing with the citrate boiling steps. An additional permeabilisation step was also added with a 2 hour incubation in 1% Triton-X, 5% DMSO in PBS before blocking for 1 hour in 1% BSA with 0.3% Triton-X. 1 in 200 dilutions for all antibodies were used. Samples were stained in 0.1% calcofluor for 40 minutes.

For the whole-mount immunolocalisation of BKn3, the samples were incubated with H<sub>2</sub>O<sub>2</sub> for 1 hour to block the endogenous peroxidases before the first blocking step with BSA. The rabbit antibodies against KNOX were detected using horse anti-rabbit biotinylated antibodies with the ABC reagent kit. The localisation was then visualised using the DAB staining kit (Vector laboratories) with the nickel substrate to get black precipitate. The reaction was stopped as soon as specific nuclear signal was seen by transferring to PBS.

### 6.6.3.3 Imaging

Samples were mounted in water and imaged using the Leica SP5 II confocal microscope using standard alexa-488, calcofluor and brightfield settings.

## **6.7 EdU/ PI Staining of maize vegetative meristems**

### **6.7.1 Plant growth conditions**

B73 maize seeds were sterilised and germinated as for the timecourse samples (see above), they were dissected down to leaf three and removed from the seed and left to recover on growth media (MS media plus glucose ) plus 0.2% Plant Preservative Mixture (PPM<sup>TM</sup>, Plant Cell Technology).

### **6.7.2 Protocol**

The method was developed by Scheissl et al, 2012 [120] and combines high resolution cell wall imaging using propidium iodide staining [119] with the incorporation of the DNA nucleotide analog 5'-ethynyl-2'-deoxyuridine (EdU) [212, 213] into newly synthesised DNA to label cells passing through the S-phase of the cell cycle. For use with maize the method was modified to include PPM in the recovery growth media to repress fungal and bacterial growth (see above). Stained samples were dissected just before mounting in 1% DABCO (not Hoyer's medium) as this protected the delicate young leaf primordia from damage during the staining protocol and mounting DABCO allowed the samples to be imaged from multiple angles easily.

### **6.7.3 Imaging**

Samples were imaged in 1% DABCO using the Leica SP5 II confocal microscope using standard Alexa-488 and propidium iodide settings (PMT detector set to 620nm-675nm).

## **6.8 Computational modelling**

Specific details for the models are given in the relevant chapters. Outlined here are the general methods and parameters for the models. All models were developed using the GPT-framework [20], implemented in Matlab using the GFTbox toolbox, freely available at <http://cmpdartsvr3.cmp.uea.ac.uk/wiki/BanghamLab/index.php/Software> .

## 6.8.1 The canvas

### 6.8.1.1 Maize leaf models

All maize leaf models started with a cylindrical canvas with the base of the cylinder parallel to the xy axis and the vertical axis parallel to the z-axis. To approximate the ring primordium, the initial cylinder was wider than it was tall with the following dimensions; 0.1mm x 0.1mm x 0.03mm. The canvas started with 1250 finite elements with 25 around the circumference and 25 in height. The elements were not split during simulation.

The base of the cylindrical canvas was fixed for all models to approximate the effect of being attached to a stem. The keyhole region was also fixed during the simulations to simulate the effect of highly restricted growth in this region.

### 6.8.1.2 Wing development models

Wing development models were based on a square canvas, with 1000 finite elements, 0.1mm height and 0.1mm in width. The elements were not split during the simulations.

## 6.8.2 The factors

Factors were used to control growth and polarity in all models. Factors are distributed across the canvas and have values at each vertex of the finite elements, they can either have fixed values, known as identity factors ( $i_{\text{factorname}}$ ), or propagate through the canvas over time, known as signalling factors ( $s_{\text{factorname}}$ ). The concentration of factors across the canvas is assumed to not dilute over time for all models. Gradients of signalling factors can also be fixed at defined timepoints.

Factors can promote growth using the function *pro*:

$$\text{Pro}(k,X) = 1 + kX$$

They can also inhibit growth using the function *inh*:

$$\text{Inh}(k,X) = 1 / (1 + kX)$$

Where “X” is the factor concerned and “k” is the coefficient for promotion or inhibition of that factor.

### 6.8.3 Networks

There are three regulatory networks involved in the modelling framework and are set up at the start of each simulation.

A gene regulatory network (GRN) controls the activity of identity and signalling factors encoded by genes. Each factor has a production rate ( $P$ ), diffusion rate ( $D$ ) and decay rate ( $De$ ).

A polariser regulatory network (PRN) controls the activity of plus and minus organisers from which tissue polarity information propagates. In the models I use the convention that polarity (indicated by arrows) points away from plus organisers and towards minus organisers. Polarity is defined by the propagation of the diffusible factor POLARISER through the canvas from plus organisers to minus organisers. POLARISER can also have a background rate of production or degradation across the canvas.

A growth regulatory network (KRN) defines how the identity or signalling factors affect specified growth rates parallel ( $K_{par}$ ) and perpendicular ( $K_{per}$ ) to the local polarity field. The KRN can also specify the growth rate in thickness ( $K_{nor}$ ). The growth rates on each surface of the canvas (a and b) can also be specified independently.

These networks are interconnected and together determine the specified growth and polarity fields across the canvas. Specified growth differs from resultant growth as the connectedness of the canvas results in different emergent properties and shape deformations.

### 6.8.4 Simulation details

Every model starts with a set-up phase, followed by the initiation of growth. At every step of the simulation the following process is followed:

1. Calculate the specified values and distribution of factors.
2. Calculate the extent of diffusion of signalling factors.
3. Based on the factors, calculate the growth tensor field.
4. Calculate the resulting displacement of each finite element vertex based on the computed growth field.
5. Calculate the region of identity factor expression in the new volume after displacement.

The most complex models take 10 minutes to run on an INTEL<sup>R</sup> CORE<sup>TM</sup> i7-2600 desktop computer 250 steps each step represents approximately 0.4 hours in the maize model.

#### **6.8.4.1 Maize leaf models**

The start of each simulation corresponds to the P1 stage of maize leaf development with the size of the canvas scaled to the size of the leaf 6 P1. There is an initial phase to each model in which the factors and networks are established, after which growth begins at time 0.2. The simulations are run until the P4/P5 stage of maize leaf development before there is significant elongation of the sheath region and the primordia is approximately 1000 $\mu$ m long and 400 $\mu$ m wide.

#### **6.8.4.2 Wing development models**

The start of each simulation is approximate to a small lemma but does not fully represent the shape as these models were used as a thought experiment. There is an initial set up phase where the factors and networks are established, after which growth begins at time 0.2. The simulation is run for 60 steps in each case.

#### **6.8.5 Polarity parameters**

Where a polarity field was used to allow specified anisotropic growth the polarity field was first established in the initial set-up phase of the simulation. The parameters for POLARISER were a diffusion rate of 0.1 and a background degradation rate of 0.1. POLARISER was always produced at plus organisers with a value of 1 and degraded at minus organisers to a value of 0. The gradient of POLARISER generated was fixed using the following:

*m.morphogenclamp((( i<sub>PLUS</sub> ==1))/( i<sub>MINUS</sub>=1)), polariser\_i)=1*

This fixed the values of POLARISER to 1 at plus organisers (defined by  $i_{PLUS}$ ) and 0 at minus organisers (defined by  $i_{MINUS}$ ). This function was used to fix the gradient of all signalling factors.

#### **6.8.5.1 Maize leaf models**

In maize leaf models where the polarity field was switched during the simulation, the polarity field was reset by introducing a new minus organiser identity factor ( $i_{TIP}$ ) at the intersection between  $i_{MIDVEIN}$  and  $i_{MARGIN}$  which defined the midvein region and the top rim margin of the

canvas respectively. As before the value of POLARISER was fixed to be 1 at the plus organiser (defined by  $i_{PLUS}$ ) and fixed to be 0 at the new minus organiser (defined by  $i_{TIP}$ ).

### 6.8.5.2 Wing models

In models where the polarity field was altered at the margins, additional minus organisers were defined at the edges, determined by the identity factor  $i_{TIP}$ .

## 6.8.6 Growth parameters

### 6.8.6.1 Maize leaf models

The factors and growth parameters are outlined in table 1 and 2 for the two most advanced wild-type models, other models built up in complexity to this. Growth was specified in two separate phases during this model and was specified to be different on the two surfaces (A and B):

Distal Tip Model, Phase 1 (Ring to Hood phase from time step 0.12 to 0.51):

$$K_{Apar} = 1.75 * inh(10, S_{OPP}) * inh(0.8, i_{EDGE}) * pro(1.5, i_{MID}) * pro(2, S_{MID}) * (S_{OPP} < 0.8) * pro(0.8, S_{PROX});$$

$$K_{Bpar} = K_{Apar};$$

$$K_{Aper} = 0.15 + 1 * pro(5, i_{EDGE}) * inh(10, i_{OPP});$$

$$K_{Bper} = 1.1 * K_{Aper};$$

$$K_{nor} = 0.1;$$

Distal Tip Model, Phase 2 (Hood to cone phase from time step 0.51 onwards):

$$K_{Apar} = 2.5 * i_{BLADE} * inh(1, S_{OPP} > 0.8) * pro(0.4, S_{PROX}) + 0.2 * i_{INTERNODE};$$

$$K_{Bpar} = K_{Apar};$$

$$K_{Aper} = 0.5 + 0.8 * pro(1, S_{MAR}) * inh(2, S_{OPP}) * inh(1, i_{OPP}) * inh(0.5, (i_{MID} * (S_{PROX} < 0.5))) * S_{PROX} * i_{BLADE}$$

$$K_{Bper} = 1.8 * K_{Aper};$$

$$K_{nor} = 0.5 + pro(0.1, S_{MID});$$

Proximo-marginal Model, Phase 1 (Ring to Hood phase from time step 0.2 to 0.85):

$$K_{Apar} = 1.75 * inh(1, S_{OPP}) . * inh(100, i_{BASE}) . * pro(0.22, S_{MID}) . *(S_{OPP} < 0.8);$$

$$K_{Bpar} = 1.5 * K_{Apar};$$

$$K_{Aper} = 0.15;$$

$$K_{Bper} = K_{Aper};$$

$$K_{nor} = 0.1;$$

Proximo-marginal Model, Phase 2 (Hood to Cone Phase from time 0.85 onwards):

$$K_{Apar} = 2.5 * i_{BLADE} . * pro(0.5, S_{BASE}) . * inh(0.4, i_{MID}) . * inh(1, i_{BASE}) . * inh(1, S_{OPP} > 0.9) . * inh(0.45, S_{MID}) \\ + \quad intgro * 0.7 * i_{INTERNODE};$$

$$K_{Bpar} = K_{Apar};$$

$$K_{Aper} = 0.8 * K_{Bper};$$

$$K_{Bper} = 0.25 + (0.5 * (inh(1, S_{OPP} > 0.9)) . * (inh(0.5, (i_{MID} * S_{BASE} < 0.15)))) . * i_{BLADE} . * pro(2, S_{MAR}) + \\ (0.7 * i_{INTERNODE});$$

$$K_{nor} = 0.5 + pro(0.1, S_{MID});$$

Factors	Location	Description	Value
$i_{MID}$	Midvein	Midvein identity	1
$i_{OPP}$	Keyhole	Keyhole identity opposite the midvein	1
$i_{BASE}$	Proximal edge	Base “attached” to stem	1
$i_{MARGIN}$	Distal edge	Margin of the future leaf blade	1
$i_{TIP}$	Intersection of midvein and distal edge	Used for polarity switch at the Hood stage	1
$i_{MINUS}$	The intersection of $i_{MARGIN}$ and $i_{MID}$ in Model 1. The distal edge in Model 2.	Sink of POLARISER	1
$i_{PLUS}$	The proximal base	Source of POLARISER	1
$i_{BLADE}$	Upper region of the hood	Blade region	1
$i_{INTERNODE}$	Upper region of the internode	Internode region	1
$i_{EDGE}$	Only in model 1, gradient from the margin, promoted by $S_{MAR}$ , inhibited by $S_{MID}$ , $S_{OPP}$ .	Defines region of high $K_{per}$ at the margin	1-0
$S_{MID}$	Produced at midvein, degraded at keyhole	Used to promote growth at the midvein in the first phase and inhibit growth in the second phase	1-0
$S_{OPP}$	Produced at keyhole, degraded at keyhole	Used to inhibit growth in the first phase and promote it in the second	1-0
$S_{MAR}$	Produced at distal edge, degraded at base	Used to promote growth at the margin	1-0
$S_{PROX}$	Produced at proximal edge	Use to change growth pattern in the second phase	1-0
POLARISER	Produced at $i_{plus}$ , degraded at $i_{minus}$ (and at $i_{tip}$ in model 2)	Used to define the axiality	1-0

Table 6.3 Factors used in the maize leaf models

Parameter	Description	Value in Model 1	Value in Model 2
P <sub>MID</sub>	Production rate of S <sub>MID</sub>	1	1
D <sub>MID</sub>	Diffusion rate of S <sub>MID</sub>	0.02	0.02
De <sub>MID</sub>	Decay rate of S <sub>MID</sub>	0.1	0.1
P <sub>MAR</sub>	Production rate of S <sub>MAR</sub>	1	1
D <sub>MAR</sub>	Diffusion rate of S <sub>MAR</sub>	0.001	0.001
De <sub>MAR</sub>	Decay rate of S <sub>MAR</sub>	0.1	0.1
P <sub>OPP</sub>	Production rate of S <sub>OPP</sub>	1	1
D <sub>OPP</sub>	Diffusion rate of S <sub>OPP</sub>	0.005	0.005
De <sub>OPP</sub>	Decay rate of S <sub>OPP</sub>	0.1	0.1
P <sub>POLARISER</sub>	Production rate of POLARISER	1	1
D <sub>POLARISER</sub>	Diffusion rate of POLARISER	0.1	0.1
De <sub>POLARISER</sub>	Decay rate of POLARISER	0.1	0.1
P <sub>PROX</sub>	Production rate of S <sub>PROX</sub>	1	1
D <sub>PROX</sub>	Diffusion rate of S <sub>PROX</sub>	0.001	0.1
De <sub>PROX</sub>	Decay rate of S <sub>PROX</sub>	0.1	0.2

Table 6.4 Parameters for the diffusible factors in the maize leaf models

### 6.8.6.2 Wing models

The factors and growth parameters are outlined in table 1 and 2 for the two most advanced wing model, other models built up in complexity to this. Growth was specified in a single phase during this model.

$$K_{Apar} = 1.2 + pro(1, S_{PROMOTE});$$

$$K_{Bpar} = K_{Apar};$$

$$K_{Aper} = 0. + pro(1, S_{PROMOTE})1;$$

$$K_{Bper} = K_{Aper};$$

$$K_{nor} = 0;$$

Factors	Location	Description	Value
$i_{MID}$	Middle of the canvas	Used to define middle region to position the $i_{TIP}$	1
$i_{MINUS}$	Distal edge	Sink of POLARISER	1
$i_{PLUS}$	Proximal edge	Source of POLARISER	1
$i_{TIP}$	Intersection of midvein and distal edge	Used for polarity switch at the Hood stage	1
$S_{PROMOTE}$	Produced at $i_{TIP}$	Used to enhance growth at $i_{TIP}$	1-0
POLARISER	Produced at $i_{PLUS}$ , degraded at $i_{MINUS}$ and $i_{TIP}$ .	Used to define the axially	1-0

Table 6.5 Factors used in the wing models

Parameter	Description	Value
$P_{POLARISER}$	Production rate of $POLARISER$	1
$D_{POLARISER}$	Diffusion rate of $POLARISER$	0.001
$De_{POLARISER}$	Decay rate of $POLARISER$	0.01
$P_{PROMOTE}$	Production rate of $S_{MID}$	1
$D_{PROMOTE}$	Diffusion rate of $S_{MID}$	0.001
$De_{PROMOTE}$	Decay rate of $S_{MID}$	0.01

Table 6.6 Parameters for diffusible factors in the wing models

## 6.9 List of plasmids generated

Plasmid Name	Description	Use	Bacterial Resistance	Plant Resistance
EC71099-pLDM-R2-PHHSPT7-Cre-HSP	Synthesised to GoldenGate, 9 repeats of DRS enhancer element with 35S minimal promoter	GoldenGate Cloning	Spectinomycin	n/a
EC71100-pLDM-R2-PHHSPT7	L1. Barley Heat shock promoter 17 with CRE	GoldenGate Cloning	Ampicillin	n/a
EC71103-pLDM-C1-L-egFP-L	Synthesised to GoldenGate, Barley Heat Shock Promoter 17	GoldenGate Cloning	Spectinomycin	n/a
EC71108-pLDM-R2-HvpP1Aa-P1N1-egFP-P1N1	Synthesised to GoldenGate, egFP for internal tagging	GoldenGate Cloning	Spectinomycin	n/a
EC71109-pLDM-R2-HvpP1Aa-P1N1-egFP-P1N1	L1. Barley P1N1a gene internally tagged with egFP at the 218th amino acid, position 2	GoldenGate Cloning	Ampicillin	n/a
EC71110-pLDM-5-HvpP1N1	Synthesised to GoldenGate, Barley P1N1a promoter (PU module)	GoldenGate Cloning	Spectinomycin	n/a
EC71111-pLDM-C2-HvpP1N1	Synthesised to GoldenGate, Barley P1N1a N-terminal for internal tagging	GoldenGate Cloning	Spectinomycin	n/a
EC71112-pLDM-T-HvpP1N1	Synthesised to GoldenGate, Barley P1N1a C-terminal for internal tagging	GoldenGate Cloning	Spectinomycin	n/a
EC71113-pLDM-R2-HvpP12.5-egFP-P1P2.5-1	Synthesised to GoldenGate, Barley P1N1a Terminator	GoldenGate Cloning	Ampicillin	n/a
EC71117-pLDM-HMHSPT7-CREUS-UBQP-lox/CYFETRIlox-BK13-mCherry-PIN6GFP	L1. Barley p1p2.5 gene N terminally tagged with egFP	GoldenGate Cloning	Spectinomycin	n/a
EC71118-pLDM-HMHSPT7-CREUS-UBQP-lox/CYFETRIlox-BK13-mCherry-PIN6GFP	L2. HSP, Znubi promoter driven lox-CYFETRI targeted, BK13-mCherry with PIN-egFP	Transformation into Barley, clonal sectors of BK13	kanamycin	Hygromycin
EC71121-pLDM-HMHSPT7.5-egFP	L2. DRS-mCherry reporter with P1N1a-egFP	Transformation into Barley, auxin and PIN reporter	kanamycin	Hygromycin
EC71125-pLDM-5-C1-BK13	L2. egFP tagged p1p2.5	Transformation into Barley, cell membrane marker	kanamycin	Hygromycin
EC71126-pLDM-PU-HMHSPT7.5	Synthesised to GoldenGate, Barley BK13 gene	GoldenGate Cloning	Spectinomycin	n/a
EC71128-pLDM-R3-UBQP-LoxP-ER-Targ-CYFET-HDELoxP-BK13-mCherry-LAQ2	Synthesised to GoldenGate, Barley p1p2.5 aquaporin gene promoter	GoldenGate Cloning	Spectinomycin	n/a
EC71129-pLDM-R3-DRS-mCherry-35S	L1. Maize ubiquitin promoter, lox bounded ER targeted CyPET, BK13 Cterminally tagged with mCherry	GoldenGate Cloning	Ampicillin	n/a
EC71131-pLDM-C-HVPIP2	L1. DRS promoter enhancer with minimal 35S promoter and free mCherry	GoldenGate Cloning	Ampicillin	n/a
EC71132-T-HVPIP2	Synthesised to GoldenGate, Barley p1p2.5 aquaporin gene for N terminal tagging	GoldenGate Cloning	Spectinomycin	n/a
EC71133-pLDM-F-P2NUBI-Htron	Synthesised to GoldenGate, Barley p1p2.5 terminator	GoldenGate Cloning	Spectinomycin	n/a
EC71145-pLDM-R4-HvpP1Aa-P1N1-egFP-P1N1	L1. Barley P1N1a gene internally tagged with egFP at the 218th amino acid, position 4	GoldenGate Cloning	Ampicillin	n/a
EC71165-pLDM-UBQ-loxmCherryRIlox-egFP	L2. Ubiquitin driven mCherry, ER localised, lox bounded, with egFP	GoldenGate Cloning	kanamycin	Hygromycin
EC71167-pLDM-R3-UBQP-LoxP-mCherry-HDEL-135S-LoxP-egFP-LAQ2	L1. Maize Ubiquitin promoter driven lox site bounded ER targeted mCherry, with free egFP	Transformation into Barley, for crossing to HSP-CRE lines	kanamycin	Hygromycin
EC71171-pLDM-CRE-US-CRE	Modified to Cre-lox with US intron at 254bp	GoldenGate, modification to stop bacterial CRE expression	Ampicillin	n/a
EC71172-pLDM-HMHSPT7-CRE	L2. barley heat shock promoter 17 driving CRE	Transformation into Barley, for crossing	kanamycin	Hygromycin
EC71173-pLDM-R2-PHHSPT7-CRE-US-CRE-HSP	L1. Barley Heat shock promoter 17 driven CRE with the US intron at 254bp	GoldenGate Cloning	Ampicillin	n/a
EC71174-pLDM-HMHSPT7-CREUS-UBQP-loxmCherryER-egFP	L2. Heat shock driven CRE with US intron, ER targeted mCherry lox bounded with egFP	Transformation into Barley, egFP clonal sector line	kanamycin	Hygromycin
TOPO_PCR4-HVK13	Fragment of Barley BK13 gene (ATG-318bp-570p) cloned into the TOPO PCR4 vector	RNA in Situ Hybridisation Probe Cloning	kanamycin	n/a
TOPO_PCR4-HVK1X1	Fragment of Barley LHX1 gene (ATG-303bp-833bp) cloned into the TOPO PCR4 vector	RNA in Situ Hybridisation Probe Cloning	kanamycin	n/a
TOPO_PCR4-HVANM	Fragment of Barley NAM gene (ATG-397bp) cloned into the TOPO PCR4 vector	RNA in Situ Hybridisation Probe Cloning	kanamycin	n/a
TOPO_PCR4-HVPI1A	Fragment of Barley P1N1a gene (ATG-248bp) cloned into the TOPO PCR4 vector	RNA in Situ Hybridisation Probe Cloning	kanamycin	n/a
TOPO_PCR4-HVPI1B	Fragment of Barley P1N1b gene (-116bp-242bp) cloned into the TOPO PCR4 vector	RNA in Situ Hybridisation Probe Cloning	kanamycin	n/a
TOPO_PCR4-HVSOPI1	Fragment of Barley Sopi1 gene (ATG-165bp-578bp) cloned into the TOPO PCR4 vector	RNA in Situ Hybridisation Probe Cloning	kanamycin	n/a
TOPO_PCR4-HVUCCA1	Fragment of Barley VUCCA1 gene (ATG-478bp) cloned into the TOPO PCR4 vector	RNA in Situ Hybridisation Probe Cloning	kanamycin	n/a

Table 6.7 Plasmids made during the project



## 7 Appendices

### 7.1 Appendix A: Developing a whole-mount immunolocalisation protocol in barley

To explore protein localisation in 3D I developed a whole-mount immunolocalisation protocol for barley tissues (this protocol does not work for maize tissues yet). I started with the protocol for whole-mount immunolocalisation protocol for *Antirrhinum* petal tissue developed by Alexandra Rebocho and based upon the protocol outline in Conti and Bradley 2007 [150] (Alexandra Rebocho, JIC, unpublished). This protocol fixed tissue in FAA overnight then immediately transferred it to the ethanol rehydration series, rinsed in water, then boiled the tissue in 10mM sodium citrate solution for 20 minutes. Once cool the tissue was washed with water then blocked for 3 hours at room temperature in 3% BSA (bovine serum albumin) and 0.3% Triton-X in PBS. The tissue was then washed in PBS and incubated at 4°C with the primary antibody in 3% BSA (1:200 dilution) overnight. Once washed with PBS and 0.3% Triton, then PBS alone, the tissue was incubated with the secondary antibody in 3% BSA (alexa-488 conjugated, 1:200 dilution) for 3 hours at room temperature. The tissue was then washed in PBS, and stained with 0.1% calcofluor for 40 minutes. This protocol, designed for *Antirrhinum* petal tissue, did not produce any specific signal in barley tissue. This may have been due to problems with antigen retrieval, therefore I explored using different combinations of methods designed to aid antigen retrieval.

In the literature I identified several different methods of antigen retrieval. Sodium citrate boiling [150] (as used by the original protocol), Proteinase K digestion (1mg/ml solution in PBS, 37°C for 1 hour), Driselase digestion (2% Driselase in PBS, 37°C for 1 hour) [214] and a cocktail of Driselase and Pectolyase (2% Driselase, 1% Pectolyase Y-23 in PBS, 37°C for 1 hour) [215].

There were also different methods of pre-treatment for tissues. Methanol incubation (100% Methanol for 10 minutes at 37°C (x3), then 99% ethanol at room temperature for 10 minutes (x2)), xylol incubation (ethanol/ xylol mix (1:1) at 37°C for 10 minutes (x3), then 98% xylol at 37°C for 10 minutes (x3), then ethanol/xylol mix (1:1) at 37°C for 10 minutes (x2), then 99% ethanol at room temperature for 10 minutes (x2)) or both combined [214], or the VIP ethanol and xylene treatment under vacuum used for the preparation of tissue for the sliced immunolocalisations (see Table 6.1, without paraffin wax steps).

Different methods for permeabilisation steps also exist. The original protocol uses 0.3% Triton-X in the blocking buffer. A solution of 3% IGEPAL CA-630 with 10% DMSO in PBS incubated for 1 hour can also be used [214], or a mix of both, using 1% Triton-X plus 5% DMSO.

Using this information I carried out a series of tests using FAA fixed barley lemma tissue, designed to explore the efficiency of different combinations of pre-treatments, antigen retrieval and permeabilisation methods. (see Figure A1 for the different combinations and their results).

Test Number	Antigen Retrieval				Pre-Treatment			Permeabilisation	
	Sodium Citrate	Proteinase K	Driselase	Pectolyase	MeOH	Xylol	VIP	IGEPAL + DMSO	Triton-X + DMSO
1	Red	Grey	Grey	Grey	Grey	Grey	Grey	Grey	Grey
2	Grey	Red	Grey	Grey	Grey	Grey	Grey	Grey	Grey
3	Red	Red	Grey	Grey	Grey	Grey	Grey	Grey	Grey
4	Red	Grey	Grey	Grey	Red	Grey	Grey	Grey	Grey
5	Red	Grey	Grey	Grey	Red	Red	Grey	Grey	Grey
6	Grey	Grey	Red	Grey	Grey	Grey	Grey	Red	Grey
7	Grey	Grey	Red	Grey	Red	Red	Grey	Red	Grey
8	Red	Red	Grey	Grey	Red	Red	Grey	Grey	Grey
9	Grey	Red	Grey	Grey	Red	Red	Grey	Grey	Grey
10	Red	Red	Grey	Grey	Red	Grey	Grey	Grey	Grey
11	Red	Grey	Grey	Grey	Grey	Grey	Red	Grey	Grey
12	Red	Red	Grey	Grey	Grey	Grey	Red	Grey	Grey
13	Red	Grey	Grey	Grey	Red	Grey	Red	Grey	Grey
14	Red	Red	Grey	Grey	Red	Grey	Red	Grey	Grey
15	Grey	Grey	Red	Red	Grey	Grey	Grey	Grey	Red
16	Grey	Grey	Red	Red	Grey	Grey	Red	Grey	Red
17	Green	Grey	Green	Green	Grey	Grey	Grey	Grey	Green
18	Green	Grey	Green	Green	Grey	Grey	Green	Grey	Green

**Figure A1 Matrix of whole-mount immunolocalisation trial conditions**

The coloured squares represent the conditions used, grey represent conditions not used, in each test. Red represents a test which failed. Green represents a test which produced specific signal.

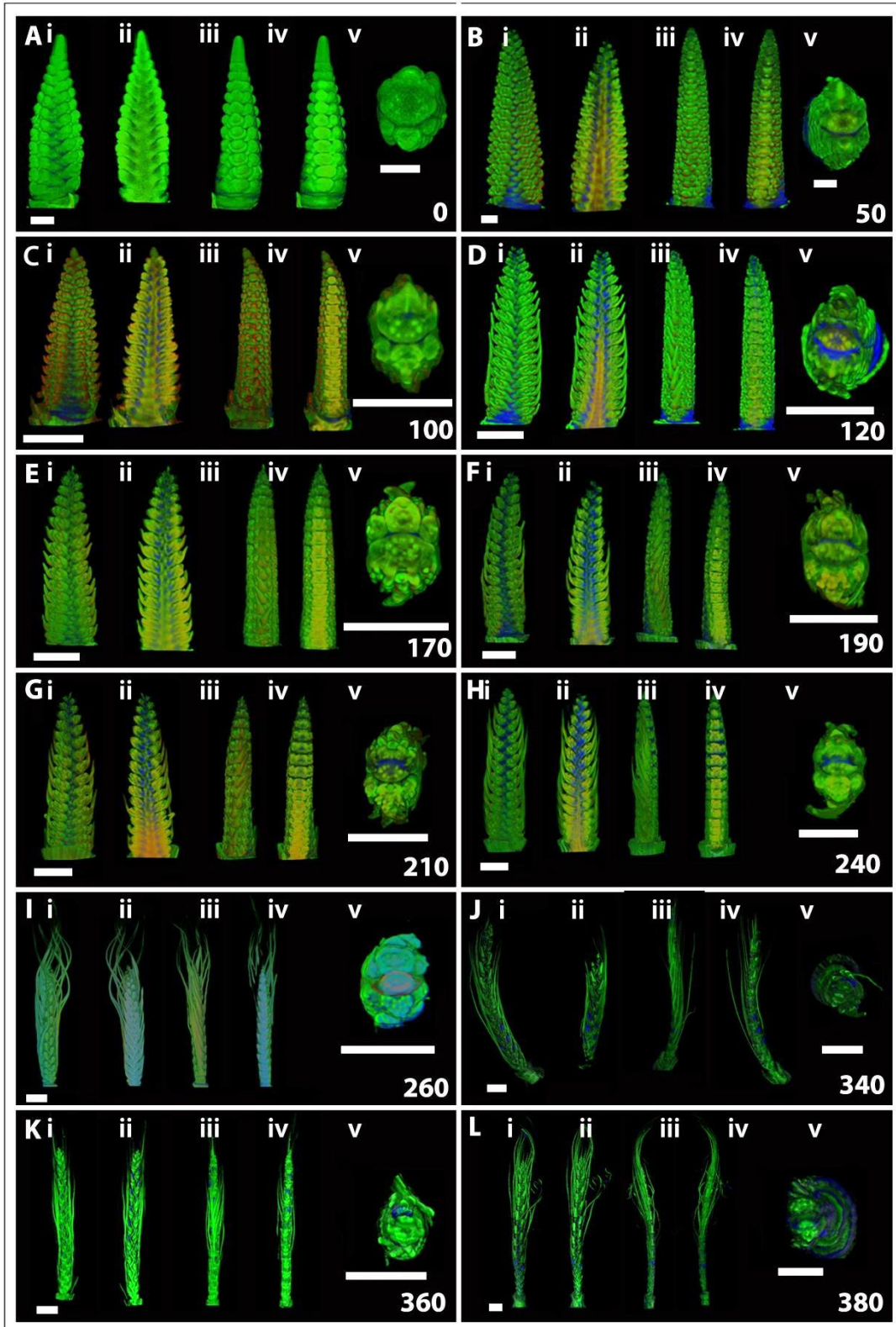
After carrying out these tests I found that the original protocol in which sodium citrate boiling was used for antigen retrieval, plus an additional antigen retrieval step of 2% Driselase, 1% Pectolyase Y-23 digestion at 37°C for 30 minutes (different tissues have differing sensitivities to the length of the digestion) combined with a 1 hour permeabilisation step at room temperature using 1% Triton-X and 5% DMSO in PBS, was able to produce specific signal in both barley lemma tissue and barley meristem and leaf primordia tissue. This could be with or without the pre-treatment in the VIP machine with cycles of xylene and ethanol treatment. The method including the VIP pre-treatment was used for all whole-mount immunolocalisations presented in this thesis.

## 7.2 Appendix B: Characterising barley morphology

As part of the barley developmental timecourse, I used OPT to characterise the morphology over time of the barley spike and flower in both the wild-type and *Hooded* backgrounds. The images in chapter 3 are a selection of the analysed images. Below are a more detailed set of images, illustrating both wild-type and *Hooded* morphology over time.

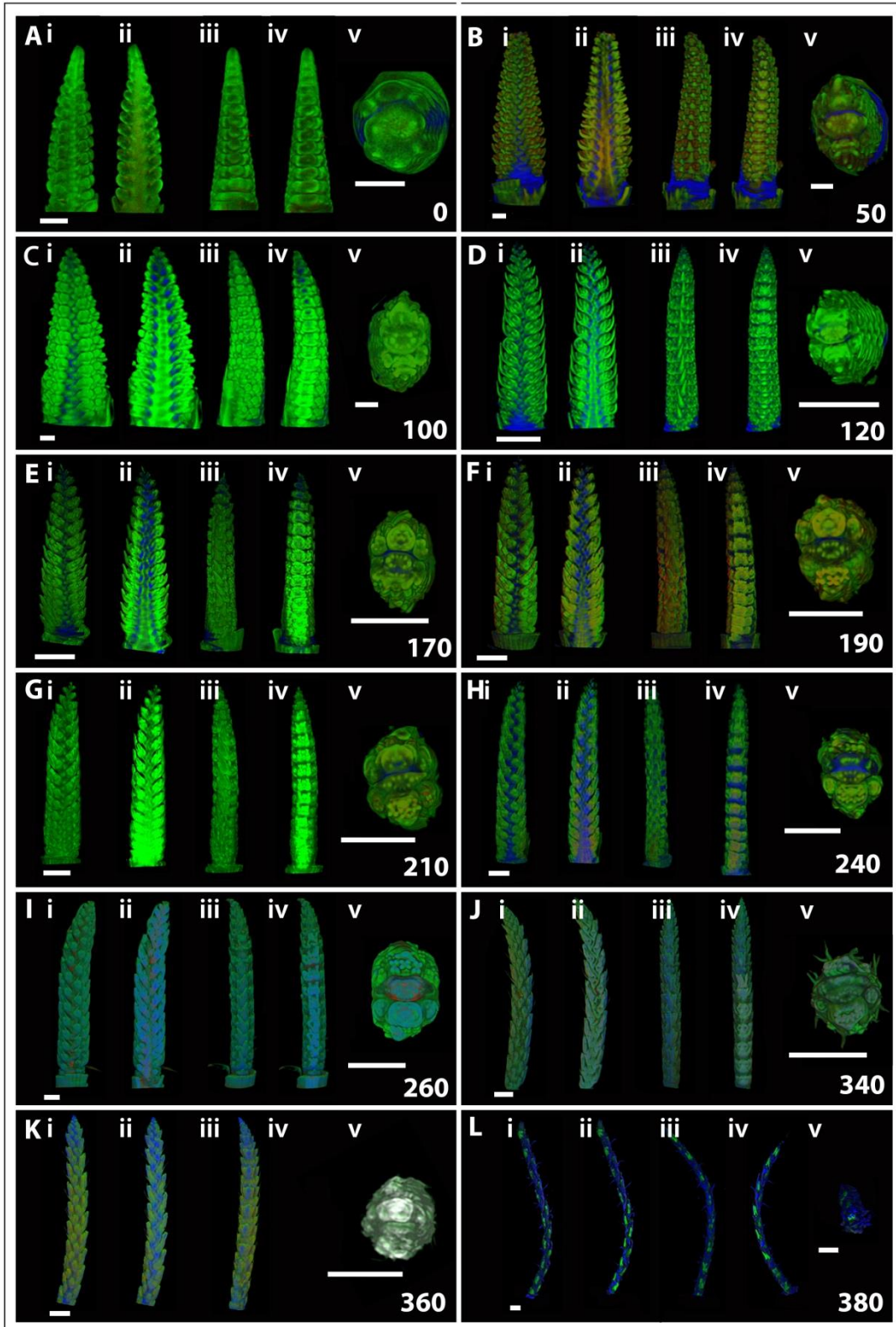
Figure B1 illustrates the development of a wild-type inflorescence spike over 380 hours of development. Starting when the lemma has been initiated as a small proximal outgrowth on floret 5 (Figure B1.A). Until lemma development is advanced, with the formation of the long distal awn which is longer than the inflorescence spike (Figure B1.L). Images of the whole spike from the front (i) and side (iii) views, longitudinal cross-sections through the 3D image illustrating the morphology of the spike and florets in the middle (i), through the base of the insertion point of the lemma into the floret base (iv), as well as transverse cross-sections through the spike at floret 5 (v) are shown. The whole spike views illustrate the change in gross morphology over time. The cross-sections illustrate the development of the lemma in relation to the rest of the floral organs. The transverse cross-sections illustrate the increase in spike width, the development of the central floret and the abortion of the lateral florets.

Figure B2 illustrates the development of the *Hooded* mutant spike over 380 hours of development. The timecourse covers the period in development from when the lemma is a small proximal outgrowth on floret 5, and until the ectopic floret on the lemma is fully formed. All of the images show the same regions as in Figure B1. Comparison between the two timecourses shows a distinct difference in morphology between wild-type and *Hooded* inflorescence development. This difference is due to the different development of the distal half of the lemma. In wild-type this develops into the awn, in *Hooded* this forms ectopic florets instead.



**Figure B1** The morphology of the wild-type barley spike over 380 hours of development. OPT images of wild-type 2 row Bowman barley during development. *i*: Full image of the front of the spike. *ii*: longitudinal cross-section through the middle of the inflorescence spike illustrating the shape of the spike and the developing lemmas. *iii*: full side view of the inflorescence spike, looking at the abaxial side of the developing lemmas. *iv*: longitudinal cross-section through the base of the developing flowers at the point of insertion of the

lemma into the flower base. *v*: transverse cross-section through the spike at floret 5. Scale bars are 200 $\mu$ m in *A-B*, 1mm in *C-I* and 2mm in *J-L*.



**Figure B2** The morphology of the *Hooded* barley spike over 380 hours of development  
 OPT images of *Hooded* 2 row Bowman barley during development. *i*: full image of the front of the spike. *ii*: longitudinal cross-section through the middles of the inflorescence spike illustrating the shape of the spike and the developing lemmas. *iii*: full side view of the inflorescence spike, looking at the abaxial side of the developing lemmas. *iv*: longitudinal cross-section through the base of the developing flowers at the point of insertion of the

lemma into the flower base. *v*: transverse cross-section through the spike at floret 5. Scale bars are 200 $\mu$ m in *A-B*, 1mm in *C-I* and 2mm in *J-L*.

The differences in lemma development (described in Chapter 3, Figure 3.4) are illustrated in more detail in Figure B3. The figure illustrates wild-type floret 5 and *Hooded* floret 5 at different timepoints over 380 hours of development. This timecourse covers from when the *Hooded* mutant lemma shares the same morphology as the wild-type (Figure B3 A-D, L-O), to the initiation of the ectopic floret on the *Hooded* lemma (170 hours, Figure B3 E), to the initiation of wing development on the *Hooded* lemma (240 hours, Figure B3 H) until the floral organs in the ectopic floret are fully developed. i and ii show whole floret morphology (ii is a longitudinal section through the middle of the floret) and iii and iv illustrate the morphology of the abaxial side of the lemma (iv shows a transverse section through the base of the lemma, there is no difference between wild-type and *Hooded* in the lower half of the lemma). The white dotted lines highlight the shape of the lemma. White arrowheads indicate the position of the ectopic flower, the wings are indicated by the red arrowheads.

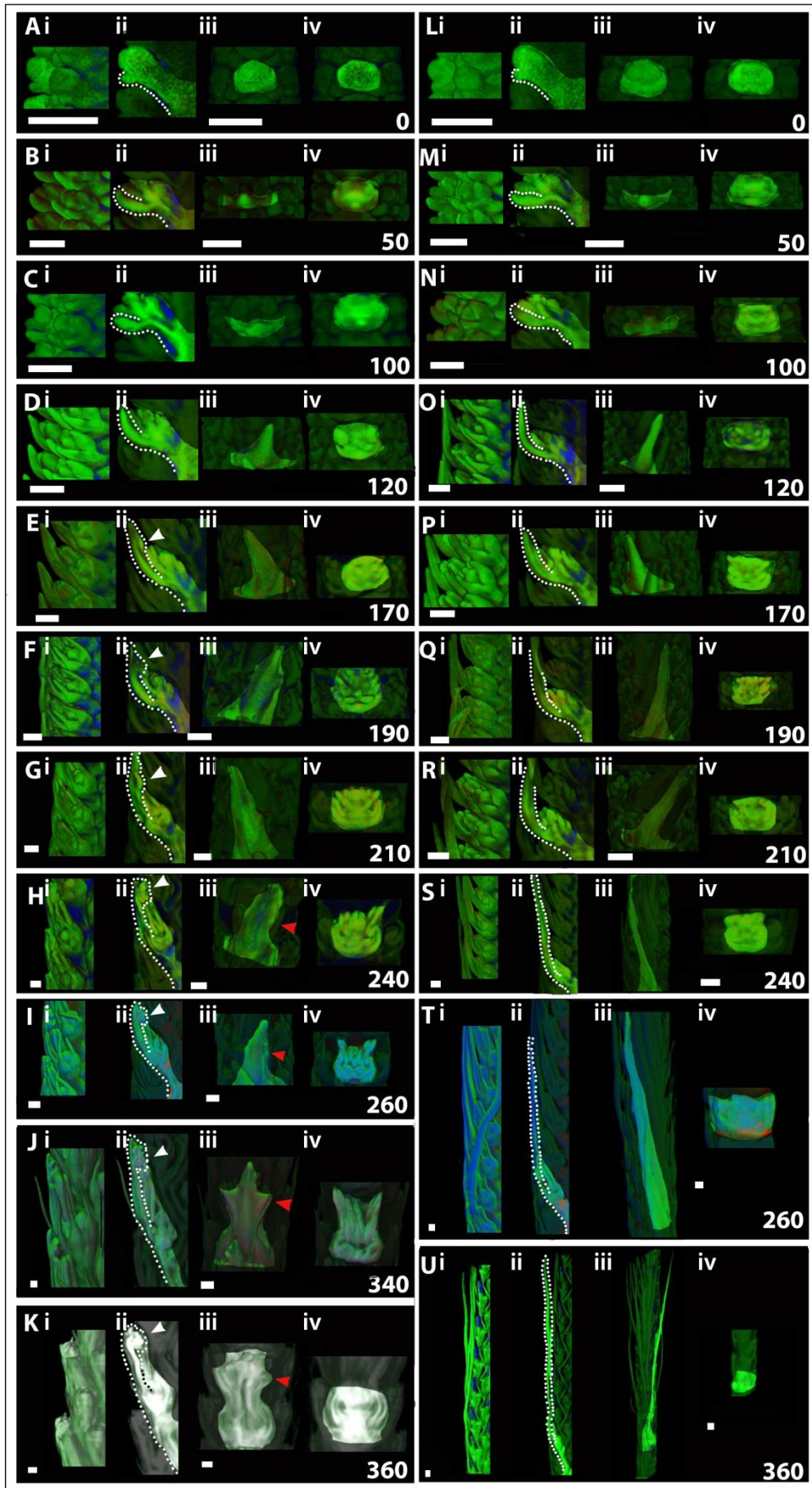


**Figure B3 The morphology of wild-type and Hooded floret 5 over 380 hours of development**

OPT

images of wild-type (*L-U*) and *Hooded* (*A-K*) Bowman barley, floret 5 during development. *i*: image of the front of the floret. *ii*: longitudinal cross-section through the middle of the floret illustrating the shape of the developing lemmas and the internal floral organs. *iii*: full side view of the floret, looking at the abaxial side of the developing lemmas. *iv*: longitudinal cross-section through the base of the developing floret at the point of insertion of the lemma into the flower base. White dotted lines highlight the shape of the floret, white arrowheads indicate the developing ectopic floret on the lemma, red arrowheads indicate the developing wings. Scale bars are 200µm.

The change in morphology over time in the adaxial surface of the lemma can be illustrated by confocal microscopy of calcofluor stained *Hooded* lemmas. (Figure B4) A selection of these images are described in detail in Chapter 3 Figure 3.6. Figure B4 illustrates the development of the ectopic flower and the wings below at a range of timepoints over 360 hours of development. From when the ectopic floral meristem is not visible (Figure B4.A) to when the floral organs have developed fully and the wings are distinct from the margin of the lemma (Figure B4.J). The white arrowheads indicate the position of the first ectopic flower and the red arrowheads indicate the position of the wings below.

SEM imaging of mature wild-type lemmas, show that hairs are only found on the adaxial surface (Figure B5.B). The abaxial surface does not have distinct hairs, but there are cells which form small distal bulges (Figure B5.B). The hairs on the adaxial surface are more dense in the upper region of the oval shaped lemma base (Figure B5.B.ii), and less dense towards the base of the lemma (Figure B5.iv) and the awn proper (Figure B5.B.i). The irrespective of position all of the hairs on the adaxial surface orient towards the distal tip of the awn (Figure B5.B, red arrows). This contrasts with the *Hooded* lemma which has distally oriented hairs in the base of the lemma, but just below the ectopic flower the hairs orient proximally (Chapter 3, Figure 3.26).

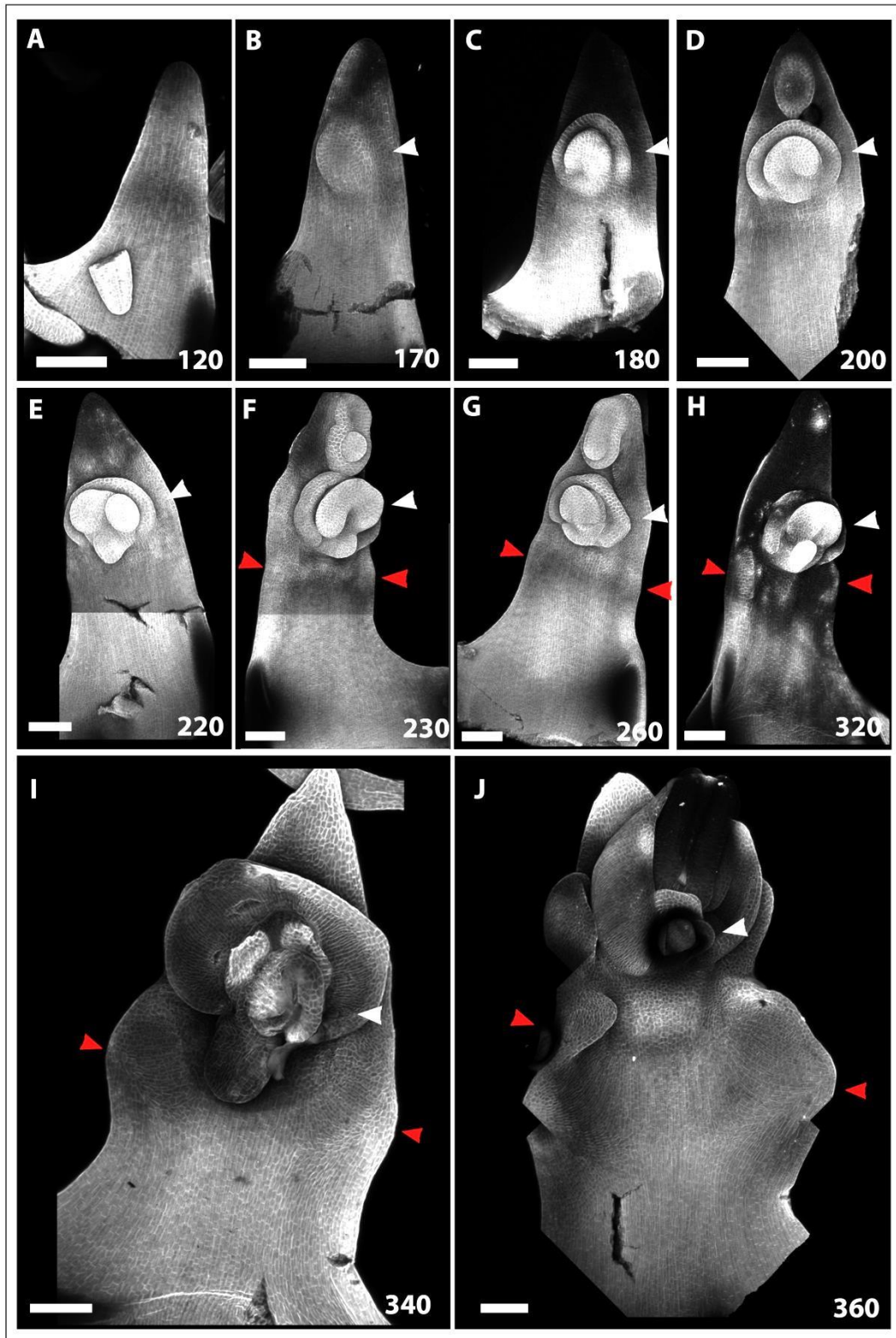
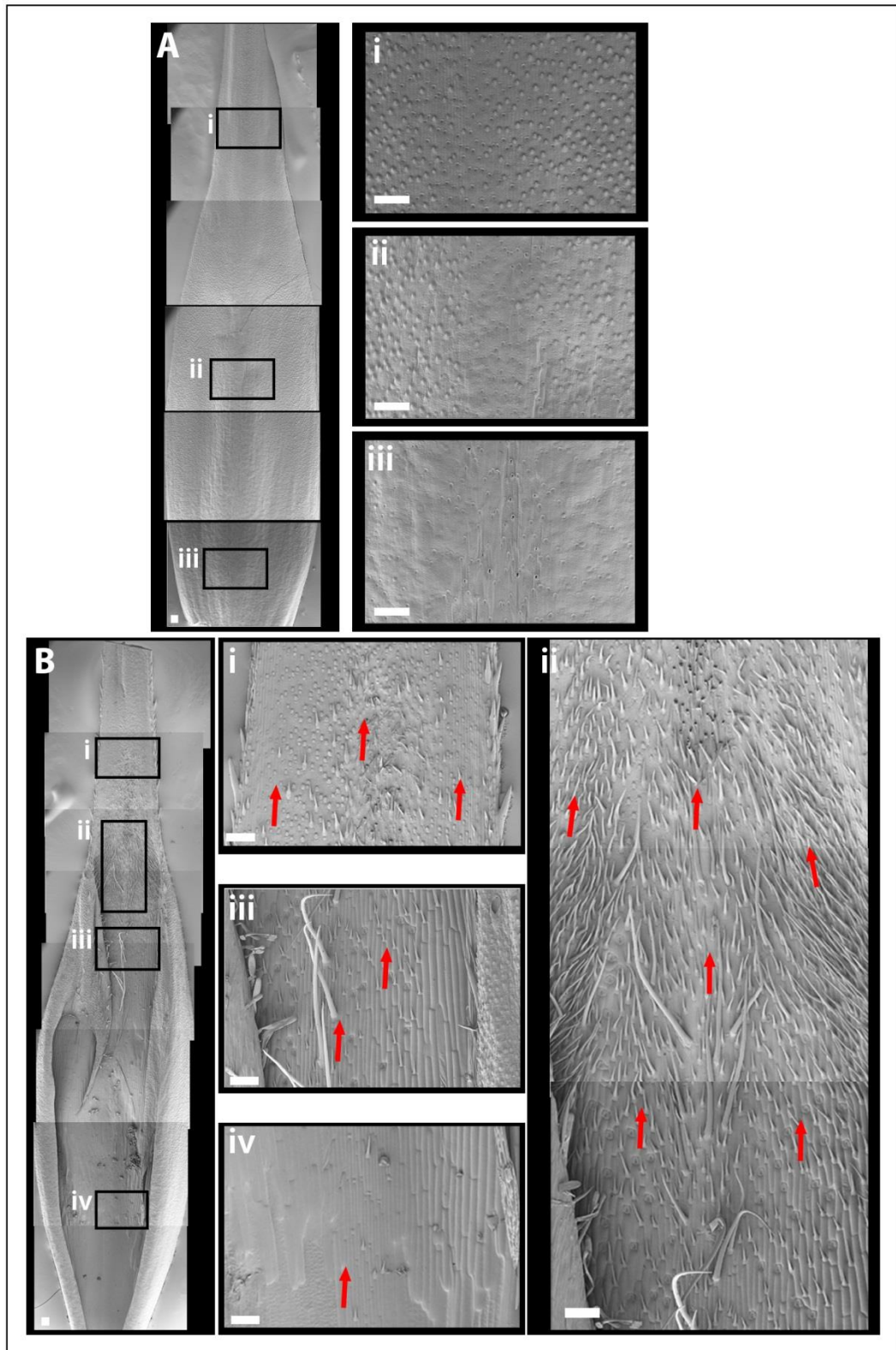


Figure B4 Confocal images of the adaxial surface of developing *Hooded* lemmas Calcofluor stained *Hooded* lemmas, looking at the adaxial surface, at various times during lemma development. White arrowheads indicate the developing ectopic floret, the red arrowheads indicate the developing wings. Scale bars are 100µm.



**Figure B 5 SEM images of a mature wild-type lemma**

Cryo SEM images (taken by Elayne Barclay), of the abaxial (*A*) and adaxial (*B*) surfaces of a mature wild-type lemma. *Ai-iii* and *Bi-iv* are zoomed-in images of the boxed areas in the main images. The red arrows indicate the orientation of the hairs. Scale bars are 100µm.

### 7.3 Appendix C: RNA *in situ* hybridisation probes

For reference, the sequences of each of the barley RNA probe targets are outlined below.

#### ***BKn3***

GCCATCAAGGCCAAGATCATCTCCCACCCCACTACTCCTCCCTCCTCGCCGCTACCTCGACTGCCA  
GAAGGTGGGGGCGCCGCCGAGGTGTCGGCGAGGCTGACGGCGGTGGCGCAGGACCTGGAGCT  
GCGGCAGCGCACGGCGCTCGGCGGCCTCGGCACCGCGACGGAGCCTGAGCTGGACCAGTTCATG  
GAGGCTTACCATGAGATGCTGGTGAAGTACCGGGAGGAGCTGACGAGGCCGCTGCAGGAGGCCA  
TGGAGTTCCTGAGGAGGGTGGAGACGCAGCTCAACTCCCTCTCCATCTCCGGCAGATCGTGC  
ATATCCTTTCCACCGGATCATCCGAGGAAGATCAAGAAGGCAGCGGAGGAGAGACAGAGCTTCT  
GAGATTGATGCCACGGAGTGGACCAGGAGCTG

#### ***LAX1***

CTACCTCATCAGCGTCCTCTACGTCGAGTACCGCTCCCGCAAGGAGAAGGAGGGCGTCAGCTTCAA  
GAACCACGTCATCCAGTGGTTCGAGGTGCTCGACGGGCTGCTGGGCCGTACTGGAAGGCGGCCG  
GGCTGGCCTTCAACTGCACGTTCTCCTCTTCGGCACCGTCATCCAGCTGATCGCCTGCGCCAGCAA  
CATCTACTACATCAACGACCGGCTGGACAAGCGGACGTGGACATACATCTTCGGCGCGTGCTGCGC  
GACGACGGTGTTCATCCCGTCTCCACAACCTACCGGATCTGATCCTTCTGGGGCTGGGCATGACC  
ACCTACACCGCCTGGTACCTCGCCATCGCCGCGCTCATCAACGGCCAGGTCGAGGGCGTCACCCAC  
ACCGGACCAACAAGCTCGTCTCTACTTACCGGCGCCACCAACATCCTCTACACCTTCGGCGGCC  
ACGCGTCACAGTGGAGATCATGCACGCGATGTGGAAGCCGCGCAAGTTCAAGTACATCTACCTGC  
A

#### ***NAM***

GAGATGGAGCGGTACGGTTCTCTGGGCATGCGGCTGGACGGCATCGGCGGCGGGGGCGGCGAGC  
TGCCGCCCCGGTTCGCTTCCACCCGACGGACGAGGAGCTCATCACCTACTACCTCCTCCGCAAGGT  
GGTTGACTGCGGCTTCTCCGGCGCCCGGCCATCGCCGAGATCGACCTCAACAAGTGGAGCCGTG  
GGAGCTGCAGGACAAGGCCTGCAAGGCCACGGCGGAGAAGGAGTGGTACTTCTACAGCCTCCGC  
GACCGCAAGTACCCACGGGCTGCGCACCAACCGCGCCACCGGCGCCGGCTACTGGAAGGCCAC  
CGGCAAGGACCGCGAGATCCGCAGCGCCGCAACGGCGCGCTCGTCCGCATGAAGAAGACGCTC  
GTCTTCTACC

#### ***PIN1a***

GATGATCACGGGCACGGACTTCTACCCCGTGATGACTGCGGTGGTGCCGCTGTACGTGGCCATGAT  
CCTCGCCTACGGCTCCGTCAAGTGGTGGGGCATCTTACGCCGGACCAGTGCTCCGGGATCAACCG  
CTTCGTGCGCTCTTCGCGTCCCGCTCCTCTCCTTCACTTCATCTCCACCAGCAACCCCTACACCAT

GAACCTGCGCTTCATCGCCGCCGACACGCTGCAGAAGCTCATGATGCTCGCCATGCTCACCGCCTG  
GAGCCACCTCTCCCGCCGCGGACGCTCGAGTGGACCATCACCTCTTCTCCCTCTCCACGCTCCCC  
AACACGCTCGTCATGGGCATCCCGCTGCTCAAGGGCATGTACGGCGACGAGTCCGGCAGCCTCATG  
GTGCAGATCGTCGTGCTCCAGTGCATC

***PIN1b***

GGAAAGGGAGATATGCCCAAGGTGACAGAGTTGGGGGAGGCCAGGGCTGGTACGGCAAGTCCG  
TCAGGAACACGCAGCTATACCACGTCATGACGGCGATGGTGCCGCTGTACGTGGTGAAGATGCTA  
GGGTACGGGTCCGCCAAGTGGTGGCGGATCTTACGCCGGACCAGTGCTCCGGGATCAACCGCTT  
CGTGGCGCTCTTCGCCGTGCCGCTGCTGTCTTCCACTTCATCTCCAGCAACAACCCCTACACCATGA  
ACCTCCGCTTCATCGCCGCCGACACCCTGCAGAAGCTCATCAAGGGCGAATTCGTTTAAACCTGCAG  
GACTAGTCCCTTAGTGAGGCTATCTAGGAC

***SoPIN1***

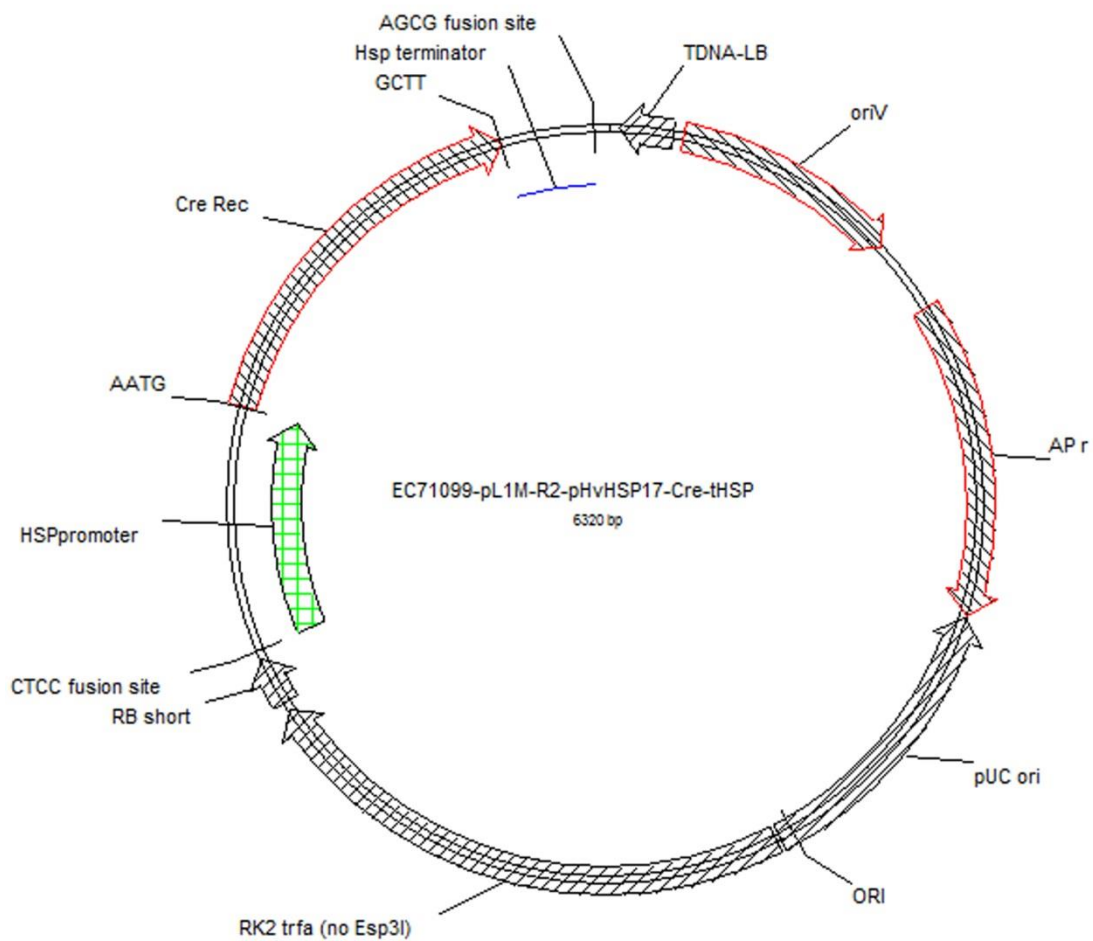
TTCCACTTCATCTCCTCCAACGACCCCTTCGCCATGAACCTCCGCTTCTCGCCGCCGACACGCTCCA  
GAAGCTCGCCGTCCTCGCGCTACTCGGCCTCTGGTGCCGCTCCGCGGGGGCTCCCTCGACTGGCT  
CATCACGCTCTTCTCCCTCTCCACGCTCCCCAACACGCTCGTCATGGGCATCCCGCTGCTCCGGGGC  
ATGTACGGCCCCGCCAGCGCCGGCACGCTCATGGTGCAGATCGTCGTGCTGCAGTGCATCATCTGG  
TACACCCTCATGCTCTTCTTTCGAGTACCGCGGGCGCAAGATGCTCGTCATGGAGCAGTTCCCCG  
ACACCGCCGCCGACATCGTCTCCTTCCGCGTCGACTCCGACGTCGTCTCGCTCGCCGGGGGCGGCG  
GGGCGGACCTGCAGGCGGAGG

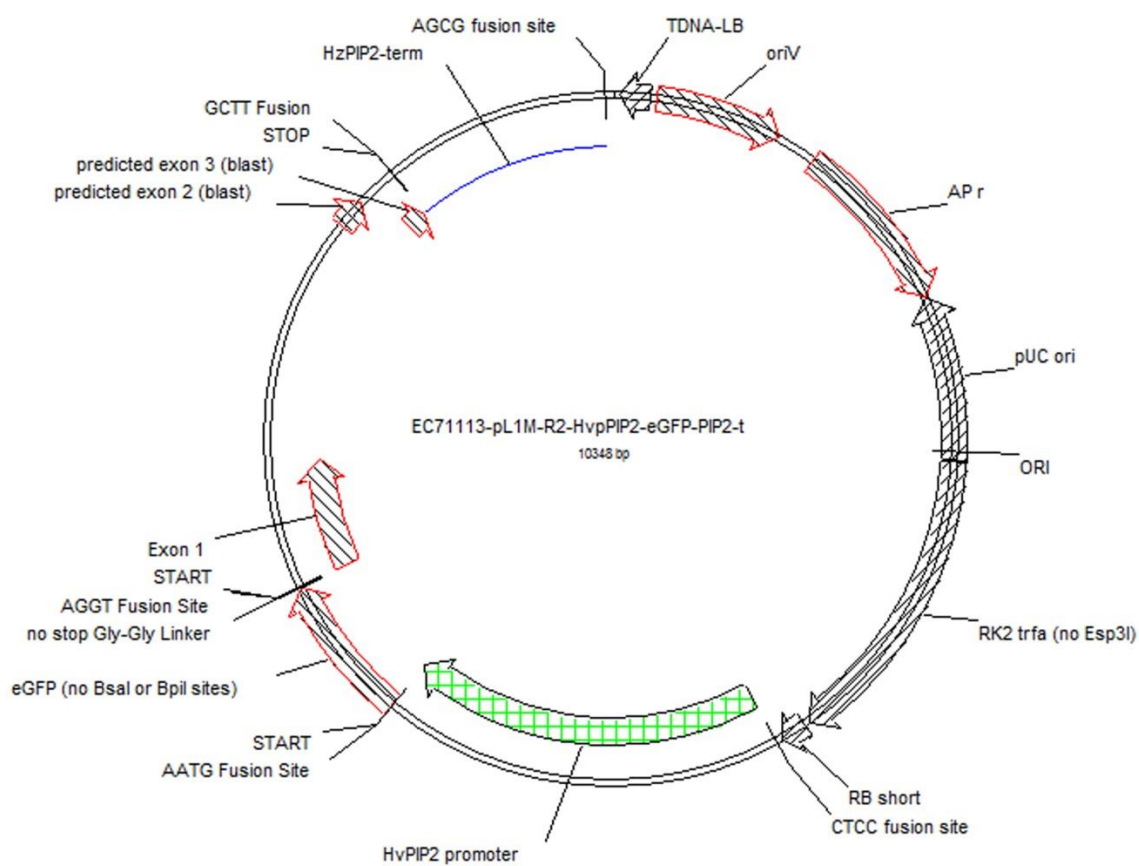
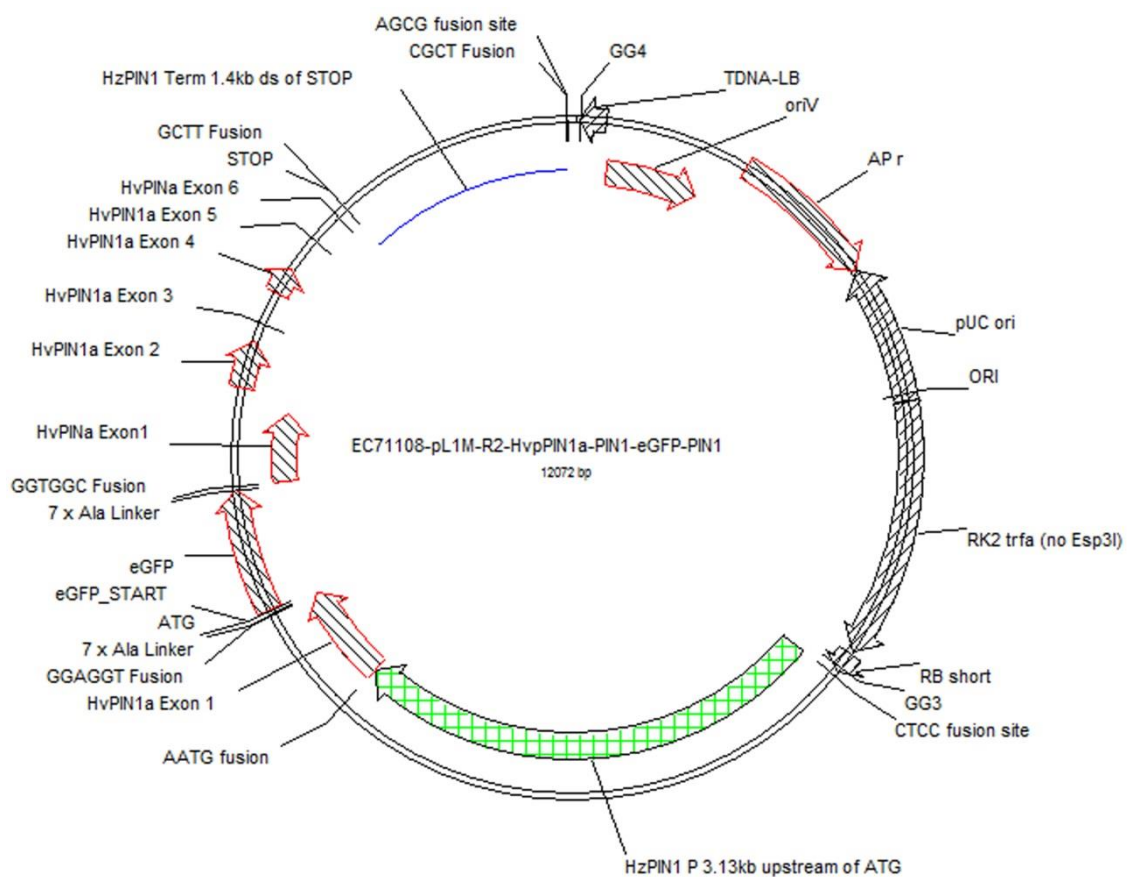
***YUCCA***

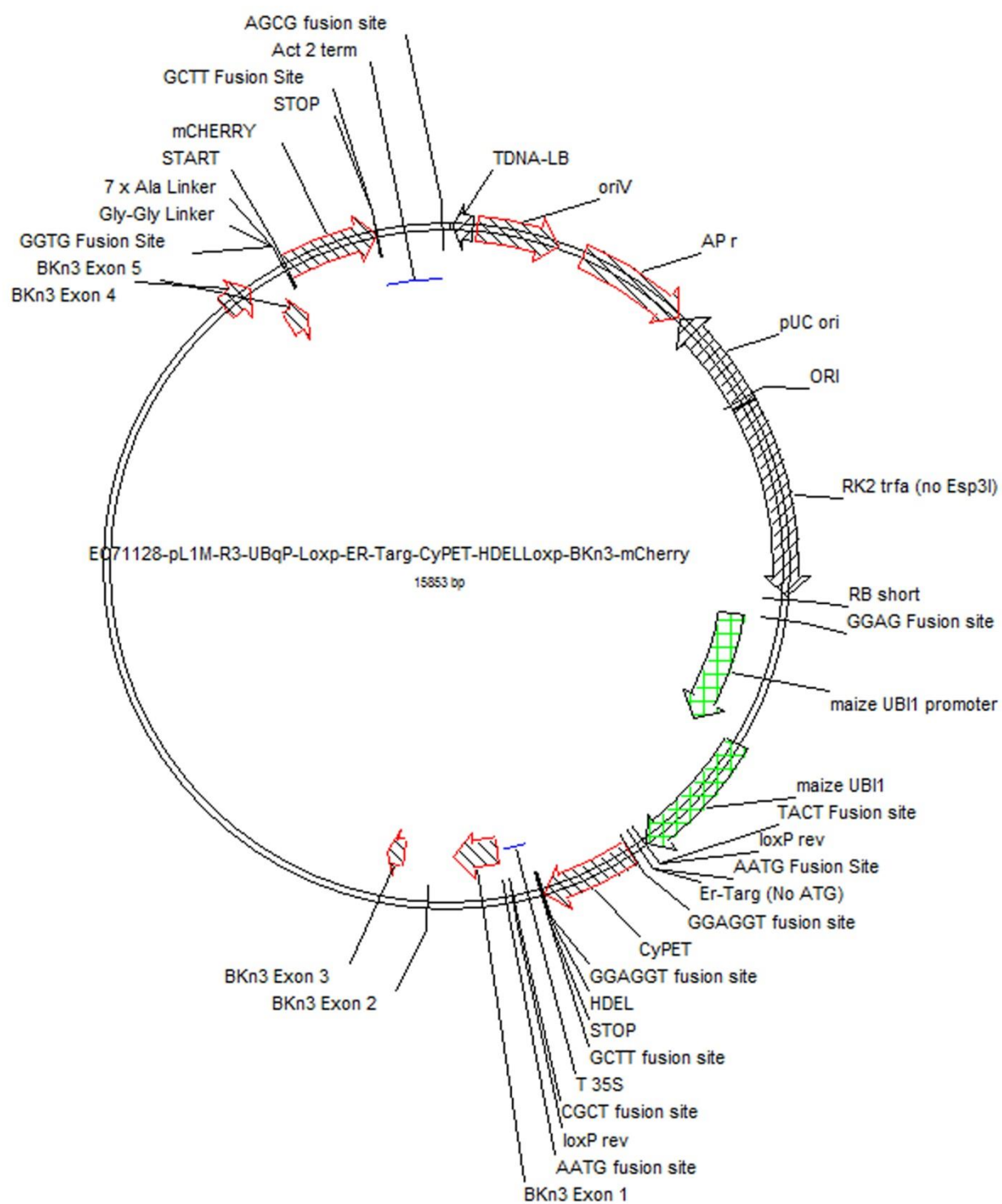
ATGGTGCTCCTGTCTAGCGATCGCATGGACAGCCTCTTCTCCCCGCGTTGCGTGTGGGTGAACGGG  
CCCATCATTATCGGCGCCGGGCGGTCGGGGCTCGCCGTGGGCGCCAGCCTCCGTGAGCAGGGCGT  
GCCGTACGTGATGCTGGAGCGGGAGGACTGCATCGCCTCTCTGTGGCAGAAGCGCACCTACGACC  
GCCTCAAGCTCCACCTCCCCAAGCAGTTCTGCCAGCTCCCCCGCATGCCCTTCCCCGCCGACTACCCC  
GAGTACCCACCCGCCGCCAGTTCATCGACTACCTCGAGGACTACGCCGCCGCTTCCACGTCAAGC  
CCGAGTTCGGCAGCACCGTGCAGTCCGCCCCGCTACGACGAGACCTCCGGGCTCTGGCGCGTGCAT  
CCTCTCGGCCAAGTCCGGCGAGATGGAGTACATCGGGCGCTGGCTCGTGGTCCGCCACCGGCGAG  
AACGCCGAGAACGTGA

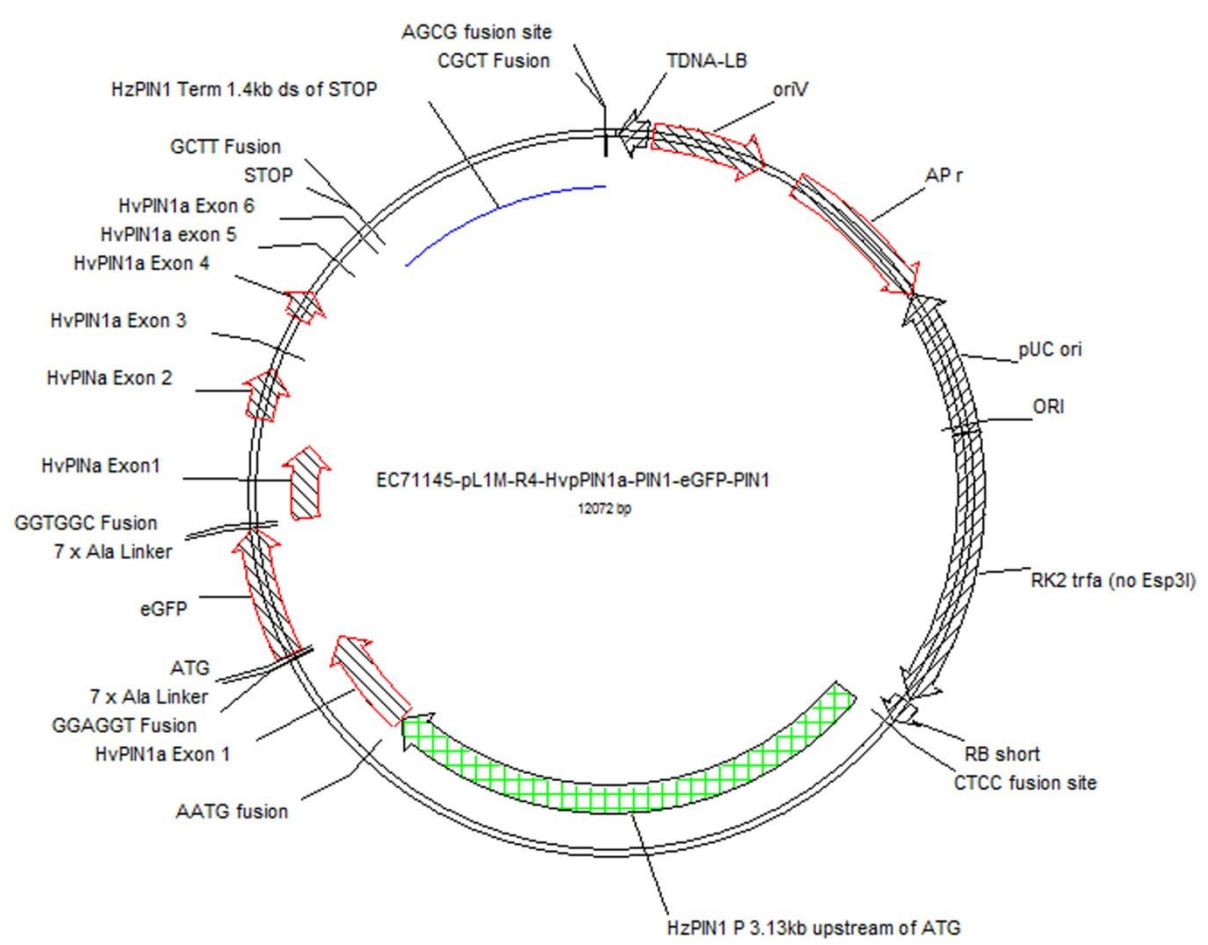
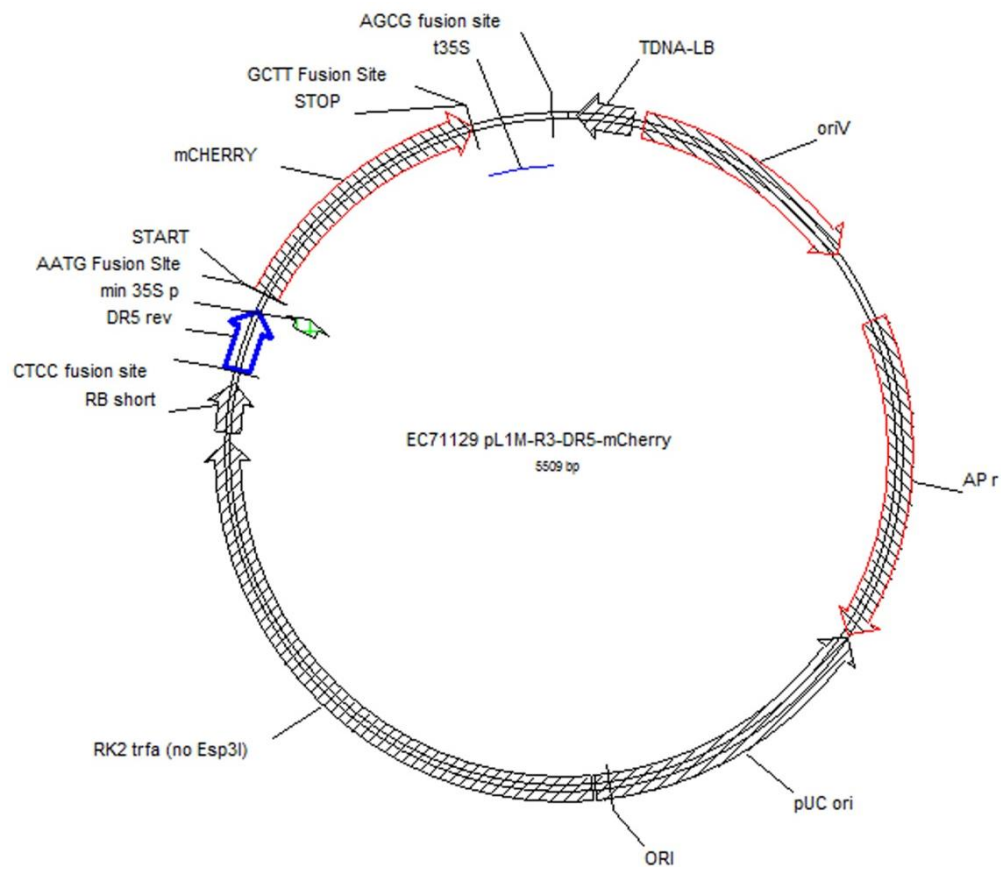
## 7.4 Appendix D: Transgenic barley constructs

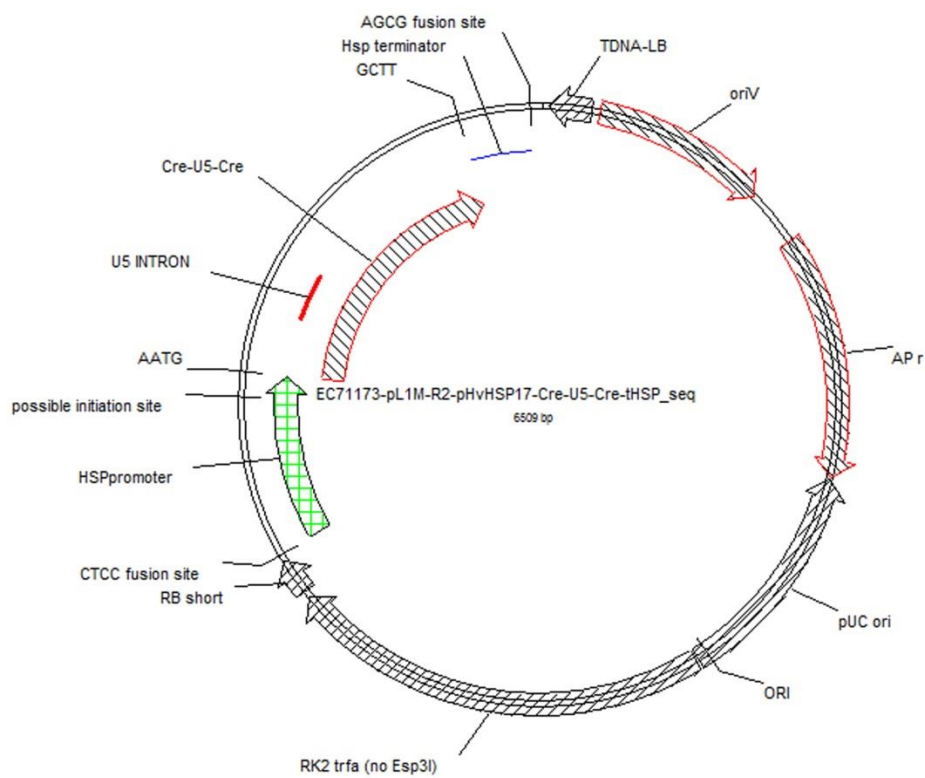
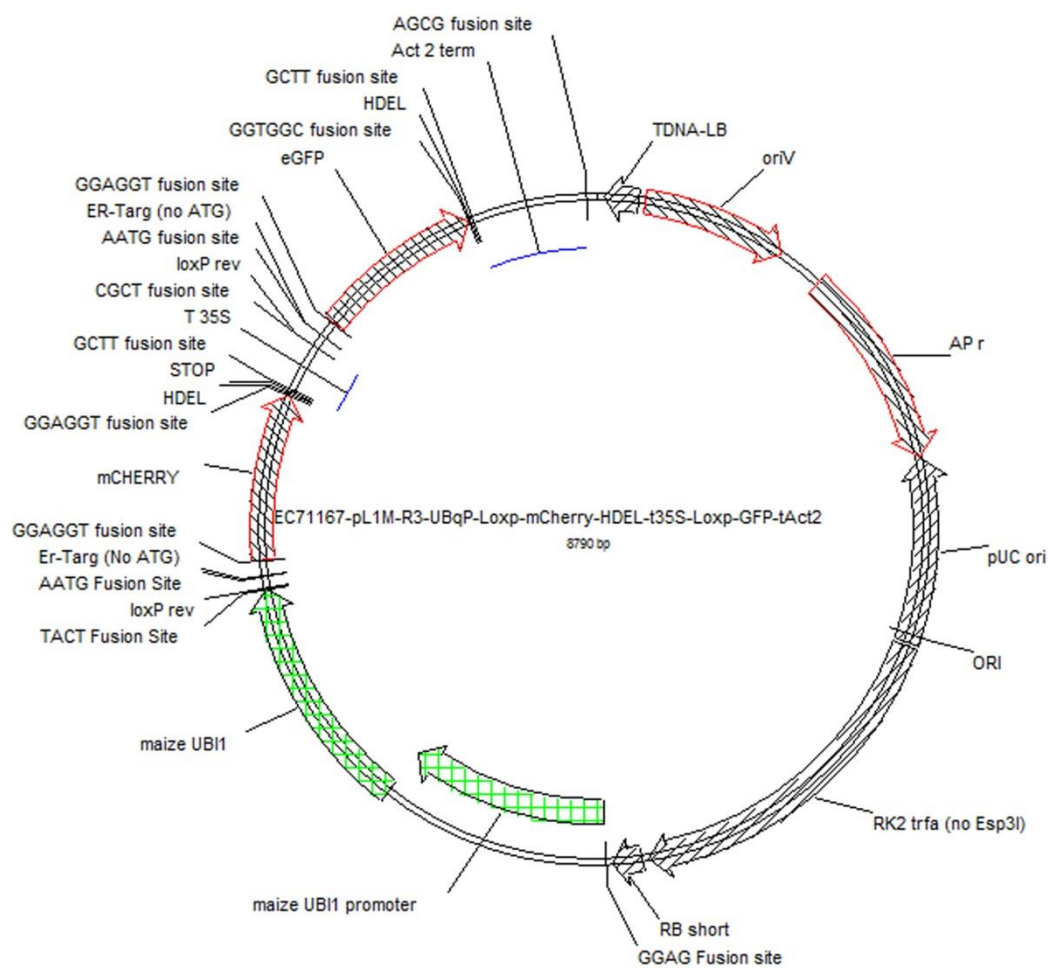
For reference below are the plasmid maps for each L1 and L2 construct made during the goldengate cloning for barley transformation. Each map is labelled with its plasmid number (see Table 6.5). The promoters are green, the exons are red, terminators are blue lines, blue outlined arrows are enhancer elements and the red line is the U5 intron. Each map has appropriate fusion sites and features labelled.

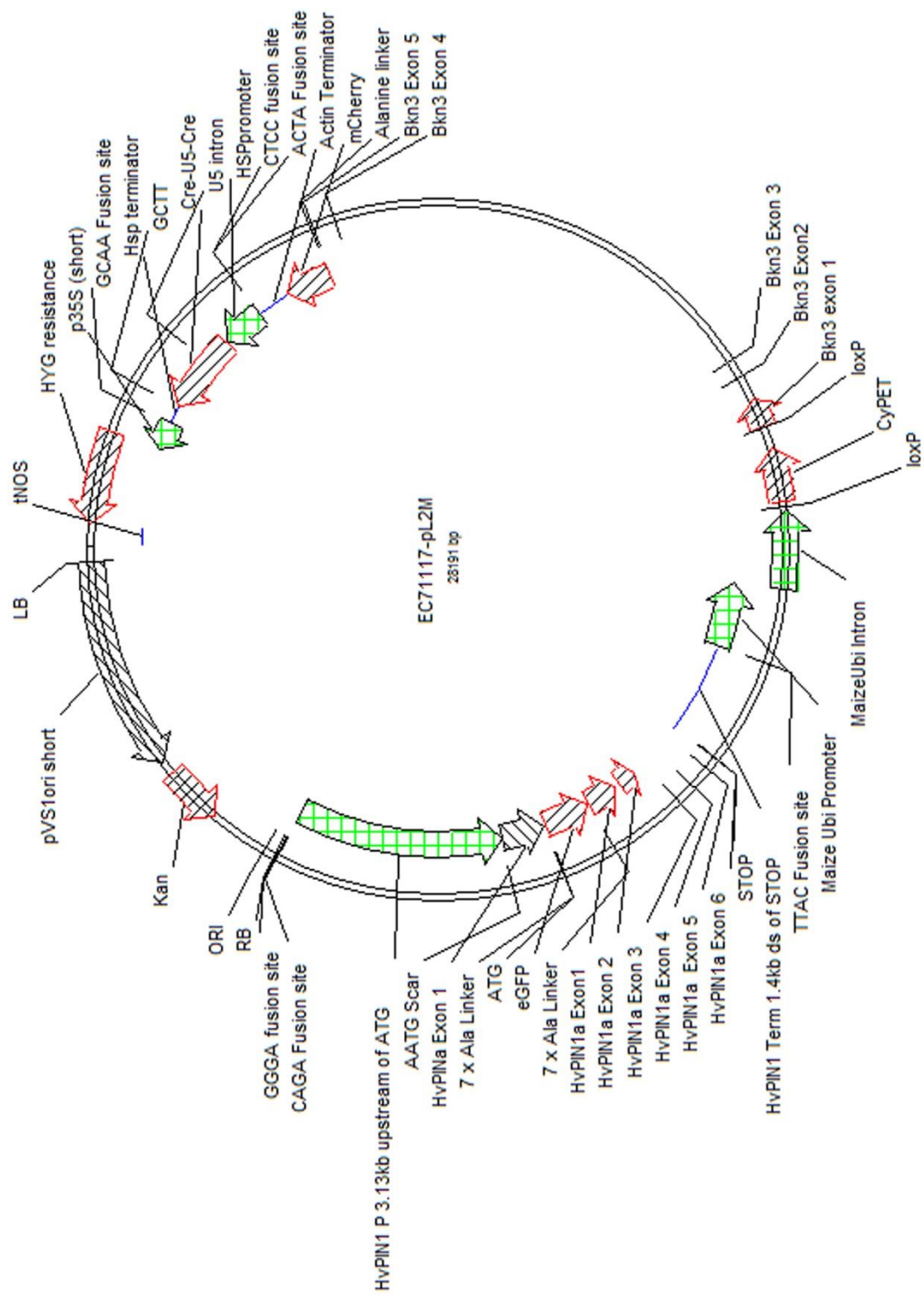


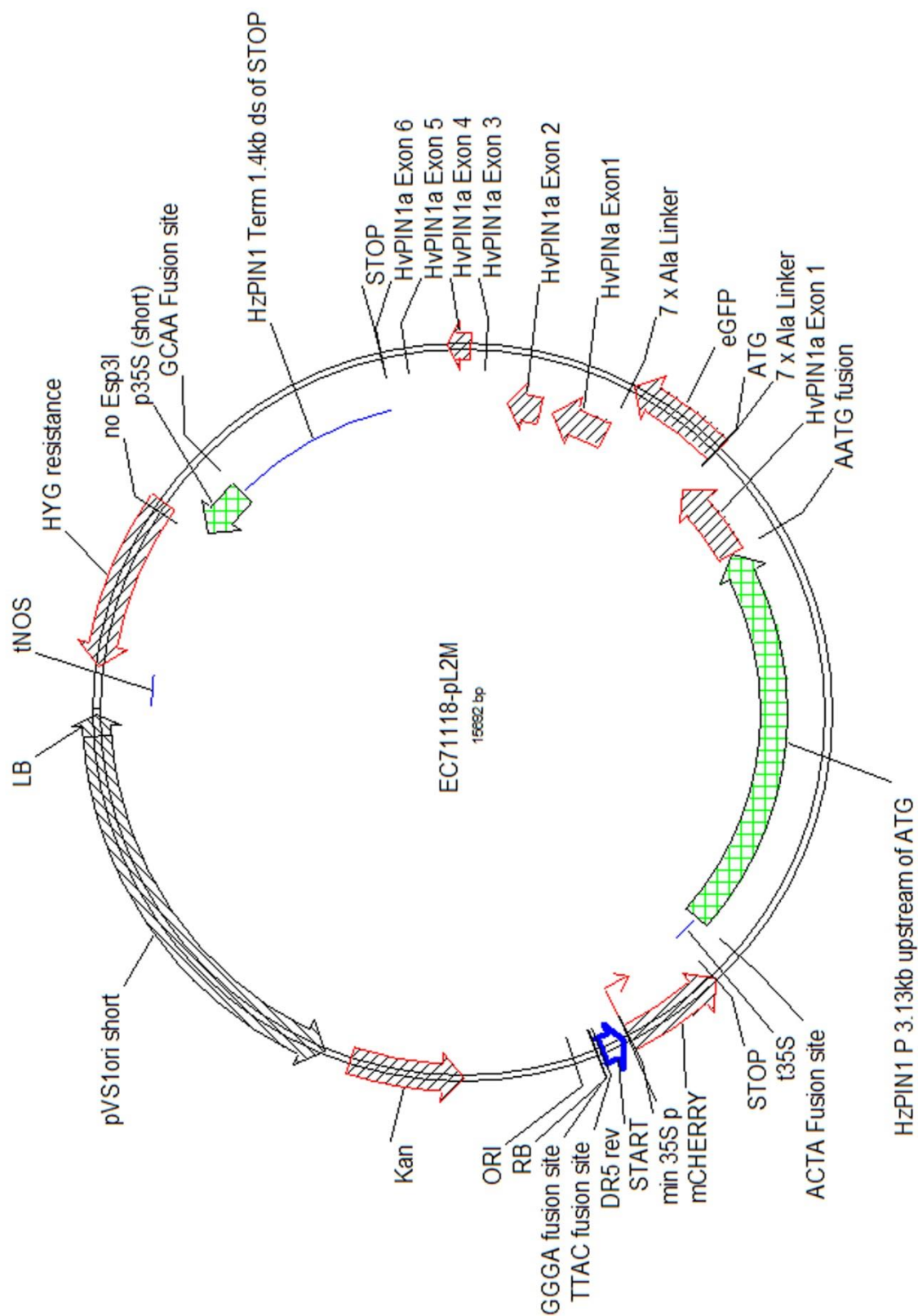


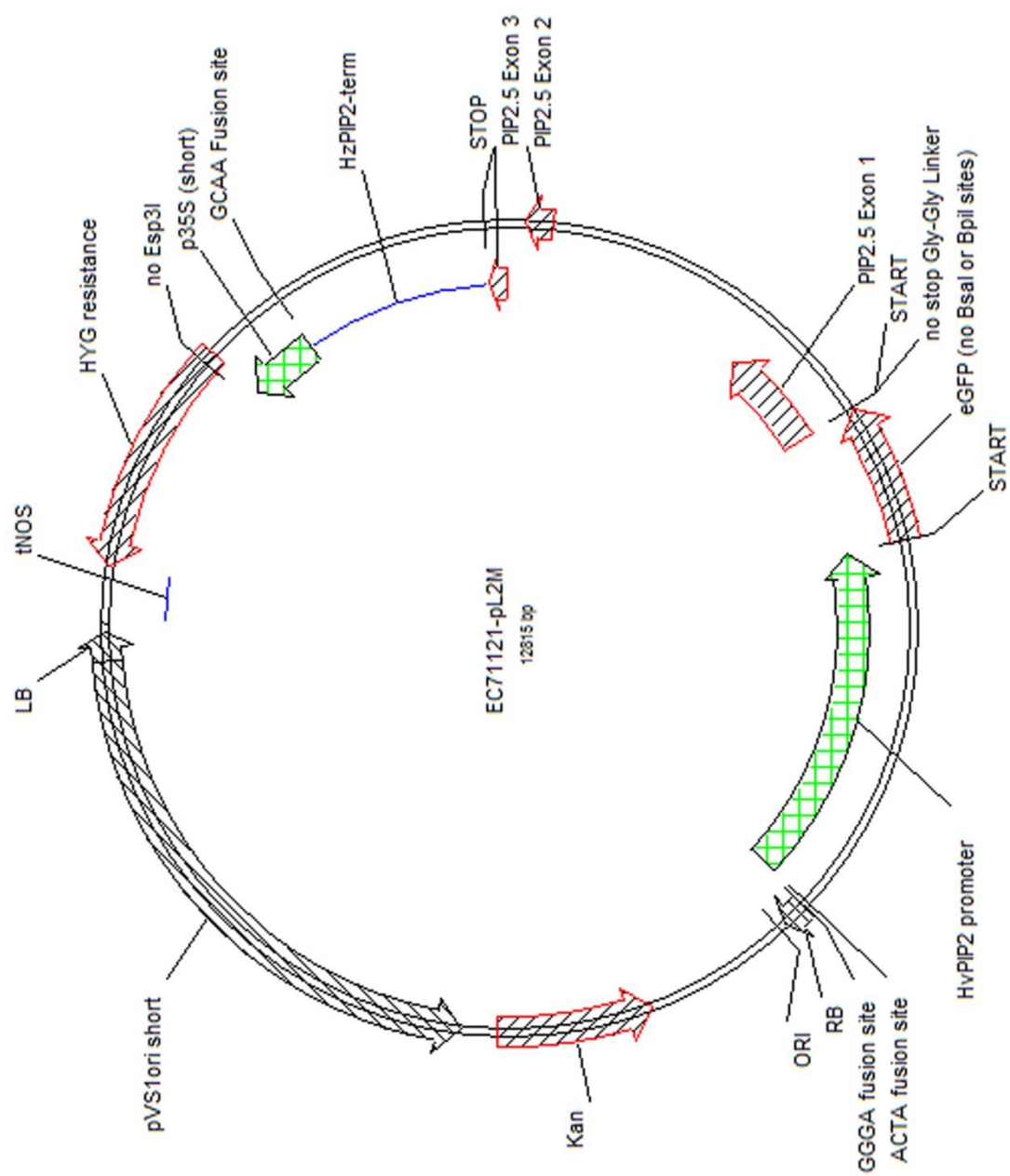


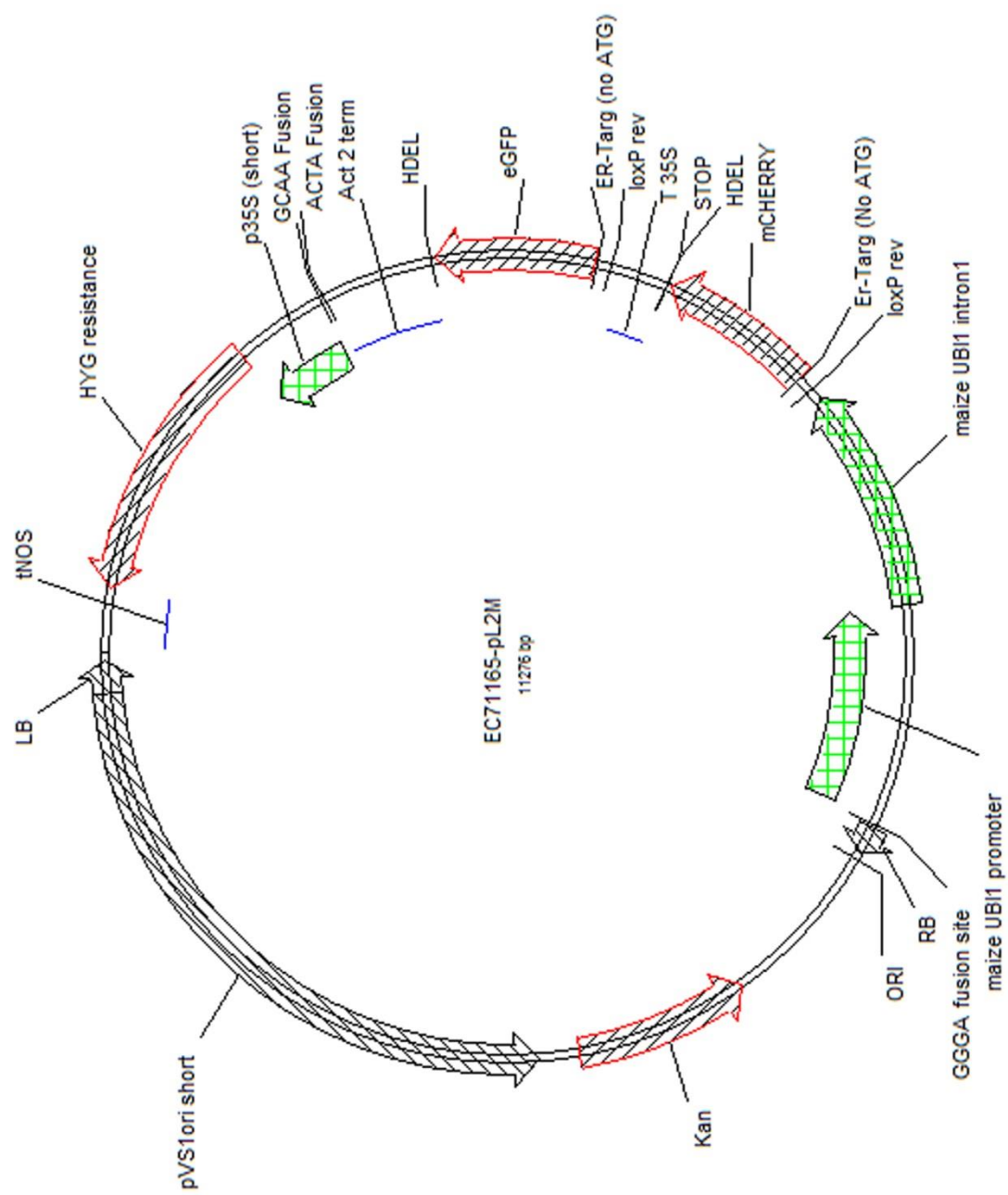


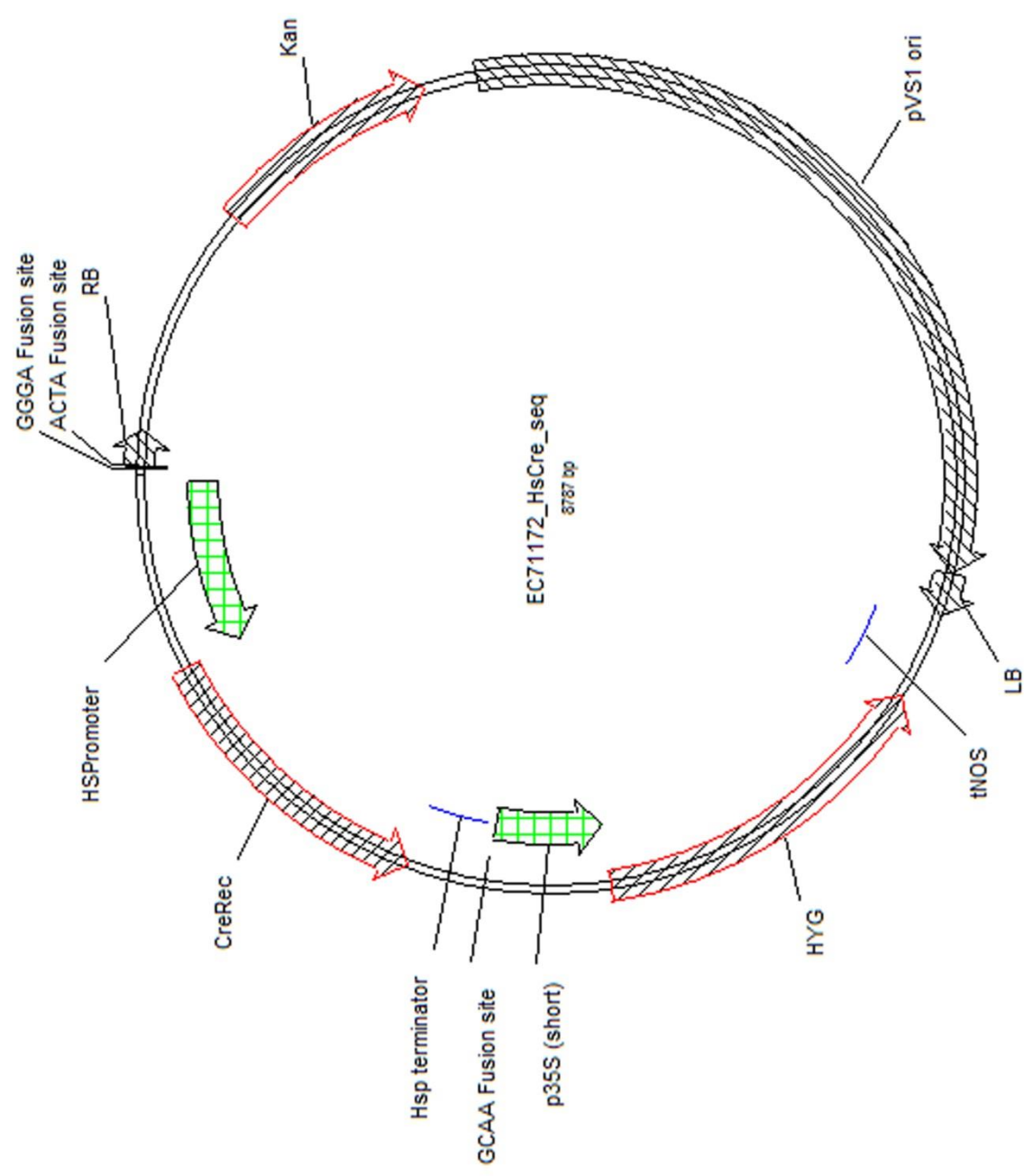


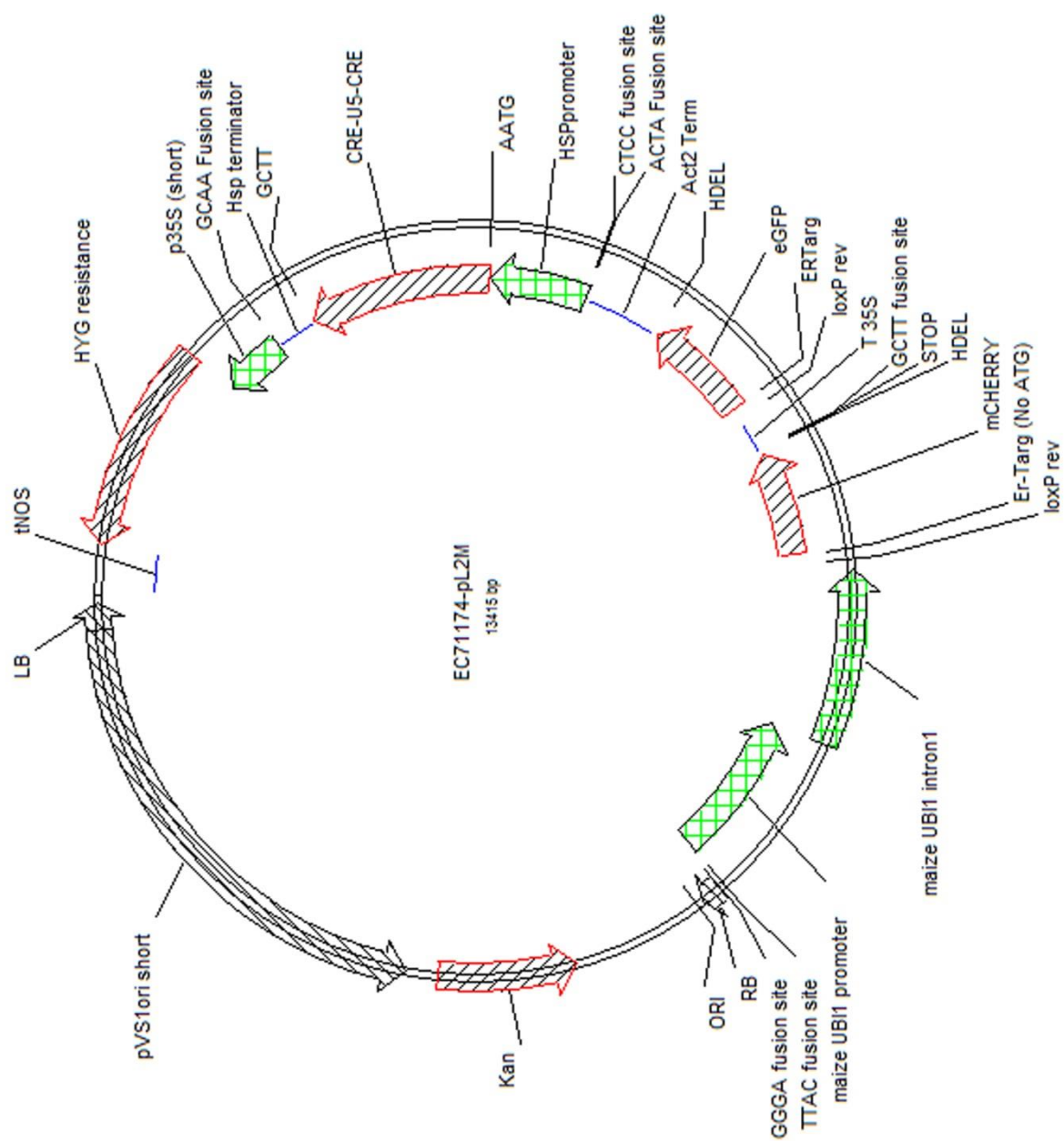












## 8 Abbreviations

BKn3	BARLEY KNOX 3
BRACT	Biotechnology Resources for Arable Crop Transformation
CT	Computerized Tomography
DAB	3,3'-Diaminobenzidine
DMSO	Dimethyl sulfoxide
EdU	5'-ethynyl-2'-deoxyuridine
ENSA	Engineering Nitrogen Symbiosis for Africa
GFP	Green Fluorescent Protein
GPT Framework	Growing Polarised Tissue framework
HD	<i>Hooded</i>
HDZIP	Homeodomain leucine zipper
HIRZ	HIRZINA
JIC	John Innes Centre
KN1	KNOTTED 1
KRN	Growth (K) Regulatory Network
L0	Level 0
L1	Level 1
L2	Level 2
LAX	LIKE AUX1
LB	Liquid Broth
LB	Lysogeny Broth
LMP	Low Melting Point
mya	million years ago
NAM	NO APICAL MERISTEM
NEB	New England Biolabs
NPA	N-1-Naphthylphthalamic Acid
OPT	Optical Projection Tomography
PI	Propidium Iodide
PIN	PINFORMED
POL	POLARISER
PRN	Polarity Regulatory Network
RCO	REDUCED COMPLEXITY
RT-PCR	Reverse Transcription PCR
SAM	Shoot Apical Meristem
SEM	Scanning Electron Microscopy
SOC	Super Optimal
STM	SHOOTMERISTEMLESS
TXR	Texas Red
UC	University of California
WOX	WUSCHEL RELATED HOMEBOX
WT	Wild Type
YFP	Yellow Fluorescent Protein

## 9 References

1. Gomez, J.M., et al., *Spatial variation in selection on corolla shape in a generalist plant is promoted by the preference patterns of its local pollinators*. Proceedings of the Royal Society of London B: Biological Sciences, 2008. **275**(1648): p. 2241-2249.
2. Nicotra, A., et al., *Leaf shape linked to photosynthetic rates and temperature optima in South African Pelargonium species*. Oecologia, 2008. **154**(4): p. 625-635.
3. Weigel, D. and O. Nilsson, *A developmental switch sufficient for flower initiation in diverse plants*. Nature, 1995. **377**(6549): p. 495-500.
4. Bilborough, G.D., et al., *Model for the regulation of Arabidopsis thaliana leaf margin development*. Proc Natl Acad Sci U S A, 2011. **108**(8): p. 3424-9.
5. Kawamura, E., G. Horiguchi, and H. Tsukaya, *Mechanisms of leaf tooth formation in Arabidopsis*. Plant J, 2010. **62**(3): p. 429-41.
6. Gunawardena, A.L.A.N., et al., *Programmed cell death and leaf morphogenesis in Monstera obliqua (Araceae)*. Planta, 2005. **221**(5): p. 607-618.
7. Nibau, C., D.J. Gibbs, and J.C. Coates, *Branching out in new directions: the control of root architecture by lateral root formation*. New Phytologist, 2008. **179**(3): p. 595-614.
8. Sears, K.E., et al., *Developmental basis of mammalian digit reduction: a case study in pigs*. Evolution & Development, 2011. **13**(6): p. 533-541.
9. Sears, K.E., *Molecular Determinants of Bat Wing Development*. Cells Tissues Organs, 2008. **187**(1): p. 6-12.
10. Scanlon, M.J. and M. Freeling, *Clonal Sectors Reveal That a Specific Meristematic Domain Is Not Utilized in the Maize Mutant narrow sheath*. Developmental Biology, 1997. **182**(1): p. 52-66.
11. Lockhart, J.A., *An analysis of irreversible plant cell elongation*. Journal of Theoretical Biology, 1965. **8**(2): p. 264-275.
12. Cosgrove, D.J., *Loosening of plant cell walls by expansins*. Nature, 2000. **407**(6802): p. 321-326.
13. McQueen-Mason, S.J. and D.J. Cosgrove, *Expansin Mode of Action on Cell Walls (Analysis of Wall Hydrolysis, Stress Relaxation, and Binding)*. Plant Physiology, 1995. **107**(1): p. 87-100.
14. Bosch, M., A.Y. Cheung, and P.K. Hepler, *Pectin Methylesterase, a Regulator of Pollen Tube Growth*. Plant Physiology, 2005. **138**(3): p. 1334-1346.

15. Baskin, T., *On the alignment of cellulose microfibrils by cortical microtubules: A review and a model*. Protoplasma, 2001. **215**(1-4): p. 150-171.
16. Heath, I.B., *A unified hypothesis for the role of membrane bound enzyme complexes and microtubules in plant cell wall synthesis*. Journal of Theoretical Biology, 1974. **48**(2): p. 445-449.
17. Williamson, R., *Alignment of Cortical Microtubules by Anisotropic Wall Stresses*. Functional Plant Biology, 1990. **17**(6): p. 601-613.
18. Bassel, G.W., et al., *Mechanical constraints imposed by 3D cellular geometry and arrangement modulate growth patterns in the Arabidopsis embryo*. Proceedings of the National Academy of Sciences of the United States of America, 2014. **111**(23): p. 8685-8690.
19. Coen, E., et al., *The genetics of geometry*. Proceedings of the National Academy of Sciences of the United States of America, 2004. **101**(14): p. 4728-4735.
20. Kennaway, R., et al., *Generation of Diverse Biological Forms through Combinatorial Interactions between Tissue Polarity and Growth*. PLoS Comput Biol, 2011. **7**(6): p. e1002071.
21. Kuchen, E.E., et al., *Generation of Leaf Shape Through Early Patterns of Growth and Tissue Polarity*. Science, 2012. **335**(6072): p. 1092-1096.
22. Sauret-Güeto, S., et al., *JAGGED Controls Arabidopsis Petal Growth and Shape by Interacting with a Divergent Polarity Field*. PLoS Biol, 2013. **11**(4): p. e1001550.
23. Yin, J., et al., *Stress-driven buckling patterns in spheroidal core/shell structures*. Proceedings of the National Academy of Sciences, 2008. **105**(49): p. 19132-19135.
24. Green, A.A., et al., *Genetic control of organ shape and tissue polarity*. PLoS Biol, 2010. **8**(11): p. e1000537.
25. Remmler, L. and A.-G. Rolland-Lagan, *Computational Method for Quantifying Growth Patterns at the Adaxial Leaf Surface in Three Dimensions*. Plant Physiology, 2012. **159**(1): p. 27-39.
26. Poethig, R.S., *Cellular Parameters of Leaf Morphogenesis in Maize and Tobacco*. Contemporary Problems in Plant Anatomy, 1984: p. 235-259.
27. Poethig, R.S., E.H. Coe Jr, and M.M. Johri, *Cell lineage patterns in maize embryogenesis: A clonal analysis*. Developmental Biology, 1986. **117**(2): p. 392-404.
28. Poethig, R.S. and I.M. Sussex, *The cellular parameters of leaf development in tobacco: a clonal analysis*. Planta, 1985. **165**(2): p. 170-184.

29. Berleth, T., E. Scarpella, and P. Prusinkiewicz, *Towards the systems biology of auxin-transport-mediated patterning*. Trends in Plant Science, 2007. **12**(4): p. 151-159.
30. Reinhardt, D., T. Mandel, and C. Kuhlemeier, *Auxin Regulates the Initiation and Radial Position of Plant Lateral Organs*. The Plant Cell, 2000. **12**(4): p. 507-518.
31. Estelle, M.A. and C. Somerville, *Auxin-resistant mutants of Arabidopsis thaliana with an altered morphology*. Molecular and General Genetics MGG, 1987. **206**(2): p. 200-206.
32. Berleth, T. and T. Sachs, *Plant morphogenesis: long-distance coordination and local patterning*. Current opinion in plant biology, 2001. **4**(1): p. 57-62.
33. Möller, B. and D. Weijers, *Auxin Control of Embryo Patterning*. Cold Spring Harbor Perspectives in Biology, 2009. **1**(5): p. a001545.
34. Vernoux, T., et al., *PIN-FORMED 1 regulates cell fate at the periphery of the shoot apical meristem*. Development, 2000. **127**(23): p. 5157-5165.
35. Smith, R.S., et al., *A plausible model of phyllotaxis*. Proceedings of the National Academy of Sciences, 2006. **103**(5): p. 1301-1306.
36. Bayer, E.M., et al., *Integration of transport-based models for phyllotaxis and midvein formation*. Genes & Development, 2009. **23**(3): p. 373-384.
37. Heisler, M.G., et al., *Alignment between PIN1 Polarity and Microtubule Orientation in the Shoot Apical Meristem Reveals a Tight Coupling between Morphogenesis and Auxin Transport*. PLoS Biol, 2010. **8**(10): p. e1000516.
38. Nakayama, N., et al., *Mechanical Regulation of Auxin-Mediated Growth*. Current Biology, 2012. **22**(16): p. 1468-1476.
39. Stoma, S., et al., *Flux-Based Transport Enhancement as a Plausible Unifying Mechanism for Auxin Transport in Meristem Development*. PLoS Comput Biol, 2008. **4**(10): p. e1000207.
40. Rolland-Lagan, A.-G. and P. Prusinkiewicz, *Reviewing models of auxin canalization in the context of leaf vein pattern formation in Arabidopsis*. The Plant Journal, 2005. **44**(5): p. 854-865.
41. Cieslak, M., A. Runions, and P. Prusinkiewicz, *Auxin-driven patterning with unidirectional fluxes*. Journal of experimental botany, 2015: p. erv262.
42. Abley, K., et al., *An intracellular partitioning-based framework for tissue cell polarity in plants and animals*. Development, 2013. **140**(10): p. 2061-2074.
43. Sauer, M. and J. Kleine-Vehn, *AUXIN BINDING PROTEIN1: The Outsider*. The Plant Cell, 2011. **23**(6): p. 2033-2043.

44. Gao, Y., et al., *Auxin binding protein 1 (ABP1) is not required for either auxin signaling or Arabidopsis development*. Proceedings of the National Academy of Sciences, 2015. **112**(7): p. 2275-2280.
45. Boutté, Y., et al., *The plasma membrane recycling pathway and cell polarity in plants: studies on PIN proteins*. Journal of Cell Science, 2006. **119**(7): p. 1255-1265.
46. Grandjean, O., et al., *In Vivo Analysis of Cell Division, Cell Growth, and Differentiation at the Shoot Apical Meristem in Arabidopsis*. The Plant Cell, 2004. **16**(1): p. 74-87.
47. Hamant, O., et al., *Developmental Patterning by Mechanical Signals in Arabidopsis*. Science, 2008. **322**(5908): p. 1650-1655.
48. Heisler, M.G., et al., *Patterns of Auxin Transport and Gene Expression during Primordium Development Revealed by Live Imaging of the Arabidopsis Inflorescence Meristem*. Current Biology, 2005. **15**(21): p. 1899-1911.
49. Scarpella, E., et al., *Control of leaf vascular patterning by polar auxin transport*. Genes & Development, 2006. **20**(8): p. 1015-1027.
50. Souer, E., et al., *The No Apical Meristem Gene of Petunia Is Required for Pattern Formation in Embryos and Flowers and Is Expressed at Meristem and Primordia Boundaries*. Cell, 1996. **85**(2): p. 159-170.
51. Aida, M., et al., *Genes involved in organ separation in Arabidopsis: an analysis of the cup-shaped cotyledon mutant*. The Plant Cell Online, 1997. **9**(6): p. 841-57.
52. Majer, C. and F. Hochholdinger, *Defining the boundaries: structure and function of LOB domain proteins*. Trends in plant science, 2011. **16**(1): p. 47-52.
53. Zhao, Y., et al., *A Role for Flavin Monooxygenase-Like Enzymes in Auxin Biosynthesis*. Science, 2001. **291**(5502): p. 306-309.
54. Yamamoto, Y., et al., *Auxin biosynthesis by the YUCCA genes in rice*. Plant physiology, 2007. **143**(3): p. 1362-1371.
55. Gallavotti, A., et al., *sparse inflorescence1 encodes a monocot-specific YUCCA-like gene required for vegetative and reproductive development in maize*. Proceedings of the National Academy of Sciences, 2008. **105**(39): p. 15196-15201.
56. Cheng, Y., X. Dai, and Y. Zhao, *Auxin Synthesized by the YUCCA Flavin Monooxygenases Is Essential for Embryogenesis and Leaf Formation in Arabidopsis*. The Plant Cell, 2007. **19**(8): p. 2430-2439.

57. Hutchison, K.W., et al., *Expansins Are Conserved in Conifers and Expressed in Hypocotyls in Response to Exogenous Auxin*. *Plant Physiology*, 1999. **120**(3): p. 827-832.
58. Boudaoud, A., *An introduction to the mechanics of morphogenesis for plant biologists*. *Trends in Plant Science*. **15**(6): p. 353-360.
59. Sistrunk, M.L., et al., *Arabidopsis TCH3 encodes a novel Ca<sup>2+</sup> binding protein and shows environmentally induced and tissue-specific regulation*. *The Plant Cell*, 1994. **6**(11): p. 1553-65.
60. Haswell, E.S., et al., *Two MscS Homologs Provide Mechanosensitive Channel Activities in the Arabidopsis Root*. *Current Biology*, 2008. **18**(10): p. 730-734.
61. Hamilton, E.S., A.M. Schlegel, and E.S. Haswell, *United in Diversity: Mechanosensitive Ion Channels in Plants*. *Annual Review of Plant Biology*, 2015. **66**(1): p. 113-137.
62. Zandomeni, K. and P. Schopfer, *Mechanosensory microtubule reorientation in the epidermis of maize coleoptiles subjected to bending stress*. *Protoplasma*, 1994. **182**(3-4): p. 96-101.
63. Lambert, R.J. and R.R. Johnson, *Leaf Angle, Tassel Morphology, and the Performance of Maize Hybrids*. *Crop Science*, 1978. **18**(3): p. 499-502.
64. Burian, A., et al., *A correlative microscopy approach relates microtubule behaviour, local organ geometry, and cell growth at the Arabidopsis shoot apical meristem*. *Journal of Experimental Botany*, 2013.
65. Grebe, M., *Ups and downs of tissue and planar polarity in plants*. *Bioessays*, 2004. **26**(7): p. 719-729.
66. Adler, P.N., *Planar signaling and morphogenesis in Drosophila*. *Developmental cell*, 2002. **2**(5): p. 525-535.
67. Fischer, U., et al., *Vectorial information for Arabidopsis planar polarity is mediated by combined AUX1, EIN2, and GNOM activity*. *Current Biology*, 2006. **16**(21): p. 2143-2149.
68. Ikeda, Y., et al., *Local auxin biosynthesis modulates gradient-directed planar polarity in Arabidopsis*. *Nature Cell Biology*, 2009. **11**(6): p. 731-738.
69. Peters, W.S. and D. Tomos, *The epidermis still in control?* *Botanica Acta*, 1996. **109**(4): p. 264-267.
70. Savaldi-Goldstein, S. and J. Chory, *Growth coordination and the shoot epidermis*. *Current opinion in plant biology*, 2008. **11**(1): p. 42-48.

71. Savaldi-Goldstein, S., C. Peto, and J. Chory, *The epidermis both drives and restricts plant shoot growth*. *Nature*, 2007. **446**(7132): p. 199-202.
72. Marcotrigiano, M., *A role for leaf epidermis in the control of leaf size and the rate and extent of mesophyll cell division*. *American journal of botany*, 2010. **97**(2): p. 224-233.
73. Bemis, S.M. and K.U. Torii, *Autonomy of cell proliferation and developmental programs during Arabidopsis aboveground organ morphogenesis*. *Developmental biology*, 2007. **304**(1): p. 367-381.
74. Kutschera, U., *The role of the epidermis in the control of elongation growth in stems and coleoptiles*. *Botanica Acta*, 1992. **105**(4): p. 246-252.
75. Boudon, F., et al., *A computational framework for 3D mechanical modeling of plant morphogenesis with cellular resolution*. *PLoS Comput Biol*, 2015. **11**(1): p. e1003950.
76. Weir, I., et al., *CUPULIFORMIS establishes lateral organ boundaries in Antirrhinum*. *Development*, 2004. **131**(4): p. 915-922.
77. Vlad, D., et al., *Leaf Shape Evolution Through Duplication, Regulatory Diversification, and Loss of a Homeobox Gene*. *Science*, 2014. **343**(6172): p. 780-783.
78. Sicard, A., et al., *Repeated evolutionary changes of leaf morphology caused by mutations to a homeobox gene*. *Current Biology*, 2014. **24**(16): p. 1880-1886.
79. Jackson, D., B. Veit, and S. Hake, *Expression of maize KNOTTED1 related homeobox genes in the shoot apical meristem predicts patterns of morphogenesis in the vegetative shoot*. *Development*, 1994. **120**(2): p. 405-413.
80. Tsiantis, M., et al., *Disruption of auxin transport is associated with aberrant leaf development in maize*. *Plant Physiology*, 1999. **121**(4): p. 1163-1168.
81. Gallavotti, A., et al., *The Relationship between auxin transport and maize branching*. *Plant Physiol*, 2008. **147**(4): p. 1913-23.
82. Scanlon, M.J., *The polar auxin transport inhibitor N-1-naphthylphthalamic acid disrupts leaf initiation, KNOX protein regulation, and formation of leaf margins in maize*. *Plant Physiol*, 2003. **133**(2): p. 597-605.
83. Bowman, J.L., *The YABBY gene family and abaxial cell fate*. *Current opinion in plant biology*, 2000. **3**(1): p. 17-22.

84. Matsumoto, N. and K. Okada, *A homeobox gene, PRESSED FLOWER, regulates lateral axis-dependent development of Arabidopsis flowers*. *Genes & development*, 2001. **15**(24): p. 3355-3364.
85. Dai, M., et al., *A WUSCHEL-LIKE HOMEBOX gene represses a YABBY gene expression required for rice leaf development*. *Plant physiology*, 2007. **144**(1): p. 380-390.
86. Tsiantis, M., et al., *The Maize rough sheath2 Gene and Leaf Development Programs in Monocot and Dicot Plants*. *Science*, 1999. **284**(5411): p. 154-156.
87. Smith, L.G., S. Hake, and A.W. Sylvester, *The tangled-1 mutation alters cell division orientations throughout maize leaf development without altering leaf shape*. *Development*, 1996. **122**(2): p. 481-489.
88. Smith, L.G., et al., *A dominant mutation in the maize homeobox gene, Knotted-1, causes its ectopic expression in leaf cells with altered fates*. *Development*, 1992. **116**(1): p. 21-30.
89. Harlan, H.V., *The Origin of Hooded Barley*. *The Journal of Heredity*, 1931. **22**(9): p. 265-272.
90. Muller, K.J., et al., *The barley Hooded mutation caused by a duplication in a homeobox gene intron*. *Nature*, 1995. **374**(6524): p. 727-30.
91. Shantz, H.L., *The Place of Grasslands in the Earth's Cover*. *Ecology*, 1954. **35**(2): p. 143-145.
92. Kellogg, E.A., *Evolutionary history of the grasses*. *Plant physiology*, 2001. **125**(3): p. 1198-1205.
93. Johnston, R., S. Leiboff, and M.J. Scanlon, *Ontogeny of the sheathing leaf base in maize (Zea mays)*. *New Phytologist*, 2015. **205**(1): p. 306-315.
94. Freeling, M., *A conceptual framework for maize leaf development*. *Developmental Biology*, 1992. **153**(1): p. 44-58.
95. Sharman, B., *Developmental anatomy of the shoot of Zea mays L.* *Annals of Botany*, 1942. **6**(2): p. 245-282.
96. Poethig, S., *Cellular parameters of leaf morphogenesis*. New York Academic Press, Contemporary problems in plant anatomy, 1983.
97. Sylvester, A.W., W.Z. Cande, and M. Freeling, *Division and differentiation during normal and liguleless-1 maize leaf development*. *Development*, 1990. **110**(3): p. 985-1000.

98. R.S. Poethig, E.J.S., *Clonal Analysis of Leaf Development in Maize* Maydica, 1995. **40**: p. 67-76.
99. Candela, H., et al., *The milkweed pod1 Gene Encodes a KANADI Protein That Is Required for Abaxial/Adaxial Patterning in Maize Leaves*. The Plant Cell Online, 2008. **20**(8): p. 2073-2087.
100. Juarez, M.T., R.W. Twigg, and M.C. Timmermans, *Specification of adaxial cell fate during maize leaf development*. Development, 2004. **131**(18): p. 4533-44.
101. Zhang, G.-H., et al., *SHALLOT-LIKE1 is a KANADI transcription factor that modulates rice leaf rolling by regulating leaf abaxial cell development*. The Plant Cell, 2009. **21**(3): p. 719-735.
102. Scanlon, M.J., R.G. Schneeberger, and M. Freeling, *The maize mutant narrow sheath fails to establish leaf margin identity in a meristematic domain*. Development, 1996. **122**(6): p. 1683-1691.
103. Timmermans, M.C., et al., *Leafbladeless1 is required for dorsoventrality of lateral organs in maize*. Development, 1998. **125**(15): p. 2813-23.
104. Moreno, M.A., et al., *liguleless1 encodes a nuclear-localized protein required for induction of ligules and auricles during maize leaf organogenesis*. Genes & Development, 1997. **11**(5): p. 616-628.
105. Lee, J., et al., *Mutations in the rice liguleless gene result in a complete loss of the auricle, ligule, and laminar joint*. Plant Molecular Biology, 2007. **65**(4): p. 487-499.
106. Walsh, J. and M. Freeling, *The liguleless2 gene of maize functions during the transition from the vegetative to the reproductive shoot apex*. Plant J, 1999. **19**(4): p. 489-95.
107. Muehlbauer, G.J., et al., *Ectopic expression of the maize homeobox gene Liguleless3 alters cell fates in the leaf*. Plant Physiology, 1999. **119**(2): p. 651-662.
108. Scanlon, M.J., *The Polar Auxin Transport Inhibitor N-1-Naphthylphthalamic Acid Disrupts Leaf Initiation, KNOX Protein Regulation, and Formation of Leaf Margins in Maize*. Plant Physiology, 2003. **133**(2): p. 597-605.
109. Lee, K., et al., *Visualizing Plant Development and Gene Expression in Three Dimensions Using Optical Projection Tomography*. The Plant Cell Online, 2006. **18**(9): p. 2145-2156.
110. Sharpe, J., et al., *Optical projection tomography as a tool for 3D microscopy and gene expression studies*. Science, 2002. **296**(5567): p. 541-5.

111. Hertweck, K.L., et al., *Phylogenetics, divergence times and diversification from three genomic partitions in monocots*. Botanical Journal of the Linnean Society, 2015. **178**(3): p. 375-393.
112. Huo, N., et al., *Structural characterization of Brachypodium genome and its syntenic relationship with rice and wheat*. Plant Molecular Biology, 2009. **70**(1-2): p. 47-61.
113. Stevens, P.F., *Angiosperm Phylogeny Website*. 2001 onwards. **Version 12**(July 2012).
114. Rudall, P.J. and M. Buzgo, *Evolutionary history of the monocot leaf*. Systematics Association Special Volume, 2002. **65**: p. 431-458.
115. Stoma, S., et al. *Using mechanics in the modelling of meristem morphogenesis*. in *5th International Workshop on Functional-Structural Plant Models*. 2007.
116. Yi, H. and V.M. Puri, *Architecture-Based Multiscale Computational Modeling of Plant Cell Wall Mechanics to Examine the Hydrogen-Bonding Hypothesis of the Cell Wall Network Structure Model*. Plant Physiology, 2012. **160**(3): p. 1281-1292.
117. Merks, R.M.H., et al., *VirtualLeaf: An Open-Source Framework for Cell-Based Modeling of Plant Tissue Growth and Development*. Plant Physiology, 2011. **155**(2): p. 656-666.
118. O'Connor, D.L., et al., *A Division in PIN-Mediated Auxin Patterning during Organ Initiation in Grasses*. PLoS Comput Biol, 2014. **10**(1): p. e1003447.
119. Truernit, E., et al., *High-resolution whole-mount imaging of three-dimensional tissue organization and gene expression enables the study of Phloem development and structure in Arabidopsis*. Plant Cell, 2008. **20**(6): p. 1494-503.
120. Schiessl, K., et al., *JAGGED Controls Growth Anisotropy and Coordination between Cell Size and Cell Cycle during Plant Organogenesis*. Current Biology, 2012. **22**(19): p. 1739-1746.
121. Barbier de Reuille, P., et al., *MorphoGraphX: A platform for quantifying morphogenesis in 4D*, ed. D.C. Bergmann. Vol. 4. 2015.
122. Rast, M.I. and R. Simon, *The meristem-to-organ boundary: more than an extremity of anything*. Current Opinion in Genetics & Development, 2008. **18**(4): p. 287-294.
123. Mohanty, A., et al., *Advancing Cell Biology and Functional Genomics in Maize Using Fluorescent Protein-Tagged Lines*. Plant Physiology, 2009. **149**(2): p. 601-605.

124. Yamaguchi, T., et al., *The YABBY gene DROOPING LEAF regulates carpel specification and midrib development in Oryza sativa*. *The Plant Cell*, 2004. **16**(2): p. 500-509.
125. Shani, E., et al., *Cytokinin Regulates Compound Leaf Development in Tomato*. *The Plant Cell*, 2010. **22**(10): p. 3206-3217.
126. Spinelli, S.V., et al., *A Mechanistic Link between STM and CUC1 during Arabidopsis Development*. *Plant Physiology*, 2011. **156**(4): p. 1894-1904.
127. Xie, K., et al., *Gradual increase of miR156 regulates temporal expression changes of numerous genes during leaf development in rice*. *Plant physiology*, 2012. **158**(3): p. 1382-1394.
128. Chen, Q., et al., *Characterization of Rolled and Erect Leaf 1 in regulating leave morphology in rice*. *Journal of Experimental Botany*, 2015.
129. Moon, J., H. Candela, and S. Hake, *The Liguleless narrow mutation affects proximal-distal signaling and leaf growth*. *Development*, 2013. **140**(2): p. 405-412.
130. Johnston, R., et al., *Transcriptomic Analyses Indicate That Maize Ligule Development Recapitulates Gene Expression Patterns That Occur during Lateral Organ Initiation*. *The Plant Cell*, 2014. **26**(12): p. 4718-4732.
131. McSteen, P., *Auxin and monocot development*. *Cold Spring Harb Perspect Biol*, 2010. **2**(3): p. a001479.
132. Cheng, Y., X. Dai, and Y. Zhao, *Auxin biosynthesis by the YUCCA flavin monooxygenases controls the formation of floral organs and vascular tissues in Arabidopsis*. *Genes & Development*, 2006. **20**(13): p. 1790-1799.
133. Péret, B., et al., *AUX/LAX genes encode a family of auxin influx transporters that perform distinct functions during Arabidopsis development*. *The Plant Cell*, 2012. **24**(7): p. 2874-2885.
134. Sinha, N.R., R.E. Williams, and S. Hake, *Overexpression of the maize homeo box gene, KNOTTED-1, causes a switch from determinate to indeterminate cell fates*. *Genes & Development*, 1993. **7**(5): p. 787-795.
135. Zhao, S.-Q., et al., *Rice leaf inclination2, a VIN3-like protein, regulates leaf angle through modulating cell division of the collar*. *Cell research*, 2010. **20**(8): p. 935-947.
136. Yan, S., et al., *ROLLED LEAF 9, encoding a GARP protein, regulates the leaf abaxial cell fate in rice*. *Plant molecular biology*, 2008. **68**(3): p. 239-250.

137. Whipple, C.J., et al., *Conservation of B class gene expression in the second whorl of a basal grass and outgroups links the origin of lodicules and petals*. Proceedings of the National Academy of Sciences, 2007. **104**(3): p. 1081-1086.
138. Williams-Carrier, R.E., et al., *Ectopic expression of the maize kn1 gene phenocopies the Hooded mutant of barley*. Development, 1997. **124**(19): p. 3737-45.
139. Stebbins, G.L. and E. Yagil, *The morphogenetic effects of the hooded gene in barley. I. The course of development in hooded and awned genotypes*. Genetics, 1966. **54**(3): p. 727-41.
140. Bonnett, O.T., *Hood and supernumerary spike development in barley*. J. Agri. Res, 1938. **57**: p. 371-377.
141. Kerstetter, R.A., et al., *Loss-of-function mutations in the maize homeobox gene, knotted1, are defective in shoot meristem maintenance*. Development, 1997. **124**(16): p. 3045-3054.
142. Hareven, D., et al., *The Making of a Compound Leaf: Genetic Manipulation of Leaf Architecture in Tomato*. Cell, 1996. **84**(5): p. 735-744.
143. Roig, C., et al., *Genetics of barley hooded suppression*. Genetics, 2004. **167**(1): p. 439-48.
144. Yagil, E. and G.L. Stebbins, *The Morphogenetic Effects of the Hooded Gene in Barley II. Cytological and Environmental Factors Affecting Gene Expression*. Genetics, 1969. **62**(2): p. 307-19.
145. Gómez, J.F. and Z.A. Wilson, *Non-destructive staging of barley reproductive development for molecular analysis based upon external morphology*. Journal of Experimental Botany, 2012.
146. Schindelin, J., et al., *Fiji: an open-source platform for biological-image analysis*. Nat Meth, 2012. **9**(7): p. 676-682.
147. Coen, E.S., et al., *floricaula: a homeotic gene required for flower development in antirrhinum majus*. Cell, 1990. **63**(6): p. 1311-22.
148. Altschul, S.F., et al., *Basic local alignment search tool*. J Mol Biol, 1990. **215**(3): p. 403-10.
149. *A physical, genetic and functional sequence assembly of the barley genome*. Nature, 2012. **491**(7426): p. 711-716.
150. Conti, L. and D. Bradley, *TERMINAL FLOWER1 Is a Mobile Signal Controlling Arabidopsis Architecture*. The Plant Cell Online, 2007. **19**(3): p. 767-778.

151. Tobeña-Santamaria, R., et al., *FLOOZY of petunia is a flavin mono-oxygenase-like protein required for the specification of leaf and flower architecture*. *Genes & Development*, 2002. **16**(6): p. 753-763.
152. Ramirez, J., et al., *Distal Expression of knotted1 in Maize Leaves Leads to Reestablishment of Proximal/Distal Patterning and Leaf Dissection*. *Plant Physiology*, 2009. **151**(4): p. 1878-1888.
153. Jackson, D., *Double Labeling of KNOTTED1 mRNA and Protein Reveals Multiple Potential Sites of Protein Trafficking in the Shoot Apex*. *Plant Physiology*, 2002. **129**(4): p. 1423-1429.
154. Golz, J.F., E.J. Keck, and A. Hudson, *Spontaneous mutations in KNOX genes give rise to a novel floral structure in Antirrhinum*. *Curr Biol*, 2002. **12**(7): p. 515-22.
155. Bolduc, N., et al., *Unraveling the KNOTTED1 regulatory network in maize meristems*. *Genes Dev*, 2012. **26**(15): p. 1685-90.
156. Fahlgren, N., et al., *Regulation of AUXIN RESPONSE FACTOR3 by TAS3 ta-siRNA Affects Developmental Timing and Patterning in Arabidopsis*. *Current Biology*, 2006. **16**(9): p. 939-944.
157. Juarez, M.T., et al., *microRNA-mediated repression of rolled leaf1 specifies maize leaf polarity*. *Nature*, 2004. **428**(6978): p. 84-8.
158. Stebbins, G.L. and V.K. Gupta, *The relation between peroxidase activity and the morphological expression of the hooded gene in barley*. *Proc Natl Acad Sci U S A*, 1969. **64**(1): p. 50-6.
159. Lin, J. and K.J. Muller, *Structure and development of epiphyllly in knox-transgenic tobacco*. *Planta*, 2002. **214**(4): p. 521-5.
160. Schneeberger, R., et al., *The rough sheath2 gene negatively regulates homeobox gene expression during maize leaf development*. *Development*, 1998. **125**(15): p. 2857-2865.
161. P. , M.C., et al., *ROUGH SHEATH2: A Myb Protein That Represses knox Homeobox Genes in Maize Lateral Organ Primordia*. *Science*, 1999. **284**(5411): p. 151-153.
162. Nelson, B.K., X. Cai, and A. Nebenfuhr, *A multicolored set of in vivo organelle markers for co-localization studies in Arabidopsis and other plants*. *Plant J*, 2007. **51**(6): p. 1126-36.
163. Johri, M.M. and E.H. Coe Jr, *Clonal analysis of corn plant development: I. The development of the tassel and the ear shoot*. *Developmental Biology*, 1983. **97**(1): p. 154-172.

164. Satina, S. and A. Blakeslee, *Periclinal chimeras in Datura stramonium in relation to development of leaf and flower*. American Journal of Botany, 1941: p. 862-871.
165. Satina, S., A. Blakeslee, and A.G. Avery, *Demonstration of the three germ layers in the shoot apex of Datura by means of induced polyploidy in periclinal chimeras*. American Journal of Botany, 1940: p. 895-905.
166. Vincent, C.A., R. Carpenter, and E.S. Coen, *Cell lineage patterns and homeotic gene activity during Antirrhinum flower development*. Current Biology, 1995. **5**(12): p. 1449-1458.
167. Gallois, J.-L., et al., *Combined SHOOT MERISTEMLESS and WUSCHEL trigger ectopic organogenesis in Arabidopsis*. Development, 2002. **129**(13): p. 3207-3217.
168. Sternberg, N. and D. Hamilton, *Bacteriophage P1 site-specific recombination: I. Recombination between loxP sites*. Journal of Molecular Biology, 1981. **150**(4): p. 467-486.
169. Sieburth, L.E., G.N. Drews, and E.M. Meyerowitz, *Non-autonomy of AGAMOUS function in flower development: use of a Cre/loxP method for mosaic analysis in Arabidopsis*. Development, 1998. **125**(21): p. 4303-4312.
170. Ulmasov, T., et al., *Aux/IAA proteins repress expression of reporter genes containing natural and highly active synthetic auxin response elements*. The Plant Cell Online, 1997. **9**(11): p. 1963-71.
171. Harwood\*, W.A., et al., *Barley Transformation Using Agrobacterium-Mediated Techniques*, in *Transgenic Wheat, Barley and Oats*, H.D. Jones and P.R. Shewry, Editors. 2009, Humana Press. p. 137-147.
172. Druka, A., et al., *Genetic Dissection of Barley Morphology and Development*. Plant Physiology, 2011. **155**(2): p. 617-627.
173. Lundqvist, U., *Scandinavian mutation research in barley - a historical review*. Hereditas, 2014. **151**(6): p. 123-31.
174. Engler, C., et al., *A Golden Gate Modular Cloning Toolbox for Plants*. ACS Synthetic Biology, 2014. **3**(11): p. 839-843.
175. Weber, E., et al., *A Modular Cloning System for Standardized Assembly of Multigene Constructs*. PLoS ONE, 2011. **6**(2): p. e16765.
176. Srivastava, V., O.D. Anderson, and D.W. Ow, *Single-copy transgenic wheat generated through the resolution of complex integration patterns*. Proceedings of the National Academy of Sciences, 1999. **96**(20): p. 11117-11121.

177. Freeman, J., et al., *Temporal and spatial control of transgene expression using a heat-inducible promoter in transgenic wheat*. *Plant Biotechnol J*, 2011. **9**(7): p. 788-96.
178. Kim, J.Y., et al., *Intercellular trafficking of a KNOTTED1 green fluorescent protein fusion in the leaf and shoot meristem of Arabidopsis*. *Proceedings of the National Academy of Sciences*, 2002. **99**(6): p. 4103-4108.
179. Kaczmarczyk, S.J. and J.E. Green, *A single vector containing modified cre recombinase and LOX recombination sequences for inducible tissue-specific amplification of gene expression*. *Nucleic Acids Research*, 2001. **29**(12): p. e56-e56.
180. Gaj, M. and M. Matuszynski, *Genetic analysis of spike characters of barley mutants*. *Barley Genetics Newsletter*, 1985. **15**: p. 32-33.
181. Pozzi, C., et al., *Genetics of mutations affecting the development of a barley floral bract*. *Genetics*, 2000. **154**(3): p. 1335-46.
182. Sauer, M., et al., *Canalization of auxin flow by Aux/IAA-ARF-dependent feedback regulation of PIN polarity*. *Genes & Development*, 2006. **20**(20): p. 2902-2911.
183. Perrot-Rechenmann, C., *Cellular responses to auxin: division versus expansion*. *Cold Spring Harbor perspectives in biology*, 2010. **2**(5): p. a001446.
184. Rayle, D.L. and R.E. Cleland, *The Acid Growth Theory of auxin-induced cell elongation is alive and well*. *Plant physiology*, 1992. **99**(4): p. 1271-1274.
185. Wolf, S., et al., *Plant cell wall homeostasis is mediated by brassinosteroid feedback signaling*. *Current Biology*, 2012. **22**(18): p. 1732-1737.
186. Rashotte, A.M., et al., *Expression Profiling of Cytokinin Action in Arabidopsis*. *Plant Physiology*, 2003. **132**(4): p. 1998-2011.
187. Vollbrecht, E., et al., *The developmental gene Knotted-1 is a member of a maize homeobox gene family*. *Nature*, 1991. **350**(6315): p. 241-243.
188. Hay, A. and M. Tsiantis, *KNOX genes: versatile regulators of plant development and diversity*. *Development*, 2010. **137**(19): p. 3153-3165.
189. Shani, E., et al., *Stage-specific regulation of Solanum lycopersicum leaf maturation by class 1 KNOTTED1-LIKE HOMEODOMAIN proteins*. *The Plant Cell*, 2009. **21**(10): p. 3078-3092.
190. Hay, A. and M. Tsiantis, *The genetic basis for differences in leaf form between Arabidopsis thaliana and its wild relative Cardamine hirsuta*. *Nat Genet*, 2006. **38**(8): p. 942-947.

191. Lincoln, C., et al., *A knotted1-like homeobox gene in Arabidopsis is expressed in the vegetative meristem and dramatically alters leaf morphology when overexpressed in transgenic plants*. *The Plant Cell*, 1994. **6**(12): p. 1859-76.
192. Hofer, J., et al., *Expression of a class 1 knotted1-like homeobox gene is down-regulated in pea compound leaf primordia*. *Plant Molecular Biology*, 2001. **45**(4): p. 387-398.
193. Champagne, C.E.M., et al., *Compound Leaf Development and Evolution in the Legumes*. *The Plant Cell*, 2007. **19**(11): p. 3369-3378.
194. Belles-Boix, E., et al., *KNAT6: An Arabidopsis Homeobox Gene Involved in Meristem Activity and Organ Separation*. *The Plant Cell*, 2006. **18**(8): p. 1900-1907.
195. Whittall, J.B. and S.A. Hodges, *Pollinator shifts drive increasingly long nectar spurs in columbine flowers*. *Nature*, 2007. **447**(7145): p. 706-709.
196. Glover, B.J., et al., *How Have Advances in Comparative Floral Development Influenced Our Understanding of Floral Evolution?* *International Journal of Plant Sciences*, 2015. **176**(4): p. 307-323.
197. Doebley, J. and L. Lukens, *Transcriptional Regulators and the Evolution of Plant Form*. *The Plant Cell*, 1998. **10**(7): p. 1075-1082.
198. McGregor, A.P., et al., *Morphological evolution through multiple cis-regulatory mutations at a single gene*. *Nature*, 2007. **448**(7153): p. 587-590.
199. Prud'homme, B., et al., *Repeated morphological evolution through cis-regulatory changes in a pleiotropic gene*. *Nature*, 2006. **440**(7087): p. 1050-1053.
200. Wray, G.A., *The evolutionary significance of cis-regulatory mutations*. *Nat Rev Genet*, 2007. **8**(3): p. 206-216.
201. Gaunt, S.J. and Y.-L. Paul, *Changes in Cis-regulatory Elements during Morphological Evolution*. *Biology*, 2012. **1**(3): p. 557-574.
202. Tamura, K., et al., *MEGA6: Molecular Evolutionary Genetics Analysis Version 6.0*. *Molecular Biology and Evolution*, 2013. **30**(12): p. 2725-2729.
203. Liao, C.-Y., et al., *Reporters for sensitive and quantitative measurement of auxin response*. *Nat Meth*, 2015. **12**(3): p. 207-210.
204. Clark, E.J.J.a.L.G., *Classification and biogeography of New World grasses: Anomochlooideae, Pharoideae, Ehrhartoideae and Bambusoideae*. *Aliso: A Journal of Systematic and Evolutionary Botany*, 2007. **23**(1): p. 303-314.
205. Sakamoto, T., et al., *Erect leaves caused by brassinosteroid deficiency increase biomass production and grain yield in rice*. *Nat Biotech*, 2006. **24**(1): p. 105-109.

206. Hake, S., et al., *The role of knox genes in plant development*. *Annu Rev Cell Dev Biol*, 2004. **20**: p. 125-51.
207. Stebbins, G.L. and H.J. Price, *The Developmental Genetics of the CALCAROIDES Gene in Barley. I. Divergent Expression at the Morphological and Histological Level*. *Genetics*, 1971. **68**(4): p. 527-38.
208. Becraft, P.W., et al., *The liguleless-1 gene acts tissue specifically in maize leaf development*. *Developmental Biology*, 1990. **141**(1): p. 220-232.
209. Guo, Y. and B. Li, *New advances in virtual plant research*. *Chinese Science Bulletin*, 2001. **46**(11): p. 888-894.
210. Vos, D.D., et al., *Simulating leaf growth dynamics through Metropolis-Monte Carlo based energy minimization*. *Journal of Computational Science*, (0).
211. Bolduc, N., et al., *Unequal redundancy in maize knox genes*. *Plant Physiology*, 2013.
212. Chehrehasa, F., et al., *EdU, a new thymidine analogue for labelling proliferating cells in the nervous system*. *Journal of Neuroscience Methods*, 2009. **177**(1): p. 122-130.
213. Salic, A. and T.J. Mitchison, *A chemical method for fast and sensitive detection of DNA synthesis in vivo*. *Proc Natl Acad Sci U S A*, 2008. **105**(7): p. 2415-20.
214. Sauer, M., et al., *Immunocytochemical techniques for whole-mount in situ protein localization in plants*. *Nat. Protocols*, 2006. **1**(1): p. 98-103.
215. Wasteneys, G.O., J. Willingale-Theune, and D. Menzel, *Freeze shattering: a simple and effective method for permeabilizing higher plant cell walls*. *Journal of Microscopy*, 1997. **188**(1): p. 51-61.